AD-A014 219

THE TURBULENT BOUNDARY LAYER: AN EXPERIMENTAL STUDY OF THE TRANSPORT OF MOMENTUM AND HEAT WITH THE EFFECT OF ROUGHNESS

Marcos M. Pimenta, et al

Stanford University

Prepared for:

Office of Naval Research

May 1975

THE TURBULENT BOUNDARY LAYER: AN EXPERIMENTAL STUDY OF THE TRANSPORT OF MOMENTUM AND HEAT WITH THE EFFECT OF ROUGHNESS

By

M. M. Pimenta, R. J. Moffat and W. M. Kays

Report No. HMT-21

Prepared with Support from

The Office of Naval Research
N00014-67-A-0112-0072

Thermosciences Division
Department of Mechanical Engineering
Stanford University
Stanford, California

May 1975

Unclassified

SECURITY CLASSIFICATION OF THIS PAGE (When Data Entered)

REPORT DOCUMENTATION PAGE		READ INSTRUCTIONS BEFORE COMPLETING FORM
1. REPORT NUMBER HMT-21	2. GOVT ACCESSION NO.	3. RECIPIENT'S CATALOG NUMBER
4. TITLE (and Subtitle) THE TURBULENT BOUNDARY LAYER: AN EXPERIMENTAL STUDY OF THE TRANSPORT OF MOMENTUM AND HEAT WITH THE EFFECT OF ROUGHNESS		5. TYPE OF REPORT & PERIOD COVERED Interim Report 6. PERFORMING ORG. REPORT NUMBER HMT-21
7. AUTHOR(s) Marcos M. Pimenta, Robert J. Moffat and William M. Kays		8. CONTRACT OR GRANT NUMBER(s) N00014-67-A-0112-0072
9. PERFORMING ORGANIZATION NAME AND ADDRESS Department of Mechanical Engineering Stanford University Stanford, California 94305		10. PROGRAM ELEMENT, PROJECT, TASK AREA & WORK UNIT NUMBERS NR094-368
11. CONTROLLING OFFICE NAME AND ADDRESS Office of Naval Research Code 473 Arlington, Virginia 22217		12. REPORT DATE May 1975 13. NUMBER OF PAGES 293
14. MONITORING AGENCY NAME & ADDRESS (if different from Controlling Office) Office of Naval Research, Resident Representative Room 165, Durand Building Stanford University Stanford, California 94305		15. SECURITY CLASS. (of this report) Unclassified 15a. DECLASSIFICATION/DOWNGRADING SCHEDULE

16. DISTRIBUTION STATEMENT (of this Report)

Unlimited

17. DISTRIBUTION STATEMENT (of the abstract entered in Block 20, if different from Report)

Unlimited

18. SUPPLEMENTARY NOTES

Duplicates contents of Ph.D. Dissertation of Marcos M. Pimenta: same title.

19. KEY WORDS (Continue on reverse side if necessary and identify by block number)

Heat Transfer
Rough Surfaces
Turbulence Structure
Turbulence
Roughness
Boundary Layer

20. ABSTRACT (Continue on reverse side if necessary and identify by block number)

The turbulent boundary on a deterministic rough wall has been examined for the cases of isothermal and non-isothermal, zero pressure gradient flows with and without transpiration. The data include temperature and velocity profiles, turbulence intensity profiles, turbulence shear stress and heat flux profiles and the correlation coefficients of both the fluid dynamic and temperature fields.

The transitionally rough state is shown to retain some characteristics of

DD FORM 1473, 1 JAN 73 EDITION OF 1 NOV 65 IS OBSOLETE
S/N 0102-014-6601

Unclassified

SECURITY CLASSIFICATION OF THIS PAGE (When Data Entered)

20. Abstract

a smooth wall layer, for example, the sharp peak in $\overline{u'^2}$ (longitudinal velocity fluctuation) very close to the wall ($y^+ \approx 15$) and a "van Driest"-like damping effect in the mixing length.

The near-wall behavior of the turbulent fluctuations in the fully rough state is markedly different from smooth wall behavior. Some effects of roughness on the turbulence structure are shown to extend over most of the layer.

The fully rough state exhibits self-similar profiles of turbulent fluctuations which are independent of free-stream velocity. The flow is fully turbulent for 99% of the layer: no viscous layer can be identified. Velocity profiles, in defect coordinates, are also shown to be similar. Temperature, T, and velocity, U, profiles are similar over most of the layer, and the T vs. U profiles are linear. The measured profiles show that the rough wall heat transfer is dominated by a very thin layer, involving the rough elements, where an apparent "jump" in temperature exists.

The correlation coefficients involving the turbulent shear stress are constant over most the layer, and their values are the same as those for smooth walls. Turbulent kinetic energy is larger throughout the layer, compared to smooth wall flows.

Constant shear stress and heat flux layers were observed very close to the wall with the mixing length ℓ given by $\ell = \kappa y$ providing a suitable virtual origin of the velocity profile is identified. Turbulent Prandtl numbers, obtained from direct measurements of turbulent shear stress, and turbulent heat flux, are shown to be reasonably constant near the wall, approximately equal to one, with the values slowly decreasing to 0.7 - 0.8 as the free-stream is approached.

THE TURBULENT BOUNDARY LAYER: AN EXPERIMENTAL STUDY OF THE TRANSPORT OF MOMENTUM AND HEAT WITH THE EFFECT OF ROUGHNESS

By

M. M. Pimenta, R. J. Moffat and W. M. Kays

Report No. HMT-21

Prepared with Support from

The Office of Naval Research

N00014-67-A-0112-0072

Thermosciences Division
Department of Mechanical Engineering
Stanford University
Stanford, California

May 1975

1a

ACKNOWLEDGMENTS

This research program was made possible by support from the Office of Naval Research, Contract N00014-67-A0112-0072. The apparatus used herein had been built under an earlier contract from the Department of the Navy, Contract N00123-71-0-0372. The authors express their deep appreciation to Dr. W. H. Thielbahr, Mr. James Patton and Dr. Ralph Roberts for their support.

The first author also wishes to sincerely thank the agencies which provided the financial support during his stay at Stanford University:

- Fundacao de Amparo a Pesquisa do Estado de Sao Paulo (FAPESP);
- Mineracao Matheus Leme Ltda;
- Escola Politecnica da Universidade de Sao Paulo.

The authors also wish to thank Mr. Robin Bircn for his meticulous construction and repair of the hot wire probes.

The authors acknowledge the measureless contributions of Mr. Hugh Coleman during the development and final writing of this report.

Monica Pimenta and Jan Moffat are responsible for the final typing of this report. Their effort made it possible.

ABSTRACT

The turbulent boundary on a deterministic rough wall has been examined for the cases of isothermal and non-isothermal, zero pressure gradient flows with and without transpiration. Both the transitionally rough and the fully rough states have been investigated. The structural features are analyzed using the measurements of integral parameters, mean temperature and velocity profiles, turbulence intensity profiles, turbulence shear stress and heat flux profiles and the correlation coefficients of both the fluid dynamic and temperature fields. The effects of transpiration on the layer structure have been measured and are analyzed. The structural features observed are compared with smooth wall cases and different degrees of roughness manifestation.

The transitionally rough state is shown to retain some characteristics of a smooth wall layer, for example, the sharp peak in $\overline{u'^2}$ (longitudinal velocity fluctuation) very close to the wall ($y^+ \approx 15$) and a "van Driest"-like damping effect in the mixing length.

The fully rough state can be identified from Stanton number or friction factor behavior (independent of Reynolds number) from mean profiles, or from turbulent fluctuation profiles. In particular, the near-wall behavior of the turbulent fluctuations is markedly different from smooth wall behavior. Some effects of roughness on the turbulence structure are shown to extend over most of the layer and the "bursting" mechanism is used to explain the shape of the intensity profiles.

The fully rough state exhibits self-similar profiles of turbulent fluctuations which are independent of free-stream velocity. The flow is fully turbulent for 99% of the layer: no viscous layer can be identified. Velocity profiles, in defect coordinates, are also shown to be similar. Temperature, T , and velocity, U , profiles are similar over most of the layer, and as a result T vs. U profiles are linear. The measured profiles show experimental verification of the hypothesis that the rough wall heat transfer is dominated by a very thin layer, involving the rough elements, where an apparent "jump" in temperature exists.

The correlation coefficients involving the turbulent shear stress are constant over most the layer, and their values are the same as those for smooth walls. This is the case despite the fact that production of turbulent kinetic energy is larger throughout the layer, compared to smooth wall flows.

Constant shear stress and heat flux layers were observed very close to the wall. The mixing length ℓ is shown to be given by $\ell = \kappa y$ for this layer, providing a suitable virtual origin of the velocity profile is identified. Turbulent Prandtl numbers, obtained from direct measurements of turbulent shear stress, and turbulent heat flux, are shown to be reasonably constant near the wall, approximately equal to one, with the values slowly decreasing to 0.7 - 0.8 as the free-stream is approached.

Blowing affects the structure of the entire layer. Friction factors and Stanton numbers are reduced; however, mean velocity and temperature profiles continue to be similar. Turbulent fluctuations are increased with transpiration, but the shear stress correlation coefficients do not change. It is shown that blowing introduces a pressure interaction mechanism which causes the wall to seem rougher to the flow, i.e., to consist of larger roughness elements. This interaction is evident from the velocity fluctuation profiles and mixing length distributions.

TABLE OF CONTENTS

Page

Page

LIST OF FIGURES

Figure		Page

Figure Page

Chapter 4

Figure		Page

Figure		Page

NOMENCLATURE

A	Van Driest damping function for a smooth surface
A^+	Van Driest dimensionless damping function = AU_τ/ν
B_f	Blowing parameter, $F/C_f/2$
B_h	Blowing parameter, F/St
C_f	Friction factor, $\tau_w/(\rho U_\infty^2/2)$
c_p	Specific heat of fluid (Btu/lbm $^\circ$F)
d	Wire diameter
E	Time averaged output from anemometer (V)
Ec	Eckert number (Equation 8.15)
e	Instantaneous output voltage from anemometer (V)
e'	Fluctuating value of anemometer output (V)
F	Blowing fraction, $\rho_o v_o/\rho_\infty U_\infty$
G	Clauser shape factor, Equation 6.13
g_c	Newton's second law proportionality factor
H	Shape factor = δ_1/δ_2
h	Heat transfer coefficient
I	Wire current
J	Mechanical equivalent of heat (778.2 ft lb/Btu)
k	Conductivity
k_s	Equivalent sand grain roughness (inch)
k^+	$k_s U_\tau/\nu$
ℓ	Mixing-length

ℓ	Length of wire
$\dot{m}''$	Mass flux through the plate surface (lbm/sec ft^2)
P	Static pressure
Pr	Molecular Prandtl number = ν/α
Pr_t	Turbulent Prandtl number = $\varepsilon_M/\varepsilon_H$
q^2	Turbulent kinetic energy = $\overline{u'^2} + \overline{v'^2} + \overline{w'^2}$
$\dot{q}''$	Heat flux
R	Wire resistance
R_{q^2}	$-\overline{u'v'}/q^2$
R_{uv}	$-\overline{u'v'}/\sqrt{\overline{u'^2}}\sqrt{\overline{v'^2}}$
R_w	Average resistance of wire
r	Ball radius (inch)
Re_k	Roughness Reynolds number = $k_s U_\tau/\nu$
Re_t	Reynolds number for the turbulence = ε_M/ν
Re_x	x-Reynolds number = xU_∞/ν
Re_{Δ_2}	Enthalpy thickness Reynolds number = $\Delta_2 U_\infty/\nu$
Re_{δ_2}	Momentum thickness Reynolds number = $\delta_2 U_\infty/\nu$
St	Stanton number = $h/G\ c_p$
$(St)_o$	Stanton number without blowing = $h/G\ c_p$
ΔSt	Stanton number error
T	Mean temperature

T_{aw}	Adiabatic wall temperature
T_m	Average wire temperature
T_t	Temperature of transpiration air beneath the porous plate
T_w	Wall temperature, wire temperature
T_τ	$(T_w - T_{\infty,o})\ St/\sqrt{C_f/2}$
T_∞	Free-stream static temperature
$T_{\infty,o}$	Free-stream total temperature
T^+	$(T_w - T)/T_\tau$
t	Instantaneous temperature
t'	Fluctuating temperature
t'_m	Fluctuating average wire temperature
t'_∞	Fluctuating free-stream temperature
$\overline{t'^2}$	Auto-correlation of temperature fluctuation
U	Time averaged velocity
U_{eff}	Time averaged effective velocity
U_τ	Friction velocity = $U_\infty \sqrt{C_f/2}$ (ft/sec)
U_∞	Free-stream velocity (ft/sec)
U^+	U/U_τ
u	Instantaneous velocity
u_{eff}	Instantaneous effective velocity for the hot wire
u'	Fluctuating longitudinal velocity
u'_{eff}	Fluctuating effective velocity

$\overline{u'^2}$	Auto-correlation of the longitudinal velocity
$\overline{u't'}$	Longitudinal velocity-temperature correlation
$\overline{u'v'}$	Turbulent shear stress
$\overline{u'w'}$	Longitudinal-tangential velocity correlation
V	Time averaged normal velocity (ft/sec)
V_o	Plate averaged normal velocity at the wall (ft/sec)
v	Instantaneous velocity normal to the test surface (ft/sec)
v'	Fluctuating normal velocity (ft/sec)
$\overline{v'^2}$	Auto-correlation of normal velocity
$\overline{v't'}$	Normal velocity-temperature correlation
$\overline{v'w'}$	Normal-tangential velocity correlation
W	Time averaged tangential velocity
w	Instantaneous tangential velocity (ft/sec)
w'	Fluctuating tangential velocity
$\overline{w'^2}$	Auto-correlation of tangential velocity
x	Streamwise coordinate
x_o	Virtual origin of momentum boundary layer
y	Distance normal to the surface (ft)
Δy	y-coordinate velocity profile virtual origin shift (ft)
y^+	$y\, U_\tau/\nu$
z	Transverse coordinate
z_o	Roughness parameter (Equation 3.2)

Greek

α	Thermal diffusivity
β	Clauser's equilibrium parameter $= \left[\delta_1/\tau_w\right](dp/dx)$
Δ_2	Enthalpy thickness $= \int_0^\infty \frac{\rho U}{\rho_\infty U_\infty}\left(\frac{T - T_\infty}{T_w - T_\infty}\right)dy$
δ	Momentum boundary layer thickness $U(\delta) = 0.99\ U_\infty$.
δ_T	Thermal boundary layer thickness $(T_w - T)/(T_w - T_\infty) = 0.99$
δ_1	Displacement thickness $= \int_0^\infty \left(1 - \frac{U}{U_\infty}\right)dy$
δ_2	Momentum thickness $= \int_0^\infty \frac{\rho U}{\rho_\infty U_\infty}\left(1 - \frac{U}{U_\infty}\right)dy$
ε_H	Eddy diffusivity for heat $= -\overline{v't'}/(dT/dy)$
ε_M	Eddy diffusivity for momentum $= -\overline{u'v'}/(dU/dy)$
κ	Karman constant
λ	Outer region mixing-length proportionality constant ($\ell = \lambda\delta$)
μ	Dynamic viscosity
ν	Kinematic viscosity $= \mu/\rho$
ρ	Density
ρ_∞	Free-stream density
τ	Shear stress, time
ξ	y-coordinate defined in Section 5.3

Subscripts

w	Wall
∞	Free-stream

Superscripts

*	Relate to constant current anemometer
—	Time averaged
$\cdot$	Rate (per second)
"	Per unit area

CHAPTER I

INTRODUCTION

The knowledge of flow resistance and heat transfer characteristics between fluids and solid surfaces is important for engineering applications. It is known that the hydrodynamic and thermal characteristics are controlled by important parameters such as fluid properties, velocity and temperature, and the shape and conditions of the solid surface. The surface condition requires special attention in applications where surface roughness is an inherent feature. The number of applications where roughness is important has motivated the present investigation, which is concentrated on the study of a turbulent boundary layer over a rough planar wall.

The behavior of friction factor and heat transfer coefficient in boundary layer flows is frequently described by means of mean velocity and temperature profiles. The shapes of the mean velocity and temperature profiles are, in turn, interpreted by considering the shear stress and heat flux distributions. Thus the behavior at each "level" is investigated by means of observations at a more detailed level. Finally, in a global sense comprehension of the boundary layer phenomenon can be achieved only by inter-relating the behaviors observed at all levels. The level by level cascade approach presumes a degree of cause-effect relationship between the levels and the organization of the different behaviors is commonly presented in terms of similarity relationships among the mean and turbulence quantities.

Works on the effects of surface roughness are found in the literature, but only a few treat more than one level at a time. The difficulty of understanding the rough wall problem might be related to the absence of systematic studies covering all levels simultaneously. The present work is an attempt to answer the need for such a multi-level study.

Engineering applications require practical and reliable correlations for friction factors and heat transfer coefficients. The generation of correlations demands not only experimental data of good quality, but also more detailed studies which bring better understanding of the flow problem. Lack of a general understanding has led various authors to propose correlations which handle their own source data but frequently miss the results from other studies (see for instance Liu et al. [1], Dvorak [2] or Gowen et al. [3]).

Furthermore, the increased use of finite difference computer programs to predict friction factor and Stanton number distributions has also increased the need for more detailed studies of the boundary layer structure than are currently available. Computer programs are capable of predicting mean velocity and temperature profiles, and the evolution of the layer under a large variety of boundary conditions, given empirical correlations for the turbulent transport properties. The required correlations are extracted from the experimental data and constitute the main output of modern boundary layer experiments. In essence, the computer program framework, plus the data correlations, constitute a more refined way of interpolating or slightly extrapolating the experimental data. The present investigation is aimed at providing such data for rough surface flows, at several different levels.

Before we discuss our experiments, let us point out some facts which have been recognized by studies with rough wall layers. Roughness normally increases friction resistance and the heat transfer coefficient compared to smooth plate values at the same Reynolds number, and, hence, enhances the boundary layer growth and entrainment of fluid from the mainstream. To account both for the surface condition and the mainstream condition, a turbulent boundary layer under the influence of wall roughness requires at least a two-parameter description for the hydrodynamics (see for instance Schlichting [5] or Nikuradse [20]). The heat transfer is sensitive to fluid Prandtl number as well as to the hydrodynamics, thus a three-parameter description is required for heat transfer (see for instance Dipprey et al. [28]). Roughness produces higher friction factors and Stanton numbers which result in larger deficits of velocity and temperature away from the wall, compared to smooth wall profiles (see for instance Hama [10] and Gowen et al. [3]). The corresponding decrements in rough wall velocity and temperature profiles relative to smooth wall values have been, tentatively, correlated as functions of a roughness size parameter. The process of correlating the data presumes some sort of "law of the wall" (an idea taken from smooth wall studies) and uses y-coordinate shifts (see for instance Clauser [19] and Jayatilleke [48]). The measurements of shear stresses and heat fluxes, and other observations at this higher level have not been presented or discussed before in the literature. Nevertheless, the most recent efforts in computer prediction programs used empirical models for the shear stress and heat flux distributions which are deduced by considering the rough layer as having similar behavior to that of a smooth wall layer. The limited success of predictive computer programs so far confirms the need for more research, particularly because experimental observations at the more detailed levels are scarce in the field of hydrodynamics of rough wall layers, and are nonexistent for the thermal field.

1.1 Main Objectives

The present study has three main objectives which are related to the problem of understanding turbulent boundary layer flows, their structural features, their interactions with a wall and their transport properties of momentum and heat.

The first objective was to provide a complete documentation of the hydrodynamic and heat transfer data for a turbulent boundary layer developing over a deterministic rough wall with and without transpiration. These data should form a consistent and reliable set of information about the mean flow and turbulence structure, which can be used in the development of new and more sophisticated boundary layer prediction models.

The second objective was to determine the extent and nature of the effects of the rough wall and the transpiration on the turbulent transport properties.

The third objective was to study and identify the fully rough state of a turbulent boundary layer with heat transfer and transpiration.

In order to accomplish these objectives the following sequence of tasks were undertaken:

1) Provide Stanton number and friction factor data for the unblown and blown cases, and independent measurements of enthalpy thickness and momentum thickness (i.e., not deduced by integration of St and $C_f/2$ data).
2) Provide Stanton numbers for the unblown case for enthalpy thicknesses larger than presented in earlier work (see Healzer [4]).
3) Develop hot-wire anemometer techniques for studying temperature and velocity fluctuations over the range of velocities and temperatures encountered in this study.
4) Adapt to our flow conditions a hot-wire technique which allows the sequential measurement, with one probe, of mean velocity and temperature.
5) Provide data and analyse the effect of a deterministic roughness and uniform transpiration on mean velocity and temperature profiles.
6) Provide data and analyse the effect of a deterministic roughness and uniform transpiration on the turbulence structure.
7) Provide data and analyse the effect of a deterministic roughness and uniform transpiration on the turbulent heat transport and temperature fluctuations.
8) Provide turbulent Prandtl number data obtained from direct measurements of the turbulent transports of momentum and heat.

1.2 Boundary Conditions Studied

The experimental part of this investigation was centered around the study of the turbulent transport properties of momentum and heat for flows over a rough wall with and without transpiration.

The fully rough state was chosen to be the primary concern and the main experimental program was conducted at a free stream velocity $U_\infty = 89$ ft/sec for which $Re_k = \frac{kU_\tau}{\nu} \geq 65$ (fully rough state according to Schlichting [5]). Two other velocities were studied: $U_\infty = 52$ ft/sec, to provide information on the transitionally rough state, and $U_\infty = 130$ ft/sec to give redundant information on the fully rough state. The free stream velocity was maintained below 150 ft/sec so that properties variations due to high velocity effects were not introduced into the problem and constant properties could be assumed.

The effects of transpiration were studied for two conditions of constant blowing fraction: $F = \rho_o V_o / \rho_\infty U_\infty = 0.002$ and 0.0039 for $U_\infty = 89$ ft/sec.

The boundary conditions can be summarized as follows:

U_∞ (ft/sec)	F
52	0.000
89	0.000
	0.002
	0.0039
130	0.000

Extensive measurements of mean values, fluctuations and correlations of the velocity and temperature fields were taken for constant wall temperature conditions. The wall to free stream temperature difference was maintained around 30°F so the flows were nearly at constant properties.

A special experiment was designed to allow the study of the heat transfer behavior at high enthalpy thicknesses. The boundary layer was thickened by means of blowing in the front section of the test section. The layer was then allowed to relax to its normal state along the rest of the test section where the transpiration was not present. Heat transfer coefficients were then measured in the downstream region for three cases with different magnitudes of blowing in the upstream region.

1.3 Preliminary Analysis

The rough surface under consideration in this study was chosen because it is repeatable, deterministic, easily describable, and also porous. It is formed by eleven densely packed layers of 0.050 inch diameter Oxygen Free High Conductivity copper balls arranged such that the surface has a regular array of hemispherical roughness elements.

The wind tunnel built to test this rough surface can presently operate with free stream air velocities up to 200 ft/sec. The free stream is maintained essentially at ambient conditions. This ensures an almost-constant property boundary layer and minimizes the effects of variable fluid properties.

Using Schlichting's [5] classical equivalent sand-grain roughness k_s ($k_s = 0.625 \times 0.050 = 0.031$ inch in our case) the operational range of this apparatus according to Healzer [4] is

$$20.0 < Re_k = \frac{k_s U_\tau}{\nu} < 150.0 \qquad (1.1)$$

where $U_\tau = \sqrt{C_f/2}\ U_\infty$ is the shear velocity and ν the kinematic viscosity. Thus, it covers part of the transitionally rough state region ($5 < Re_k < 65$) and part of the fully rough state region ($Re_k > 65$).

For air flowing over the surface, U_τ varies in the range

$$1.24 < U_\tau < 9.3 \text{ (ft/sec)} \quad . \qquad (1.2)$$

The fully rough state occurs for $U_\tau \geq 4.0$ ft/sec.

If one assumes that the effect of molecular transport is contained in a layer where $y^+ = \frac{yU_\tau}{\nu} < 30$, the extent of this layer, which can be named y_b, is given by:

$$0.046 > y_b > 0.006 \text{ (inch)} \quad . \qquad (1.3)$$

In the fully rough state we have $y_b < 0.014$ inch.

Healzer [4] suggested for the present surface that the virtual origin of velocity profiles is located approximately at 0.010 inches below the top of the rough elements. If y_b were equal to or less than 0.014 inches, no molecular effect could be detected for the fully rough state of an air boundary layer over this surface, with any available probe.

Heat transfer, which is dominated by the molecular resistance at the fluid-surface interface, depends on the details of the flow very near the wall, on the activity among the roughness elements and on the remnants of the viscous layer embedded in between the rough elements. These aspects are dependent on the roughness element size, shape and distribution. Thus, it is believed that the thermal and hydrodynamical behavior of this thin region still have to be accounted for. Our very limited range of operation (in terms of roughness Reynolds number and fluid Prandtl number) can not shed light upon this problem. Any model of what happens in the region very next to the wall must remain speculative until measurements are made within the flow in that region.

1.4 General Organization

The analysis of the experimental results was divided into three main blocks:

1) The effects of the roughness as identified by comparison with smooth wall studies.
2) The fully rough state.
3) The effects of transpiration.

Block 1 is presented in Chapter II and blocks 2 and 3 are presented in Chapter III. In these two chapters the boundary layer structure should be considered in an "elliptical" way, that is, all aspects must be considered simultaneously to understand the interconnections.

Chapter IV contains the description of the apparatus, instrumentation and measurements techniques.

Chapters V thru VIII contain the detailed presentation of the data with some side considerations.

Chapter IX includes a summary of the important results.

CHAPTER II

STRUCTURE OF A TURBULENT BOUNDARY LAYER UNDER THE INFLUENCE OF A DETERMINISTIC ROUGH WALL

In smooth wall boundary layer research the concepts of an outer flow module and a wall layer module have proven very useful, as Offen [6] stresses in his studies. The outer flow and the wall layer interact, with the main feature of this interaction being the "bursting" phenomenon, e.g., see Kim et al. [7]. "Bursting" represents a periodic cycle of events, in which inrush of high momentum fluid toward the wall is followed by a "lift-up" of low momentum fluid from the wall. The "lift-up" fluid crosses a good part of the layer, and interacts with the outer flow. Flow visualization has shown an apparent local destruction of the wall sublayer before each lift-up.

Grass [8], in a roughened-wall open channel flow experiment, has also observed the "bursting" phenomenon. He found the free surface to have a wavy shape, for his fully-developed flow, which he attributed to the violent "lift-up" coming from in between the rough elements. He suggested that the low velocity fluid, which had been decelerated by the roughness elements, constituted a new flow module which should replace the smooth wall sublayer as the flow module that interacts with the outer flow.

Certainly, the protuberances on a rough wall disturb or destroy the wall sublayer. Pressure forces appear as form drag and contribute to the flow resistance. Higher turbulent mixing results from eddy shedding, from flow separation, or from shear layers starting from the roughness protuberances. We should expect that the changes in the inner flow might bring about modifications in either the level or nature of some of the interactions with the outer flow.

The search for classes of flows with similar behaviors has proven useful in the study of turbulence mechanisms and structure. Because we believe in cause-effect relations, the existence of similar behavior is frequently interpreted to mean that similar mechanisms and interactions are present. Similarities in the face of different boundary conditions is taken as an indication of "equilibrium mechanisms" or "universal behavior." Normally, the starting point in looking for such behavior is provided by dimensional analysis, which guides the development of the similarity rules, parameters and variables.

We know that the smooth wall outer flow is only weakly affected by the direct effects of viscosity. The large-scale motions in the outer flow are the most energetic and control the main features of the flow. It is only for the very-small scale motions which dissipate turbulence energy (which are most important near the wall) that viscosity plays an important role. In the outer flow the length and velocity scales are respectively the boundary layer thickness δ and shear velocity U_τ, and, since ν effects are small, the flow is independent of Reynolds number. The defect-velocity similarity law confirms the appropriateness of these scales (see for instance Tennekes et al. [25]).

The smooth wall sublayer is dominated by viscous action and is under high shearing stresses (note that we are not referring to flows near to separation, when $\tau \cong 0$ at the wall, because we are interested in zero pressure gradient flows). The viscosity sets a new length scale to the flow, and mean flow field similarity is present in U^+ and y^+ coordinates.

Finally, the region of overlap of the two layers has the famous logarithmic behavior that results in the traditional similarity "law of the wall" and most, if not all, of the cornerstones of boundary layer prediction schemes.

One further aspect we should stress is how boundary conditions have been chosen for structural studies. The non-linearity of the fluid flow problem has led several investigators to come up with ideas such as "equilibrium layers," "quasi-equilibrium layers," "self-preserving layers" and "asymptotic layers." These layers result from boundary conditions artificially set to produce some kind of similarity in one or more mean profiles after the proper length and velocities are identified. Similar profiles or turbulence quantities are not necessarily obtained for these conditions. Some factors have been recognized, for example, which strongly influence turbulence profiles, without having any significant effect on the mean profiles, e.g., the free-stream turbulence level.

Much important information on turbulence, its mechanisms and its interaction with a flow have been obtained under "simplified" boundary conditions leading to similarity conditions. Mean profiles, rms values of the velocity components, spectral measurements, flow visualization, and conditional sampling have provided us with much information. Controlling the boundary conditions becomes a way of controlling the flow phenomenon.

Prior studies have mostly referred to the simple smooth wall case. Laufer [9] would argue that we should start first with even simpler flows, like jet flows, and try to understand all mechanisms in them before putting in any wall effect. He proposes that a better understanding of the large scale motions and their interactions with the main flow is needed because the turbulence extracts its energy from the mean flow through those interactions. He stresses that the wall complicates the problem by imposing a region where viscosity ν necessarily affects the flow with the introduction of another length scale, ν/U_τ. It is a region where the mean flow has part of its energy directly dissipated, and both turbulence production and dissipation are augmented. Furthermore, the wall puts a physical constraint to the size of the large eddies. Thus the mean flow - turbulence interaction is more complicated for boundary layers and less suitable to understanding or prediction than are free shear flows, i.e., jets.

Several studies with rough wall boundary layers have shown that, in the fully rough flow regime, the viscous sublayer disappears. The development of the boundary layer is still, however, controlled by a thin region next to and around the rough elements.

Results from works like those of Hama [10] and Corrsin et al. [11] led Perry [12] and others to conclude that the effect of the roughness is restricted to the region very near the surface and the profiles of mean velocity and turbulent fluctuations in the outer flow are independent of the detailed nature of the wall roughness, if properly normalized on outer layer scale factors.

Unfortunately most of the evidence presented to support the latter conclusion were mean velocity profiles and skin friction distributions. This is sufficient for an engineer who is mainly interested on total "drag forces" or total resistance to the flow, but for the purpose of this study, this is not sufficient.

The apparently universal relationship between shear stress and mean velocity profile is responsible for the success of the methods of Schlichting [5], Hama [10], Perry et al. [12], and of other models for treating roughness studies. As was recently pointed out by Yaglom et al. [13], and by Powe et al. [14], one might expect in some cases this "universality" to not apply, making the classical approach not tenable.

As we want to have better knowledge of the structure of the turbulent layer developing under the influence of a deterministic roughness, it seems reasonable that we should measure velocity and temperature fluctuations, cross-correlations, correlation coefficients distributions, in addition to mean velocity and temperature profiles.

Absolute levels of turbulence quantities from different experiments and apparatus may not be easily compared. The performance and characteristics of rough wall turbulent boundary layers can however be contrasted with those for a smooth wall which forms a baseline data set. The ideal would be to have the smooth and rough data from the same apparatus, so free stream conditions are preserved as well as other parameters inherent to the equipment. As we were not able to do this we will refer to Klebanoff's [15] already classical data for smooth wall layer. We have to keep in mind, as Bradshaw [16] points out, that mean velocity and shear stress profiles are very insensitive to the distribution of turbulence quantities. In fact, one can have distinctly different profiles of turbulence quantities while associated with identical mean profiles. Orlando [17] and Sharan [18] discuss cases with the latter characteristics.

We will now turn our attention to the similarities and dissimilarities between our rough wall flow and the representative smooth wall boundary layer characteristics. We expect that the characteristics of a flow close to a rough wall are dependent on shape, size and distribution of the rough elements, which for our study corresponds to the densely packed, uniform ball, rough wall boundary layer case.

Roughness, as we will see, affects the development of a turbulent boundary layer in all three levels of the measurements made: integral parameters, mean profiles and turbulence quantities (fluctuations, correlations, etc.). Roughness effects are shown graphically in Figures 2.1-7 where some of our rough wall profiles are contrasted to the smooth wall layer case. The plots use smooth wall parameters and accepted similarity rules.

All figures sketched in this chapter refer to data which is plotted and discussed in detail in later chapters. References shown in each sketch will identify the detailed figure summarized by the sketch. Only the correct levels and trends are represented here for purpose of easier comparison.

Figure 2.1 and 2.2 show distributions of $C_f/2$ and St . In either case the smooth wall correlation is a unique function of Re_x , but the rough wall distributions depend on the free stream velocity, U_∞ .

From Figure 2.3 we see rough and smooth mean velocity profiles for the same value of U_τ . The shapes are different and the two layers are of different thickness. No viscous layer exists for the rough profile. Figures 2.4 and 2.5 show another aspect: despite its larger absolute value of velocity defect, the rough wall flow has the same outer region profile in velocity defect coordinates as does the smooth wall. The rough wall boundary layer does not, however, have a sharp velocity gradient in the near wall region, as does the smooth wall. Another feature of this difference is shown in Figure 2.6. The mean temperature-velocity profile for the rough wall is nearly linear for all U/U_∞ but, for the smooth wall case, a pronounced dip in temperature appears in the low velocity region.

Finally, from Figure 2.7 it is apparent that the rough wall distribution of the longitudinal velocity fluctuation has a higher level than the smooth wall case and in addition its distribution has no sharp peak near the wall.

It was possible to collect a large variety of information on the characteristics of a rough wall layer. Measurements were made at three levels (integral parameters, mean profiles and turbulence quantities profiles). As shown in Figure 2.0, integral parameters, mean profiles, and turbulence intensities constitute the means we will use to analyze the structural characteristics. It is an "elliptical" view of the structure, i.e., all aspects must be considered simultaneously to understand the interconnections.

2.1 Fully Rough and Transitionally Rough Behaviors

The most extensively studied rough walls have been classified as "k" surfaces by Perry et al. [12]. These surfaces follow the usual Clauser [19], Nikuradse [20], or Schlichting [21] scheme. Integral parameters, skin friction and velocity profiles can be correlated to flow parameters with inclusion of the roughness Reynolds number, Re_k,

$$Re_k = \frac{k_s U_\tau}{\nu} \tag{2.1}$$

where k_s is the sand-grain roughness and $U_\tau = \sqrt{\tau_w/\rho}$ is the shear velocity. The behavior of the traditional "k" surfaces studied is usually divided into the following flow regimes:

$Re_k \leq 5$ - "hydraulically smooth"

$5 \leq Re_k \leq 65$ - "transitionally rough"

$65 \leq Re_k$ - "fully rough"

We will not use this classification as a means of describing the flow regime in our case. We are not assuming that our surface behaves like a "k" surface nor analyzing its performance using the sand-grain roughness parameter. We will, instead, identify the state of "fully rough" flow for our surface according to certain similarity characteristics of the flow that are defined below. Figures 2.8-12 show Stanton number, friction factor, enthalpy thickness and momentum thickness distributions, each measured on the rough wall for different free-stream velocities. Flows with an 89 and 130 ft/sec free stream are described as "fully rough" because

$$St = f(\Delta_2/r) \tag{2.2}$$

$$C_f/2 = g(\delta_2/r) \tag{2.3}$$

$$\Delta_2 = \bar{f}(x) \tag{2.4}$$

$$\delta_2 = \bar{g}(x) \tag{2.5}$$

and the flow characteristics (integral parameters) are all independent of Reynolds number.

This fact was also reported by Healzer [4] for this surface. Figure 2.12, which was taken from Healzer's work, shows the momentum thickness δ_2 as a function of the downstream distance x, alone, for $U_\infty \geq 89$ ft/sec. He had some doubts on the state of his 32 ft/sec case. He tentatively classified it as "fully rough", but our 52 ft/sec flow is "transitionally rough", so a lower free-stream velocity would very likely render the layer transitional.

Therefore, our $U_\infty = 52$ ft/sec run represents the transitional state and both the $U_\infty = 89$ and 130 ft/sec runs constitute fully rough state flows.

The differences in distributions of $C_f/2$ and St for rough and smooth walls, already shown in Figures 2.1-2, can be further appreciated in Figures 2.13-14. The smooth wall variation of friction factor and δ_2, with δ_2 and x, respectively, are different from those just seen for the rough wall. The smooth $C_f/2$ variation is, according to Kays [22],

$$\frac{C_f}{2} = 0.0128 \, Re_{\delta_2}^{-.25} \quad . \tag{2.6}$$

2.2 Mean Velocity and Temperature Profiles

For the velocities investigated we have looked for, but not found, three-dimensional variations in mean profiles for measurements as close as 0.007 inch from the top of the balls. The resolution of measurements corresponds to the hot-wire length which, by coincidence, is nearly equal to the diameter of the copper balls making up the rough wall.

Typical "fully rough", non-dimensional mean velocity and temperature profiles are shown in Figures 2.15-16.

The non-existence of a viscous sublayer is confirmed by the absence of any sharp velocity gradient near the wall. A shift of the virtual origin, as suggested by Moore [23], Perry et al. [12], Liu et al. [1], Monin et al. [24], and others, would render to the profile a logarithmic region extending from the first point (only 0.007" from the top of the balls) up to 10% of the layer thickness, where, therefore, an inertial sublayer exists from the top of the balls. Consequently, viscosity or molecular action is negligible across at least 99% of the layer thickness. In between the rough elements the effect of viscosity was not tested, because of physical limitations of probe dimensions, but it is apparent that the effects of pressure forces are overwhelming, at least for the "fully rough" state. According to Tennekes and Lumley [25] we should expect an inertial sublayer whenever $yw/\nu \gg 1$, $y/\delta \ll 1$ and $k/\delta \ll 1$ simultaneously (w is a characteristic velocity scale of the turbulence fluctuations and k is a characteristic length of the rough elements). The above stated conditions were satisfied near the wall for all measured profiles of fully rough flows, and an inertial sublayer exists, therefore, from the top of the balls.

The last argument can be better appreciated by looking at Figure 2.17 which shows the velocity-defect profiles $(U_\infty - U)/U_\tau$ plotted against y/δ. The profiles follow Coles' [26] law of the wake for smooth wall layers with zero pressure gradient, for all points from $y/\delta = 0.01$ out:

$$\frac{U_\infty - U}{U_\tau} = -2.5 \ln \frac{y}{\delta} + 1.38 \left\{2 - w\left(\frac{y}{\delta}\right)\right\} \tag{2.7}$$

where $w(y/\delta)$ is an empirical function determined by Coles [26]. So in some sense it is valid to say that the outer flow in our "fully rough" regime constitutes 99% of the thickness and, at least for mean values, the fluid dynamical behavior is the same as in the smooth wall outer layer region.

But this similarity, in our case, is not restricted to mean velocity profiles — the temperature profiles exhibit it also. Using the same virtual origin shift, the temperature profile has a logarithmic region of about the same extent as does the velocity profile.

The virtual origin shift is the same for the mean velocity and temperature profiles, and this fact leads to important consequences. Figure 2.18 shows the fully rough profile of the non-dimensional temperature $(T_w - T)/(T_w - T_\infty)$ plotted against the non-dimensional velocity U/U_∞ at the same y position. A peculiarity of this plot is that it is independent of the coordinate y and also independent of the ambiguous definition of the virtual position of the wall. Two striking facts may be observed. First, the plot is a straight line over a wide range of velocity (this results from the similar shapes of the velocity and temperature profiles). Secondly, one should notice the extrapolated "non-zero" value of the non-dimensional temperature when the velocity goes to zero. In the same figure we contrast the rough wall zero offset to a representative smooth wall profile according to Blackwell [27]. The smooth case clearly shows the molecular transport effects of a $Pr = 0.72$ fluid. The two profiles differ completely for low velocity ratios. In fact, the smooth wall profile for very low velocities follows the equation

$$T^+ = Pr\ U^+ \tag{2.8}$$

which is valid for the viscous sublayer. At large velocity ratios the two profiles come together and have similar distribution. This corresponds to the end of the smooth wall log-region and the whole wake-region.

The non-existence of a viscous sublayer is revealed by another characteristic of the fully rough profiles. As we can see in Figure 2.18 the rough wall profile has no tendency to follow the sublayer Equation (2.8). Molecular transport appears to be negligible above the top of the balls, and the flow is "fully turbulent" for the whole layer. It is also clear that there is no "buffer" layer, as in smooth wall boundary layers. The absence of molecular transport results in the momentum and heat transfer being determined, within the layer, solely by the turbulent mixing.

The linearity of the rough wall profile shown in Figure 2.18 indicates a wider inertial sublayer, compared to smooth wall layers, with a long logarithmic region. As a consequence, the momentum and energy equations for our zero pressure gradient case are similar. The turbulent Prandtl number can be expected to have a value around 1, and the turbulent heat flux to be controlled by the turbulent momentum flux.

The linearity of the profile as shown in Figure 2.18 also indicates that the direct viscous dissipation of the mean flow kinetic energy is negligible. Consequently, constant properties behavior can be assumed and high velocity effects are negligible, as is discussed in Chapter VIII, where we assert that the Eckert number of the flows considered in this study is small (Ec << 1).

As we can observe from Figures 2.15, -16, and -17, there is, in fact, good similarity between mean velocity and temperature profiles. So the linearity we are discussing should not have come as a surprise, and we can expect a similarity in the distribution of the diffusivities of momentum and heat. The mean temperature profiles and the heat flux are determined, then, by the fluid dynamics. The ratio between the diffusivities, i.e., the turbulent Prandtl number, is bound to be approximately constant or vary only slightly close to the wall. This we expect to be verified in the region of the layer sufficiently close to the wall where the "Couette flow" assumptions are valid and convection by the mean flow is negligible. (This is usually called the constant shear stress or heat flux layer.)

Because of the rough wall action disturbing the flow, there is higher turbulent mixing and the rough wall case shows more motions of small time scale than in the smooth wall case. Molecular diffusion does not "have time" to become important in the heat transfer within the boundary layer.

The non-zero intercept, shown in Figure 2.18, has not been referred to before in the literature. It supports hypotheses concerning the existence of a "super-thin" layer next to the surface (around and in between the balls) which determines the heat transfer characteristics of the surface. Molecular action is viewed as concentrated in that layer, where most of the resistance to the heat transfer is located. The existence of this layer has been suggested by several investigators -- Dipprey et al. [28], Owen et al. [29], Yaglom et al. [13], Lewis [30], and others -- using either intuition or dimensional arguments to generate its definition.

In view of the non-zero temperature intercept, it is unreasonable in any modeling attempt for computer boundary layer predictions to force the origins of the velocity profiles and temperature profiles to coincide. In fact, the idea of "slip" velocity and temperature profiles at the top of the rough elements is more suitable. Lewis [30] discusses this idea and the velocity and temperature profiles can be represented for "k" rough surfaces as in Figure 2.19. Functions R and g are the roughness functions, that for sand-grain roughness or "k" roughness are functions of roughness Reynolds number, $R(k^+)$, with g depending also on the Prandtl number $g(k^+,Pr)$. They provide the matching conditions necessary, or the boundary conditions for the outer flow. $R(k^+)$ can be the function studied by Clauser [19], among others. $g(k^+,Pr)$ can be the function proposed by Dipprey et al. [28] and others.

2.3 First Level of Turbulence Quantities

In Figure 2.20 we have plotted, on linear scales, two velocity profiles for the region very close to the wall. One is for our rough wall and the other is for a smooth wall having the same shear velocity, $U_\tau = \sqrt{\tau_w/\rho}$ and following

$$U^+ = y^+ \ , \ y \to 0 \ . \tag{2.9}$$

Figure 2.20 indicates that the position of the "virtual origin" appears to be below the top of the balls. As one can see, the rough wall "arrests" the flow much more efficiently. In other words, the rough wall velocity must drop to zero in a shorter distance than is the case for smooth walls. This is compatible with the higher resultant friction factor for rough walls. Because the friction factor becomes independent of Reynolds number for fully rough behavior, bluff body or "pressure" drag must be responsible for most of the resistance to the flow over the rough surface. The drag results from pressure forces, in the x-direction, acting on the rough elements. Such "pressure" drag gives total resistance forces that are proportional to U_∞^2, and thereby to a friction factor that is independent of the Reynolds number. The local, small-scale pressure forces are expected to overwhelm the viscous action in between the protuberances and are the main agents for the strong deceleration of the fluid particles near the wall. In the heat transfer problem, however, there is no counterpart for the pressure forces, and all heat transfer, at the interface solid-fluid, must be by molecular action, as discussed before.

The stronger "arrest" capability of a rough wall, previously mentioned, is introduced and discussed by Grass [8], and the large pressure forces will be considered next in the course of analysis of the turbulence intensities profiles.

Figure 2.21, -22, and -23 show typical distributions for the three components of the turbulence intensity.

Figure 2.21 is taken from Klebanoff's [15] well-known work for smooth wall boundary layers. The $\sqrt{\overline{u'^2}}/U_\tau$ profile shows a sharp increase very close to the wall, reaching a peak at $y^+ \approx 15$. This is in the zone of maximum production of turbulent energy ($-\overline{u'v'}\ \partial U/\partial y$ is maximum) and is also the outer edge of the viscous sublayer. The largest non-isotropy in the fluctuating components of the velocity occurs in the sublayer, because the large eddies are very elongated in the streamwise direction, a fact observed by several authors. This observation is consistent with the notion that the largest eddies are the energy-containing eddies and responsible for most of the turbulence intensity. Thus the fact that $\overline{u'^2} >> \overline{v'^2}$ is to be expected in conjunction with the existence of the streamwise elongated eddies, and vice-versa.

When the effect of roughness is introduced, the sharp peak in $\overline{u'^2}$ is reduced and compressed into a small distance from the wall in y/δ coordinates. The maximum value in $\overline{u'^2}$ occurs at smaller y/δ compared to the smooth wall case. In place of the sharp peak, a broad region of high turbulent mixing appears, as observed in Figure 2.22, for a surface with transitionally rough behavior.

In the fully rough regime, as shown in Figure 2.23, the peak is broad and displaced away from the wall.

In Figure 2.24 the major difference between transitionally and fully rough behaviors can be observed. The major difference is restricted to the region where $y/\delta < 0.05$, which is of the order of the ball diameter used for this case. Otherwise, in the outer part of the layer $\sqrt{\overline{u'^2}}/U_\tau$ is independent of the Reynolds number effects.

The higher value for $\sqrt{\overline{u'^2}}/U_\tau$ shown in Figure 2.23 over most of the rough layer, compared to Klebanoff's [15] smooth data, can not be explained by a higher free-stream turbulence. Both profiles tend to be the same values for large y/δ. Apparently, the effect of roughness on the turbulence structure extends out much farther from the wall than reported in previous works (see, for instance, Hinze [32]). We should also expect that, for the zone close to the wall, the large eddies will not be so elongated as they are for smooth walls. If "streaks" are present (see Kline [31]) they interact much faster and stronger with the wall compared to the smooth wall case, and as a result generate a more energetic "bursting".

As we can see from Figure 2.23, in the fully rough case, $\sqrt{\overline{u'^2}}/U_\tau$ attains a maximum at $y/\delta \approx 0.1$ and decreases toward the wall. We know that viscous action is negligible in this region and that the turbulence production $(-\overline{u'v'}\ \partial U/\partial y)$ does not reach a maximum there. These facts do not agree with the observations of Corrsin et al. [11] for a two-dimensional "corrugated paper" roughness element. Hinze [32], using Corrsin's results, concluded that turbulence profiles, when properly non-dimensionalized, were universal for smooth and smooth and rough walls boundary layers. This argument has been used by other investigators such as Perry et al. [33] and Grass [8] in their analyses. Probably the general features observed for $\overline{u'^2}$ profiles are inherent to our three-dimensional roughness surface but are not representative of two-dimensional surface elements.

The drop in $\overline{u'^2}$ near the wall can tentatively be justified using either of two lines of argument. One line is based on observations by Grass [8] in his open-channel flow study. He found the rough wall to have a much stronger "arrest" mechanism than a smooth wall, which has only the viscous action. The "bursting phenomenon" (see Kim et al. [7] and Offen [6]) is the main interaction mechanism between the outer flow and the fluid near the rough elements. The inrushing fluid from the outer region of a rough wall flow is decelerated by pressure forces while still relatively far from the wall. The outrushing fluid which results from "lift ups" that originate in between the rough elements moves with a nearly vertical trajectory and interacts with the flow much farther away from the wall. Both of these actions tend to result in low values of $\overline{u'^2}$ in the near wall region and higher intensities in the outer region, compared to smooth wall flows. Near the wall, a reduction in $\overline{u'^2}$, by continuity requirements, results in an increase in $\overline{v'^2}$ or $\overline{w'^2}$, or both. The resultant turbulent field is more isotropic. Consequently, as we have advanced the eddies are not so elongated as they are for the smooth wall case.

The other argument is based on observations reported in a recent systematic study by Powe et al. [34]. They analyzed the production, transport and dissipation of turbulent kinetic energy for turbulent flow in rough pipes. They measured most of the terms of the turbulent kinetic energy balance equation. This equation for a two-dimensional boundary layer (Klebanoff [15] and Townsend [35]) is:

$$\underbrace{\overline{u'v'}\,\frac{\partial U}{\partial y}}_{(1)} + \underbrace{\frac{1}{2}\frac{\partial}{\partial y}\left(\overline{v'q^2}\right)}_{(2)} + \underbrace{\frac{1}{\rho}\frac{\partial}{\partial y}\overline{p'v'}}_{(3)} + \underbrace{\frac{1}{2}U\frac{\partial}{\partial x}q^2 + \frac{1}{2}V\frac{\partial}{\partial y}q^2}_{(4)} - \underbrace{\nu\frac{\partial^2}{\partial y^2}q^2}_{(5)} + \underbrace{D}_{(6)} = 0 \qquad (2.10)$$

where term

(1) represents the production of turbulent energy from the mean motion,

(2) represents the turbulent energy diffusion,

(3) represents the pressure diffusion,

(4) represents the convection of turbulent energy by the mean motion,

(5) represents the diffusion of turbulent energy by molecular action, and

(6) represents the dissipation of turbulent energy.

The effect of roughness was incorporated into the equation by means of three-dimensional perturbations in the mean velocity. The final equation (see Powe et al. [34]), to all intents and purposes, has six terms similar to those of Equation (2.10).

Powe et al. [34] observed large turbulent and pressure diffusion terms (similar to (2) and (3) of Equation (2.10)) compared to smooth wall measurements (Laufer [36]) in a layer next to the wall, a layer that had a thickness of the order of the size of the roughness element. The consequence is a larger loss of turbulent kinetic energy due to diffusion of turbulent energy, using the same language of Klebanoff [15] and Laufer [9].

We should expect from the rough wall pressure forces action a more intense redistribution of energy inside the layer very close to the wall. As Tennekes et al. [25] points out, the turbulent kinetic energy production $(-\overline{u'v'}\ \partial U/\partial y)$ is the source for the longitudinal fluctuation $\overline{u'^2}$. This component then interacts with the pressure force fluctuations and redistributes the energy to the $\overline{v'^2}$ and $\overline{w'^2}$ components. Thus, despite the fact that turbulence production is the largest at the top of the balls, the level of turbulence intensity is not largest there because more energy is extracted from the mean flow there and redistributed inside the layer by diffusion.

Figure 2.25 shows transitionally and fully rough distributions for the temperature fluctuations. The $\sqrt{\overline{t'^2}}/T_\tau$ profile distributions are similar to those for $\sqrt{\overline{u'^2}}/U_\tau$. As the flow velocity is increased, the layer reaches the fully rough state and the peak in this profile becomes broader and moves away from the wall. Similarity of the $\overline{u'^2}$ and $\overline{t'^2}$ profiles supports the idea that the velocity field controls the temperature field. A high degree of $\overline{u't'}$ correlation is to be expected.

A representative behavior of $\sqrt{\overline{t'^2}}/T_\tau$ for a smooth wall boundary layer, shown in Figure 2.26, is taken from Orlando [17], as discussed in Chapter VII. As we can see, a sharp peak occurs very close to the wall, near $y^+ \approx 15$, where $\sqrt{\overline{u'^2}}/U_\tau$ also attains its maximum value.

The temperature fluctuations profiles change in a manner similar to the change in $\overline{u'^2}$ profiles as we go from smooth wall behavior through transitionally rough to fully rough state.

2.4 Second Level of Turbulence Quantities

From our results it appears that the change in boundary condition (smooth to rough wall) does not alter the relationship between the turbulent shear stress and the components of the fluctuating velocity. This point is amplified in the following paragraphs.

The shear stress distribution $-\overline{u'v'}$ and its values normalized by U_τ^2, $\sqrt{\overline{u'^2}}\sqrt{\overline{v'^2}}$, and q^2 for the rough wall are shown in Figures 2.27, -28 and -29. The distribution is independent of mean flow velocity for the rough case, but, as we see from Figure 2.27 the rough wall values of $-\overline{u'v'}/U_\tau^2$ are larger than those of Klebanoff's [15] smooth wall data for $y/\delta \gtrsim 0.1$. A constant shear stress layer appears to exist up to $y/\delta = 0.1$, as in the case of smooth walls.

As we saw before, the values of $\overline{u'^2}$ and $\overline{v'^2}$ are larger in our case, but the correlation coefficient,

$$R_{uv} = \frac{-\overline{u'v'}}{\sqrt{\overline{u'^2}}\sqrt{\overline{v'^2}}} \tag{2.11}$$

is approximately constant across most of the layer and equal to 0.45, as in a smooth wall layer.

The ratio between $-\overline{u'v'}$ and the turbulent kinetic energy q^2 is also the same as for a smooth wall, with a value of 0.15.

The "smooth-wall" values have been reported by several authors (Townsend [37], Bradshaw [38], and Orlando [17]) and appear to be "universal" values for the turbulence phenomena in constant pressure boundary layers.

So, apparently, there is a universal character of the turbulence interactions in the outer layer that is independent of its interaction with the inner flow, no matter whether the wall is rough or smooth. This fact, plus the similarity obtained in defect coordinates for the velocity profile, suggests further similarities in other parameters, e.g., consider the "mixing length", ℓ, defined as

$$\ell = \frac{\sqrt{-\overline{u'v'}}}{dU/dy} \quad . \tag{2.12}$$

Its distribution, compared to a typical smooth wall case is shown in Figures 2.30 and 2.31.

For $y/\delta > 0.1$, the mixing-length distributions are quite similar. For $y/\delta < 0.1$, the effect of viscosity is evident for the smooth wall, and a "damping" effect appears (as discussed by Hinze [32] and others). For the rough wall, $\ell = \kappa y$ $(\kappa = 0.41)$ remains valid down to the first data point.

Fully rough temperature-velocity correlation coefficients are shown in Figures 2.32 and -33. Only a few data like this have been reported for smooth walls (see Orlando [17]) due to the difficulty and high consumption of time required for its determination.

First, note the constancy in the value of the correlation between the temperature and the streamwise velocity fluctuations. For most of the layer,

$$\frac{-\overline{u't'}}{\sqrt{\overline{u'^2}}\sqrt{\overline{t'^2}}} \approx 0.75 \quad . \tag{2.13}$$

The correlation coefficient between the temperature and the normal velocity fluctuation is also nearly constant at a value,

$$\frac{-\overline{v't'}}{\sqrt{\overline{v'^2}}\sqrt{\overline{t'^2}}} \approx 0.6 \tag{2.14}$$

throughout most of the layer.

The higher value obtained for the correlation coefficient between the temperature and the streamwise velocity fluctuations is consistent with the description of the interaction between the outer flow and the "near wall" flow. The high coherence between u' and t' is a natural result, because these fluctuations originate primarily by the inrush and ejection mechanism, during "bursting", as discussed in previous sections. Very close to the wall, however, there is no tendency of this correlation to increase and reach a value ≈ 1.0, as has been reported for smooth wall layers (see for instance Orlando [17]).

The value of the correlation coefficient between the temperature and the normal velocity fluctuations reported here is in good agreement with those reported in the literature for the flat plate case over smooth walls. Thus, there is no apparent effect of the rough wall on this coefficient.

2.5 Turbulent Prandtl Number

Experimental data for smooth plate studies have suggested that both the molecular Prandtl number and the flow field determine the turbulent Prandtl number. The scatter in the data is large, but two definite characteristics are generally reported for boundary layers in air with no axial pressure gradient. The turbulent Prandtl number is larger than 1.0 close to the wall. It decreases to 0.9 in the logarithmic region, and to a value around 0.5 to 0.7 near the free stream. This has been reported by several authors, for example, Simpson [39], Kearney [40], and Orlando [17].

Several investigators have shown that close to a smooth wall we have

$$-\overline{u'v'} \propto y^3 + O(y^4) \tag{2.15}$$

and

$$\overline{v't'} \propto y^3 + O(y^4) \quad . \tag{2.16}$$

Thus

$$\frac{\overline{u'v'}}{\overline{v't'}} \approx \text{constant} \quad . \tag{2.17}$$

We will refer now, again, to the profile of mean temperature versus mean velocity $\left((T_w-T)/(T_w-T_\infty) \times U/U_\infty \right)$, as shown in Figure 2.34 . As one can see, the derivative dT/dy for the smooth wall case increases as $y \to 0$ (or as $U \to 0$). It reaches, at the wall, a value proportional to the laminar Prandtl number according to the sublayer equation

$$T^+ = Pr\, U^+ \quad . \tag{2.18}$$

The turbulent Prandtl number can be obtained from

$$Pr_t = \frac{\overline{u'v'}}{\overline{v't'}} \frac{dT}{dU} \tag{2.19}$$

according to the discussion in Chapter VIII. Therefore, because of the result in Equation (2.17), the behavior of Pr_t close to the wall is mostly due to the variation of dT/dU.

We are reporting in Figure 2.35, for the first time, a rough wall turbulent Prandtl number distribution, obtained using Equation (2.19), for which each term was individually measured.

The linearity in the profile of $((T_w-T)/(T_w-T_\infty) \times U/U_\infty)$ for the rough wall, as again seen in Figure 2.34, gives $dT/dU \sim$ constant close to the wall.

In Figures 2.36 and 2.37 we show the profiles $-\overline{u'v'}/U_\tau^2$ and $\overline{v't'}/U_\tau T_\tau$ for the rough wall. As we see for the region very close to the wall, where both the convection by the mean flow and the molecular transport are negligible, we have a constant turbulent shear stress and heat flux layer. Thus, we have

$$\frac{\overline{u'v'}}{\overline{v't'}} \approx \frac{U_\tau}{T_\tau} = \text{constant} \quad . \tag{2.20}$$

Using Equation (2.19) we expect, therefore

$$Pr_t \approx \text{constant} \quad . \tag{2.21}$$

This near constancy of the turbulent Prandtl number is in agreement with the observed similarity in mean velocity and temperature profiles. Finally, a value around 1.0 is obtained for low values of y, as conjectured by Dipprey et al. [28], Owen et al. [29], and others. However, the assumption $Pr_t = 1.0$ throughout the layer, which they used, is seen not to be valid.

The determination of Pr_t is very uncertain ($\approx$ 18%), so it is difficult to compare our results with the smooth case. The direct way used in this study for the determination of Pr_t is more accurate than previous methods such as that described by Simpson [39] and others, which require derivatives of mean profiles with respect to the y-coordinate. Kearney's [40] uncertainty envelope (see Figure 2.38) for Pr_t contains both the smooth wall and the rough wall results. Both have in common the monotonic decrease as the free stream is approached. The major difference appears in the region very close to the wall, where in our case there is no indication that Pr_t will have a value larger than 1.0, as is the case for smooth walls. Let us stress the fact that we do not have measurements very close to the wall but that we have reached the above conclusion indirectly.

In the inertial sublayer for the rough wall case, since the molecular effects are negligible, one can write

$$Pr_t = \frac{\overline{u'v'}}{\overline{v't'}} \frac{dT}{dU} = \frac{C_f/2}{St} \frac{d\left(\dfrac{T_w-T}{T_w-T_\infty}\right)}{d(U/U_\infty)} \frac{T_w-T_\infty}{T_w-T_{aw}} \quad . \tag{2.22}$$

The adiabatic wall temperature T_{aw} appears in this equation because of the definition of Stanton number used in this work, $St = \dot{q}''/(\rho G(T_w-T_{aw}))$. (Note that $T_{aw} \approx T_{\infty,o}$ and we have used in this study the $T_{\infty,o}$ value.) The values obtained from both expressions in Equation (2.22) agree to within 5%. Thus, we suggest the use of the second expression for estimating the turbulent Prandtl number in the near wall region for fully rough flows.

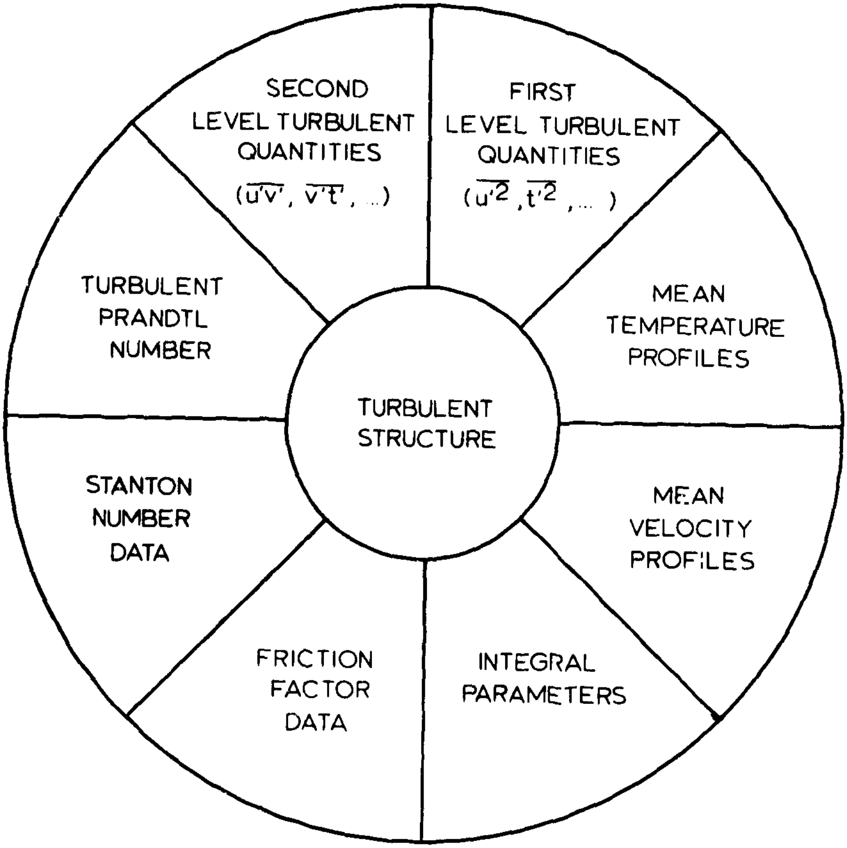

Fig. 2.0 Turbulent structure analysis.

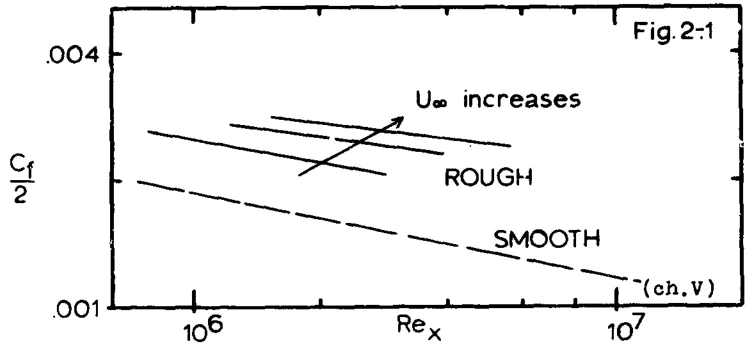

Fig. 2.1 Rough vs. smooth friction factor distributions.

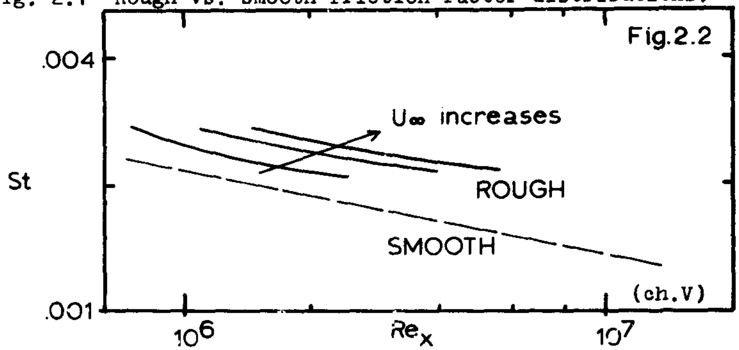

Fig. 2.2 Rough vs. smooth Stanton number distributions.

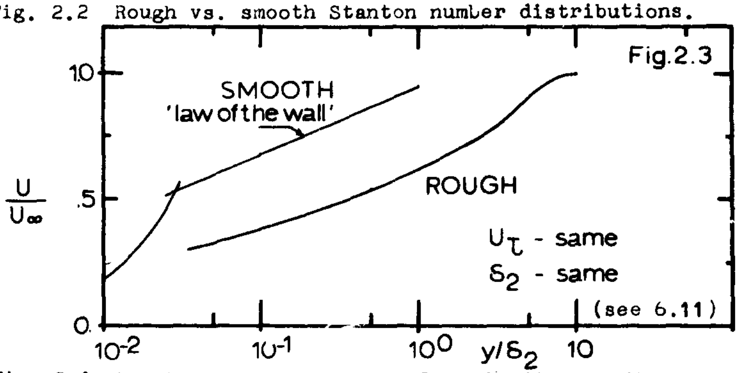

Fig. 2.3 Rough vs. smo ι near wall velocity profiles.

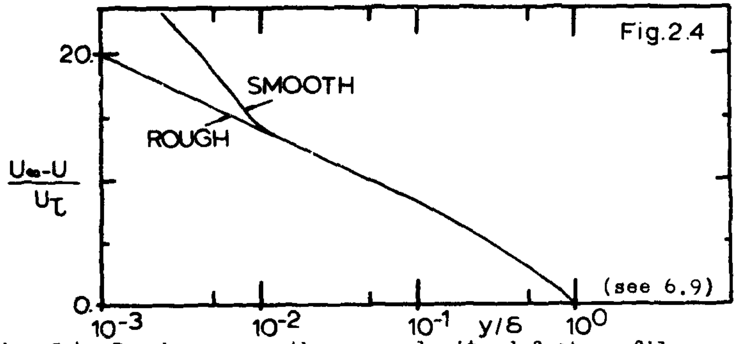

Fig. 2.4 Rough vs. smooth mean velocity defect profiles.

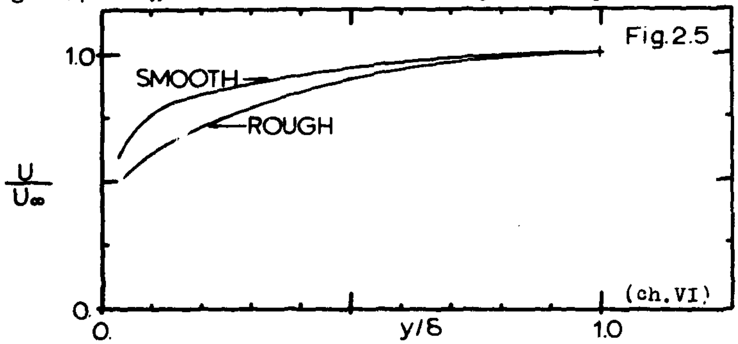

Fig. 2.5 Rough vs. smooth mean velocity profiles.

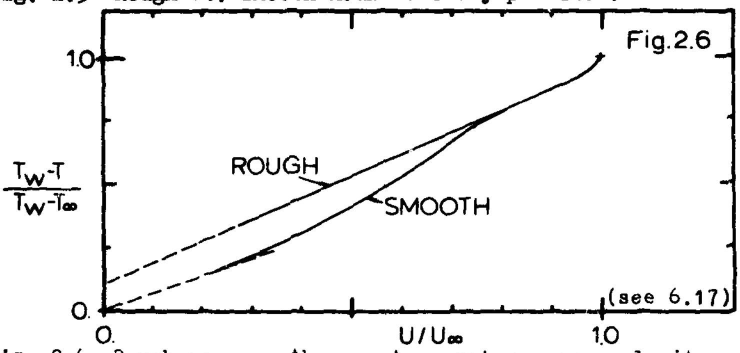

Fig. 2.6 Rough vs. smooth mean temperature-mean velocity profiles.

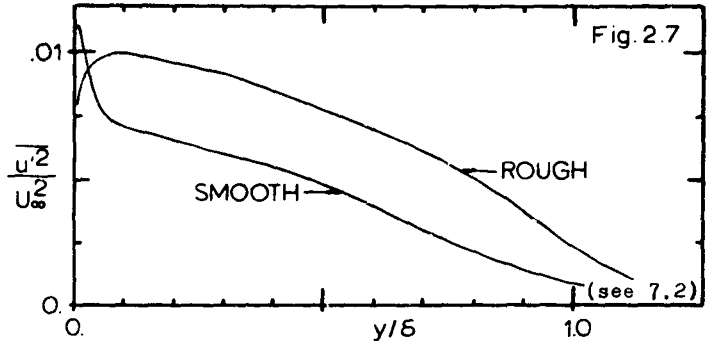

Fig. 2.7 Rough vs. smooth axial velocity fluctuations.

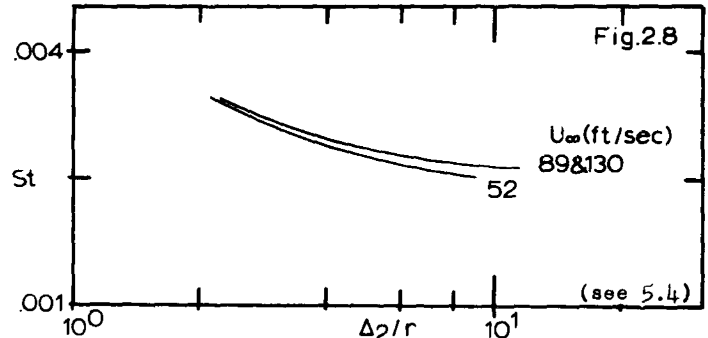

Fig. 2.8 Rough surface Stanton number distributions.

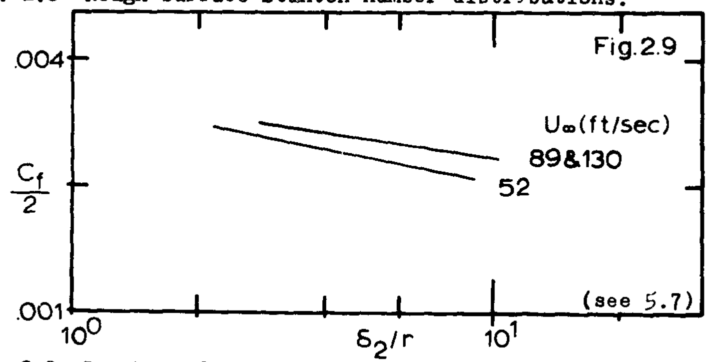

Fig. 2.9 Rough surface friction factor distributions.

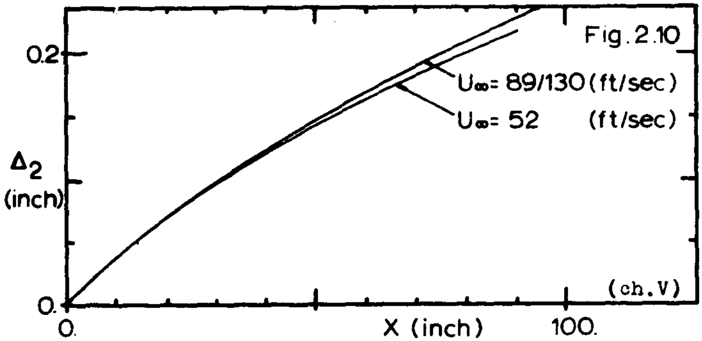

Fig. 2.10 Enthalpy thickness variation with x-distance.

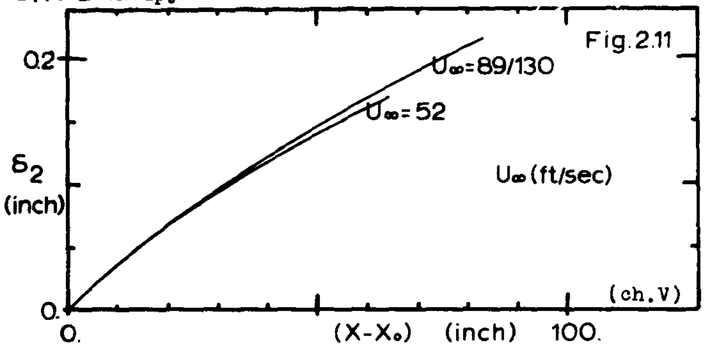

Fig. 2.11 Momentum thickness variation with x-distance.

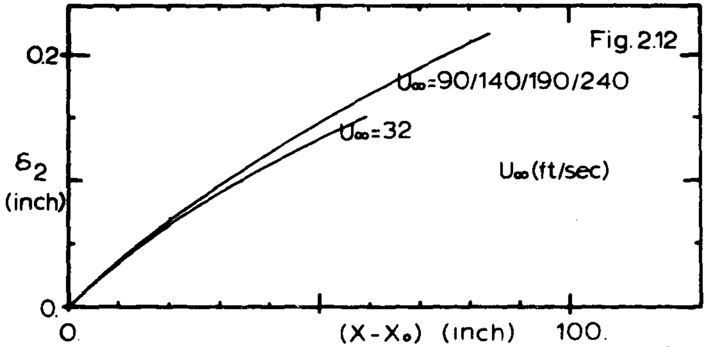

Fig. 2.12 Momentum thickness distribution from Healzer(4).

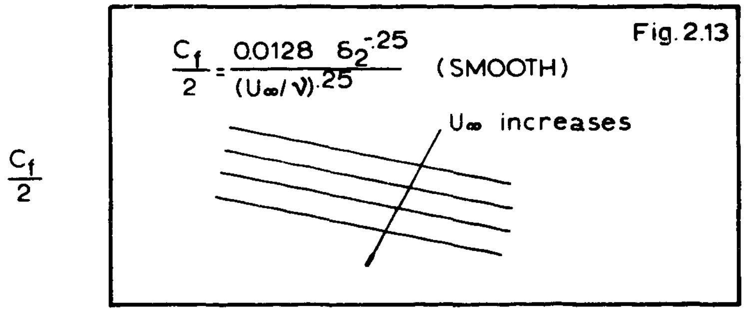

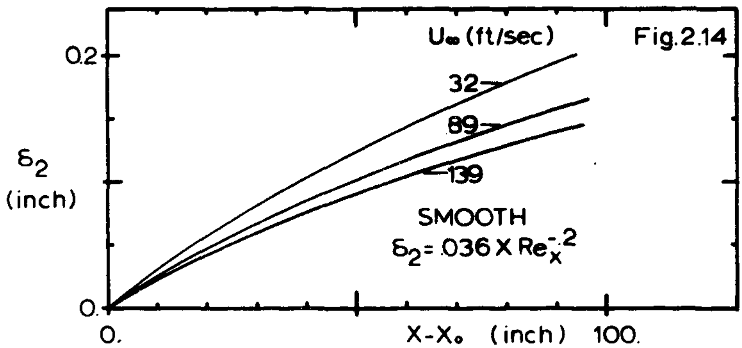

Figs. 2.13-14 Smooth $C_f/2$ and δ_2 distributions.

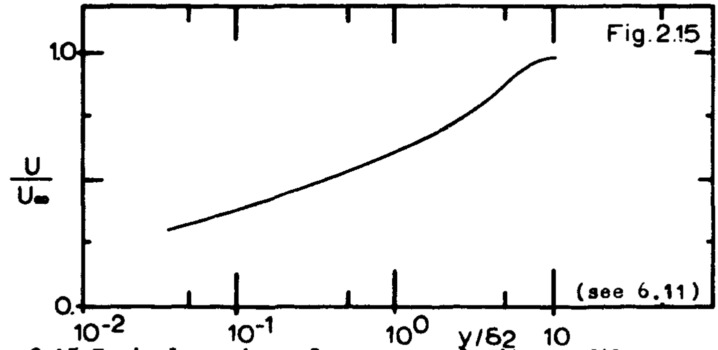

Fig. 2.15 Typical rough surface mean velocity profile.

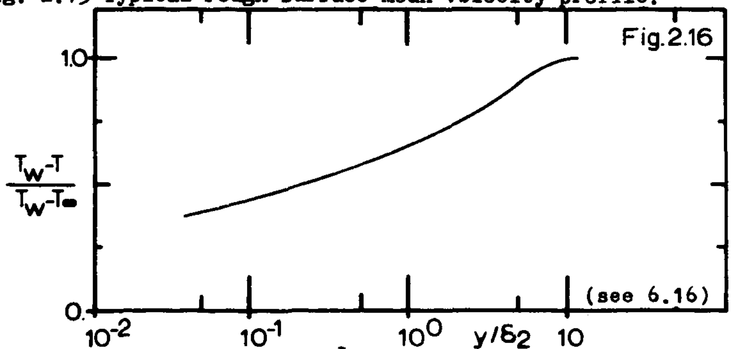

Fig. 2.16 Typical rough surface mean temperature profile.

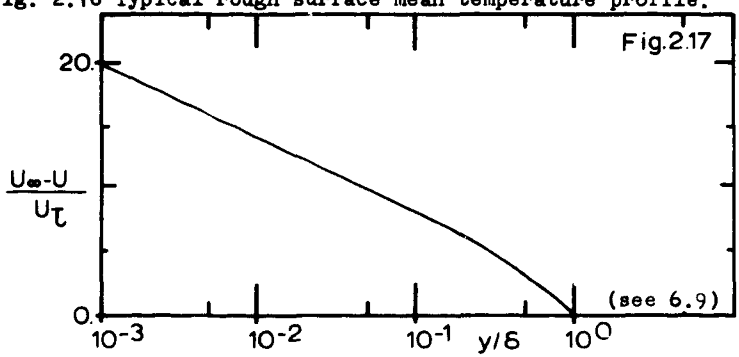

Fig. 2.17 Rough surface velocity defect profile.

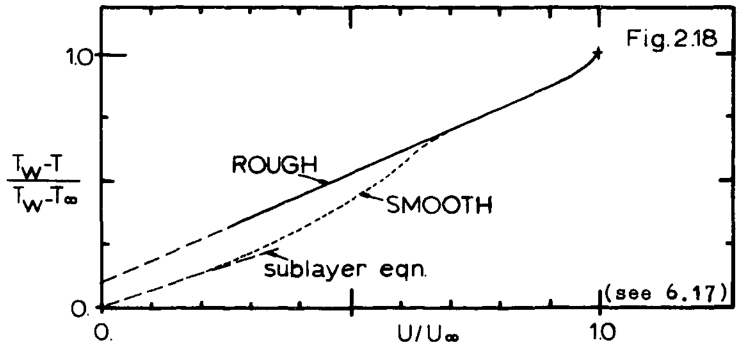

Fig. 2.18 Typical mean temperature-mean velocity profile.

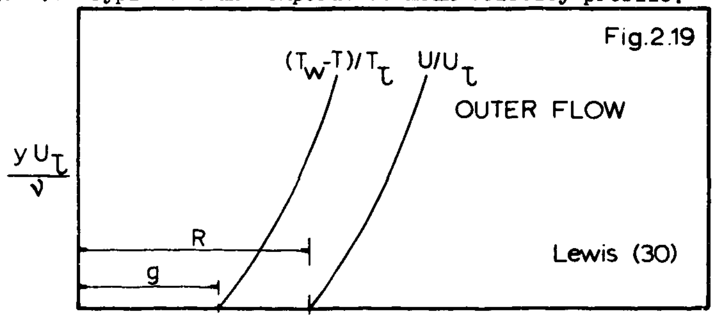

Fig. 2.19 Outer flow of a rough wall layer and wall functions R and g according to Lewis.

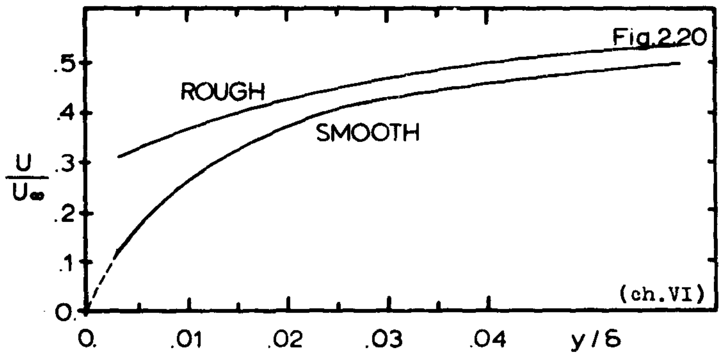

Fig. 2.20 Near wall velocity profiles for rough and smooth wall boundary layers.

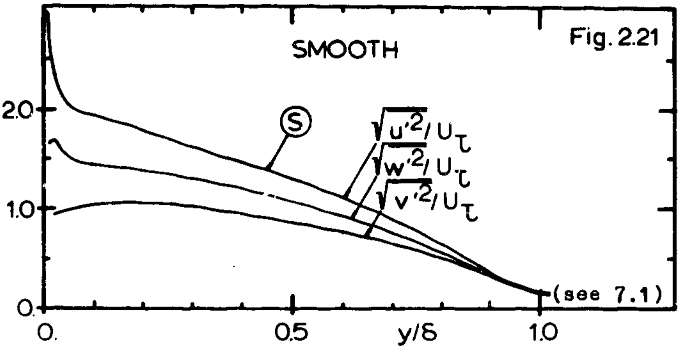

Fig. 2.21 Turbulence intensities: smooth wall.

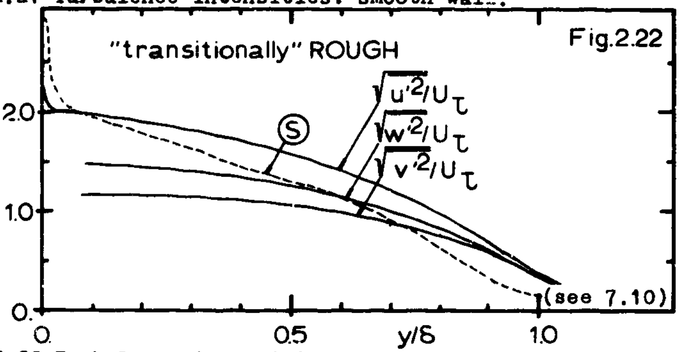

Fig. 2.22 Turbulence intensities: rough surface.

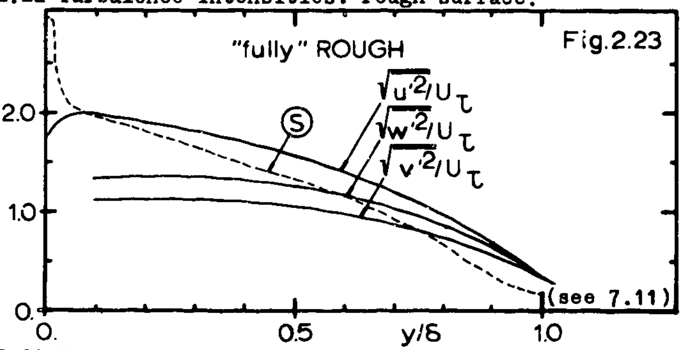

Fig. 2.23 Turbulence intensities: rough surface.

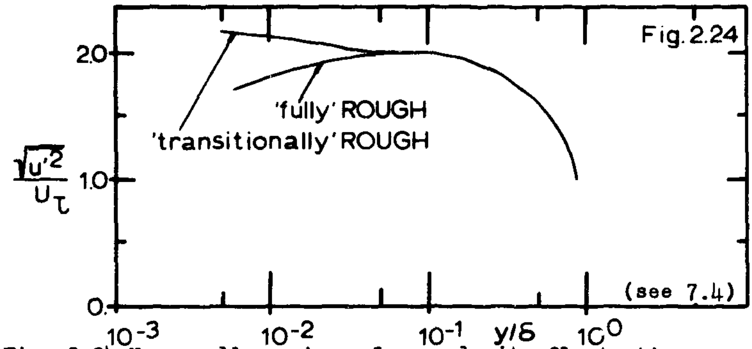

Fig. 2.24 Near wall rough surface velocity fluctuations.

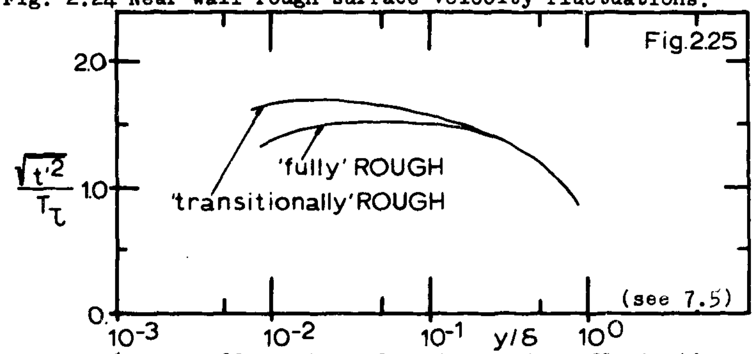

Fig. 2.25 Near wall rough surface temperature fluctuations.

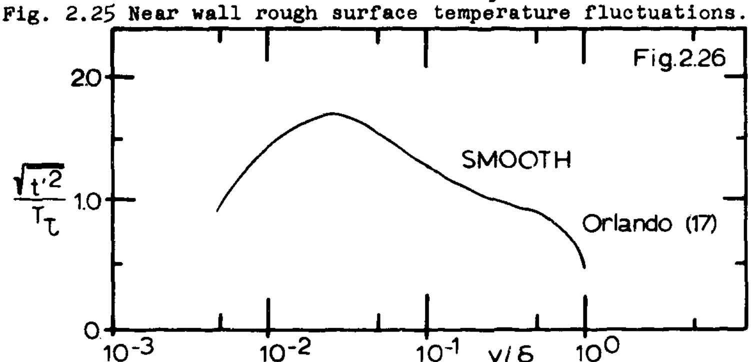

Fig. 2.26 Near wall smooth surface temperature fluctuations.

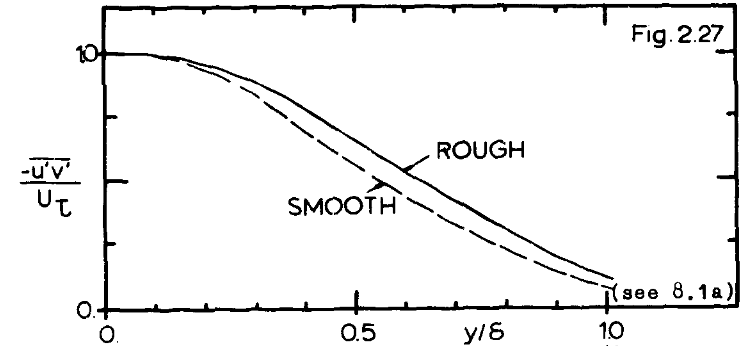

Fig. 2.27 Turbulent shear stress: rough vs. smooth.

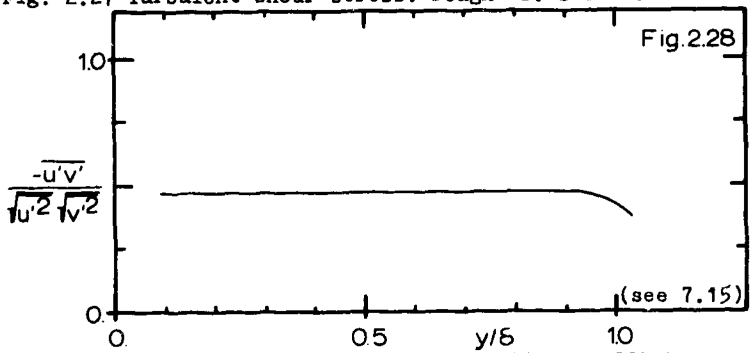

Fig. 2.28 Turbulent shear stress correlation coefficient.

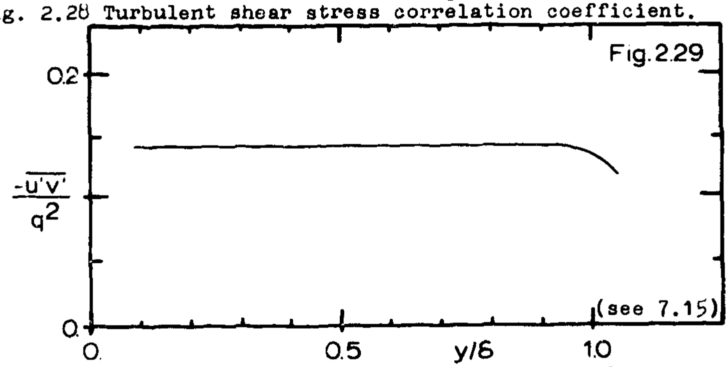

Fig. 2.29 Ratio between turbulent shear stress and turbulent kinetic energy.

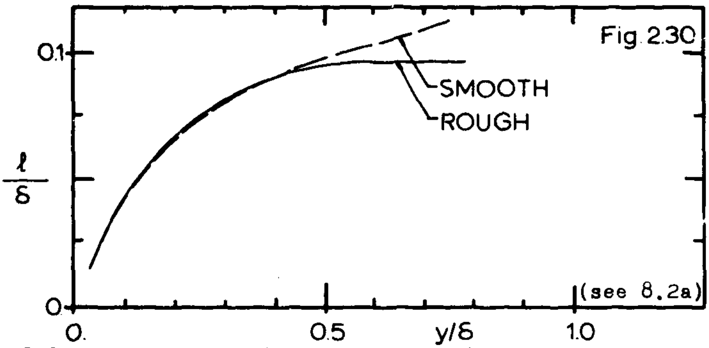

Fig. 2.30 Outer flow mixing-length distribution.

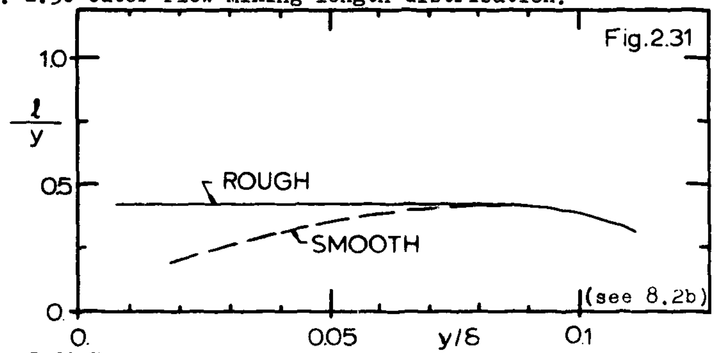

Fig. 2.31 Near wall mixing-length distribution.

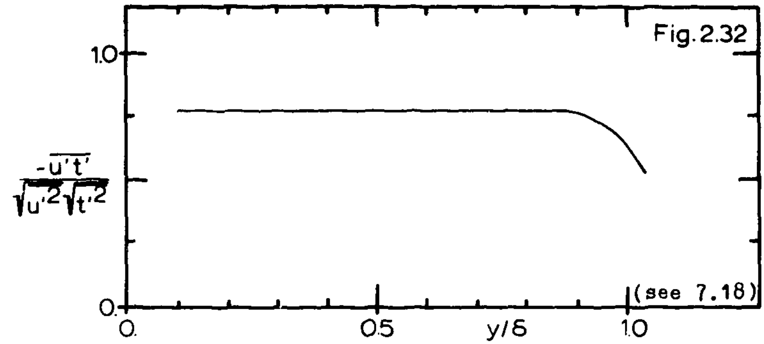

Fig. 2.32 Axial velocity-temperature correlation coefficient.

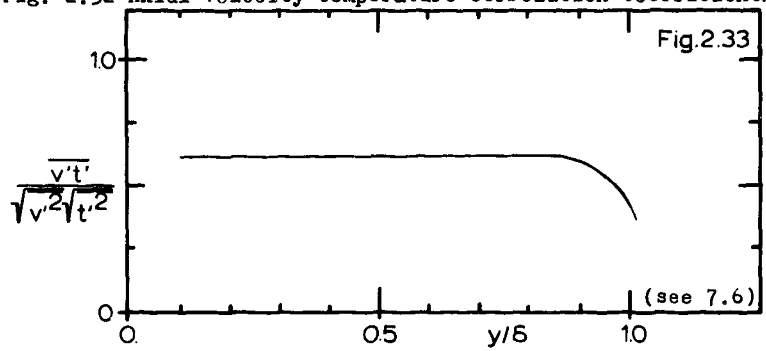

Fig. 2.33 Turbulent heat flux correlation coefficient.

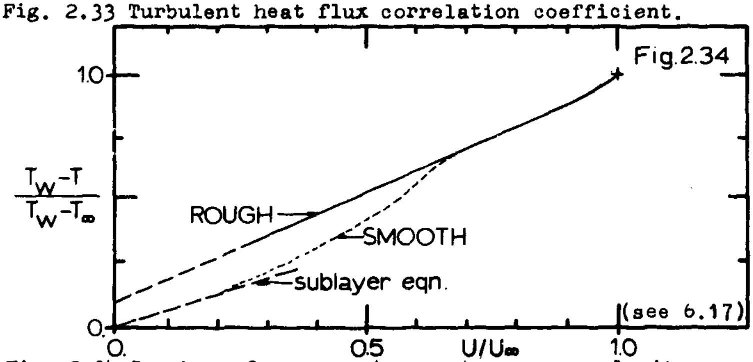

Fig. 2.34 Rough surface mean temperature-mean velocity profile.

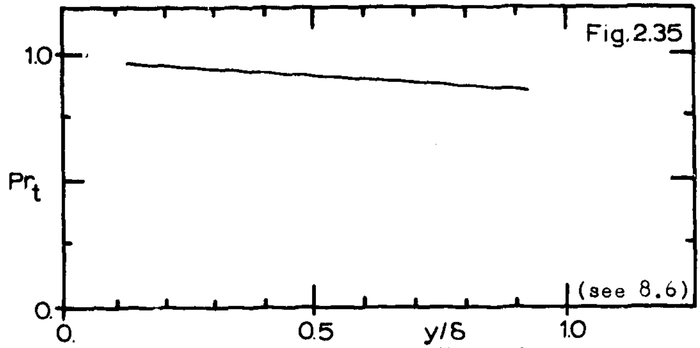

Fig. 2.35 Rough surface turbulent Prandtl number .

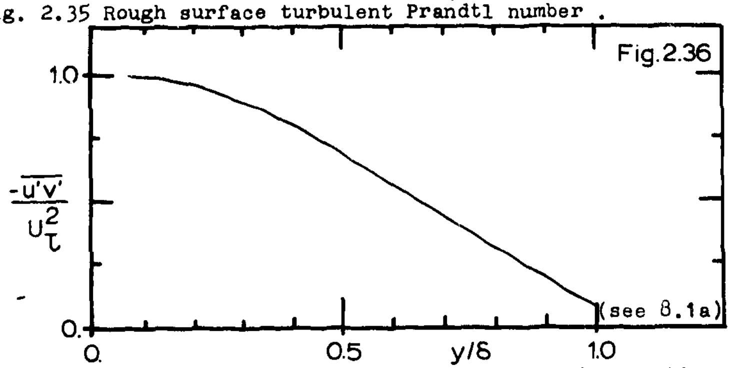

Fig. 2.36 Rough surface turbulent shear stress distribution.

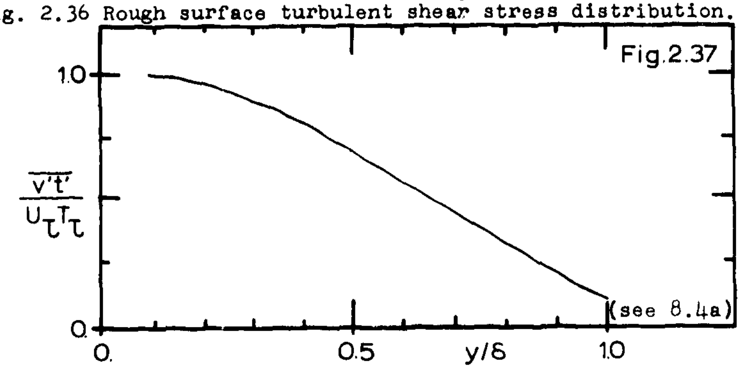

Fig. 2.37 Rough surface turbulent heat flux distribution.

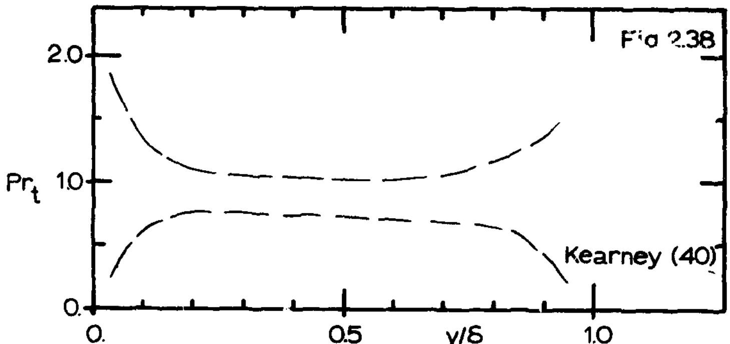

Fig. 2.38 Uncertainty envelope of smooth wall turbulent Prandtl number according to Kearney.

CHAPTER III

THE FULLY ROUGH STATE OF A TURBULENT BOUNDARY LAYER

Several interesting peculiarities of the fully rough regime over our deterministic surface have been discussed in the previous Chapter II. An "elliptical" line of argument was drawn having as its objective the comparison with the smooth wall for all aspects of behavior.

To the present point we have avoided a thorough discussion of the fully rough regime itself. A systematic study of this regime was conducted, introducing two new aspects almost never considered before in experimental work with roughness: non-isothermal boundary layer flows and transpiration. These two boundary conditions are encountered in applied problems such as thermal protection of surfaces like turbine blades, nose-tips of re-entry vehicles, etc. But in the overall this study becomes a contribution in the coupled problem of fluid dynamics, heat transfer and mass transfer (injection) with the effect of roughness. Further, due to the novelty of this study, one does not have much experimental data to compare with, except for unblown, isothermal data, so it was important to identify and well define the fully rough state. (From time to time we will refer to Healzer's [4] work which is one of the pioneers in this area.)

The boundary conditions for the flow were chosen as to produce the fully rough state and to allow the study of the effects of heat transfer and transpiration. The fully rough state for our surface has been defined to be that state in which the observed Stanton number and friction factor distributions are independent of Reynolds number. Figures 3.1 and 3.2 represent these characteristics, and free-stream velocities of 89 ft/sec and 130 ft/sec runs correspond to this flow regime.

Transpiration rates of $F = 0.002$ and $F = 0.004$ for the $U_\infty =$ 89 ft/sec were considered for the study of mass injection and its effects.

A heated wall with constant and uniform temperature was considered for studies of heat transfer. The free-stream was maintained at a lower constant temperature setting: on average there was a 27°F driving potential.

The analysis of the fully rough regime will be considered in two sections (see Figure 3.0):

1) fully rough state and other works
2) fully rough state and transpiration.

3.1 The Fully Rough State and Other Works

As Yaglom [13] points out, a rough surface can at best be described by parametrically representing size, shape and distribution of the rough elements, which would correspond to three parameters. It is interesting to note that several attempts have been made to identify each surface with the use of only one parameter, and describe its performance as a function of this parameter, as it has been done by several authors after works by Nikuradse [20], Schlichting [21], Clauser [19], Hama [10] and others.

Regardless of their main objectives, the experimental works in roughness effects have, in general, dealt mostly with integral parameters: mean velocity profiles, skin friction, and Stanton number distributions. Several surfaces and fluids have been used to compare and determine the performance of each class of surfaces.

Therefore, there is not much data which can be directly used for comparison with our results. Only a few works have treated the fluid dynamics of rough wall boundary layers, almost none the heat transfer problem, and none have used a deterministic roughness except for woven screens. We will, tentatively, try to compare our results with some available correlations and data.

Most of the reported results on the roughness effects were obtained from pipe flow experiments and are tentatively extended to boundary layers over plates. This is in essence, what Schlichting and Prandtl [21] did. This classical work established the procedure used for a long time in rough wall problems. It introduces the definition of "equivalent sand-grain roughness", k_s for rough surfaces, so the friction factor results and correlations of Nikuradse's pipe flows (rough walls made with uniform sand grains) can be extended for these surfaces (see Schlichting [5] for details). For instance, for a surface like ours, densely packed spheres, they recommended 0.625 times the ball diameter, or $k_s = 0.031$ inches.

From work by Schlichting [5] the velocity profile for the fully rough regime of a sand-grain roughness wall was given by

$$U^+ = \frac{1}{\kappa} \ln \left(\frac{y}{k_s}\right) + 8.5 \quad . \tag{3.1}$$

Other methods of analyzing the data have been proposed by different authors. Thus, another way of comparing data from different experiments has been done by using the roughness parameter z_o, as Monin et al. [24] and Reynolds [42] suggested. Data is correlated by z_o defined by

$$U^+ = \frac{U}{U_\tau} = \frac{1}{\kappa} \ln \left(\frac{y}{z_o}\right) \tag{3.2}$$

which fits velocity profiles in the logarithmic region, when z_o is properly determined.

In an extensive work Jayatilleke et al. [48], with $Re_k = \frac{kU_\tau}{\nu}$, determined that

$$U^+ = \frac{1}{\kappa} \ln \left(\frac{30}{Re_k}\right) y^+ \tag{3.3}$$

gives a better fit for the available fully rough data. Note that this last result would give a value of 8.3 instead of 8.5 in Equation 3.1.

Thus for the fully rough state from Equation 3.2 one gets

$$z_o = \frac{k_s}{30} \tag{3.4}$$

and z_o has a constant value. The data for our surface as presented in Chapter VI has z_o in the range $0.90 \lesssim z_o \times 10^3 \lesssim 1.10$, which is compatible with $k_s = 0.031$ inches.

This method is analogous to that which Jayatilleke et al. [48] proposed with

$$U^+ = \frac{1}{\kappa} \ln (Ey^+) \tag{3.5}$$

$$E = \frac{30}{Re_k} \tag{3.6}$$

and which has been adopted by Spalding et al. [43].

We show in Figure 3.3a the values of E calculated from some of our profiles. In the fully rough range, the agreement of these values is rather good. The "k" surface character of our test surface is confirmed by this observation, and thus, the hydrodynamics of the flows reported here agrees with the accepted data for the fully rough regime.

We have also represented in Figure 3.3a the transitionally rough behavior of a "k_s" surface, which is defined to have the same behavior as Nikuradse's sand-grain pipe flows in the transition region. As we can see, our surface does not follow the k_s surface behavior in the transitionally rough regime. Hama [10] has shown that the transitional regime is very dependent on the rough surface nature.

A fact one should mention here refers to the correlation that Schlichting and Prandtl [21] suggested for the fully rough skin friction variation

$$\frac{C_f}{2} = 0.5 \left(2.87 + 1.58 \,\ell og\, \frac{x}{k_s}\right)^{-2.5} \quad . \tag{3.7}$$

This correlation has been used by several investigators for comparison of their data.

As a matter of record we show in Figure 3.3 this correlation and our "fully rough" skin friction distribution as discussed in Chapter V. Our data have a different shape. Could this difference be attributed to the ambiguity in defining the distance x from a virtual origin? This is not reasonable since for $\frac{x}{k_s} = 10^3$ the "error" in x would amount to more than 22 inches; while for $\frac{x}{k_s} = 10^4$ this "error" goes to 100 inches. Moore [23] and White [41] have already discussed the possibility of necessary changes in the coefficients in Equation 3.7 for correlating more recent data, and our data confirms this necessity.

Rough surfaces experiments in heat transfer have been performed for pipe flows. Some authors have proposed two-layer models for the heat transfer. The rough surface is replaced by an equivalent smooth wall, at some distance below the tip of the rough elements. The boundary layer is, then, assumed to be two-dimensional and formed by two layers. One is a super-thin layer next to the wall in which are concentrated all molecular effects on heat transfer and which simulates the fluid involving the protuberances. Above this layer would lie a "fully turbulent" layer. Assumptions like the validity of Reynolds analogy, turbulent Prandtl number equal to one, same distribution of eddy-diffusivity as for smooth walls, etc., form the basis for the matching between the two layers. We can refer to works by Gowen and Smith [3], Kolar [44], Yaglom and Kader [13], Nikitin [45], Owen and Thomson [29], Dipprey and Sabersky [28], Nunner [46], etc. The result, normally, comes out in the form of a correlation

$$St = f\left(\frac{C_f}{2}, Re_k, Pr\right) \quad . \tag{3.8}$$

Comparisons should be made with experimental results and correlations derived for air as the working fluid. Two works can be cited here: Nunner's [46] study of heat transfer in pipes having ribs attached to the walls, and Gowen and Smith's [3] who used different kinds of rough elements.

Nunner correlated his data with the expression

$$St = \frac{C_f/2}{1 + 1.5\, Re^{-0.125}\, Pr^{-0.166}(Pr\; C_f/C_{f_{smooth}} - 1)} \quad . \tag{3.9}$$

Gowen and Smith proposed a different expression which correlates heat transfer data for fluids with three different Prandtl numbers (0.7 - 13.0)

$$St = \frac{\sqrt{C_f/2}}{\psi + 4.5} \tag{3.9a}$$

where,

$$\psi = \left[0.155\ (Re_k\ \frac{D}{k})^{0.54} + \sqrt{\frac{2}{C_f}}\right] Pr^{0.5} \quad . \tag{3.9b}$$

These expressions were proposed for pipe flows and the Reynolds number dependence involves the pipe diameter, D . In the shown format, they are not suitable for comparison with our data. However, in order to have a feeling for their predicted values in the normal range of applications let us show some numbers.

Equation (3.9) for the range $10^4 < Re < 10^5$ gives

$$0.68 \lesssim \frac{St}{C_f/2} \lesssim 0.74 \qquad \text{(Nunner)}$$

Assuming the levels $Re_k \approx 70.0$, $\frac{C_f}{2} \approx 0.00230$, $\frac{D}{k} \approx \frac{2\delta}{k} \approx 94.0$, $Pr =$ 0.72 which corresponds to our 89 ft/sec case, Equation (3.9a) gives

$$\frac{St}{C_f/2} \approx 0.56 \qquad \text{(Gowen and Smith)}$$

Our fully rough case gives $St/(C_f/2) \approx 0.96$, and therefore the ratios calculated above by either method underestimate the value of Stanton number. This fact suggests that these correlations obtained for pipe flows are not suitable for boundary layer flows.

Dipprey et al. used water as the flowing medium for heat transfer experiments in rough wall pipe flows and the molecular Prandtl number was varied by running the experiments at different temperatures. The expression correlating their experimental data is

$$\frac{1}{\sqrt{C_f/2}}\left[\frac{C_f/2}{St} - 1\right] + 8.48 = 5.19\, Re_k^{0.2}\, Pr^{0.44} = g(Re_k\ , Pr) \qquad (3.9c)$$

It does not involve the pipe diameter D , which makes it suitable for comparisons with boundary layer flows. Note that it can only, tentatively, be extrapolated to the range $Pr = 0.72$ (air).

Figure 3.4 shows this correlation and our data for $U_\infty = 89$ ft/sec and $U_\infty = 130$ ft/sec. We have also represented the average variation of g calculated with the curve-fitted expressions for $C_f/2$ and St , as discussed in Chapter V. ^ur data falls below the correlation and seems to be just slightly sensitive to Re_k . We would expect a better agreement because Equation (3.9c) was derived with $Pr_t = 1$, which is not a bad assumption for our case as we see in Chapter VIII.

These comparisons suggest, at least, that heat transfer results for rough pipe flows are not suitable to be extrapolated to boundary layer flows.

Studies of heat transfer from rough plates scarcely appear in the literature. Some Russian works have been reported (see Kryukov et al. [49]) but their unorthodox presentations of the data allow no comparisons.

Unfortunately, due to the lack of data on rough plates boundary layers, comparisons with previous works can only be related to Stanton number from pipe flow studies, and skin friction.

We will next discuss the fully rough state of our surface, by analyzing the measured profiles at the different levels.

3.1.1 Mean Velocity and Temperature Profiles

Distinguishable features of the "fully rough" state are the different similarities observed for profiles of mean quantities and turbulence intensities when the proper velocity and length scales are used. These similarities occur regardless of the free-stream velocity as a consequence of Reynolds number independence.

The first characteristic to be noted in the development of the turbulent boundary layer over our rough wall is that the shape factor $H = \delta_1/\delta_2$ is slowly decreasing along the test section. For the fully rough regime a value of approximately 1.46 is reached at the end of the test section. Figure 3.5 shows H as function of x. The value 1.46 is in agreement with measurements by Moore [23], Tillman [47] and Hama [10].

In the region where H is only slowly varying, similarity in U/U_∞ profiles can be obtained as a function of similarity variables like y/δ_2 or y/δ both for changes in x-position and changes in U_∞. Figure 3.6 shows the velocity profile U/U_∞, for the two free-stream velocities we considered, corresponding to plate 19, and the similarity is easily seen.

Velocity profile similarity in these coordinates can be expected for boundary layers where there is no Reynolds number dependence, and in our case it refers to the whole layer.

A good way of further showing this similarity is to plot the previous velocity profiles in defect coordinates. Figure 3.7 shows $(U_\infty - U)/U_\tau$ for plate 19. As we saw in Chapter II the velocity-defect profile corresponds to the one given by Coles [26] law of the wake for smooth surfaces.

These similarities come about in the fully rough state where

$$\delta = f_1(x) \tag{3.10}$$

$$\delta_1 = f_2(x) \tag{3.11}$$

$$\delta_2 = f_3(x) \tag{3.12}$$

$$\frac{C_f}{2} = \bar{f}(x) \tag{3.13}$$

so, for the same x

$$U_\tau \;\alpha\; U_\infty \tag{3.14}$$

These peculiarities have been analyzed by Schlichting [5], and are confirmed by the present data.

However, similarity in our case is not restricted to mean velocity profiles: the temperature profiles exhibit it also. It can be seen from a T^+ versus U^+ plot. In our special case, however, for the same x distance, irrespective of the free-stream velocity, we have approximately the same Stanton number and friction factor, and the same behavior is observable from $(T_w - T)/(T_w - T_\infty)$ versus U/U_∞ profiles. Figure 3.8 shows it clearly. The linearity of the plot is remarkable and its consequences have been discussed in the previous chapter.

3.1.2 First Level of Turbulence Quantities

Similarities in mean profiles have been reported before by Hama [10], Clauser [19], and Moore [23], but only with reference to mean velocity. Turbulent intensities profiles and their correlation coefficients have been reported in a few works, most of them referring to two-dimensional roughness elements. Similarities have not been much commented or analyzed for the present kind of surface. In order to discuss these similarities one has to define the scales to be used.

It has been shown for smooth wall layers that U_τ is the velocity scale for turbulence intensities in the wall layer, and the behavior in the outer layer is normally scaled in U_∞ (see Hinze [32]).

Figures 3.9 and 3.10 show the $\overline{u'^2}$ profiles for the three velocities we analyzed. The 52 ft/sec run profile was only represented for the outer region. The profiles normalized by U_τ collapse better.

The nature of the hydrodynamical behavior of the fully rough state makes U_τ and U_∞ both possible candidates for the velocity scale. According to Hinze, who analyzed the rough wall boundary layer data of Corrsin et al. [11], normalizing the shear velocity U_τ would make rough and smooth turbulence intensity profiles nearly coincide in the outer region of the layer.

Figures 3.9a and 3.10a also compare the longitudinal velocity fluctuation, $\overline{u'^2}$, for the fully rough state and two smooth wall experiments. These last profiles refer to works by Klebanoff [15] with very low free stream turbulence level and Orlando [17] with a level similar to our apparatus. The normalizing velocity scales are U_∞ and U_τ in Figures 3.9a and 3.10a, respectively. The agreement in the outer region proposed by Hinze does not occur. The rough wall is certainly affecting the flow over the whole layer. Further evidence of this fact is discussed in the Pr_t section 3.1.4. Near the wall, where a constant shear stress layer exists (see Section 3.1.3), the velocity scale certainly is U_τ, because $\overline{u'v'} \propto U_\tau^2$. It is, then, a natural step to use U_τ over the whole layer as the velocity scale.

The last assertion can be even better appreciated from Figure 3.11 where the three components of velocity fluctuations are shown. All three were non-dimensionalized by U_τ, for 89 and 130 ft/sec.

Analogous features are then expected to exist for the temperature fluctuations, at least to be in line with the heat transfer behavior and the similarity between velocity and temperature profiles.

Figure 3.12 shows $\sqrt{\overline{t'^2}}/T_\tau$ for the 89 and 130 ft/sec cases. The noticeable similarity in distribution confirms our expectation and, again, that T_τ, the near wall temperature scale, can be used as the scale for the whole layer.

3.1.3 Second Level of Turbulence Quantities

Apparently the fully rough state scales well on the shear velocity U_τ . Figure 3.13 shows the turbulent shear stress distribution for $U_\infty = 89$ and 130 ft/sec. They are almost identical and show a constant shear stress layer near the wall.

The similar $\sqrt{\overline{u'^2}}/U_\tau$, $\sqrt{\overline{v'^2}}/U_\tau$ and turbulent shear stress distributions for the two free-stream velocities result in

$$R_{uv} = \frac{-\overline{u'v'}}{\sqrt{\overline{u'^2}}\sqrt{\overline{v'^2}}} \tag{3.15}$$

being approximately constant, and a value of 0.44 is found.

Despite the fact that, for higher velocities, U_τ is larger, the interactions are such that the turbulence quantities scale proportionally to each other and R_{uv} is the same as for smooth walls (see Townsend [35]). This correlation seems to be more universal than one would expect.

Figure 3.14 show R_{uv} and $-\overline{u'v'}/q^2$ with their constant values. Further, similarity in the mean velocity - shear stress profiles can be contrasted in Figures 3.15 and 16 where the mixing-length distributions have been plotted. Close to the wall $\ell = \kappa y$ seems to be non-dependent on velocity, shear velocity or whatever.

With respect to the temperature fluctuations field, profiles of $\overline{v't'}/\sqrt{\overline{v'^2}}\sqrt{\overline{t'^2}}$ and $-\overline{u't'}/\sqrt{\overline{u'^2}}\sqrt{\overline{t'^2}}$ have never before been reported for fully rough state. Variation of the correlation coefficients with free-stream velocity are not expected to be measureable, based on the scaling of turbulence quantities observed in the previous section.

The correlation coefficients $\overline{v't'}/\sqrt{\overline{v'^2}}\sqrt{\overline{t'^2}}$ and $-\overline{u't'}/\sqrt{\overline{u'^2}}\sqrt{\overline{t'^2}}$ are shown in Figures 3.17 and 18. The constancy of their values over a good part of the layer confirms the expectation.

Finally, the turbulent heat flux $\overline{v't'}$ is non-dimensionalized by $U_\tau T_\tau$ and its distribution is shown in Figure 3.19. The turbulent heat flux is similar for the two velocities as the shear stress was, and the value ~1.0 close to the wall justifies the existence of a constant heat flux layer.

3.1.4 Turbulent Prandtl Number

Figure 3.20 shows the turbulent Prandtl number variation for the fully rough state. Very close to the wall a value of approximately 0.95 is attained in both cases analyzed. A smooth wall turbulent Prandtl number variation taken from Orlando's [17] work is also shown in Figure 3.20. It can be seen that the smooth Pr_t value significantly decreases near the edge of the layer. The rough profile, however, maintains its level over most of the layer, and this fact is another evidence that the rough wall is affecting the whole layer.

The behavior in the mean temperature - mean velocity (T-U) profile and the existence of a constant shear stress and heat flux layers for low y/δ produces a region with $Pr_t \approx$ constant.

3.2 Fully Rough State and Transpiration

Transpiration has been used as a means of boundary layer control and thermal protection of surfaces.

A systematic study of transpiration effects in smooth wall boundary layers has been conducted at Stanford by Kays [50], Moffat [51] and co-workers. Among several observed features three come specially to attention:

1) for low blowing fractions $F = \rho_o V_o / \rho_\infty U_\infty \leq 0.008$ there is a region near the wall where Couette flow assumptions are valid.

2) for these cases there is a region not too close to the wall but sufficiently close ($y/\delta < 0.1$) where the mixing-length distribution is $\ell = \kappa y$.

3) for the region next to the wall it is possible to correlate the data by means of only one length scale A^+ made a function of $V_o^+ = \frac{V_o U_\tau}{\nu}$. This has been done through

$$\ell = \kappa y(1 - \exp(-y^+/A^+(V_o^+))) = \frac{\sqrt{-\overline{u'v'}}}{dU/dy} \tag{3.16}$$

This is a variation of well known van Driest [52] scheme. Andersen [53] discusses the role of A^+ as a measure of a "sublayer thickness", however it is first of all a length scale. The simplicity and success of this method justifies its generalized use.

The first study in transpired rough walls has, recently, been presented by Healzer [4]. The general effect of blowing on friction factor and Stanton number are the same for smooth and rough walls. Both decrease with increase in the blowing fraction. Figures 3.21 and 22 show the results for the present study. A systematic study on these parameters and the effect of blowing is given by Healzer [4].

Our major concern in this study is the identification of the effects of roughness with blowing on the flow and how this compares with the transpired smooth wall case.

3.2.1 Mean Velocity and Temperature Profile

Figure 3.23 shows the velocity profiles for three transpiration rates $F = 0.0$, 0.002 and 0.004, corresponding to the same x position and having the same free-stream velocity $U_\infty = 89$ ft/sec. It is clearly seen that the velocity-defect increases near the wall, because fluid with no x-momentum is being injected through the porous wall. Apparently, no special change in the fluid dynamics is happening near the wall since the general shape of the curves is preserved.

As a contrast we show from Moffat [51] typical velocity profiles for smooth walls with the same transpiration rates. As we see from Figure 3.28 as the transpiration rate increases the profile becomes more "rough-like". For the unblown profile a clear "knee" is observed in the curve, which occurs in the "buffer-zone" where the boundary of the viscous sublayer is located. For the transpired cases, however, the "knee" becomes flatter and occurs at smaller y/δ. At the highest rate it is almost imperceptible. Therefore, the sublayer thickness apparently decreases with increasing blowing rates. For sufficiently high value of F we would not be able to see a "knee", and it would look as if no viscous sublayer is present.

At a first glance, a highly blown smooth layer velocity profile resembles our unblown rough wall profile. This is an interesting observation and may provide a clue as to how to empirically model the layer behavior. Coincidentally, Reynolds [42] in a recently published book mentions the possibility of a smooth wall transpired layer to have some "rough wall-like" characteristics. He comments on this fact, which has been overlooked in the past. It seems reasonable to us that for high enough blowing rate the discrete distribution of the pore in any real porous surface will have some effect on the boundary layer. When transpiration is taking place, this distribution results in an array of jets, even though the Reynolds number based on pore diameter is small ($1.0 < Re < 20.0$). The evidence that jets exist, for the present rough surface, was given by Pimenta [54] who showed that for some conditions the jets coalesced to form a stable pattern of large jets (5 to 10 times the spacing of the surface jets). This coalescing effect displayed a repeatable pattern and a repeatable critical velocity for onset and disappearance (different from the onset) when tested with no free-stream flow. Tests with a mean flow showed no abrupt change on the heat transfer behavior of the surface associated with the onset of coalescence. It was concluded that the shear flow in the boundary layer defeated the tendency for the jets to agglomerate. The very existence of the coalescent jet effect, however, proves that there must have been discrete, identifiable, jets at the surface even at these low Reynolds numbers. If these jets are admitted to exist, then a mechanism is present by which even a "smooth" porous surface can seem to become rough when transpiration is present. We know that a wall affects a boundary layer flow through pressure forces and shear forces, these resulting necessarily from the no-slip condition. The static pressure field around each small jet, plus the shear interaction, can simulate the interaction between a solid protuberance and the flow if part of the pressure force reaction is taken out by the solid. Thus the wall can be "seen" by the mean flow as if it were "rougher". Further arguments in support of this idea will come with the analysis of the longitudinal velocity fluctuations, $\overline{u'^2}$.

Let us refer back to our rough wall data. For each constant F case, similarity in velocity-defect coordinates, $(U_\infty - U)/U_\tau$, is obtained for profiles at two different x-stations. This similarity has been observed for smooth walls by Simpson [39] and Andersen [53] and cases of constant F with no axial pressure gradient are classified as "near-equilibrium" flows. Thus, the uniformly blown rough wall layer also reaches the "near-equilibrium" state. The velocity distributions, however, are not the same for the cases with different values of F. Figure 3.25 shows one of such distributions for the case $F = 0.002$.

One of the major features observed from the rough wall velocity profiles is that they conform to a Stevenson's [55] type of law of the wall.

This law was first developed by Stevenson for uniformly transpired smooth wall and as presented by Eckert [57] read as

$$\frac{2U_\tau}{V_o}\left[\left(\frac{V_o}{U_\tau} U^+ + 1\right)^{1/2} - 1\right] = \frac{1}{\kappa} \ln y^+ + C \tag{3.17}$$

As discussed in Chapter VI, this expression is obtained with two assumptions: 1) "Couette-flow", i.e., $\frac{\partial}{\partial x} = 0$, and 2) mixing-length $\ell = \kappa y$.

For smooth walls Stevenson [55] proposes that C should be the same as in the $V_o = 0$ case. Simpson [39], however, suggests C to be determined from

$$U^+ = y^+ = 11.0 \tag{3.18}$$

which works reasonably well for mild values of V_o.

Coles suggests that Equation 3.17 is reasonable for $-0.004 \leq \frac{V_o}{U_\infty} \leq 0.01$, when the mixing-length results are realistic.

In our case we are measuring the y-coordinates from the top of the rough elements. So, as discussed in Chapter VI, Equation 3.17 can be put in the form

$$\frac{2}{V_o}(U_\tau^2 + UV_o)^{1/2} = \frac{1}{\kappa} \ln\left(\frac{y + \Delta y}{z_o}\right) \tag{3.19}$$

where Δy and z_o are functions of the blowing fraction F. Figure 3.26 shows the good agreement of Equation 3.19 with a typical velocity profile which exists for $y/\delta_2 < 1$. As it is discussed in Chapter VI, as well as in Section 3.2.3, the Equation 3.19 renders a mixing-length distribution $\ell = \kappa y$. It is very clear that no viscous layer exists also for the blown profiles, so we can expect no Reynolds number dependence also for the constant F runs. This is apparent from our data, and is confirmed by Healzer's [4] work. As we already mentioned the characteristics of the flow depends on the value of F.

The temperature profile is depressed with blowing in the near wall region. Figure 3.27 shows a typical temperature profile with the general shape similar to that of the velocity profile. This is confirmed by the plot of $(T_w - T)/(T_w - T_\infty)$ versus U/U_∞ which is independent of the y-coordinate. Figure 3.28 shows a typical profile for $F = 0.002$. Two features must be stressed again: the linearity and the "non-zero" intercept for non-dimensional temperature as $U/U_\infty \to 0$. The linearity could not be anticipated from "Couette-flow" analysis of x-momentum and energy equations as seen in Chapter V. It constitutes strong evidence of similarity between velocity and temperature profiles. The linearity implies that the sublayer is certainly non-existent, and that the turbulent Prandtl number is approximately constant and close to one (1.0).

The "non-zero" intercept constitutes a good evidence of a very "thin" layer next to a solid-fluid interface which is responsible for most of the resistance to heat transfer.

Thus, transpiration is not changing these features which characterized the unblown case.

3.2.2 First Level of Turbulence Quantities

Figures 3.29, 30 and 31 show the turbulence intensity ($\overline{u'^2}$, $\overline{v'^2}$ and $\overline{w'^2}$) distributions for the three transpiration rates studied, $F = 0.0$, 0.002 and 0.004.

The plots for $\overline{v'^2}$ and $\overline{w'^2}$ seems to indicate that blowing is not much affecting their distribution near the wall. Unfortunately, due to physical size limitation no data could be obtained for very low y/δ. Transpiration makes $\overline{v'^2}$ and $\overline{w'^2}$ distributions to be more similar, and the anisotropy is decreased.

Interesting features can be observed from Figure 3.32 where the near wall region is magnified in a plot of the stream-wise fluctuations. The peak of $\overline{u'^2}/U_\infty^2$ appears to be at the same $y/\delta \approx 0.1$. Blowing increases

$\overline{u'^2}$ for $y/\delta > 0.1$. However, very close to the wall the trend is the opposite.

If one recalls the analysis of the $\overline{u'^2}$ profile given in the previous chapter, one can put forward a tentative explanation for this strange behavior. Let us consider again the "arrest" mechanism capability of a rough surface. As we saw, the strong deceleration imposed by the wall into the flow in a short distance can explain why $\overline{u'^2}$ decreased near the wall in the unblown case. In other words, the "inrush" of high momentum fluid toward the wall is very effectively "arrested" near it, by the rough elements.

Referring back to our discussion in Section 3.2.1, one might be tempted to say that the blown rough wall acts like it were "rougher". This is because a larger F reduces $\overline{u'^2}$ near the wall. The present argument is not too strong, but a couple of other evidences seem to support it. First, Healzer [4] in his computer prediction attempts of his transpired heat transfer data had to artificially make the wall look rougher. Secondly, as we will discuss in the next section the "shift" in virtual origin was larger for higher F . The shift seems to be proportional to the roughness size. This suggests that the transpired wall is seen by the flow as if the wall had larger rough elements.

We are reproducing, for the purpose of comparisons, in Figures 3.33, 34 and 35 the $\overline{u'^2}$, $\overline{v'^2}$ and $\overline{w'^2}$ distributions for a smooth wall boundary layer with transpiration. They correspond to $F = 0.0$, 0.005 and 0.01. These results have been taken from a recent work by Polyayev et al. [56].

From Figure 3.33 we can see that for $F \leq 0.005$ there is clearly a peak in $\overline{u'^2}$ close to the wall, indicating the existence of a sublayer.

Comparing [illegible] rough wall results, we see that for large blowing rate the [illegible] files are very similar. At high blowing rate, however, we have to be careful because not much influence of the outer layer "diffuses toward the wall". The smooth wall distributions of turbulence intensities, however, are not similar when we have no blowing or just some blowing. It is interesting to note that the turbulent intensities distributions for the smooth wall with $F = 0.005$ resemble those of our rough wall for $U_\infty = 52$ ft/sec.

Therefore, transpiration in the smooth wall case directly affects the mechanism near the wall, but it does not cause dramatic changes for the fully rough state.

Finally, we show in Figure 3.36 the temperature fluctuation profiles. Certainly T_τ is not any longer the temperature scale, and $(T_w - T_\infty)$ seems to be a more realistic scale. The $\overline{t'^2}$ profile shape is similar to the one of $\overline{u'^2}$, but does not exhibit the same near-wall trends. We can expect a lower $\overline{u't'}$ correlation in this case.

3.2.3 Second Level of Turbulence Quantities

The applicability of smooth wall mechanisms of interaction between inner flow and outer flow is very well reflected by the correlation coefficient R_{uv}

$$R_{uv} = \frac{-\overline{u'v'}}{\sqrt{\overline{u'^2}}\sqrt{\overline{v'^2}}} \tag{3.20}$$

as well as

$$R_{q^2} = \frac{-\overline{u'v'}}{q^2} \quad . \tag{3.21}$$

Distributions of these coefficients are shown in Figure 3.37. They have, over most of the layer, approximately constant values of 0.44 and 0.14, respectively, for $0.05 \lesssim y/\delta \lesssim 0.85$.

We should emphasize, now, that these two values are the same as those for our unblown rough data and also for smooth data, as reported by Polyayev [56], Lumley et al. [25]. It suggests some kind of "universality" in the interactions between mean flow - turbulence in the outer flow.

The persistent behavior of R_{uv} and R_{q^2} for the present surface regardless of the transpiration (blowing) boundary condition comes as a good support of structural models for the turbulent shear stress. These models as discussed by Reynolds [42] use equations for Reynolds stress components or turbulent kinetic energy, with some empirical relations to achieve closure of the syst‹ ˜ differential equations. We are here referring to the model developed by Townsend [37] and used by Bradshaw et al. [58], with

$$-\overline{u'v'} \approx 0.15\, q^2 \tag{3.22}$$

Figure 3.38 shows the turbulent shear stress distributions for the transpired cases. The turbulence production $P = -\overline{u'v'}\, \partial U/\partial y$, increases over most of the layer because for the blowing case $\overline{u'v'}$ and $\partial U/\partial y$ are larger for the same $y/\delta (y/\delta \gtrsim 0.1)$. This is responsible for increases in $\overline{u'^2}$, $\overline{v'^2}$ and $\overline{w'^2}$ for $F > 0$.

As discussed in Chapters V and VI, the Couette flow assumption works well near the wall $(y/\delta \lesssim 0.1)$, and

$$\frac{-\overline{u'v'}}{U_\infty^2} \cong \frac{C_f}{2} + \frac{V_o}{U_\infty}\frac{U}{U_\infty} \tag{3.23}$$

fits the data in this region.

One of the most interesting aspects of the transpired rough boundary layer comes with the analysis of the mixing-length ℓ distribution. Figures 3.39 and 40 show ℓ distribution for the three transpiration rates.

No significant changes occur to ℓ/δ as we increase F from zero. However, it seems that a fit like

$$\frac{\ell}{\delta} \cong \text{constant} = \lambda_\infty \tag{3.24}$$

for the outer flow, would ask for a lower constant λ_∞ for larger values of F. An average value for this constant λ_∞ can be estimated as $\lambda_\infty = 0.09$. This value is somewhat higher than one for smooth surfaces reported by Andersen [53], $\lambda_{\infty,\text{smooth}} = 0.0779$.

Now let us refer to Figure 3.40. It shows that $\ell = \kappa(y + \Delta y)$ for low y/δ. The important fact is that Δy increases with blowing. In our case

$F = 0.0 \qquad \Delta y \cong 6.0 \times 10^{-3}$ inch

$F = 0.002 \qquad \Delta y \cong 8.0 \times 10^{-3}$ inch

$F = 0.004 \qquad \Delta y \cong 9.0 \times 10^{-3}$ inch

This fact supports the argument that the wall "looks rougher" with blowing. Since for $F = 0.0$, $\Delta y \cong$ constant one can expect that

$$\Delta y \alpha \text{ roughness size} \tag{3.25}$$

Thus, Δy increases with F and so does the apparent size of the roughness.

As we mentioned before, Healzer [4] has noticed that when he tried to predict the skin friction variation using the computer prediction scheme developed by Kays [50], he had to artificially make the wall "rougher" for $F > 0$ in order to predict reasonable $C_f/2$ distributions.

The behavior of the mixing-length ℓ distribution for transpired smooth wall boundary layers, according to Kays [50] or Andersen [53] using the van Driest [52] scheme, is represented in Figure 3.41. Its distribution has been correlated by

$$\frac{\ell}{y} = \kappa\{1 - \exp(-y/A)\} \tag{3.26}$$

where $\kappa = 0.41$, $A = A(V_o)$ and A decreases for increasing V_o . This is compatible with the velocity profiles shown in Figure 3.24, and was obtained with the assumption that the wall shear τ_w is given by

$$\frac{\tau_w}{\rho} = \nu \left.\frac{dU}{dy}\right|_o \tag{3.27}$$

As we see from this figure the ℓ distribution for smooth wall approaches the rough wall distribution (dashed line at $\ell/y = 0.41$) as F increases.

Referring back to our discussion in Section 3.2.1, there might be an extra term in the right hand side of Equation 3.27 corresponding to a pressure force interaction introduced by the blowing. We have advanced that blowing makes a surface to seem rough: if this is due to local pressure "islands" around the discrete jets, then these pressure "islands" can transmit a net force in the x-direction between the surface and the fluid.

Nothing extraordinary happened with velocity-temperature correlation coefficients with the introduction of blowing.

Figure 3.42 shows the correlation coefficient between the streamwise velocity and temperature fluctuations $\overline{u't'}/\sqrt{\overline{u'^2}}\sqrt{\overline{t'^2}}$ for the transpired cases. The near constancy of its value is preserved, but now its value is around 0.6, lower than for the unblown case as it has been anticipated.

The same distribution and level can be seen in Figure 3.43 for the correlation coefficient between the normal velocity and temperature fluctuations $\overline{v't'}/\sqrt{\overline{v'^2}}\sqrt{\overline{t'^2}}$.

3.2.4 Turbulent Prandtl Number

Finally, we show in Figure 3.44 the turbulent Prandtl number distribution for the transpired cases. No discernible changes can be observed from the rough, unblown case, which was somewhat expected because

$$Pr_t = \frac{-\overline{u'v'}}{\overline{v't'}} \frac{dT}{dU} \tag{3.28}$$

and the $\overline{u'v'}$ and $\overline{v't'}$ distributions were similar, and dT/dU is approximately constant for $U/U_\infty \lessapprox 0.8$.

This again reassures the near absence of molecular transport of heat throughout the layer, and that it is controlled by the fluid dynamics.

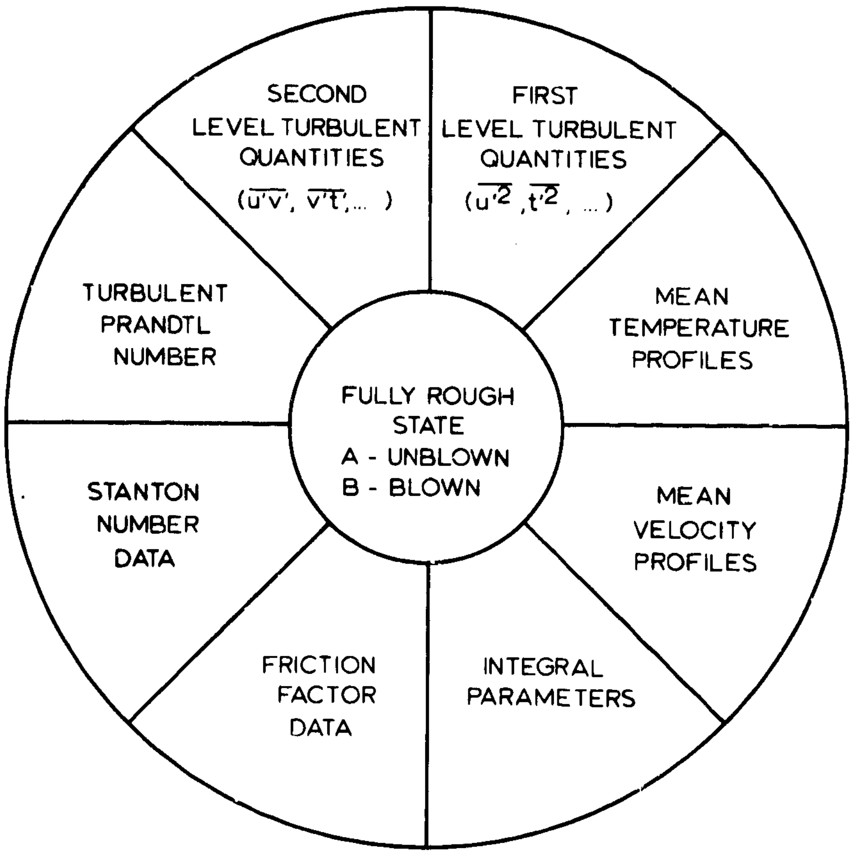

Fig. 3.0 Fully rough state analysis.

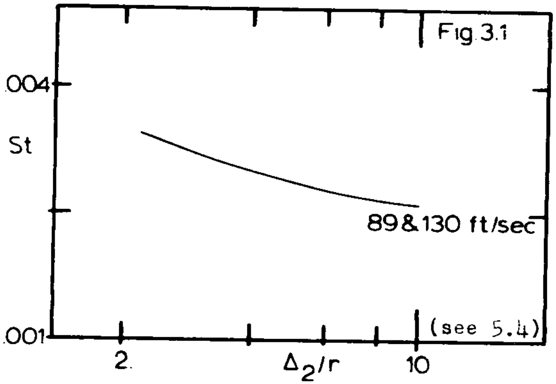

Fig. 3.1 Fully rough Stanton number.

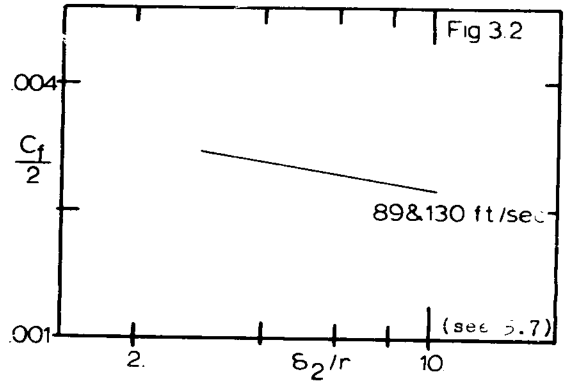

Fig. 3.2 Fully rough friction factor.

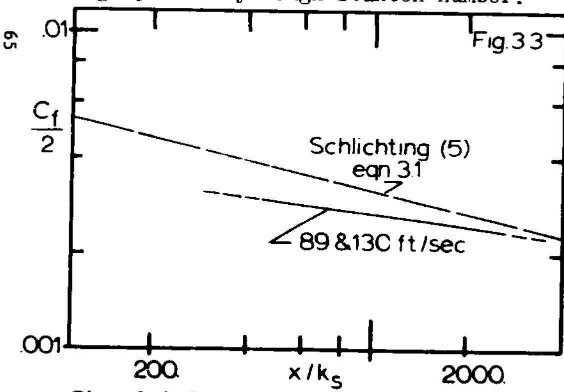

Fig. 3.3 Comparison with Schlichting's $C_f/2$ correlation.

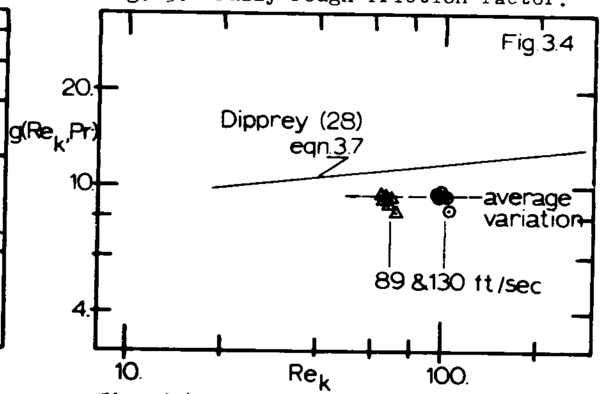

Fig. 3.4 Comparison with Dipprey's g function correlation.

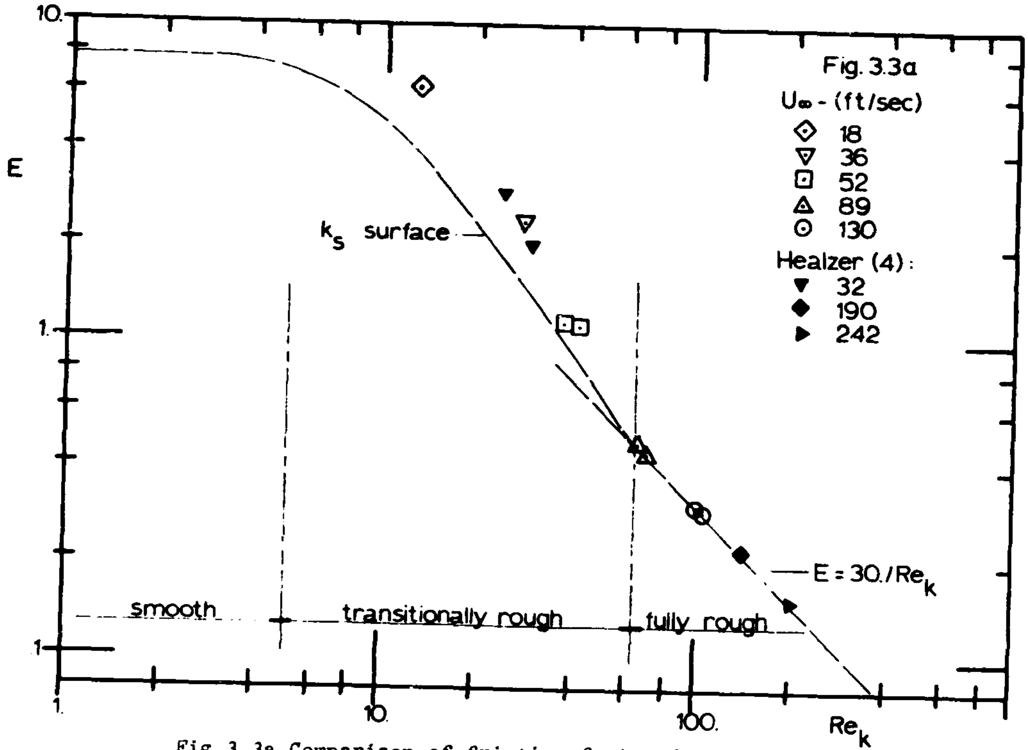

Fig 3.3a Comparison of friction factor data in terms of E with "k" and "k_s" surfaces behaviors.

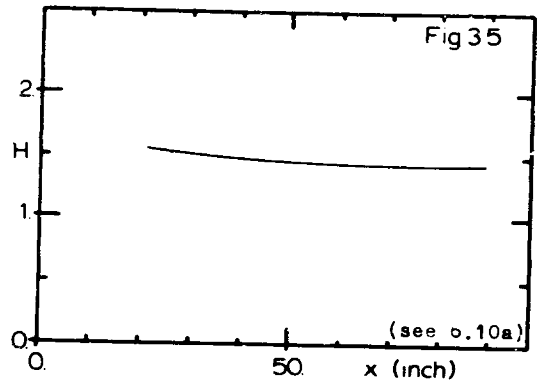

Fig. 3.5 Shape factor variation.

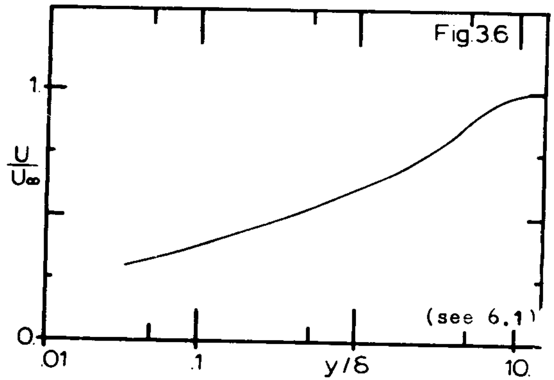

Fig. 3.6 Mean velocity profile.

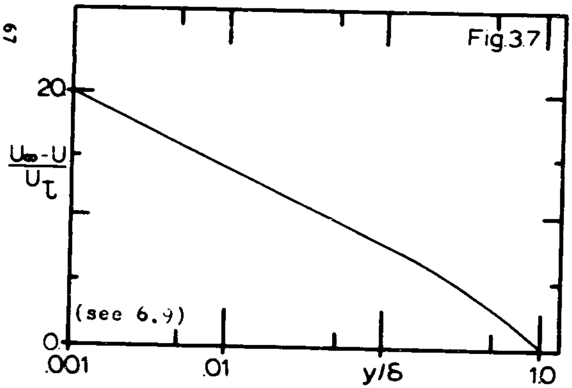

Fig. 3.7 Velocity defect profile.

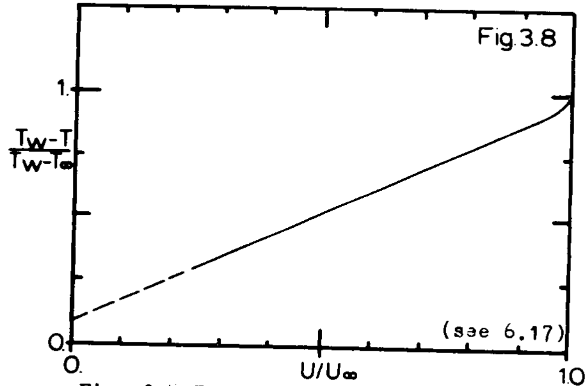

Fig. 3.8 Fully rough mean temperature-mean velocity profile.

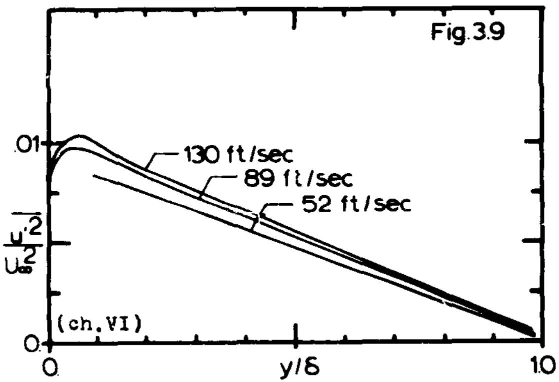

Fig. 3.9 Rough surface axial velocity fluctuation normalized by U_∞

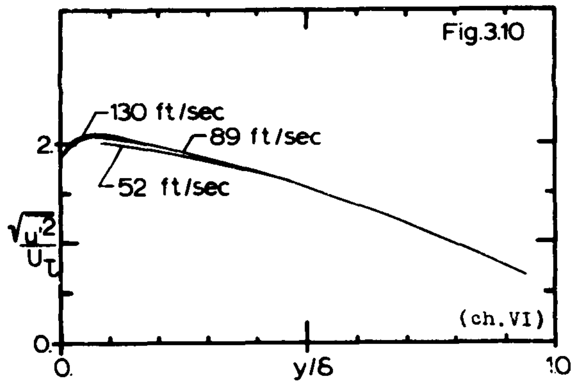

Fig. 3.10 Rough surface axial velocity fluctuation normalized by U_τ

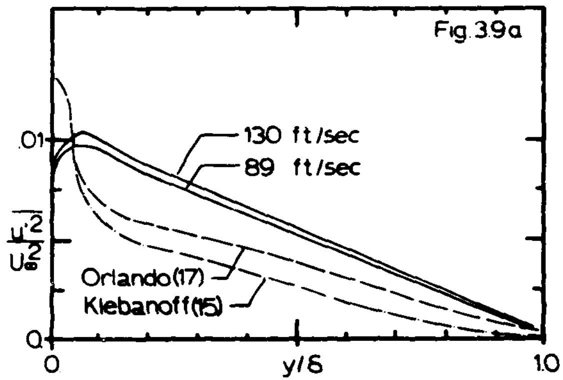

Fig. 3.9a $\overline{u'^2}/U_\infty^2$: rough vs. smooth.

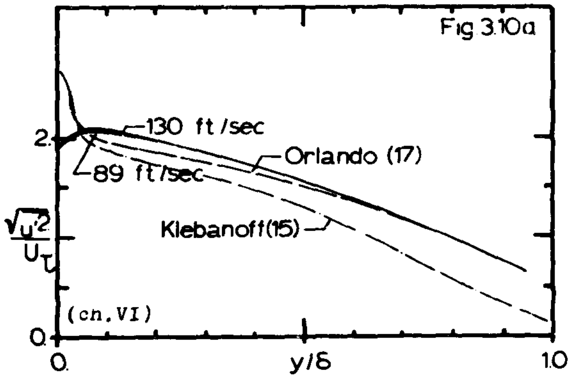

Fig. 3.10a $\sqrt{\overline{u'^2}}/U_\tau$: rough vs. smooth.

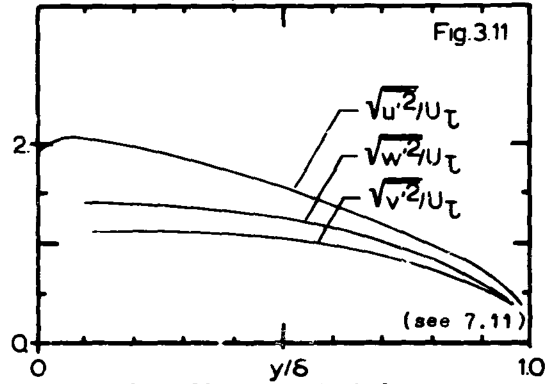

Fig. 3.11 Fully rough turbulence intensities.

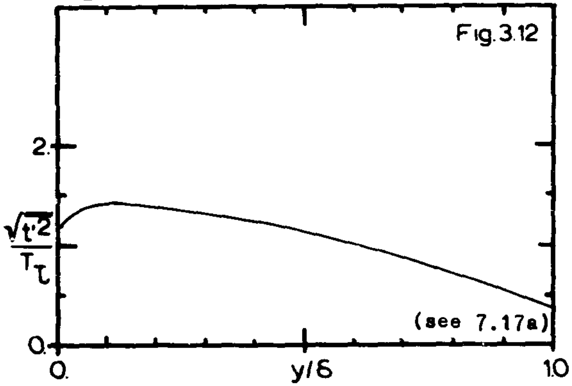

Fig. 3.12 Fully rough temperature fluctuations.

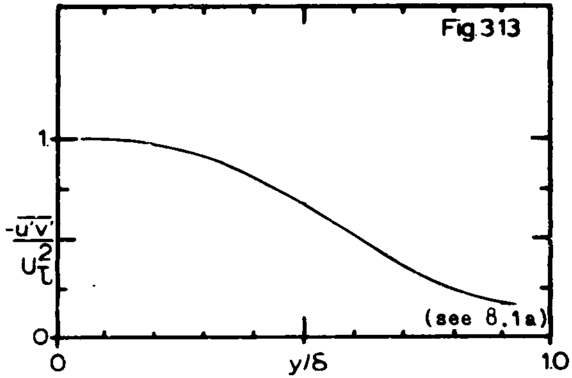

Fig. 3.13 Turbulent shear stress.

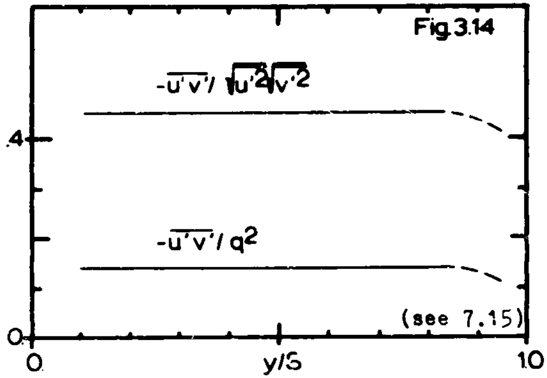

Fig. 3.14 $-\overline{u'v'}$ correlations.

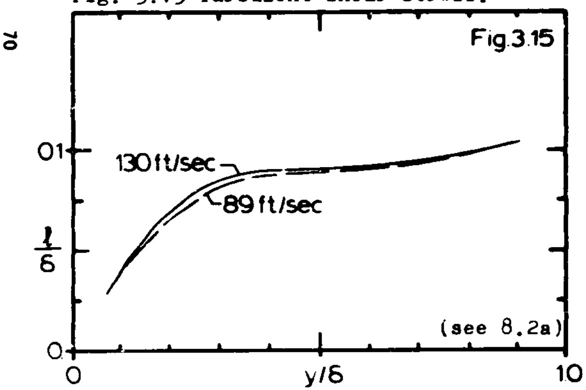

Fig. 3.15 Outer region mixing-length.

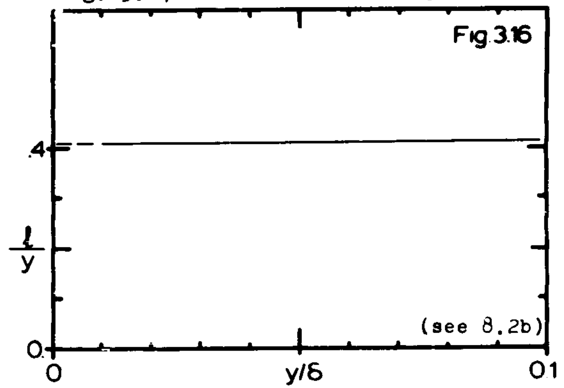

Fig. 3.16 Near wall mixing-length.

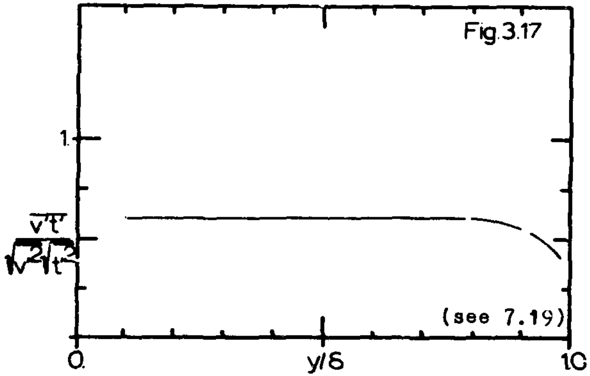

Fig. 3.17 $\overline{v't'}$ correlation coefficient.

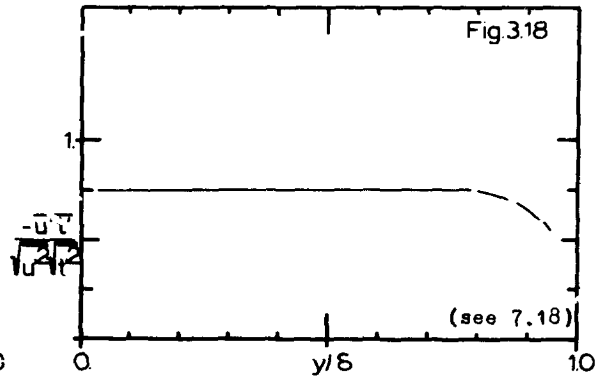

Fig. 3.18 $-\overline{u't'}$ correlation coefficient.

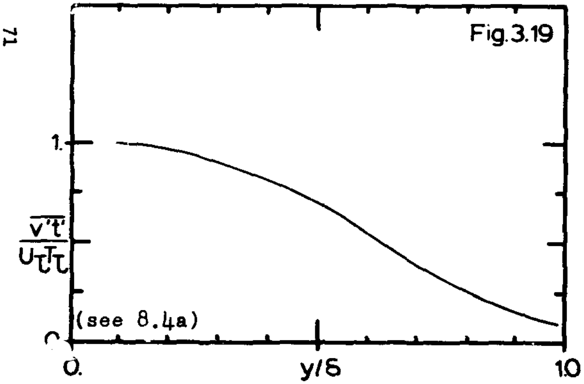

Fig. 3.19 Turbulent heat flux.

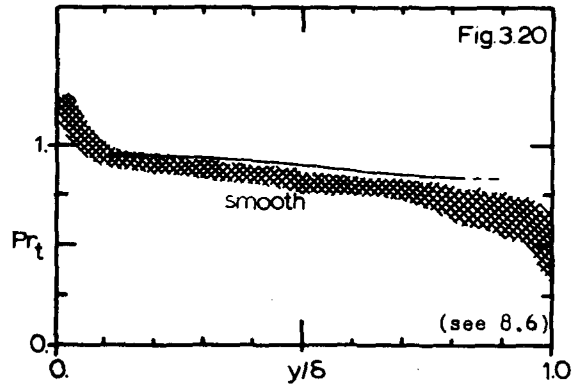

Fig. 3.20 Pr_t: rough vs. smooth.

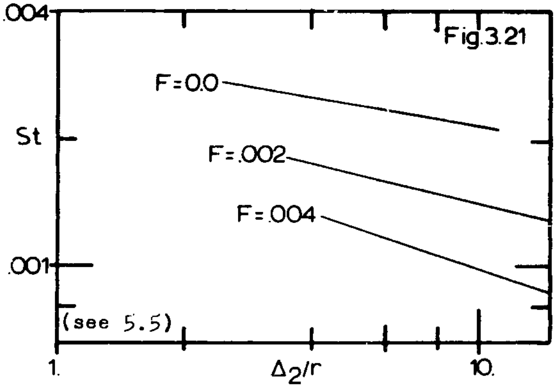

Fig. 3.21 Stanton number with blowing.

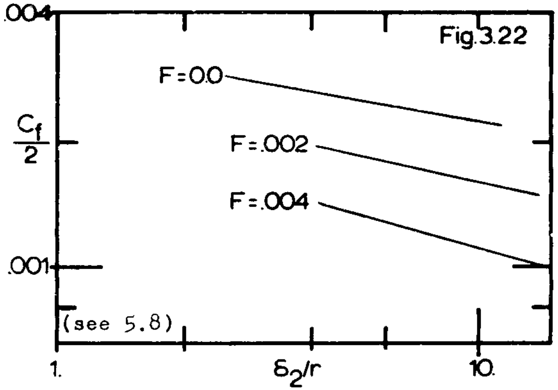

Fig. 3.22 Friction factor with blowing.

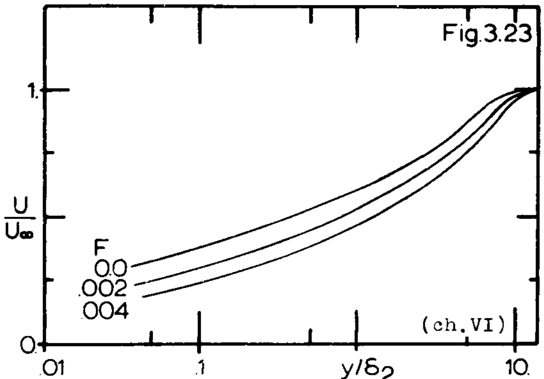

Fig. 3.23 Rough surface mean velocity profiles with different F.

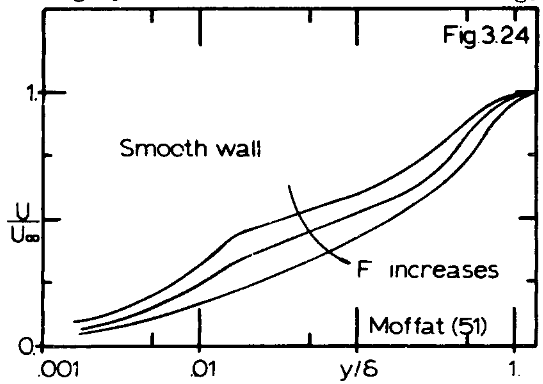

Fig. 3.24 Smooth wall mean velocity profiles with different F.

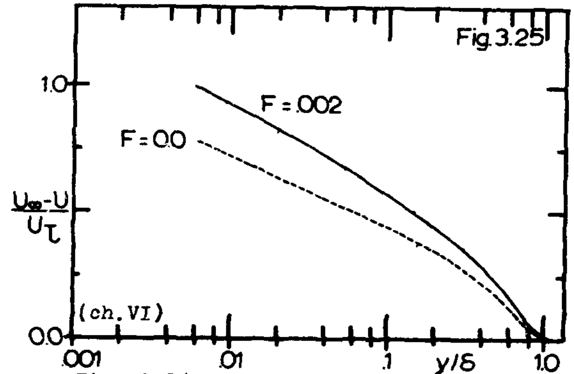

Fig. 3.25 Effect of blowing on velocity defect profile.

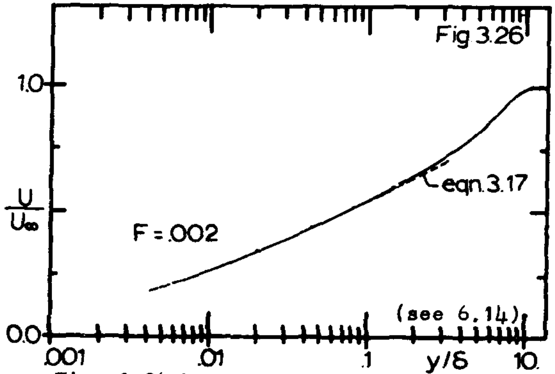

Fig. 3.26 Near wall velocity profile with blowing.

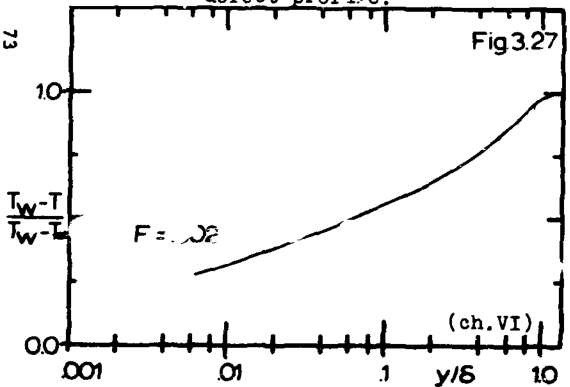

Fig. 3.27 Near wall temperature profile with blowing.

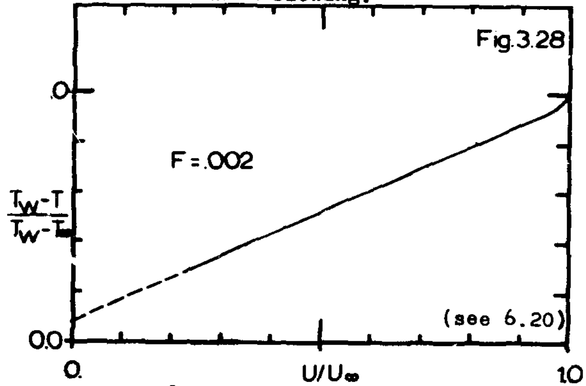

Fig. 3.28 Mean temperature-mean velocity profile with blowing.

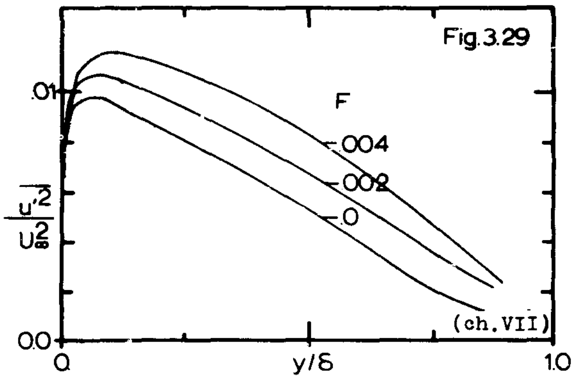

Fig. 3.29 Effect of blowing on $\overline{u'^2}/U_\infty^2$.

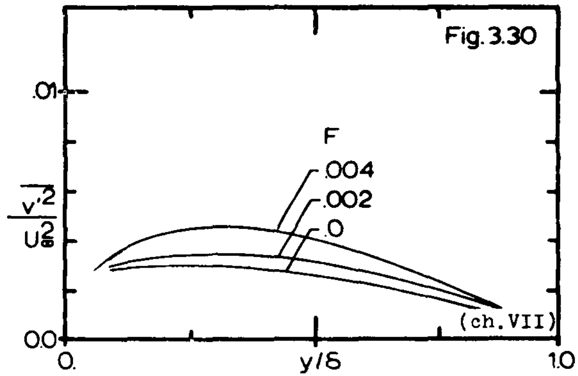

Fig. 3.30 Effect of blowing on $\overline{v'^2}/U_\infty^2$.

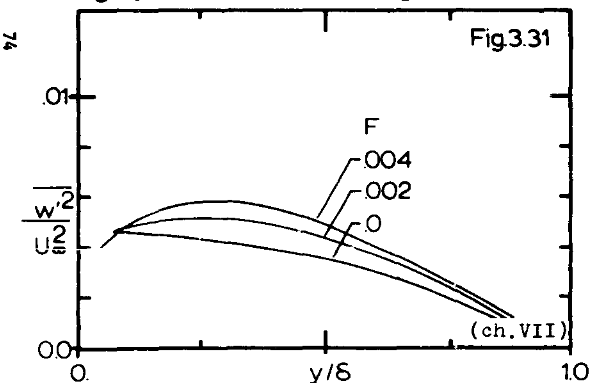

Fig. 3.31 Effect of blowing on $\overline{w'^2}/U_\infty^2$.

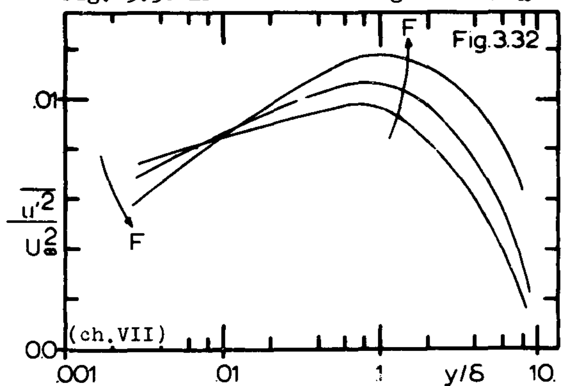

Fig. 3.32 Near wall behavior of $\overline{u'^2}/U_\infty^2$ with different F.

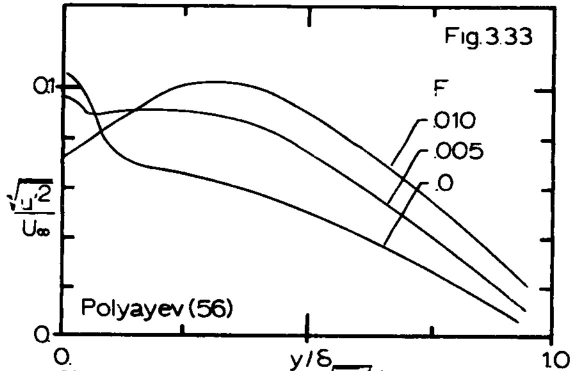

Fig. 3.33 Smooth wall $\sqrt{u'^2}/U_\infty$ profiles with different F.

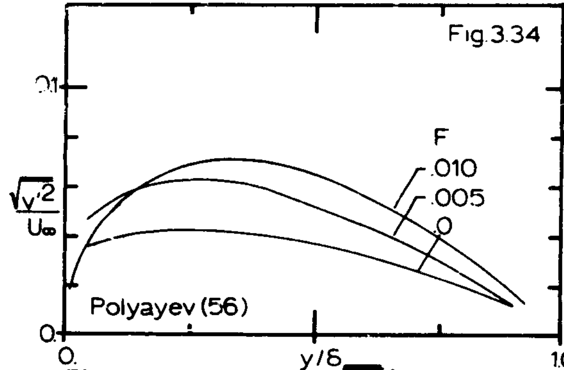

Fig. 3.34 Smooth wall $\sqrt{v'^2}/U_\infty$ profiles with different F.

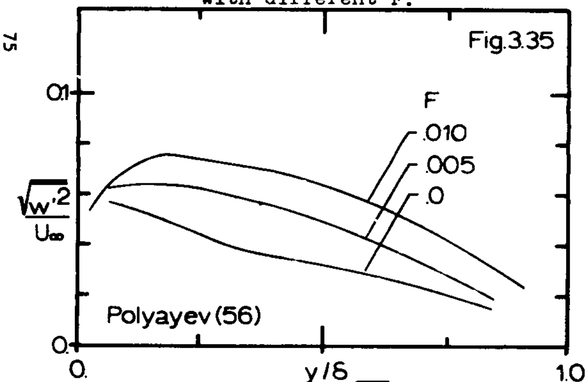

Fig. 3.35 Smooth wall $\sqrt{w'^2}/U_\infty$ profiles with different F.

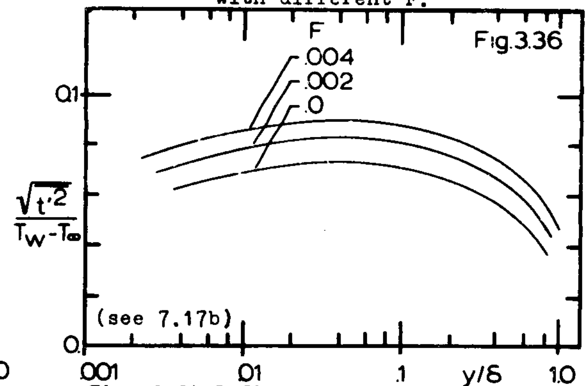

Fig. 3.36 Influence of blowing on temperature fluctuations.

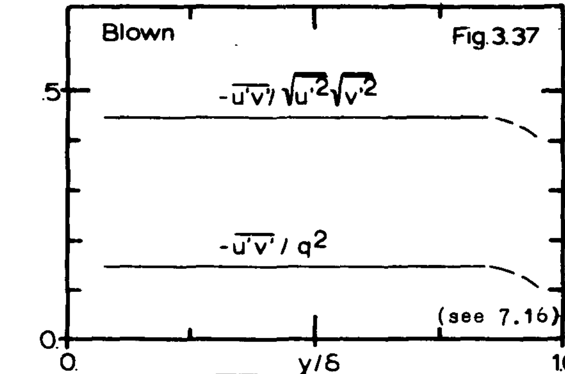

Fig. 3.37 $-\overline{u'v'}$: effect of blowing on correlations.

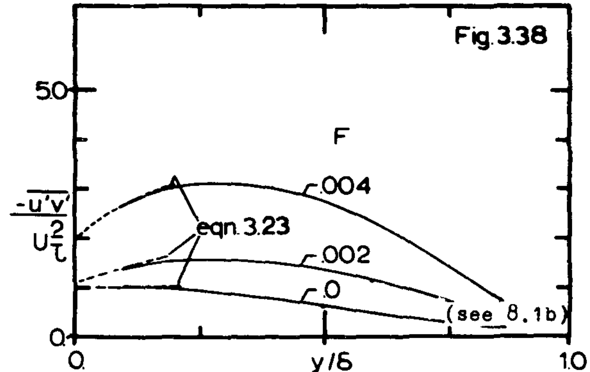

Fig. 3.38 Turbulent shear stress with blowing.

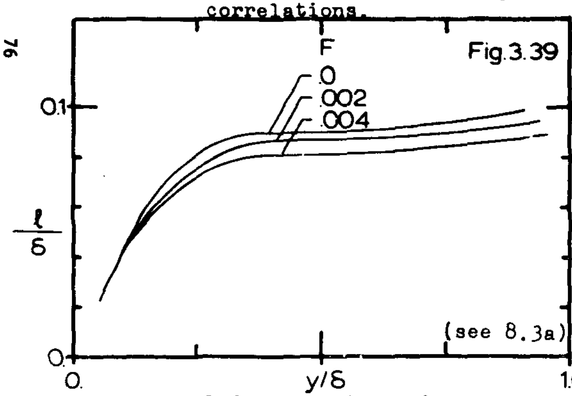

Fig. 3.39 Influence of blowing on outer region mixing-length.

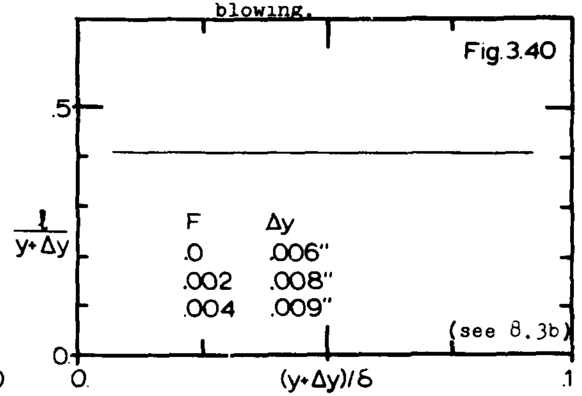

Fig. 3.40 Near wall mixing-length.

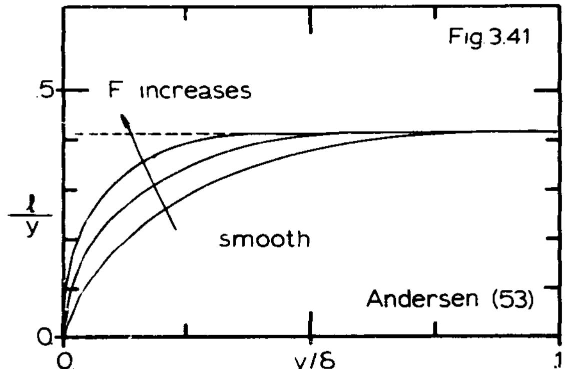

Fig. 3.41 Influence of blowing on near smooth wall mixing-length.

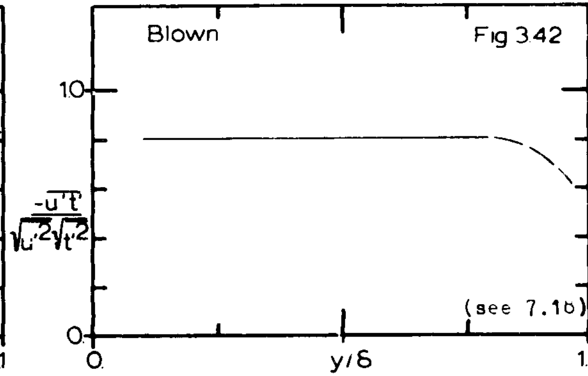

Fig. 3.42 $-\overline{u't'}$: correlation coefficient.

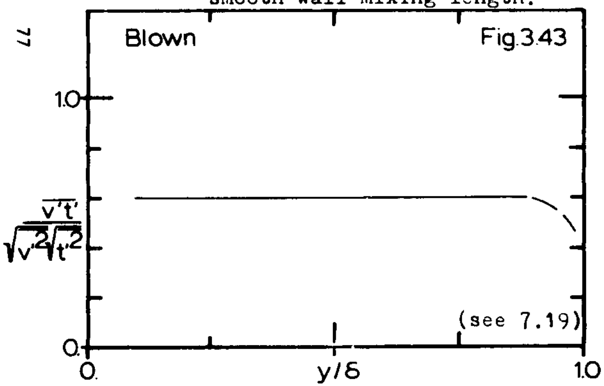

Fig. 3.43 $\overline{v't'}$: correlation coefficient

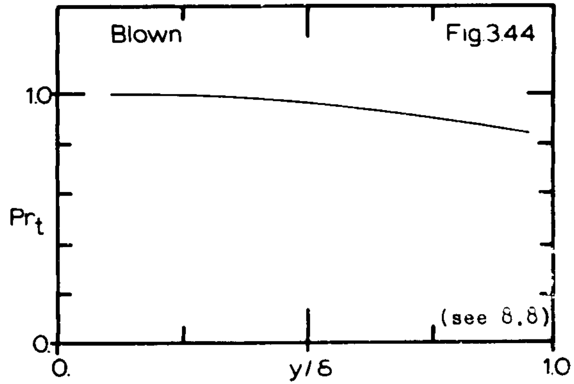

Fig. 3.44 Turbulent Prandtl number.

CHAPTER IV

APPARATUS AND INSTRUMENTATION

The apparatus used in this study was built by Healzer [4] for his experiments in heat transfer with blowing. It will be referred to as the Roughness Rig. The Roughness Rig has its basic design based on another existing heat transfer facility that has been used over the past few years by the Heat and Mass Transfer (HMT) Group at Stanford. Several studies on the transpired turbulent boundary layer on a smooth surface were conducted in this HMT apparatus, which was described first by Moffat [51]. References [39,40,53,59,60,61,62] describe the modifications made to it along the years.

The Roughness Rig is a closed loop wind tunnel using air at approximately atmospheric conditions. The test section, which is 4 x 20 inches at the inlet, consists of a rectangular, variable height duct, 8 feet in length. Its test surface consists of a 24 - segment porous plate, 18 inches wide, forming the bottom wall of the duct. Figure 4.1 shows a flow diagram of the rig which has four main systems: the main air system, the transpiration air system, the plate heater electrical power system, and the heat exchanger cooling water system. A photograph of the Roughness Rig is shown in Figure 4.2. A brief description of the four main rig systems will be given below, having in mind Figure 4.1.

4.1 The Main Air System

The main air flow path is: (1) main air blower and velocity control, (2) overhead ducting to an oblique header, (3) main-stream heat exchanger, (4) screen box and filter, (5) nozzle to test section inlet, (6) 8 feet long test section and (7) a multistage diffuser which returns the mainstream air back to the blower.

The main air supply blower is a 445-BL Class 3 Buffalo Blower that delivers 8300 cfm at 12 inches of water and is driven by a 20 horsepower motor by means of pulleys and belts. They are mounted on a seismic base, so as to minimize vibration. Flexible boot connections reduce the transmission of mechanical vibrations from the blower to the remainder of the tunnel and test section.

The main air stream velocity in the test section is varied by changing pulleys and belts on the blower and drive, and by means of a controllable restriction imposed on the flow at the outlet of the blower. In order to obtain a continuous variation of air velocity a gate valve was designed and inserted in the main air system. This represents a modification on Healzer's [4] original apparatus. It consists of a plywood box having two 1/8" thick aluminum plates as gate valves running perpendicular to each other. This allows continuous control from zero-flow to unrestricted flow, and increased the capabilities of the rig that had a discrete set of pulleys and belts.

A 24" dia. galvanized sheet metal overhead duct delivers the air to an oblique inlet header on the main-stream heat exchanger. The header was designed to provide uniform flow distribution and low pressure loss.

The main air stream temperature is controlled by means of a 5 row, 33" x 48" heat exchanger, which is supplied with cooling water continuously pumped from a holding tank. The cooling water temperature is adjusted until the desired main-stream air temperature is achieved. The measurement of turbulent quantities usually required an eight to ten hour period, during which the control of this temperature was critical. As main air temperature fluctuations can impair those measurements special attention was given to this control.

The cooling water is pumped through the main-stream heat exchanger and the transpiration heat exchanger, forming a composite system with a slow response to adjustments. But despite this and the sizeable ambient temperature variations during the day, the drift in main-stream temperature was always less than $0.3^{\circ}F$ for each one of the measurement time periods.

Following the heat exchanger there is a filter and a screen box. The insertion of a filter made of a single sheet of linen was made after a succession of hot wire probes broke due to dust inside the wind tunnel. The screen box contains four stainless steel, #40 mesh, .0055" dia. wire screens. The function of this set of screens is to reduce non-uniformities in the mean field velocity and the turbulence level of the main air stream.

Following the screens, the flow enters a nozzle with a 19.8 to 1 area contraction. A two-dimensional contraction nozzle was designed to smoothly accelerate the flow with no separation at the nozzle inlet or outlet.

The test section consists of the test plate assembly, the two side walls and a flexible top wall. These walls are made of 1/2 inch thick plexiglass. The top wall can be adjusted to give a variable flow area in the flow direction. In these experiments it was conformed so as to produce a zero static pressure gradient along the test section.

The side walls contain two sets of static pressure taps, 2 and 12 inches apart in the flow direction. The second set was used to position the top wall to produce the run condition. An aluminum probe sled, which spans the test section, locks onto the side walls in fixed positions over the center of each of the 24 test plates. This sled supported the probes used in this experiment, which extended down through access holes in the flexible top wall.

The air coming from the test section flows into a ≈ 7:1 multistage vaned diffuser. Its inlet section has an adjustable top so it can be kept aligned with the test section top. There follow three separate, vaned, two-dimensional diffusion sections that open to a plenum box. This diffuser recovers approximately 40% of the kinetic energy head.

Finally, a small charging blower attached to the plenum box is used to control the static pressure of the test section and maintain it equal to the ambient pressure.

We should stress that in all runs, as in Healzer's [4], no boundary layer trip was used, so natural transition to the turbulent state was obtained.

4.1.1 The Test Plate Assembly

The bottom wall of the test section constitutes the test surface of the Roughness Rig. It consists of 24 individual porous plates mounted in four separate aluminum base castings. A cross section through one of the plates and casting is shown in Figure 4.3. It shows a typical transpiration compartment and plate assembly.

Transpiration air coming through the delivery ducts is diverted by a baffle-plate and enters a pre-chamber. The upper surface of this inlet plenum is a porous bronze preplate which protects the test plate and serves to decrease a possible maldistribution of air flow to the test plate.

The transpiration air temperature is monitored by a thermocouple located in the center of a small chamber above the pre-plate. The air then passes through a layer of honeycomb having openings with 3/16 inch dia. and 3/8 inch thick, attached to the bottom surface of the test plate.

The aluminum castings have their temperature controlled by cooling water tubes and monitored by thermocouples, both installed in the casting webs.

Each test plate has the dimensions 18.0 x 4.0 x .5 inches. They are made of O.F.H.C. copper balls, .050 inches in diameter, arranged in eleven layers in their most dense array. The balls received a plating of .005 inches of electroless nickel and were then brazed together. The plates have a well defined surface roughness pattern and are uniformly porous for the transpiration experiments. Uniformity in plate permeability was checked in place, with everything assembled. As discussed by Healzer [4] and Pimenta [54] no significant variation of the porosity was noticed. A close-up picture of the plate is shown in Figure 4.4. Details of its construction are discussed in Healzer [4].

Each plate is supported along its long edges by a 1/32 inch thick phenolic stand-off that thermally insulates it from the base casting and prevents air leakage between compartments. The plate ends are insulated from the casting sides by strips of balsa wood.

Plate thermocouples were embedded to a depth of .068 inches below the top of the surface layer, which located their junctions at the center of the ball layer just below the surface layer. There are five of them wired in parallel, so an average temperature of each plate is measured.

4.2 The Transpiration Air System

The transpiration air flow path is: (1) filter box, (2) transpiration blower, (3) transpiration heat exchanger, (4) header box, (5) delivery tubes (one to each porous plate).

Air enters the system through a filter box, made using 5 micron retention filter felt material.

The transpiration air supply blower is a Buffalo type V, size 25 blower driven by a 15 horsepower, 3600 rpm motor. The flow rate is controlled by individual ball valves in each delivery tube.

Air is delivered by a 10 inch diameter flexible duct to a box containing the transpiration air heat exchanger with a by-pass system to control mixing. This 5 row, 18 x 24 inches heat exchanger receives its cooling water continuously pumped from the storage tank. The water runs in series through the heat exchangers for the main and the transpiration air.

Transpiration air, then, leaves to a header box that distributes it to each supply line, one for each of the 24 porous plates.

The 3 feet long, 1 inch dia. delivery tube connects the header box to the control ball valves. At midway of each tube is located a constant current hot-wire type flowmeter. Each flowmeter was calibrated for the range 1 to 70 cfm. This design was selected due to a wide range of operations needed for the Roughness Rig. A thorough discussion of this system is found in Healzer [4].

The delivery lines and header box have been insulated to minimize the interaction between the transpiration air and the surroundings, and to guarantee a uniform temperature of the delivered air to each test plate assembly.

Finally, a 1 inch flexible hose connects each control valve to the test plate assembly.

4.3 The Plate Heater Electrical Power System

A 750 amp, 24 kw Lincoln Arc Welder supplies power to the plate heater. Its constant 22 volts D.C. output is delivered to a bus bar box mounted on the side of the Roughness Rig through an overhead copper bus bar system. From the bus bar system, power goes to each heater. Each plate has its own heater wire glued into eight equally spaced grooves in the underface. The heater consists of a single piece of #26 AWG stranded copper wire with irradiated PVC insulation. This allows one to vary the power to each plate individually and to maintain a uniform surface temperature. Plate power is controlled by individual solid state amplifier circuits, one for each plate, by which one can adjust the heater voltage. A detailed description of the power control is given in Healzer [4]. One heater lead is connected to a precision ammeter shunt, one for each plate, and the other lead to a power transistor which is part of the power controls.

Measurement of the power delivered to each heater is made by measuring the voltage drop across the heater and across the precision shunt in the heater circuit. The heater and shunt voltages are read in selector switch read-out boxes. The power amplifiers play no role here: the data are independently read, not "presumed" from amplifier settings.

4.4 The Heat Exchanger Cooling Water System

Cooling water continuously pumped from a holding tank is supplied to the two heat exchangers in a series circuit. A flow rate of about 31 gpm is maintained with the objective of minimizing temperature gradients in the heat exchangers and insuring uniform air temperature.

Temperature control of the cooling water is by means of make-up water from the building supply line, replacing a portion of the water returning from the heat exchanger, which is dumped. The make-up water is mixed in the holding tank to provide damping of possible temperature fluctuations in the supply water. It was later verified that in off-peak hours, this holds a more constant temperature than we expected.

4.5 Rig Instrumentation

4.5.1 Temperature Instrumentation

Temperature measurements on the Roughness Rig are made using iron-constantan thermocouples. This does not include the boundary layer probing, which was done using hot wire anemometry. The thermocouples are all brought together at a common test console zone box. Rotary switches select individual thermocouples for read-out. The entire thermocouple circuit uses a single ice-bath reference junction and the output is measured with a Hewlett-Packard Integrating Digital Voltmeter, Model 2401C.

Despite all the care taken by Healzer [4] with the insulation of the zone box, extra effort was put into it. It was found that sun light during the day, even diffusively, hit the zone box causing temperature stratification problems. An additional layer of insulation material was applied to the zone box and a plywood cover now protects it from being damaged.

The ice-bath received also special attention. Our normal runs, usually, took eight or more hours, longer than the Dewar flask would remain full of ice. Temperature drifts of $1^{o}F$ were observed in the reference temperature during this long period of time. To avoid this, we replaced the ice-bath with a new one every two or three hours.

4.5.2 Pressure Measurement

Pressure measurements were made with manometers and transducers. The tunnel static pressures were measured using an inclined Meriam manometer, with a 0.824 specific gravity fluid of 3.0 inch range. This manometer was calibrated against a 30" Meriam Micromanometer model 34FB2.

The mainstream total pressure and pressures used in calibration of the hot wire velocity probes (in the calibrator) were measured with two pressure transducers. They consisted of two Statham unbonded strain gauge differential pressure transducers.

a PM5 : pressure range 0 to 0.5 psi
practical air velocity range ~50 to ~250 ft/sec

a PM97 : pressure range 0 to 0.05 psi
practical air velocity range ~5 to ~50 ft/sec.

Each unit was provided with a zeroing circuit and carefully calibrated in the Thermosciences Measurements Center against the 30" Meriam Micromanometer with compensation for ambient temperature variation. The calibration curve was checked several times. Each was found to be linear and stable to ± 0.001 inches of water for the interval 10% to 80% of its range. The Hewlett-Packard integrating digital voltmeter model 2401C with an external quartz crystal oscillator clock was used to read the transducers. We always integrated the signal for 10 seconds, and very low signals for 100 seconds.

4.5.3 Flow Rate

Transpiration air flow rates for each plate were measured by means of a specially designed hot-wire type flow meters using a differential thermocouple sensor The signal coming from the differential thermocouple, proportional to hot-wire to air temperature difference, was calibrated as a function of flow rate. The hot-wire operated in the constant current mode. The flowmeter heater current was always set exactly the same as during calibration.

Measurement of relative humidity, of the inlet air pressure by means of a water manometer and of inlet air temperature to the delivery pipe by a thermocouple allowed calculation of the actual flow rate from the reading, the calibration curve, and the data.

The same conversion computer program, FLOMET, used by Healzer [4] was used throughout this study.

The flowmeters were calibrated against ASME orifice meters in the Thermosciences flow bench, and a 1% accuracy is attributed to this calibration.

4.5.4 Electric Power Measurement

The D.C. electric power delivered to each plate is measured in a simple way. The voltage drop across each plate heater was measured directly. Each heater current was measured individually using a calibrated ammeter shunt and measuring the voltage drop. These shunts had their resistances checked periodically during the research. The values were stable.

All voltages were read using the Hewlett-Packard 2401C IDVM.

Plate power calculations were made in a computer data reduction program. This takes also into account energy losses, energy exchanged with the transpired air and, by an energy balance operation, gives the energy transfer to the boundary layer and Stanton numbers. This is further discussed in Chapter V.

4.5.5 Main-stream Conditions

The main-stream conditions: temperature, total-to-static pressure, and static pressure distribution along the test section were carefully set, controlled and monitored for each run.

Main-stream temperature was measured using a calibrated probe made of 0.004 inch iron-constantan thermocouple wire. This probe was a fixed position version of the traversing probe described by Kearney [40]. The probe was calibrated in an oil bath at the Thermosciences Measurement Center against a Hewlett-Packard Model DY-2801A quartz thermometer. A linear curve fit to the calibration points was used with a maximum difference of $\pm 0.07^{\circ}F$ observed.

The main-stream total pressures were measured with a Kiel-type probe located in the center of the potential flow region. Static pressures were taken from the wall taps in the same cross-section of the tunnel. Each static wall tap has an 0.040 inch diameter hole with sharp edges at the wall plane. The pressures were taken using the pressure transducers.

The static pressure distribution for each run was set to produce zero pressure gradient and to have its level as close as possible to ambient conditions. It was measured through the wall taps by the 3" inclined manometer.

4.6 Set-up of Boundary Conditions

Special care was taken as each run was being set-up. This was considered important to insure the reproducibility of the rough w oundary layer data.

For all runs considered in this study the boundary conditions were:

- constant and uniform wall temperature,
- constant and uniform blowing rate,
- steady and constant free-stream velocity along the test section (or zero static pressure x-gradient),
- steady and constant free-stream temperature .

The major adjustments were made with the flow field still isothermal, i.e., without heating the plates. The proper combination of pulleys were chosen for the main blower, and then, using the control valve, the desired air velocity was set at exit of the nozzle.

Next, the flexible top wall was adjusted to give a zero pressure gradient (uniform main-stream velocity). Static pressures were measured from 12 inches apart wall pressure taps. For all runs no change between two taps was more than 0.003 inches of water. This was done at the same time the transpiration air flow rates were being set and the tunnel static pressure maintained with the charging blower at atmospheric value. The whole procedure was iterative and was performed working from the nozzle, down the test section to the diffuser.

As the wind tunnel is closed loop, every adjustment interacted with each of the others in the most complicated way. The process was time consuming but normally the final free-stream velocity was within a couple of percent of the desired values. Care was taken to repeat this velocity within 1% of its value, so readjustments were sometimes made necessary.

The plates were then heated for the non-isothermal [illegible]s, and the power to them iteratively adjusted to obtain a constant [illegible] temperature ($\pm 0.5^{o}$F maximum). The small wall-to-free stream temperat[illegible] difference (25 - 30^{o}F) had no appreciable effects on the hydrodynamic conditions already set. Both the hydrodynamic and thermal conditions were reset before each run to take into account different ambient conditions.

The main-stream temperature was controlled by varying the amount of make-up water admitted to the holding tank from the supply line. During each run it was monitored by a calibrated thermocouple using a separate VIDAR digital voltmeter from a VIDAR 5206 D-DAS Data Acquisition System employing a D.E.C. PDP 8/L Computer. Readings were taken every half minute, and the free-stream temperature could then be controlled so as to not vary more than 0.2^{o}F from set value.

4.7 Hot Wire Instrumentation

The instrumentation used throughout this study is schematically represented in Figure 4.5. It consisted of:

A DISA 55D01 system used as a constant temperature anemometer. Gains and filters used guaranteed flat anemometer response for all frequencies encountered in our flow conditions. Input adjustments for cable compensation were made to render both probes used (horizontal and slant wires) to have balanced bridges. These adjustments were somewhat tricky and required special choice and matching of cables and probes. They were not altered in any circumstance for a given pair of probes throughout their useful lives.

A DISA 55M01 unit used with a constant current bridge (DISA 55M20). This unit has low levels of noise and amplifier drift, and high sensitivity for temperature measurements can be obtained with very high amplifier gains (3500). Velocity contamination in the anemometer response for temperature measurements can almost be eliminated by using very low probe currents: 2 mA for the two 5 microns tungsten wires.

A DISA 55D65 Probe Selector with very low contact resistance was used to switch the hot wire probe between the constant current mode of operation (connection to 55M01) to the constant temperature mode of operation (connection to 55D01).

A DISA 55D15 true rms meter. This unit was calibrated at the Thermosciences Measurement Center against standard sine waves having known rms values to give a 1% accuracy on the measured value.

(Note that no linearizer was used)

A Hewlett-Packard 2401C integrating digital voltmeter for reading the anemometer and rms meter outputs. An external crystal excited clock was used to control the integration time of the HP 2401C unit 1, 10 or 100 seconds.

Two hot-wire probes mounted on specially designed probe holders.

One DISA 55P05, a 5 micron tungsten wire, gold-plated, boundary layer probe (horizontal wire).

One DISA 55F02, a 5 micron tungsten wire, gold-plated, 45° slant probe (slant wire).

Both probes can be seen in Figure 4.6.

4.8 Hot Wire Probes

4.8.1 Horizontal Wire

The horizontal wire probe and its support is represented schematically in Figure 4.7. It is very similar to the ones used by Andersen [53] and Orlando [17], but was built specially for our application.

The hot wire element is a DISA 55P05 boundary layer probe. The wire is 3 mm long, 5 microns in diameter, gold plated to a diameter of 30 microns outside of the sensitive portion, which in our case was 1.2 mm long.

This probe was chosen due to the low aerodynamic interference of its supports, as suggested by Rasmussen et al. [63] for good measurements. Also, because its long prongs are of the boundary layer type, it is good for temperature measurement according to Maye [64]. In use, its prongs were always kept oriented parallel to the direction of the mean flow, to reduce prong interference (Thinh [65]).

The size of the probe allowed measurements very close to the wall, in fact, 0.007 inch from the top of the balls.

The probe has a keel that prevents the wire from hitting the wall. This keel acts like a wall stop, and was specially designed for our application. It is 0.110 inch long and 0.055 inch wide, so in its closest position to the wall it is always hitting the crest of at least one ball of the surface layer. Let us recall that the copper balls have 0.050 inch diameter and are arranged in the densest way, with their crests coplanar.

The distance from the wire to the plane of the bottom of the keel was measured by an optical comparator for every wire we used. This distance was 0.006 or 0.007 inch depending on the case. We must stress that several wire probes were used with the same probe holder.

When the wire probe was mounted to the holder, an optical comparator was used to check its alignment.

During boundary layer traverses the probe holder was supported by a special sled that spanned the tunnel and rested on the side walls. Two locating pins and two set screws fixed the sled to the walls perpendicular to the side walls. The horizontal wire was aligned with the flow by matching machined marks on the holder and sled. This alignment is not too crucial because the horizontal wire response was found to be insensitive to yaw misalignments of up to 5°.

The probe was translated by means of a micrometer head traverse mechanism. The probe was lowered until, visually, one could see the keel touch the wall. The probe was then advanced 0.002 inch to compensate for micrometer backlash, and then the traverse begun. Readings of velocity and temperature were then taken for every 0.001 inch, until two successive settings gave different values of temperature and velocity. At this point one assumed the probe had left the wall. This, according to Orlando [17], gives a maximum uncertainty band of ± 0.001 inch.

The horizontal wire was used for measurements of quantities such as:

U mean velocity profile,

T mean temperature profile,

$\overline{u'^2}$ longitudinal velocity fluctuation profile,

$\overline{t'^2}$ temperature fluctuation profile,

$\overline{u't'}$ longitudinal velocity-temperature correlation.

4.8.2 Slant Wire

The slant wire probe and its supports are represented schematically in Figure 4.8. It is similar to the ones used by Andersen [53] and Orlando [17], but was built specially for our application.

The hot wire element is a DISA 55F02 5 micron tungsten, 45° slant wire. The wire is 3 mm long, with 1.2 mm sensitive center portion and gold plated ends. It is mounted on a rotatable spindle of the probe holder, and has its prongs parallel to the mean flow direction at any angle of rotation.

The choice of this probe was based on the experience gained by the use of similar probes by Andersen [53] and Orlando [17]. Also, its directional sensitivities are well known and documented in Jorgensen's [66] work as discussed in Appendix B.

The hot wire probe has its rotatable spindle activated by a cable drive, which can be operated with the probe inside the tunnel. The "lock-drum" system of the spindle has eight radially drilled holes spaced at 45°. A lever located on top of the micrometer traverse mechanism activates a spring loaded pin that locks the spindle in place by fitting into one of the holes. For our probe the wire can be oriented at eight different angles:

$$\theta_n = n\frac{\pi}{4} \; ; \; n = 1, \ldots, 8$$

The angle values were chosen to insure maximum versatility in measurements. $\theta = 90°$ was used for those mean velocity measurements needed for determining the sensitivity coefficient used in fluctuation measurements. Other angles were used for measurement of shear stress, two-dimensionality check, etc. No mean velocity, as such, is reported from slant wire results.

This probe conforms to standards of low prong interference described by Rasmussen et al. [63].

The size of the probe and spindle limited how closely one could approach the wall. A minimum distance of 0.125 inch was used. The probe has also a keel designed for our application. It is cylindrical, 0.110 inch long and has 0.250 inch diameter. When the keel touches the wall the hot wire has its center 0.125 inch from the top of the balls. This distance was measured with an optical comparator. The positioning error was estimated to be ±0.002 inch. To start the measurements the probe was lowered until the keel touched the wall lightly but the spindle could still be smoothly rotated.

The angles of the prong system with respect to the wall for the different holes in the lock-drum were measured by means of a toolmaker's microscope. They were verified to be 45° apart with a maximum difference of less than 0.5°. The measurement of the wire angle and its positioning in the spindle during mounting procedure was done using an optical comparator. For each different probe used, the wire angle was within about $\pm 0.75^{\circ}$ of the nominal value of 45°. The actual angle was used in all data reduction.

When the probe was in place supported by the sled, the alignment of the hot wire spindle with the mean flow direction was done in the freestream as in Orlando's [17] work. The wire was placed in the horizontal plane ($\theta = 90^{\circ}$, 270°) and measurements of the velocity were made in this plane for the two θ's . The whole probe holder body was then rotated around its axis, changing the yaw angle of the probe until the difference between the two electrical signals ($\theta = 90$, $\theta = 270^{\circ}$) read by the Hewlett-Packard IDVM was less than 3 mV from a 3 V signal. This corresponds to an error of less than 0.2 ft/sec in mean velocity. Because of the slant wire's high angular sensitivity this procedure was used instead of a mechanical one.

The slant wire was used for measurements of quantities such as:

$\overline{u'v'}$ shear stress,

$\overline{v'w'}$, $\overline{u'w'}$ Reynolds stress components,

$\overline{v'^2}$ normal velocity fluctuation profile,

$\overline{w'^2}$ transverse velocity fluctuation profile,

$\overline{v't'}$ turbulent heat flux .

4.8.3 Mysterious Wire Breakage

A great deal of effort and time was put in this study to prevent the breakage of hot wires. It was expected from Andersen's [53] and Orlando's [17] previous experience that the probes DISA 55P05 and 55F02 would be strong and survive all measurements and calibrations.

Several wires had to be used and calibrated during this study.

A filter was introduced in the tunnel loop to reduce the dust in the air fearing that the closed loop tunnel was working as a dust trap. This reduced the frequency of broken wires, but even after the filter was installed, the slant wire probes systematically broke without any perceptible reason. During four months eight wires failed, each representing nearly 50 hours of effort in fabrication and calibration.

Finally, strain gages were attached to the probe spindle and stem, to allow us to investigate the problem of shock and vibration in service, and to determine whether or not the system had any resonant frequency which was excited at any operating condition. We operated the hot wire following all normal procedures during calibration and data-taking, monitoring the output with an oscilloscope. The only abnormal behavior, which we observed, occurred when the set-screw of the probe holder was being tightened. Very sharp oscillations were produced in the probe stem as a result of stick-slip behavior in the set-screw. The threads were cleaned up and lubricated. The same procedure was repeated and no shocks were observed. Although the "cure" seemed trivial, and unlikely to succeed, the problem seemed to be solved, and no further wires were broken.

4.9 Hot Wire Procedure and Calibration

The mean velocity and temperature across the boundary layer were sequentially measured with the same hot wire probe at the <u>same</u> physical location. This means that, during a boundary layer traverse, the probe was brought to each location and held there while measurements were made of both velocity and temperature.

First, the temperature was measured using the constant current anemometer, the probe working as a resistance thermometer. The probe was then switched to the constant temperature anemometer and the velocity measured.

This method was used based on the experience gained from Orlando's [17] work. Two objectives were in mind:

eliminate spatial uncertainty in location of the probe which arises from having to combine isothermal velocity profile data with temperature profile data taken at a different time;

save time since our primary concern was non-isothermal cases involving heat transfer.

As no temperature compensating probe was used, and we also wanted information about the temperature field, a linearizer circuit was not employed. Measurements without a linearizer have been reported in the literature (Klebanoff [15], Orlando [17], Watts [67]). As we never had turbulence intensity larger than 25% of the local mean value, the linearizer circuit was not needed. According to Sandborn [68] no improvement in measurement quality would be obtained with its use in our case.

4.9.1 Calibration for Temperature Measurements

The calibration of both probes: horizontal and slant wires, for temperature measurements used the same procedure and equipment as in Orlando's [17] work.

It was done in a variable temperature oil bath (Rosemount Engineering Co. Model 910A) controlled by a Thermotrol Model 910-508 with a resistance thermometer sensor. The oil bath temperature was monitored by a Hewlett-Packard Model DY-2801A quartz thermometer.

The wire probe was placed inside a 1/2 inch diameter copper tube, to protect and avoid its contamination. The tube was sealed with a rubber cork and immersed in the oil bath. The air gap inside the tube was baffled to prevent circulation in an attempt to make the air isothermal near the wire.

The circuit used (cables, switches, probes, etc.) for calibration was the same as that used for measurements (see Figure 4.5) throughout this work: the DISA 55M01 unit with the constant current bridge DISA 55M20. The output was read by the Hewlett-Packard 2401C integrating digital voltmeter.

Calibrations were performed for the range of temperatures between $60^{\circ}F$ - $110^{\circ}F$, using at least 12 points, evenly spaced, over this range.

For each temperature the anemometer time averaged output E^* and the wire resistance R_w were measured. The superscript * refers to the constant current mode of operation. A straight line curve fit was used for both, giving:

$$E^* = A^*T + B^* \tag{4.1}$$

$$R = C^*T + D^* \tag{4.2}$$

A^* and C^* are real constants for each wire and calibration. B^* and D^* were shown by Orlando [17] to vary slightly for the same wire and cables, with each connection and disconnection of the plugs. This variation was attributed to changes in contact resistances of different plugs of the cables. This situation has largely determined the procedure which had to be followed during the measurements, as it is discussed in Section 4.10. Values of A^* varied around -0.062 V/°F and values of C^* varied around 0.0075Ω/°F for the temperature wires. The maximum departure from the straight lines fitted through the calibration points was always less than 0.08°F.

4.9.2 Calibration for Velocity Measurements

a. CALIBRATOR

The calibration of the horizontal and slant wire probes for velocity measurement was made in a variable temperature and variable velocity air jet. This jet was provided by an apparatus especially designed for this purpose which will be referred to as the CALIBRATOR. A schematic diagram is shown in Figure 4.9. It is operated using air supplied by the transpiration air system blower, and has its temperature controlled by the secondary heat exchanger.

The air velocity is controlled in the control box. Gate valves partly block the flow and dump some of the air to the room. The air then goes through a heater that gives a finer control of the air temperature. The heater is made of a long Alumel coil suspended inside a 1-inch dia. PVC pipe and is electrically heated. A rheostat controls the power to the heater element. Leaving the heater the air enters the CALIBRATOR through a mixing chamber and air filter, both thermally insulated. The mixing chamber is to insure temperature uniformity and the filter takes out dust to minimize wire breakage.

A thermally insulated 3-inch dia. PVC pipe, 3 feet long follows the filter. At the inlet a set of honeycomb flow straighteners and a set of screens, take out the swirl and damp the fluctuations of the air flow. The long pipe insures a fully developed flow and was dimensioned according to ASME recommendations.

The probes were calibrated in the free jet at the exit of this pipe where there is a 20:1 contraction ASME nozzle. The probe holder is held by an external support attached to the CALIBRATOR.

The aluminum nozzle is heated from the outside by an electrical resistor wrapped around it to minimize heat loss to the ambient. Its temperature is monitored and maintained exactly at the air temperature flowing inside the duct.

There is a static pressure tap in the pipe wall located before the entrance to the nozzle following ASME recommendations. The air temperature is measured by a calibrated iron-constantan thermocouple located on the centerline and half way up the pipe, also following ASME recommendations.

The distribution of air velocity in the jet was checked with a total pressure probe. It was uniform across most of the jet, and for the range 0-250 ft/sec it could be determined from the plenum chamber static pressure measurement with no measurable error. This defined a workable region in shape of a cone with 1/2 inch in height and 1/2 inch in base diameter. The temperature was also very uniform. The jet turbulence level depended somewhat on the blower used, but in our operations with the transpiration air blower this level was less than 0.8%.

The static pressure in the plenum which is equal to the total pressure of the jet at the nozzle exit, was read by the pressure transducers. We used the Hewlett-Packard 2401C integrating digital voltmeter, with an external oscillator, to give an integration time of 10 seconds. This voltmeter was also used to read the thermocouples and the anemometer output.

The CALIBRATOR allows expeditious velocity calibrations at various constant air temperatures that, otherwise, could not be done in our closed-loop wind tunnel. It can cover all the velocity range of interest.

b. Calibration

We used the circuit shown in Figure 4.5, having the constant temperature anemometer DISA 55D01, for calibration and measurements.

Each wire was calibrated twice, having two different operating wire resistances R_w. The calibrations, at two overheating ratios, were: one with overheat of around 2.5 ohms (high overheat ratio) and the other with overheat of around 1.5 ohms (low overheat ratio). Thus, two calibrations per wire were made for the range of velocities 15 ft/sec to 150 ft/sec, at a constant air jet temperature between $75^{o}F$ and 80^{o}. This temperature range was chosen because it corresponds to the average temperature expected in the boundary layer traverses. These calibrations were used for the data reduction throughout this study.

For each calibration point (over 35 points covering the velocity range) it was determined:

E anemometer time averaged output using the Hewlett-Packard 2401C with 10 seconds of integration,

R cold resistance of the wire,

U air velocity .

The calibration was correlated in the form

$$\frac{E^2}{R_w - R} = f(U) \tag{4.3}$$

This was chosen following suggestions by Sandborn [68] and Orlando [17].

A curve fit of the data provided us with a functional form for $f(U)$. The data was divided into two intervals because of our very extensive range. A spline curve fit, matching the values of the functions $f_1(U)$ and $f_2(U)$, and the first and second derivatives of f_1 and f_2 at an intermediate point gave:

$$\frac{E^2}{R_w - R} = f_1(U) = A_1 + B_1U^{0.5} + C_1U + D_1U^{1.5} \qquad (4.4)$$

for $E < E_b$

$$\frac{E^2}{R_w - R} = f_2(U) = A_2 + B_2U^{0.5} + C_2U + D_2U^{1.5} \qquad (4.5)$$

for $E > E_b$

E_b corresponded to velocity $\simeq$ 75 ft/sec.

A curve fit was made for each of the two overheat ratios, and for each fit no deviation greater than 0.5% in velocity was found for the measured data. The excellent quality of the fit made us decide to use it, throughout this work, for the determination of velocity U and sensitivities $\partial E/\partial U$, $\partial E/\partial T$.

A typical calibration is shown in Figure 4.10. Note that for each overheat ratio it corresponds a curve $E^2/(R_w - R) = f(U)$.

Several calibrations were run at different air temperatures to test the validity of the correlation given by Equation (4.3). These test calibrations were made at air temperatures in the range 60°F to 90°F, or, within ±15°F from the normal calibration temperature (75°F - 80°F). No departure was observed among those, showing that Equation (4.3) correlates the data to better than 1% in velocity. From this study it was concluded that for our range of temperatures and velocities one can write

$$E^2 = (R_w - R(T))\ f(U) \qquad (4.6)$$

where

R_w is the constant wire operating resistance

$R(T) = C^*T + D^*$ (Equation 4.2) wire cold resistance

$f(U)$ the functions of velocity obtained by curve fit (Equations (4.4) and (4.5)).

This result agrees very well with what Sandborn [68] recommends for an expression correlating the constant temperature anemometer output.

4.10 Measurement of Mean Temperature and Velocity

a. Mean Temperature

Mean temperature was measured using the horizontal wire with constant current anemometer. The probe was put into the free-stream before and after each profile and the anemometer output E^*_∞ and wire resistance R_∞ were measured. The free-stream temperature T_∞ was measured with the calibrated thermocouple, whose reading was corrected for the velocity effect using a recovery factor of 0.86. Following Sandborn's [68] recommendation the wire probe was assumed to have unity recovery.

For all the boundary layer traverses we measured the output E^* (sequentially measured after the velocity).

Recalling the fact that B^* and D^* of Equations 4.1 and 4.2 change slightly with each disconnection of the probe (necessary to probe different stations) the following procedure had to be followed to determine the values of B^* and D^*. Placing the wire in the free-stream, the anemometer output E^*_∞ and the wire resistance R_∞ were determined. The free-stream temperature was measured by a calibrated thermocouple. These measurements were made before and after each profile was taken, it served to define the values of B^* and D^*, and to guard against changes during a traverse. We could also verify, from these two checks, whether or not the overall calibration had drifted or the wire had become dirty.

Using Equations (4.1) and (4.2) we get

cold wire temperature:

$$T_f = \frac{1}{A^*}(E^* - E^*_\infty) + T_\infty \qquad (4.7)$$

wire cold resistance:

$$R = C^*(T_f - T_\infty) + R_\infty \qquad (4.8)$$

air temperature:

$$T = T_f - \frac{U^2}{2g_c J c_p} \tag{4.9}$$

The velocity effect correction is small for most cases considered here.

The resistance temperature curve for each probe had the same slope for different calibrations, but a slightly different level. That is why we followed the procedure described here. All integration times were 10 seconds.

Uncertainty in T measurement: $\pm 0.2^{\circ}$F .

b. Mean Velocity

Mean velocity was measured using the horizontal wire with the constant temperature anemometer. For all the boundary layer traverses we measured E (the output at constant temperature), right after E^* (the output at constant current).

Using Equation (4.3) yields:

$$\frac{E^2}{R_w - R} = f(U) \tag{4.3}$$

where

E is known (the time averaged output of the anemometer)

R_w is constant

R is obtained from Equation (4.8)

and we can get U from curve fits.

All integration times were 10 seconds. No correction for wall proximity was made in the data. Minimum observed velocity was 18 ft/sec even at only 0.005 inch of the ball top, and corrections do not apply in this case (see Repik [72] for instance).

Uncertainty in U measurements: 1% of U .

4.11 Measurements of Turbulence Quantities

The measurement of turbulence quantities is based on the fact that the wire responds to both temperature and velocity fluctuations.

From Appendix B for small fluctuations:

$$e' = \frac{\partial e}{\partial u_{eff}} u'_{eff} + \frac{\partial e}{\partial t} t' \tag{4.10}$$

which for the horizontal wire reduces to

$$e' = \frac{\partial e}{\partial u} u' + \frac{\partial e}{\partial t} t' \tag{4.11}$$

and for the slant wire reduces to

$$e' = \frac{\partial e}{\partial u} \{u' + \frac{D}{2A} v' + \frac{F}{2A} w'\} + \frac{\partial e}{\partial t} t' \tag{4.12}$$

The sensitivities $\frac{\partial e}{\partial u}$ and $\frac{\partial e}{\partial t}$ were obtained from Equation (4.3). Here enters one basic assumption, i.e., that the instantaneous values are related in the same way as Equation (4.3) or

$$e^2 = (R_w - R) f(u)$$

so

$$\frac{\partial E}{\partial U} = \overline{\frac{\partial e}{\partial u}} = \frac{R_w - R}{2E} \frac{df}{dU} \tag{4.13}$$

$$\frac{\partial E}{\partial T} = \overline{\frac{\partial e}{\partial t}} = - \frac{E}{2(R_w - R)} \frac{\partial R}{\partial T} = - \frac{EC^*}{2(R_w - R)} \tag{4.14}$$

The last step uses Equation (4.2) and the assumption $\partial/\partial T = \partial/\partial T_f$ (this assumption is necessary only at high velocities - at low velocities it follows from the definition of T_f and T) is very good for our applications. A similar method is discussed by Sandborn [68] and used by Corrsin [71], Fulachier et al. [73], and others.

Finally, as we did not use a linearizer circuit the velocity had to be measured for each position.

4.11.1 Horizontal Wire

a. $\overline{u'^2}$

All measurements of $\overline{u'^2}$ were done in isothermal flow fields in order to improve accuracy.

The technique is discussed in Appendix B and uses the circuit in Figure 4.5. Equation (B.11) gives

$$\overline{e'^2} = \left(\frac{\partial E}{\partial U}\right)^2 \overline{u'^2} \tag{4.15}$$

$\overline{e'^2}$ is the rms value of the anemometer output integrated for 100 seconds.

$\frac{\partial E}{\partial U}$ is obtained from Equation (4.13), and as we are not using a linearizer, the measurement of the mean velocity is necessary.

Uncertainty of measurement of $\sqrt{\overline{u'^2}}$: $\pm 3\%$.

b. $\overline{t'^2}$

The measurements of $\overline{t'^2}$ were made using the resistance thermometer approach discussed in Appendix A.

We used the circuit in Figure 4.5 and Equation (A.5):

$$\overline{e^{*'2}} = \left(\frac{\partial E^*}{\partial T}\right)^2 \overline{t'^2} \tag{4.16}$$

$\overline{e^{*'2}}$ is the rms value of anemometer output.

$\frac{\partial E^*}{\partial T}$ is obtained from calibration (Equation (4.1)).

The value of t' is corrected for conduction errors, as discussed in Appendix A.

Uncertainty of measurement of $\sqrt{\overline{t'^2}}$: $\pm 12\%$.

c. $\overline{u't'}$

The measurements of the streamwise velocity-temperature correlation are discussed in Appendix B. A similar measurement technique has been used by Corrsin [71], Bremhorst et al. [74] and others, using an equation like (B.14):

$$\overline{e'^2} = \left(\frac{\partial E}{\partial U}\right)^2 \overline{u'^2} + \left(\frac{\partial E}{\partial T}\right)^2 \overline{t'^2} + 2\,\frac{\partial E}{\partial U}\frac{\partial E}{\partial T}\,\overline{u't'} \qquad (4.17)$$

for which we measure sequentially the rms output $\overline{e'^2}$ of the constant temperature anemometer and the value of $\overline{t'^2}$ using the resistance thermometer technique discussed in subsection b. The value of $\overline{u'^2}$ is taken from isothermal flow measurements. This procedure is justified in Appendix B. For our case we are making the reasonable assumption that the isothermal Reynolds stress components are preserved. The sensitivities $\partial E/\partial U$, $\partial E/\partial T$ are obtained from Equations (4.13) and (4.14) and use the value of mean velocity U, measured by the slant wire with $\theta = 90^{\circ}$.

In order to decrease the scatter of the data two measurements at two different wire temperatures were taken. As different sensitivities result from two wire temperatures, we obtained two estimates of $\overline{u't'}$. The average of them was taken to be $\overline{u't'}$.

Accuracy of measurement of $\overline{u't'}$: $\pm 15\%$.

4.11.2 Slant Wire

a. $\overline{v'^2}$, $\overline{w'^2}$ and $\overline{u'v'}$

For the measurements of the Reynolds stress tensor components we have used a method inspired by the work of Fujita and Kovasznay [69]. This same method was used by Andersen [53] and Orlando [17]. It uses a single rotatable slant wire and is discussed in Appendix B.

All these components were determined for the isothermal field. By taking t' out of the picture we improved the accuracy.

Several measurements, of $\overline{u'w'}$ and $\overline{v'w'}$ were made, for the range of conditions we analyzed, and demonstrated that the 2-dimensional flow field hypothesis is valid for the Roughness Rig. This was shown to be true, at least, for $y \geq 0.125$ inches, which is the closest we could get to the wall. The measured values of $\overline{u'w'}$ and $\overline{v'w'}$ were no larger than 1% of $\overline{u'v'}$ and we have assumed them equal to zero.

This last hypothesis simplifies the method so that only three measurements of $\overline{e'^2}$ are necessary. They were taken for $\theta = 0^\circ$, 45° and 135° (angle between vertical and wire-prongs plane), with one wire temperature (high overheat). Note that $\overline{u'v'}$ alone can be obtained from measurements at $\theta = 45^\circ$ and 135° .

According to Equation (B.13) (See Appendix B) the reduction of the data uses the isothermal $\overline{u'^2}$ value measured with the horizontal wire, for the same flow conditions and in the same day of run.

The measurements of the mean velocity, necessary for determination of the sensitivity $\partial E/\partial U$, were taken for $\theta = 90^\circ$ (wire parallel to wall). At this angle there is no velocity gradient along the wire and the effect of fluctuations is reduced.

The uncertainties of measurement of $\overline{u'v'}$, $\overline{v'^2}$ and $\overline{w'^2}$ are estimated to be $\pm 10\%$.

b. $\overline{v't'}$

Measurement of the normal velocity-temperature correlation uses the method discussed in Appendix B. It is similar to methods used by Arya and Plate [70], Corrsin [71], Orlando [17] and others.

From Equation (B.16)

$$\overline{e'^2}\Big|_{\theta = \pm 45^\circ} - \overline{e'^2}\Big|_{\theta = \pm 135^\circ} - a\,\overline{u'v'} = b\,\overline{v't'} \qquad (4.18)$$

where a and b are functions of the sensitivities $\partial E/\partial U$, $\partial E/\partial T$ and the directional properties of the wire.

Values of $\overline{u'v'}$ (Reynolds shear stress) were borrowed from the isothermal runs. These values, in conjunction with measurements of $\overline{e'^2}$ at two symmetric angles with respect to horizontal for a given wire temperature (R_w = constant) gave us an estimate of $\overline{v't'}$. Again, the validity of this method is discussed in Appendix B. The small wall-to-free stream temperature difference we have in our study led us to the assumption that $\overline{u'v'}$ is the same for both isothermal and non-isothermal flows.

In order to improve accuracy and decrease scatter in the data four estimates of $\overline{v't'}$ were measured, and their average was taken to be the final $\overline{v't'}$. The estimates were obtained from the combinations:

(2) - $\theta = +45^\circ$ & 135°, high overheat

(2) - $\theta = -45^\circ$ & -135°, low overheat .

As one can see from the final data, this indeed contributed to reduce the scatter.

Uncertainty of the measurement of $\overline{v't'}$ is estimated to be ±15%.

4.12 Some Considerations on Qualification Tests

The qualification of the apparatus was done by Healzer [4]. He describes a long series of tests, which we did not repeat since this study was conducted right after his.

The tests consisted of:

- boundary layer energy balances,
- transpiration energy balances,
- uniformity of mean velocity traverses across the test section,
- check of all instrumentation.

Stanton number results from this and Healzer's [4] work for the same boundary conditions are in agreement within 0.0001 Stanton number units. This is the estimated uncertainty for these measurements, so this excellent agreement is taken as a check of the apparatus reliability.

The qualification of the measurements techniques for velocity and temperature follows from Orlando's [17] work. This study was envisaged and, partly, carried out at the same time as Orlando's [17]. The fact that no previous profile data exist for this Roughness Apparatus makes it necessary to establish the reliability of the results by careful qualification of the techniques.

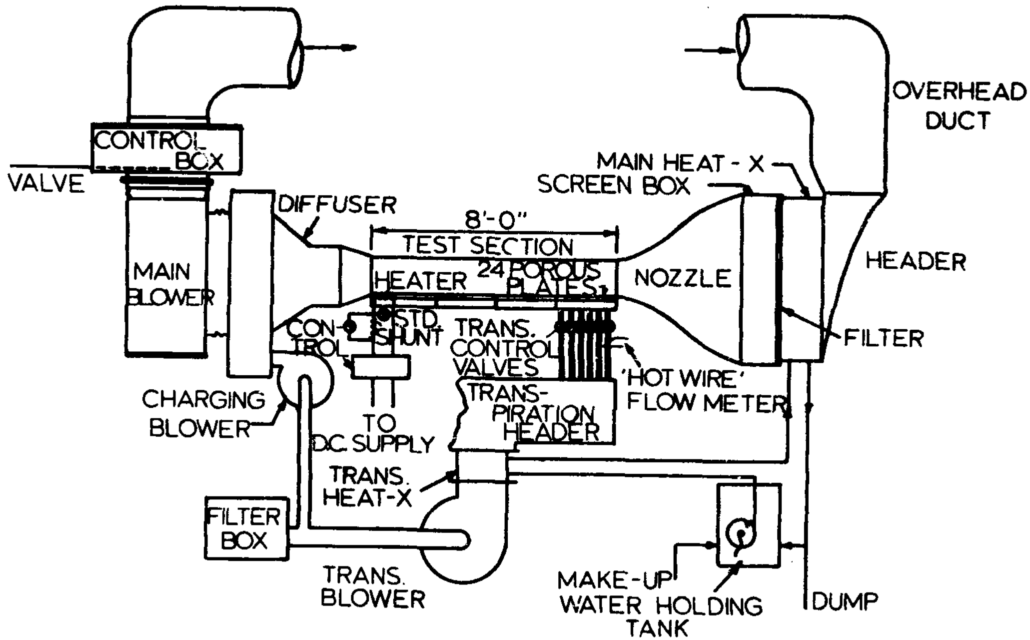

Fig. 4.1 Schematic of the rough surface wind tunnel.

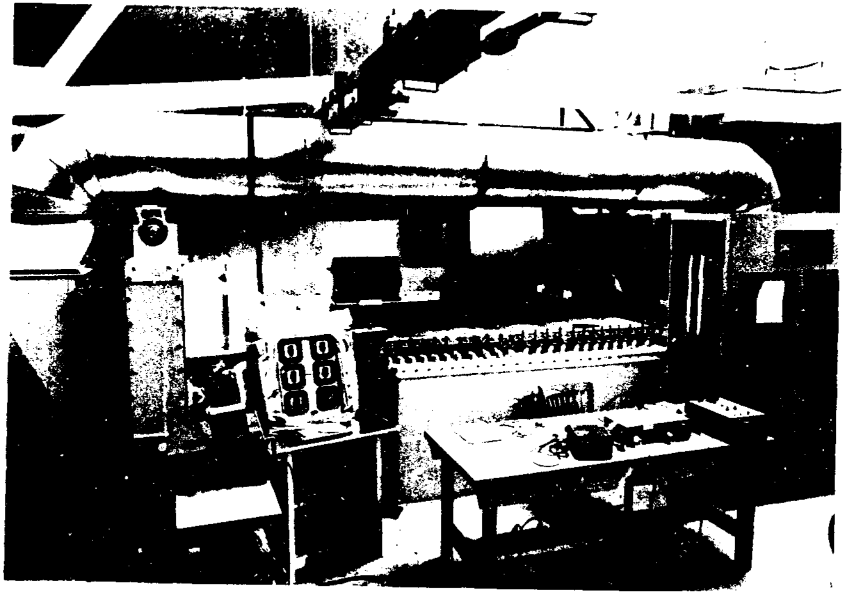

Fig. 4.2 Photograph of the roughness apparatus.

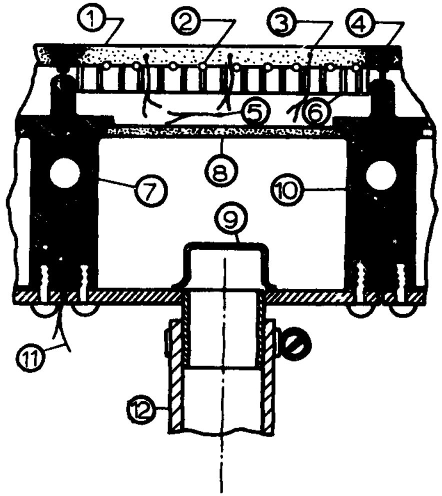

1. POROUS PLATE
2. HEATER WIRES
3. THERMOCOUPLES
4. SUPPORT WEB
5. TRANS. AIR THERMOCOUPLE
6. HONEY COMB
7. CAST. WATER PASSAGE
8. PRE-PLATE
9. TRANS. AIR DEFLECTOR
10. CASTING
11. CASTING THERMOCOUPLE
12. TRANS. AIR DELIVERY TUBE

Fig. 4.3 Cross section view of typical porous plate compartment.

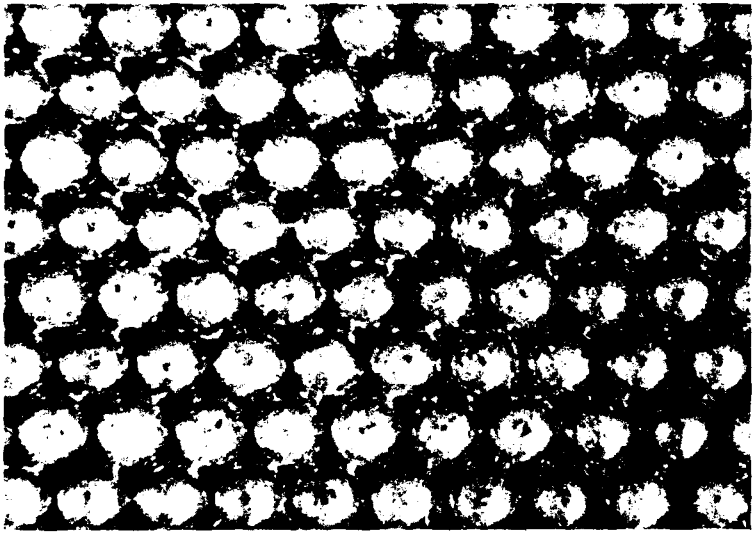

Fig. 4.4   Close-up photograph of the test rough surface.

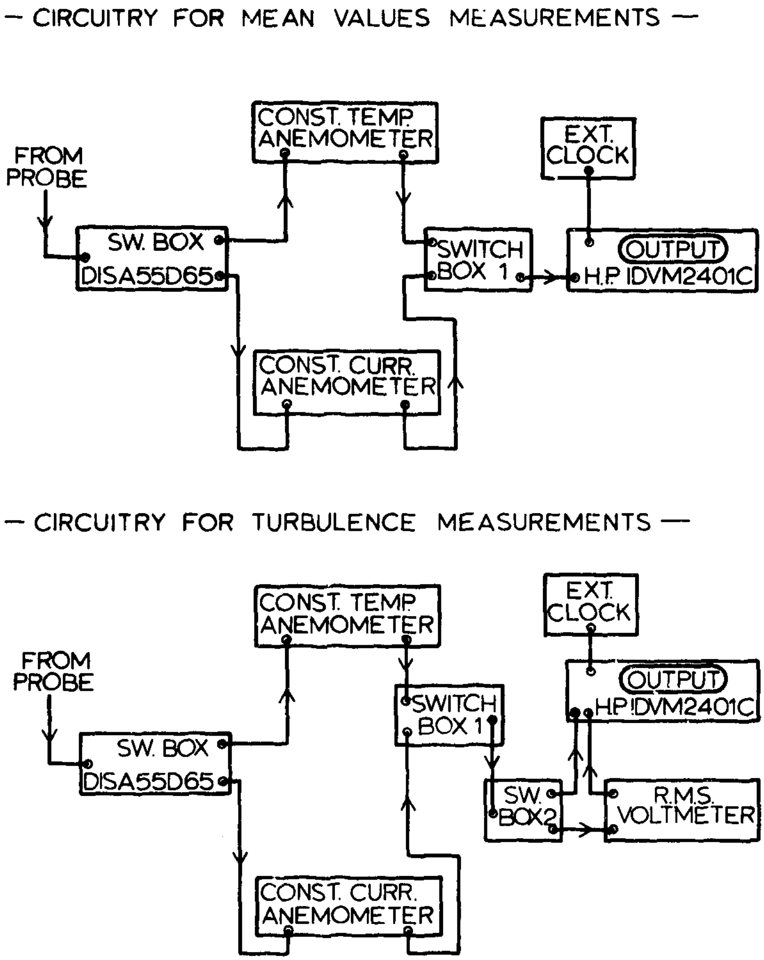

Fig. 4.5 Schematic of the hot-wire instrumentation and circuitry.

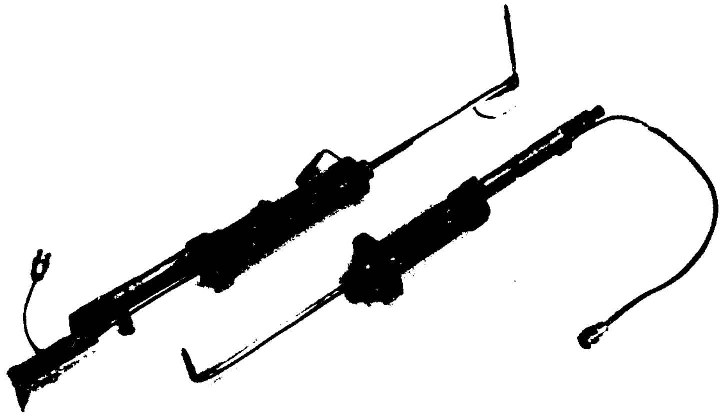

Fig. 4.6 Photograph of the hot-wire probes.

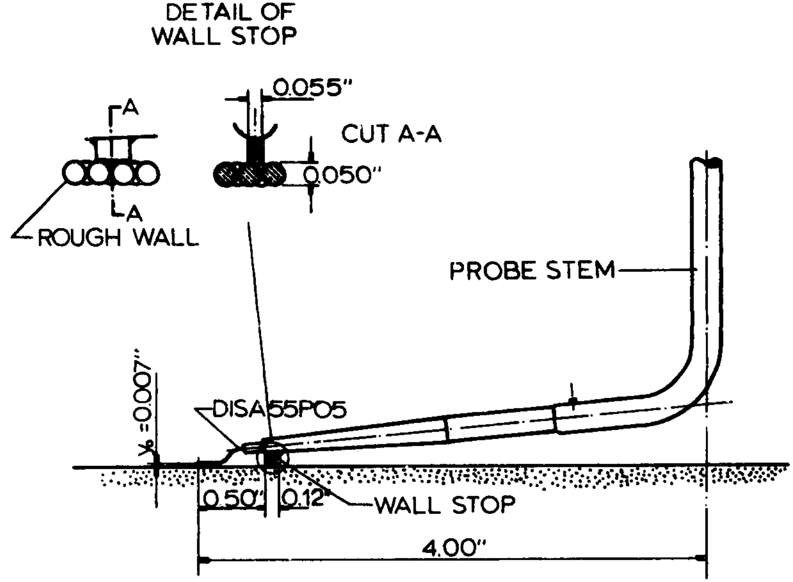

Fig. 4.7 Schematic of the horizontal hot-wire probe.

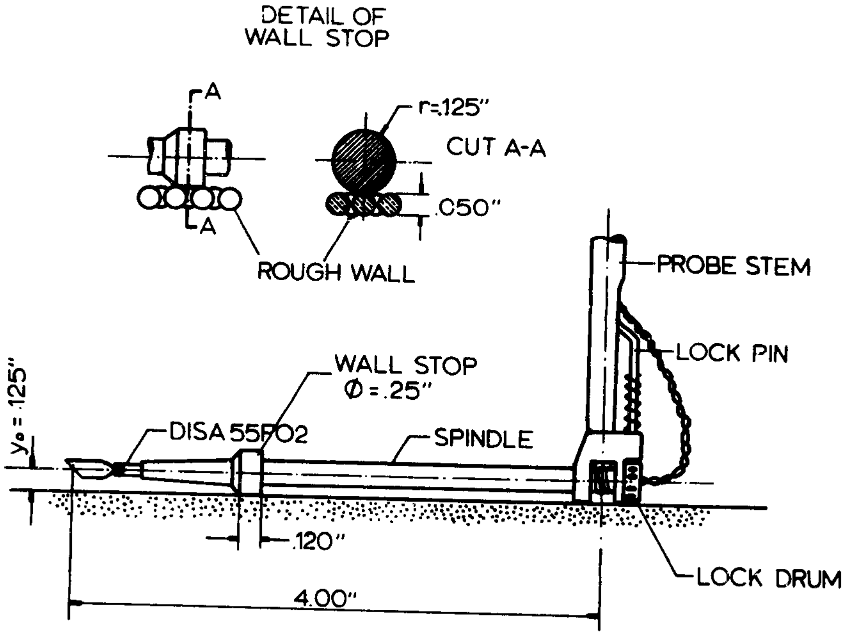

Fig. 4.8 Schematic of the slant hot-wire probe.

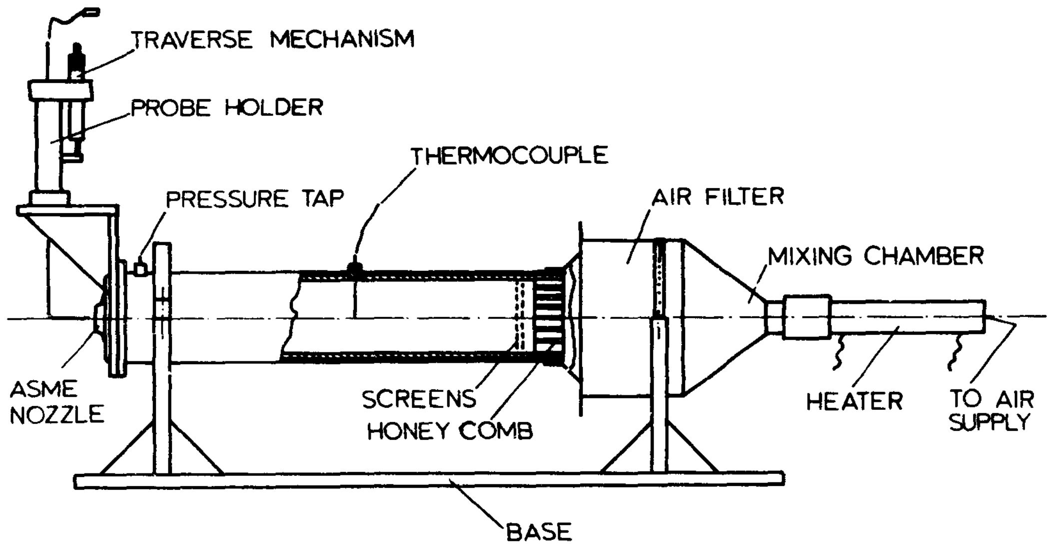

Fig. 4.9 Schematic of the CALIBRATOR.

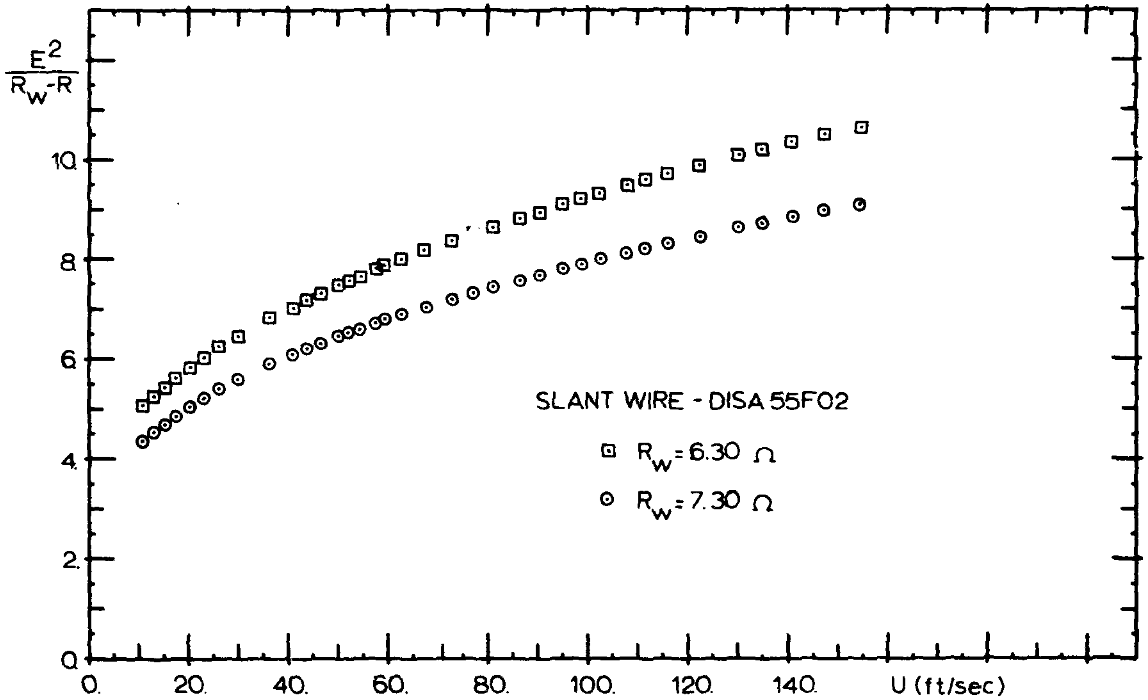

Fig. 4.10 Typical slant-wire calibration curves.

CHAPTER V

STANTON NUMBER AND FRICTION FACTORS

The determination of the Stanton numbers and friction factors for each of the cases studied was undertaken primarily to supply the parameters necessary for the non-dimensionalization of the different measured profiles. These cases will be referred to as base line data.

A small extension of Healzer's [4] experiments was also conducted with the intention of testing two conclusions that can be drawn from his results. First, that the heat transfer data exhibited "fully rough" behavior for low free stream velocity, sufficiently low to reduce the roughness Reynolds number down to 14. According to the well-accepted flow regime classification (see Schlichting [5], White [41], or Reynolds [42]), roughness Reynolds numbers between 5 and 65 correspond to the "transitionally rough" regime. Second, that the Stanton number data show a tendency to leveling-off at high values of enthalpy thickness. In other words, the boundary layer might be reaching an asymptotic state, where

$$\Delta_2 \propto x \qquad (5.1)$$

or

$$St = \frac{d\Delta_2}{dx} = \text{const.} \qquad (5.2)$$

Figure 5.1, taken from Healzer's work [4], illustrates the two points just raised.

Further, if Reynolds' analogy holds for the present experiments, similar trends would be observed for the friction factors.

Hydrodynamic asymptotic behavior has been observed for "d-type" rough surfaces by Perry et al. [33].

Stanton numbers and friction factors, their determinations and distributions are analyzed next.

5.1 Stanton Number Determination

Stanton numbers were determined by means of an energy balance taken for a control volume involving each plate segment.

In equation form it is:

$$St = \frac{(\text{plate power}) - \dot{m}''c_p(T_w - T_t) - (\text{losses})}{Gc_p(T_w - T_{aw})} . \qquad (5.3)$$

The losses include: radiant loss from top and bottom of the plates, conduction from plates to casting (and through the stagnant air beneath the plate when there is no transpiration).

Models for those losses were developed and incorporated into a computer data reduction program that calculates St using Equation (5.3). The models and the program are extensively described by Healzer [4]. Based on his qualification tests the uncertainty of the Stanton number is estimated to be ± 0.0001 Stanton number units over the range of conditions tested in this work.

5.2 Base-line Stanton Number Data

Stanton numbers for the base line data were taken four or five times, and an average value has been chosen to represent the actual condition. The simplicity of the process justified the repetition of the data-taking for each non-isothermal run made.

The enthalpy thicknesses presented in this chapter were obtained by means of numerically integrating the two-dimensional boundary layer integral energy equation. They compare very well with the values acquired by probing the boundary layer for temperature and velocity profiles, the agreement being good to 5%. We have decided not to use the profile values because only six profiles were taken for each run, and they, if interpolated, would represent only poorly the actual value for the 24 test plate stations.

Stanton number plots are shown in Figures 5.2, 5.3, 5.4, and 5.5. Two coordinate systems are used, one having as abscissa the enthalpy thickness Reynolds number and the other the enthalpy thickness Δ_2 normalized by the ball radius r.

Values of Stanton numbers for the 89 ft/sec runs agree with those of Healzer [4] within ± 0.0001, which is the uncertainty for these measurements.

From Figure 5.2 the effect of roughness is evident as we compare Stanton numbers with those corresponding to a smooth wall. According to Kays [22], the well-accepted correlation for air over a smooth wall is

$$St = 0.0153 \, Re_{\Delta_2}^{-0.25} \quad . \tag{5.4}$$

Figure 5.3 shows the two blown runs analyzed in this work. Figures 5.4 and 5.5 are interesting, showing Stanton numbers plotted against Δ_2/r.

Healzer [4] showed that for the present surface the fully rough regime data correlate well in these coordinates. Stanton numbers for the 89 and 130 ft/sec seem to be only functions of Δ_2/r, i.e., independent of the free stream velocity. The data points for 52 ft/sec fall below the other two cases, and this case corresponds to a different kind of regime. It might seem unjustified to assign so much significance to such a small difference in the data. However, structural study of the 52 ft/sec case clearly showed different behavior from the fully rough behavior. This observation suggests that the Stanton number difference is both real and significant, and that the Stanton number and friction data must be interpreted in the light of the evidence from the structural studies.

The study of structural properties of the turbulent boundary layer constitutes the objective of this work. The interpretation of all heat transfer and skin friction data included in this chapter take into account the structural evidence discussed in other chapters.

The following expression is suggested for the fully rough regime:

$$St = 0.00317 \left(\frac{\Delta_2}{r}\right)^{-0.175} \tag{5.5}$$

for the interval $4.0 < \frac{\Delta_2}{r} < 15$ (for this interval the effects of natural transition from laminar flow have ceased). The power was chosen to match the fit to the skin friction distribution discussed in Section 5.4. The curve corresponding to Equation (5.5) is plotted in Figure 5.4.

The blown data are well correlated by the expression

$$\left.\frac{St}{(St)_o}\right|_{\Delta_2} = \left[\frac{\ell n(1 + B_h)}{B_h}\right]^{1.175} (1 + B_h)^{0.175} \tag{5.6}$$

where for the same enthalpy thickness Δ_2:

... St is the Stanton number,

... $(St)_o$ is the Stanton number for the unblown case,

... $B_h = F/St$ is the blowing parameter.

This correlates St as shown in Figure 5.5 .

This relation is similar to that developed by Whitten [59] for transpired smooth walls and proposed by Healzer [4] for the present surface.

5.3 Friction Factors Determination

Healzer [4] has determined the friction factors using the two-dimensional boundary layer momentum integral equation, which for a transpired layer can be written as

$$\frac{C_f}{2} = \frac{d\delta_2}{dx} - F \tag{5.7}$$

where δ_2 is the momentum thickness and F is the blowing fraction. The derivative was performed after least-squares fitting an expression of the form

$$\delta_2 = a(x - x_o)^b \tag{5.8}$$

through the momentum thicknesses. These were obtained for eight (on the average) stations by probing the boundary layer, measuring the velocity profiles.

This method is convenient because it requires only mean velocity measurements, but it introduces uncertainties of two types. First, it always renders a logarithmic variation of $C_f/2$ with x. Second, it is very sensitive to whether the high or the low Reynolds number data are more heavily weighted.

In order to illustrate this point, we represent in Figure 5.6 the data points for the 52 ft/sec run with $x_o = 0.0$. If we do not include the first two points, the other data points would lie on a straight line with a virtual origin at $x = 0.0$. This shows how subjective is a logarithmic curve fitting of δ_2 data. The determination of the friction factors by curve fitting δ_2 is dependent on the number and choice of the data points (distribution, spacing, etc.). Bradshaw [16] discusses the problem of curve-fitting in order to obtain the derivative of a continuous function through data points. The derivative depends on the number of data points, the shape of distribution and type of function chosen to fit the data.

In an attempt to avoid these problems we have used Andersen's [53] shear stress method, which Orlando [17] also applied to obtain friction factor, but in this case with further considerations.

Consider a distance ξ from the top of the balls. We will assume that the flow is parallel, i.e., two dimensional, for distances larger than ξ. This assumption is reasonable based on our tests of flow two-dimensionality for the mean velocity profiles as well as for the Reynolds stress components, discussed, respectively, in Chapters VI and IV. Further, we have only considered in our measurements those stations where the boundary layer thickness was at least one order of magnitude larger than the spherical rough elements diameter. We would have some doubts concerning the validity of this assumption for very large roughness, especially if we consider the recent work by Powe et al. [34].

The time-averaged continuity equation and x-momentum boundary layer equation for constant properties and no-pressure gradient can be written for $y > \xi$ as

$$\frac{\partial U}{\partial x} + \frac{\partial V}{\partial y} = 0 \tag{5.9}$$

and

$$U \frac{\partial U}{\partial x} + V \frac{\partial U}{\partial y} = \frac{1}{\rho} \frac{\partial}{\partial y} \tau \tag{5.10}$$

where, for $y > \xi$,

$$\frac{\tau}{\rho} = \nu \frac{\partial U}{\partial y} - \overline{u'v'} .$$

The x-momentum equation can be put into the form

$$U\left(\frac{\partial U}{\partial x}-\frac{\partial V}{\partial y}\right)+\frac{\partial}{\partial y}UV = \frac{\partial}{\partial y}\left(\frac{\tau}{\rho}\right) , \tag{5.11}$$

or, using the continuity equation and rearranging,

$$\frac{1}{\rho}\frac{\partial \tau}{\partial y} = \frac{\partial}{\partial y}UV+\frac{\partial U^2}{\partial x} . \tag{5.12}$$

Now, integrating from ξ to y, one obtains

$$\frac{\tau(y)}{\rho} = \frac{\tau(\xi)}{\rho}+U(y)V(y) - U(\xi)V(\xi)+\frac{\partial}{\partial x}\int_{\xi}^{y}U^2dy . \tag{5.13}$$

Finally, using Equation (5.9) to calculate $V(y)$,

$$\frac{\tau(y)}{\rho} = \frac{\tau(\xi)}{\rho}+[U(y)-U(\xi)]\ V(\xi) - U(y)\frac{\partial}{\partial x}\int_{\xi}^{y}Udy+\frac{\partial}{\partial x}\int_{\xi}^{y}U^2dy . \tag{5.14}$$

As is discussed in Appendix C, the first two terms in the right-hand side can be expressed, for small ξ, as

$$\frac{\tau(\xi)}{\rho}+[U(y)-U(\xi)]\ V(\xi) = \frac{C_f}{2}U_\infty^2+U(y)V_o .$$

Thus, introducing the definition of $\tau(y)$, one obtains

$$\frac{C_f}{2}+\frac{U(y)V_o}{U_\infty^2} = \frac{\nu}{U_\infty^2}\left.\frac{\partial U}{\partial y}\right|_y - \frac{\overline{u'v'}(y)}{U_\infty^2}+\frac{U(y)}{U_o^2}\frac{\partial}{\partial x}\int_{\xi}^{y}Udy - \frac{1}{U_\infty^2}\int_{\xi}^{y}\frac{\partial U^2}{\partial x}dy . \tag{5.15}$$

All the terms on the right-hand side can be measured or numerically obtained from mean velocity profiles. The same is true for $U(y)V_o/U_\infty^2$, and therefore $C_f/2$ can be calculated. Equation (5.15) was used for the determination of all friction factors shown in this study. We have measured $-\overline{u'v'}(y)$ and taken mean velocity profiles at six different x-stations for each flow condition.

The Reynolds shear stress $-\overline{u'v'}$ was measured for all x-stations for which mean velocity profiles were taken and always at the location

$y = 0.130''$. (The closest one could get to the wall, with the slant wire, was $0.125''$.) The determination of $-\overline{u'v'}$ is discussed in Section 4.11.2.

As discussed in Chapter VI, the assumption of 2-D flow holds, down to $y = 0.007''$, which is the closest to the wall where mean velocities were measured. Therefore, for all cases we set $\xi = 0.007''$.

Referring to Equation (5.15), the determination of friction factors throughout the experiments revealed all terms in the right-hand side as being negligible compared to $-\overline{u'v'}$ (less than 2%).

Thus,

$$\frac{C_f}{2} \approx \frac{-\overline{u'v'}(y)}{U_\infty^2} - \frac{U(y)V_o}{U_\infty^2} \tag{5.16}$$

for $y = 0.130''$.

5.4 Base-Line Friction Factor Data

Figure (5.7) shows the friction factors for the three unblown base-line runs plotted against the momentum thickness δ_2 normalized by the ball radius r. Here, both the $C_f/2$ and δ_2 were determined from independent sets of measurements, so their relationship is independent of any subjective input. The coordinate δ_2/r was shown by Healzer [4] to be appropriate for discussing the effect of the deterministic roughness.

As we can see from Figure 5.7, it is apparent that for 89 and 130 ft/sec $C_f/2$ is only a function of δ_2/r, independent of free stream velocity, i.e., the boundary layer is at the same state for $U_\infty = 89$ and 130 ft/sec. The corresponding roughness Reynolds numbers based on Schlichting's [5] equivalent sand-grain roughness k_s are larger than 65, so the layer is in fully rough state by either criterion.

Note that the 52 ft/sec data lie below the 89 and 130. Structural differences observed also confirm that the 52 ft/sec boundary layer was in a different state than the 89 and 130 layers, i.e., not fully rough.

A good fit to our data in the fully rough state is

$$\frac{C_f}{2} = 0.00328 \left(\frac{\delta_2}{r}\right)^{-0.175} \tag{5.17}$$

for $0.1 < \frac{\delta_2}{r} < 1.0$, where the effects of natural transition on structural properties of the layer have ceased.

The differences between smooth and rough behavior can also be observed in Figure 5.7 . The friction factor distributions for a turbulent boundary layer over a smooth plate have been represented for the three free stream velocities, according to the well-accepted correlation for air (Kays [22]):

$$\text{smooth:} \qquad \frac{C_f}{2} = 0.0128\ Re_{\delta_2}^{-0.25} \ . \tag{5.18}$$

Roughness increases the friction factor.

Figure 5.8 shows the skin friction for the complete base-line data set at 90 ft/sec, including the two blowing cases.

The following relation is proposed to correlate the data:

$$\left.\frac{C_f/2}{(C_f/2)_o}\right|_{\delta_2} = \left(\frac{\ln(1 + B_f)}{B_f}\right)^{1.175} (1 + B_f)^{0.205} \tag{5.19}$$

where, for the same momentum thickness δ_2:

... $\frac{C_f}{2}$ is the blown friction factor,

... $\left(\frac{C_f}{2}\right)_o$ is the unblown fruction factor,

... $B_f = \frac{F}{C_f/2}$ is the blowing parameter.

Such a correlation interpolates $C_f/2$ as shown in Figure 5.8, and is valid for the range $0.1 < \delta_2/r < 1.0$.

Using the two-dimensional momentum integral equation (Equation (5.7)) and the $C_f/2$ curve-fitted distribution (Equation (5.17)), one gets

$$\delta_2 = 0.00509\ (x - x_o)^{0.851} \tag{5.20}$$

where x_o corresponds to the virtual origin of the layer.

A plot of the measured momentum thickness δ_2 for the unblown, fully rough cases is shown in Figure 5.9. We have estimated $x_o \cong 1.5"$ for the 89 ft/sec run and $x_o \cong -1.0"$ for the 130 ft/sec run. The good agreement of Eqn. (5.20) with the measured values qualifies our $C_f/2$ determinations.

5.5 Transitionally Rough versus Fully Rough State

We can now discuss one of the points raised in the beginning of this chapter. The present study shows that the boundary layer does show transitionally rough structural characteristics at 52 ft/sec. Healzer [4], based on surface heat transfer measurements only, tentatively reported the layer to be fully rough for velocities as low as 32 ft/sec.

Figures 5.4 and 5.7 show the St and $C_f/2$ data for 52 ft/sec having a lower level compared to those for the higher velocities. The depressions, though small, are believable in view of the structural features observed and discussed in a later section. They follow the expectation, since for the 52 ft/sec run the roughness Reynolds number is less than 65 (see Schlichting [5]), using roughness Reynolds number defined by $U_\tau k_s/\nu$, with k_s as the equivalent sand-grain roughness (0.031" in our case).

5.6 Asymptotic Behavior of the Layer

The plot of Stanton number distributions shown in Figure 5.1 from Healzer [4] seems to be leveling off for large enthalpy thickness Δ_2.

As a side study, an experiment was designed to expand the range of Δ_2, so we would have more data points in the region where St appears to be heading toward a constant value.

A layer with a constant St would have reached an asymptotic state when $\Delta_2 \propto x$. We know only one reference to the existence of such a state for a rough wall, reported by Perry et al. [33]. Their study referred to the fluid dynamics of a turbulent boundary layer developing over a "d" kind of rough wall. The "d" roughness consisted of a smooth wall containing a two-dimensional pattern of narrow cavities. Perry et al. reported that an asymptotic layer with constant $C_f/2$ was attained for sufficiently large δ_2.

Our surface, however, has three-dimensional elements, and no prior report has suggested such a surface might have an asymptotic state. Schlichting [5] classified a surface like ours as a "k"-type roughness.

For sufficiently large x or δ_2, a turbulent boundary layer developing over it would be expected to evolve from the fully or transitionally rough state toward the hydraulic smooth state.

Studies of heat transfer to smooth walls suggest that a turbulent boundary layer forgets its previous history within a few boundary-layer thicknesses (two or three). Another observed fact is that transpiration increases the momentum and enthalpy thicknesses. Thus, a layer can be augmented with blowing along part of the test section and then, stopping the blowing, it will relax to its natural state.

Based on this idea, three runs with $U_\infty = 89$ ft/sec were made. First, we transpired with $F = 0.002$ through the six plates of the first casting. An increase, with respect to the unblown case, of 50% in Δ_2 was obtained for plate 6, which corresponds to the initial enthalpy thickness for the relaxing region. Later, we transpired with $F = 0.004$ through the first nine plates. In this case we obtained an increase of 100% in Δ_2 for plate 9.

Finally, we transpired with $F = 0.004$ through three more plates, i.e., through the first 12 plates. With this technique we artificially almost doubled the range of Re_{Δ_2} for the 89 ft/sec, and obtained a continuous expanded Stanton number distribution. This was possible because of the capabilities of the present apparatus, for otherwise a test section at least twice as long would be necessary.

Figure 5.10 shows the result of this test. In the first run St recovers to the $F = 0.0$ run in a couple of plates and then follows it quite well. This run verified for the first time the validity of the augmentation process for rough plates. The test also supported an additional expectation: the protuberances generate higher turbulence intensities near the wall, and as a result the layer relaxes very rapidly toward its normal state.

The second and third runs are the most interesting. They show a slower relaxation than the previous run, however, the last six plates show a nearly constant Stanton number. This suggests that an asymptotic state is about to be reached, with St a constant, independent of Δ_2 .

If true, this last suggestion would contradict the belief that a flow over a rough plate would tend to reach the smooth behavior after a long distance. It seems to be the case, at least, for the heat transfer characteristics of this surface. In Figure 5.10 we represented also the distribution of Stanton number for a smooth flat plate case, according to Equation (5.4). It is apparent that for our surface no matter how high Re_{Δ_2} gets the Stanton number distribution will not reach the smooth one -- there is no tendency for the rough data to drop towards the smooth line.

However, the constancy of St would be expected if the layer reaches a "d" roughness behavior, according to Perry et al. [33]. His analysis for the fluid dynamics of "d" surfaces can also be put in terms of the temperature field. For the layer at the asymptotic state, the temperature profiles would develop in a way such that

$$\frac{T_w - T}{T_w - T_\infty} = \Phi^* (y/\delta_T) \quad , \tag{5.21}$$

where Φ^* is an universal function. If this is the case, the only length scale pertinent to the problem would be one representative of the thickness. The same would be the case for the velocity profiles,

$$\frac{U}{U_\infty} = \Phi (y/\delta) \quad . \tag{5.22}$$

In fact, velocity profiles were taken, and Equation (5.22) was verified to hold for large x for the three runs represented in Figure 5.10 .

A necessary condition for an asymptotic layer is that the different length scales are proportional to each other and grow linearly with x

$$\delta \propto \delta_T \propto \Delta_2 \propto x \quad . \tag{5.23}$$

The invariant profile plus the linear growth together result in

$$St \rightarrow \text{constant} \quad . \tag{5.24}$$

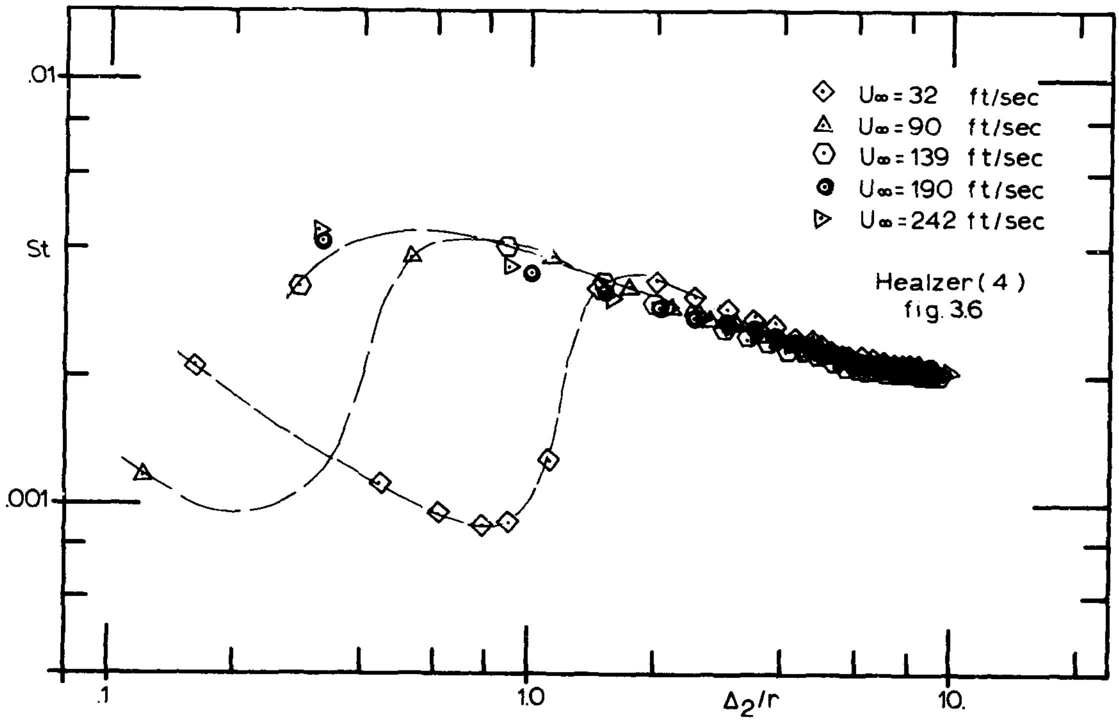

Fig. 5.1 Stanton number versus (enthalpy thickness)/(ball radius) - rough surface unblown data of Healzer.

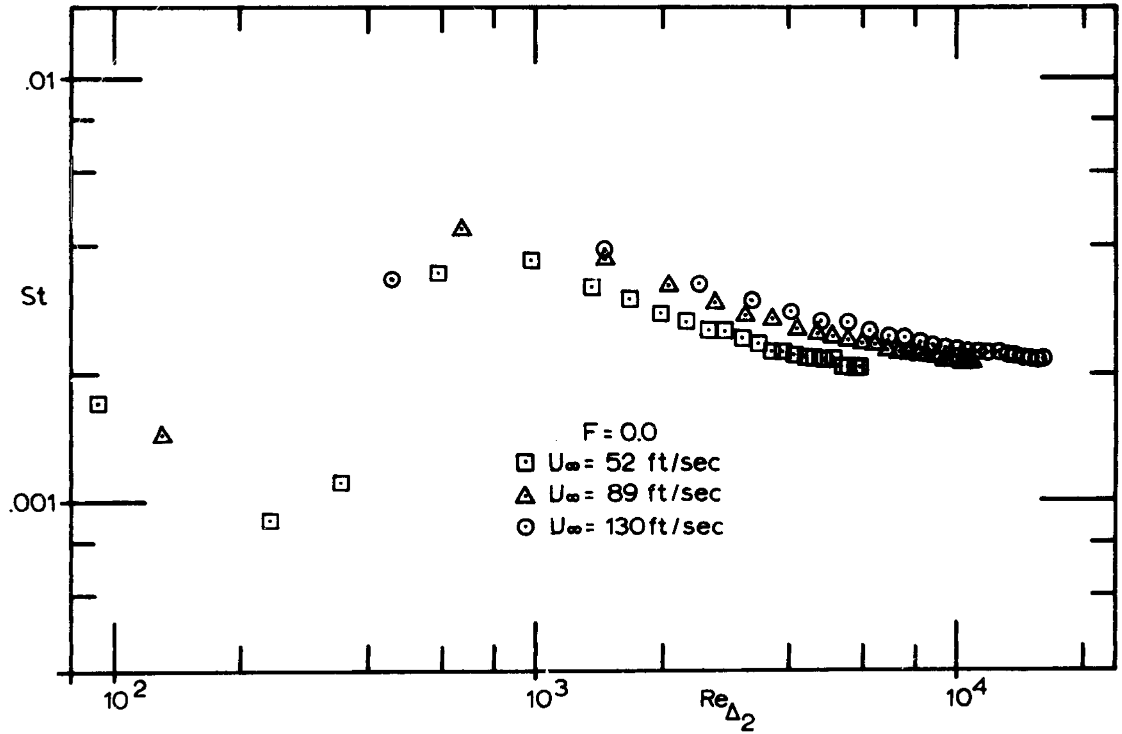

Fig. 5.2 Stanton number versus enthalpy thickness Reynolds number - rough surface unblown data.

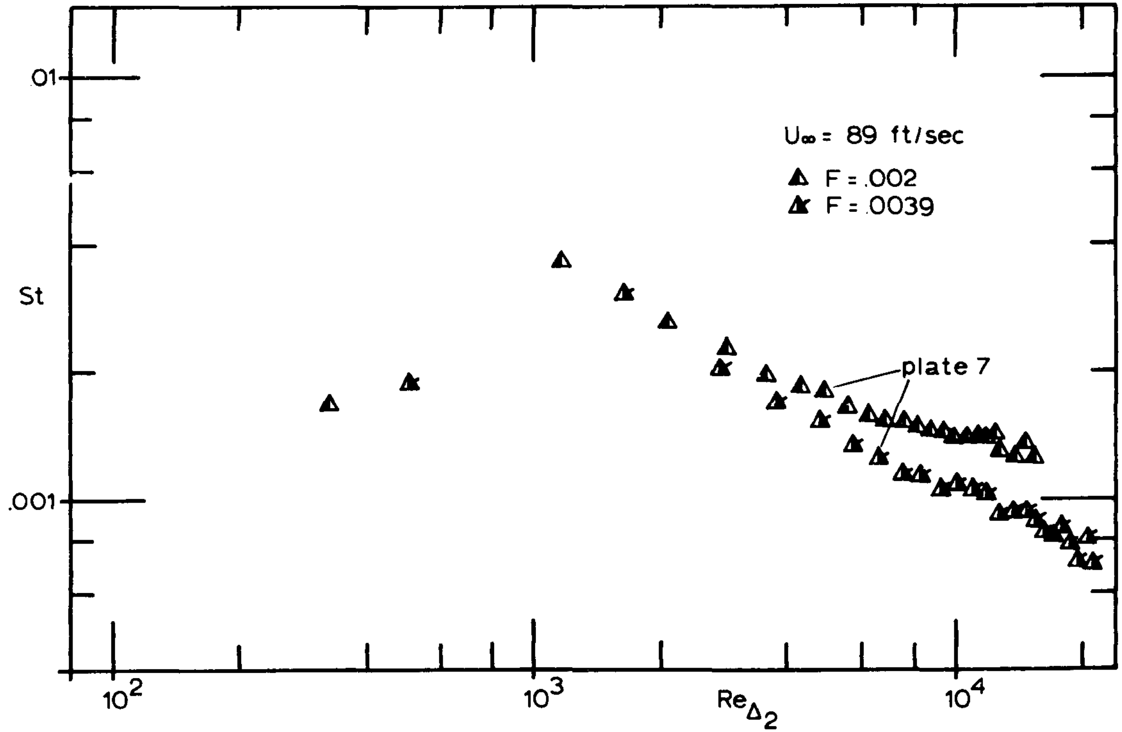

Fig. 5.3 Stanton number versus enthalpy thickness Reynolds number - rough surface for different blowing fractions.

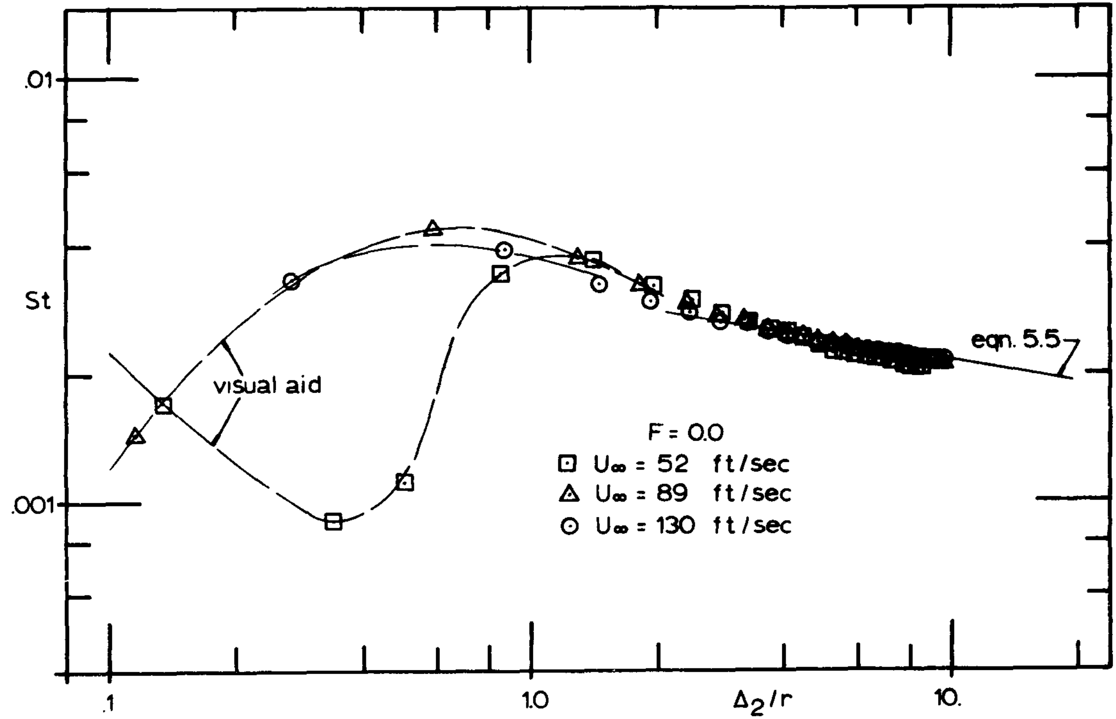

Fig. 5.4 Stanton number versus (enthalpy thickness)/(ball radius) - rough surface unblown data and correlation (Eqn. 5.5).

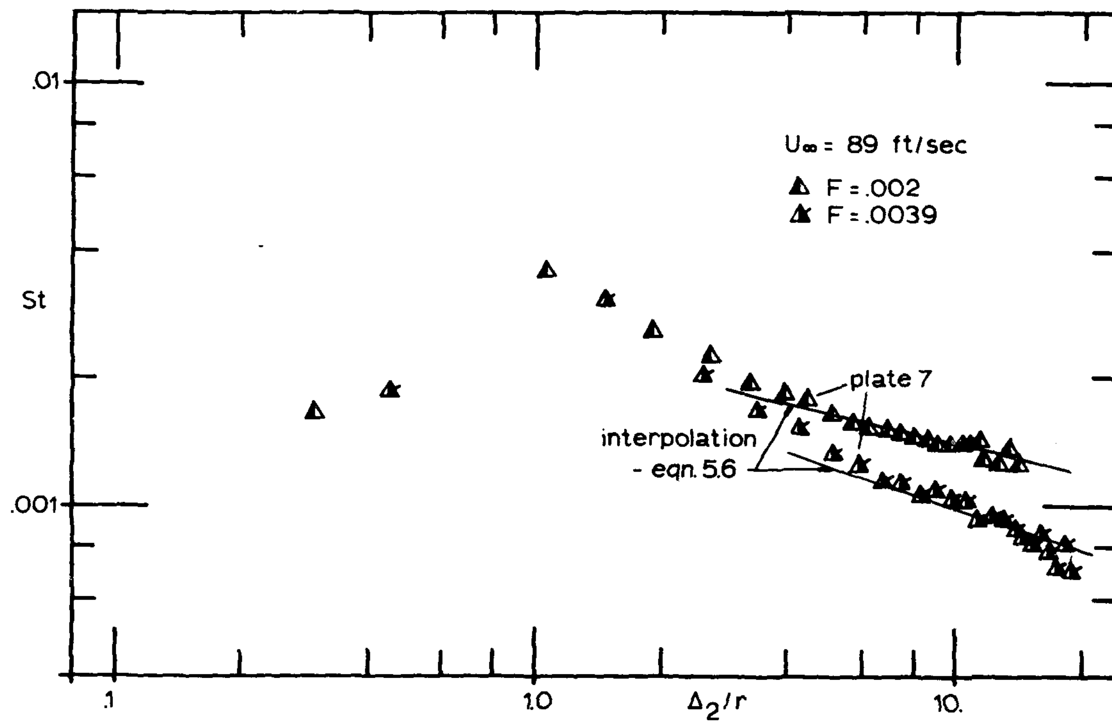

Fig. 5.5 Stanton number versus (enthalpy thickness)/(ball radius) - rough surface data for different blowing fractions and interpolating expression (Eqn. 5.6).

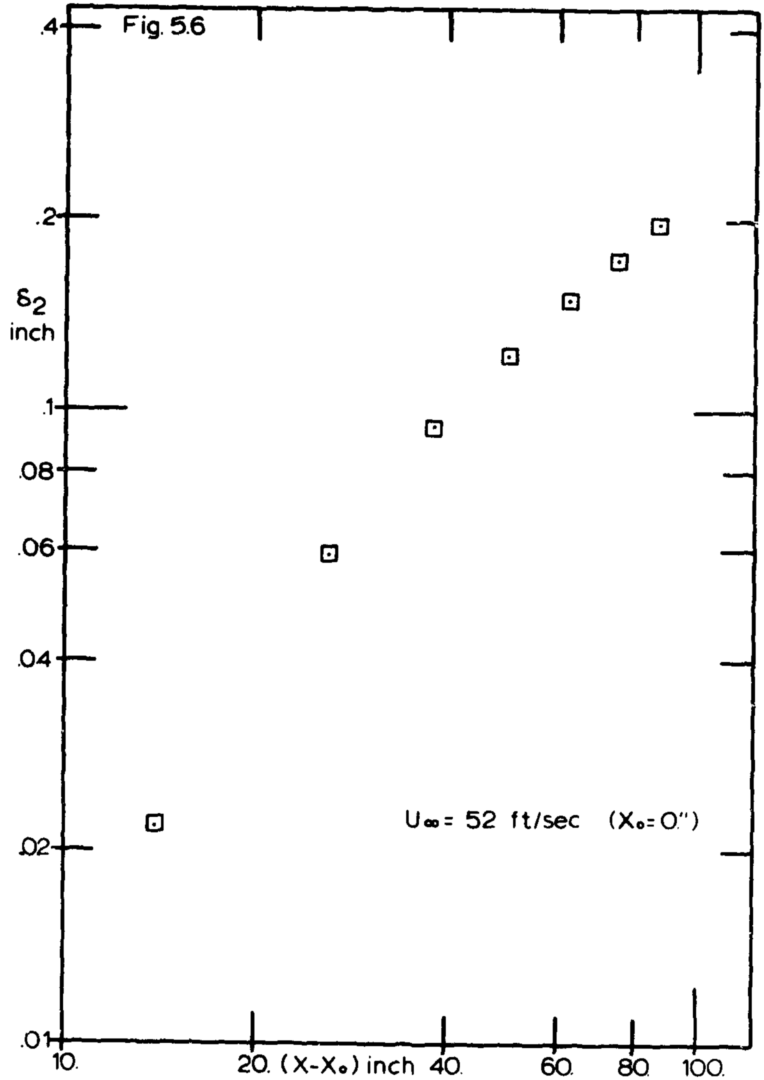

Fig. 5.6 Measured momentum thichnesses at different x-stations - transitionally rough state.

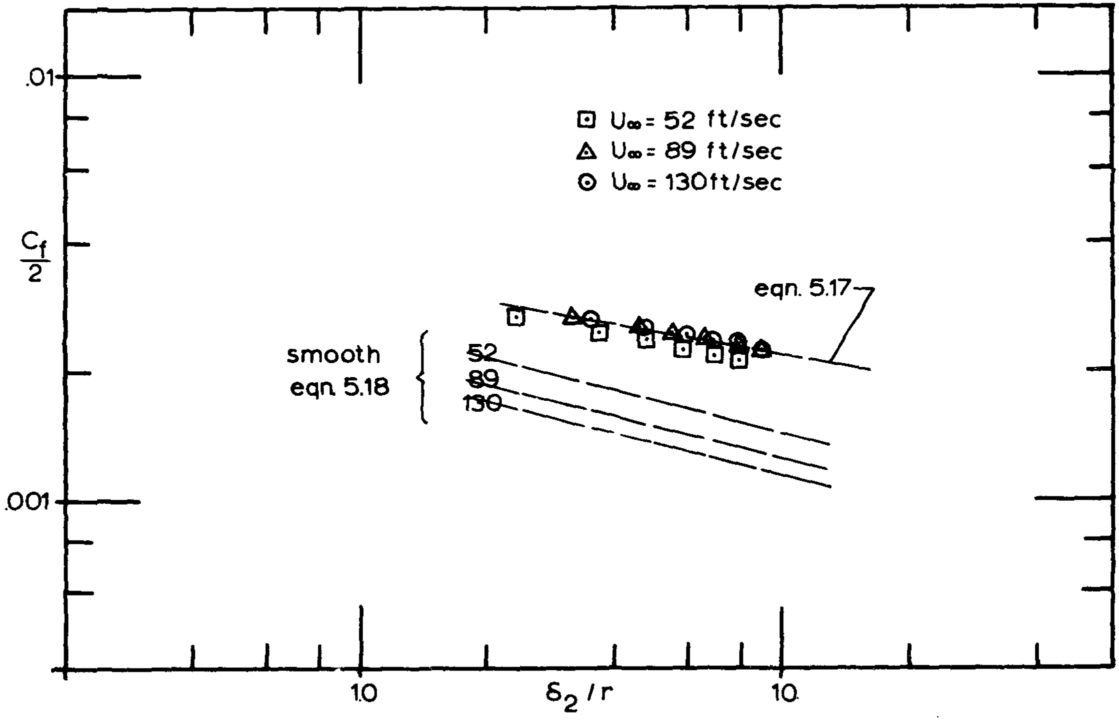

Fig. 5.7 Friction factors versus (momentum thickness)/(ball radius) - transitionally and fully rough states compared with smooth wall behavior.

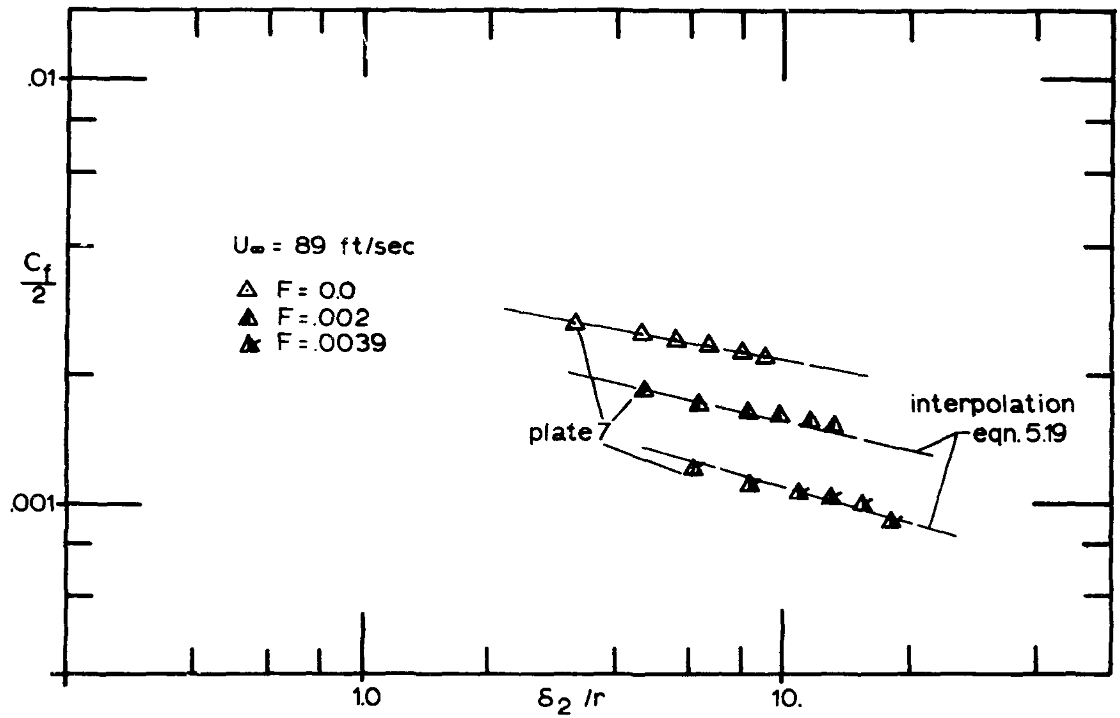

Fig. 5.8 Influence of blowing on the friction factors and interpolating expression (Eqn. 5.19).

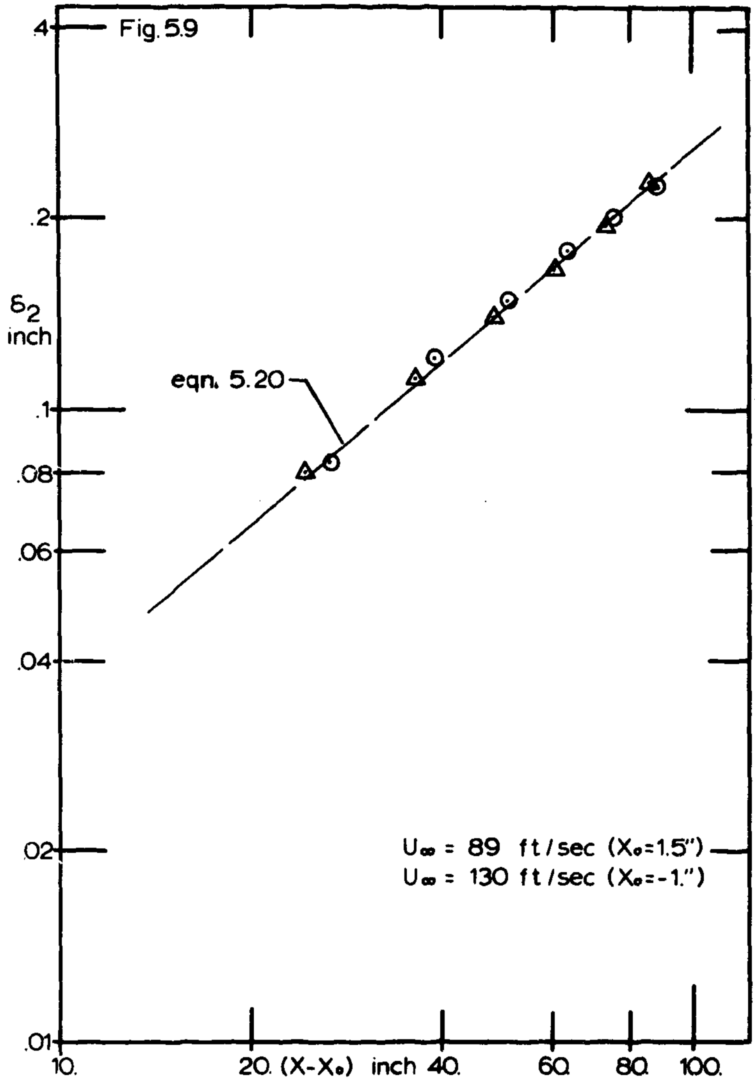

Fig. 5.9 Momentum thickness distribution for the fully rough state.

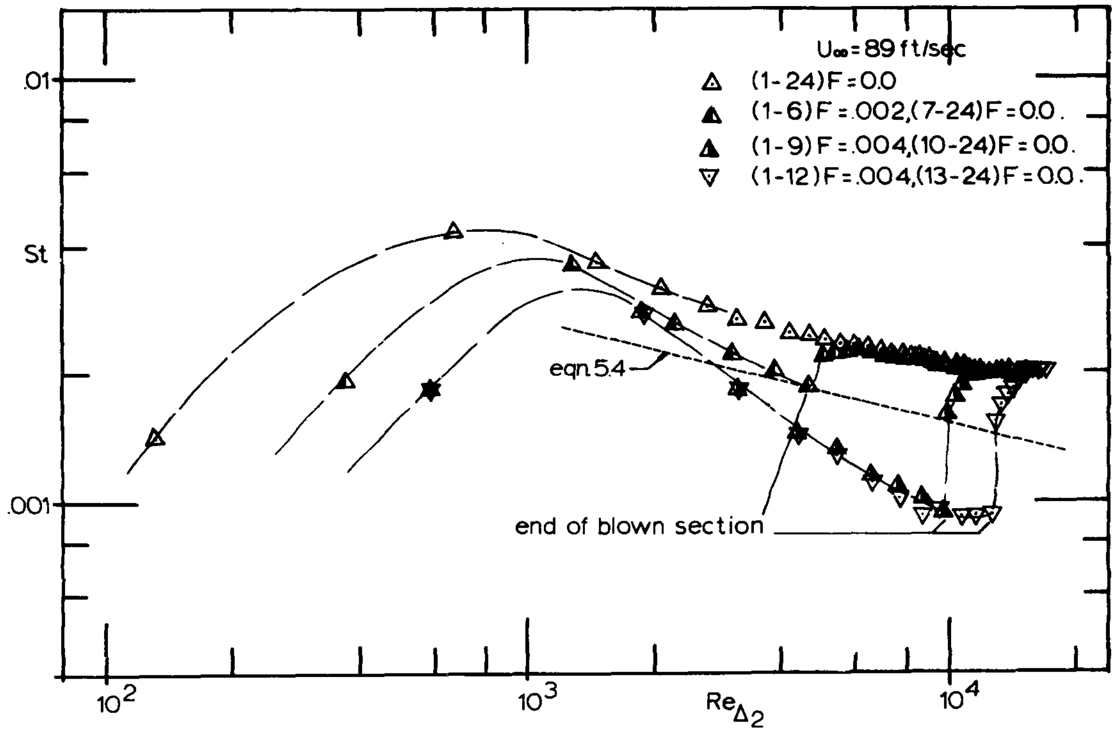

Fig. 5.10 Asymptotic Stanton number behavior for high enthalpy thickness Reynolds number.

CHAPTER VI

MEAN VELOCITY AND TEMPERATURE PROFILES

As discussed in Chapter IV mean velocity and temperature profiles were sequentially measured with the same probe at each position. Besides the thoroughly probed cases with heat transfer (three free-stream velocities: 52, 89 and 130 ft/sec), some isothermal velocity profiles were taken for 18 and 32 ft/sec during the preliminary runs.

The profiles shown here have the y-coordinate referred to the plane of the top of the balls, unless otherwise specified. Some aspects of the question of how to define an apparent wall are discussed in this chapter.

The uncertainties are estimated to be $\pm 1\%$ for velocity and ± 0.2°F for temperature.

6.1 Near Wall Tridimensionality and Other Tests

Because of the three dimensional nature of our rough wall protuberances we decided that the region close to the wall should be carefully studied. There is no doubt that the flow around the balls is three-dimensional, but there is the question as to how far above them the flow is affected. It was our intention to consider the boundary layer, wherever possible, as being two-dimensional. This feature simplifies the analysis of the flow.

Tests for checking the three-dimensionality were conducted for two flow conditions: unblown ($F = 0.0$) and blown ($F = 0.002$). A free-stream velocity of 89 ft/sec and a 27°F wall-to-free-stream temperature difference were maintained for both cases. Mean velocity and temperature profiles were taken with the horizontal wire at plate 19. The centered position for Station 19 corresponds to $x_{19} = 74$ inches and $z_{19} = 0.0$ inch. At data taking conditions, the wire and pronges were always parallel to a horizontal plane tangent to the ball tops and the wire axis was orthogonal to the x(streamwise) direction, which, in the free-stream, is the mean velocity direction. Then, maintaining the wire orientation, boundary layer traverses were made for the positions

$$(x_{19} , z_{19})$$

$$(x_{19} , z_{19} - 0.025")$$

$$(x_{19} - 0.025" , z_{19} - 0.025") \quad .$$

The displacement of 0.025" was carefully measured with feeler gauges and was accomplished by moving the sled that holds probes and the traverse mechanism. The wall was located using the technique discussed in Chapter V, and the first point corresponds to $y = 0.007"$. The spacings were chosen to take advantage of the periodicity of the surface. The compact arrangement of the balls makes the rough surface periodic in the x (streamwise) direction, as well as in the z (spanwise) direction. This can be seen in Figure 4.4. The radius of each copper ball is 0.025".

Some results of this test are shown in Figure 6.1 and 6.2, respectively, the mean velocity and temperature profiles for the unblown run. In order to magnify possible differences between the profiles, we have presented them in dimensional form. The slight differences observed for the first points are attributed to the uncertainty of ± 0.0005 in the position of the first point with respect to the wall. The test shows no evidence of flow three-dimensionality as close to the wall as $y = 0.007"$. The profiles for the blown run gave the same results.

It is our conclusion that our horizontal wire, with its 0.047 inch sensing length, takes some kind of a spatial average of the mean quantities, and this average shows no detectable three-dimensional effects in the mean profiles.

Before this test was conducted several measurements were made of mean velocity profiles for the same free-stream velocity, using isothermal and non-isothermal conditions. These profiles qualified our measurement technique since no difference could be observed in U/U_∞ profiles for the two conditions. The preservation of isothermal U/U_∞ profiles for low wall-to-free-stream temperature differences runs has been verified by Thielbahr [61] and Orlando [17]. Figure 6.3 shows, for a typical run case, the isothermal and non-isothermal mean velocity profiles, which agree very well within the ±1% uncertainty. As a result of these tests it was decided to take only non-isothermal profiles using the sequential technique.

6.2 Laminar Boundary Layer Over a Rough Wall and Transition

As it has been reported in the literature (for instance, see Schlichting [5]), when the Reynolds number is sufficiently low one can have a laminar boundary layer over a rough plate. It is implicit that the layer thickness has to be an order of magnitude larger than the representative roughness height, if one talks of a layer with gross two-dimensional characteristics. It is believed that for such a low Reynolds number the disturbances generated by the rough elements are damped out and do not trigger instabilities which would result in a turbulent layer. As the flow evolves along the plate, the Reynolds number gets larger and finally transition occurs. Healzer [4] reported for the porous surface an interesting result: transition from laminar to turbulent behavior for unblown and blown layers, occurs for momentum thickness Reynolds number around 400. This is the same momentum thickness Reynolds number that would be expected for transition on a smooth plate.

We have not tripped the boundary layer, so in all our cases it had a natural transition. During our preliminary runs, we decided to investigate somewhat further this natural transition. Therefore, isothermal velocity profiles were taken for free-stream velocities of 18 ft/sec and 36 ft/sec. Transition occurred in a matter of two to three local layer thicknesses. For 18 ft/sec, it was located between plates 12 and 14 ($x \cong 50.$ inch) and for 36 ft/sec, between plates 10 and 12 ($x \cong 42.$ inch). A sequence of mean velocity profiles for the 36 ft/sec case is presented in Figure 6.4. It shows how dramatic the change of their shape appears.

We have, in Figure 6.5, represented a Blasius [85] profile solution for a laminar boundary layer. It can be observed from Figure 6.5 that a change of ~5 mils in the origin of the y-coordinate makes the measured laminar profiles follow Blasius solution. These measurements were performed in isothermal flows. It was observed that heating the plates for Stanton numbers determination caused the transition region to move upstream, 2 or 3 plates, in the test section, compared to the isothermal flow. This fact was also observed by Schlichting [5] and others. It seems likely that heat transfer destabilizes the layer and transition is triggered earlier, compared to isothermal cases. The on-set of transition also occurred for momentum thickness Reynolds number around 400, which is the same as Healzer [4] reported.

This study, thus revealed that the laminar portion of the layer preceding the transition has a Blasius mean velocity profile. The transition takes place within one plate-segment length (4 inches) and all major changes in the mean profiles occur in such a short distance. The response of the turbulence field to transition is reported in Chapter VII.

6.3 Determination of the Virtual Origin of the Velocity Profiles

The virtual origin of velocity profiles is, by far, the most avoided subject of discussion in reports on rough wall boundary layer and pipe flow studies. The difficulty in defining the position of the rough wall arises from two practices inherited from earlier smooth wall studies. First, the two-dimensional character of a layer can only be maintained if the no-slip boundary condition is set for a flat or axi-symmetric surface. Second, velocity profiles are compared in semilog coordinates and analyzed with respect to their deviation from the logarithmic law of the wall.

The virtual or apparent surface of a rough plate is, therefore, a subjective concept. The constraints on its definition depend on the way the profiles are going to be interpreted and analyzed. This problem is handled in different ways by different investigators. Several authors simply do not mention it. Some, such as Tsuji and Iida [75] measured velocity profiles from the crests of the roughness elements. Others, such as Liu [1], Moore [23] and Perry [33], place the profile origin below the rough element crests. In fact, Perry uses the technique suggested by Clauser [19] and adjust the y-coordinate until the velocity profile exhibits the familiar 'log' region. Healzer [4] used otherwise a "french-curve" fit of the data, near the wall, to find it.

In the present study, knowledge of the apparent wall position was not necessary. Mean velocity and temperature profiles were measured sequentially with the same probe and their slopes at the wall were not sought. In the interest of consistency the y-coordinate was always referred to the top of the balls. Nevertheless, the virtual origin problem was considered during the development of this experiment, and the most satisfactory way for its determination is discussed next.

6.3.1 Unblown Cases

Monin and Yaglom [24] discuss a systematic way of finding the Δy - shift of the y-coordinate which locates the apparent wall position. This technique is repeatable, and sharply discriminates Δy and was used for all the data.

The basic assumption of this method is the same as Clauser's [19]. We assume that for a two-dimensional unblown boundary layer in zero presure gradient there is a region in y-space where

$$\frac{\partial U}{\partial y} \propto \frac{1}{y + \Delta y} \tag{6.1}$$

where $\Delta y = 0$ for smooth walls and $\Delta y \neq 0$, in general, for rough walls. The proportionality constant has been shown to be U_τ/κ for smooth walls and, tentatively, is extrapolated and used in rough wall cases. We will assume this constant to be U_τ/κ, due to the lack of better information.

Tennekes [25] argues that Equation (6.1) can be obtained by dimensional analysis for the inertial sublayer where $q^2 (y + \Delta y)/\nu >> 1$, $(y + \Delta y)/\delta << 1$ and $(y + \Delta y)/k_s > 1$ (for rough walls). Thus, it would not be considered as an assumption.

Equation (6.1) can be integrated to

$$U = \frac{U_\tau}{\kappa} \ln \frac{y + \Delta y}{z_o} \tag{6.2}$$

where

U_τ - shear velocity

κ - Karman constant (= 0.41)

z_o - constant

Δy - y-shift

For our surface, Δy refers to the position of the apparent wall with respect to the top of the balls.

The constant z_o is directly related to Schlichting's [5] constant B which he considers to be a function of the roughness Reynolds number Re_k. A function like $z_o = z_o(Re_k)$ can equally well describe the hydrodynamical performance of a rough surface.

Note that Equation (6.2) is another form of the law of the wall and can be obtained from Prandtl [76] mixing-length model. Near the wall with Couette flow assumptions the momentum equation gives

$$\tau/\rho = -\overline{u'v'} = \tau_w/\rho = U_\tau^2 \tag{6.3}$$

and

$$\tau/\rho = \ell^2\left(\frac{dU}{dy}\right)^2 \tag{6.4}$$

where

$$\ell = \kappa\,(y + \Delta y) \quad . \tag{6.5}$$

Equation (6.2) follows from the previous equations.

The determination of Δy is made by plotting z_o versus $y + \Delta y$, and choosing Δy that gives the longest plateau of constant z_o. Figures 6.6a and 6.6b show this exercise for typical velocity profiles. As we can see this process is very sensitive to small changes in Δy, which can be determined to within 0.001 inch, the uncertainty in positioning the probe with respect to the wall.

Plots of $z_o \times y$ were made for most of the unblown profiles, and as a result we got $\Delta y = 0.006'' \pm 0.0005''$. This means that for the conditions of this study the position of the "apparent" wall is constant. Note that the value of Δy (= 0.006") for the turbulent profiles is, within the positioning uncertaint , the same as that for the laminar profile, which was shown to be $\Delta y = 0.005''$ in Section 6.2. From this fact, one can see Δy as a characteristic length scale of this surface, which probably is proportional to the roughness size k.

6.3.2 Blown Cases

Based on the process of determining Δy for unblown cases, we have developed a similar method for the blown cases. We are assuming that a linear mixing-length relates the turbulent shear stress to the local velocity gradient. Then, as before

$$\frac{\tau}{\rho} = \kappa^2 (y + \Delta y)^2 \left(\frac{\partial U}{\partial y}\right)^2 \tag{6.6}$$

This assumption is substituted into the momentum and continuity equations for the mean flow in a two-dimensional turbulent boundary layer with zero pressure gradient. The region considered here is for $y > \xi$, where the flow is two-dimensional, following Chapter V and Appendix C.

According to the derivation given in Appendix C, for the region close to the wall and with the Couette flow assumption $(\partial/\partial_x \approx 0)$, the wall-shear stress can be defined as

$$\frac{\tau_w}{\rho} = \frac{C_f}{2} U_\infty^2 = U_\tau^2 \tag{6.7}$$

We obtain from Equation (C.18)

$$\frac{\tau}{\rho} = U_\tau^2 + UV_o \tag{6.8}$$

If Equation (6.6) is substituted into Equation (6.8), then

$$\kappa^2 (y + \Delta y)^2 \left(\frac{\partial U}{\partial y}\right)^2 = U_\tau^2 + UV_o \tag{6.9}$$

Equation (6.9) can be integrated to give

$$\frac{2}{V_o} (U_\tau^2 + UV_o)^{1/2} = \frac{1}{\kappa} \ln \left(\frac{y + \Delta y}{z_o}\right) \tag{6.10}$$

As Baker [78] discusses, the assumptions involved here should not be expected to hold near the wall for very large injection rates (F), i.e., when $\partial U/\partial y$ approaches zero. In our case, purposely, F was made small: 0.002 and 0.004 .

Equation (6.10) is the mathematical representation for the law of the wall for transpired rough wall boundary layers. Studies like those of Stevenson [55] and Simpson [39] have proposed similar forms of Equation (6.10) for smooth walls.

As for the unblown case, the determination of Δy is made by plotting z_o versus $y + \Delta y$, and choosing Δy that gives the longest plateau of constant z_o. This value of z_o can be correlated to the roughness Reynolds number and blowing fraction F or V_o, to represent the hydrodynamical performance of a transpired rough surface.

For the case $F = 0.002$, Δy corresponded to 0.008 inch as Figure 6.7 indicates. The case $F = 0.004$, Figure 6.8 shows a $\Delta y = 0.0095$ inch. This study serves to indicate that Δy is not only a function of the geometry of the surface but also of the transpiration rate. Therefore, Δy, which constitutes a measure of the apparent roughness size, is increased by the transpiration. This fact comes in support of the idea we have introduced in Chapter III: the static pressure field around each small jet, resulting from transpiration through the pores, simulates the interaction between a solid protuberance and the flow. The wall looks "rougher" to the flow, when blowing is present, and the effect of blowing is enhanced for larger F ratios.

6.4 Outer Region Similarity for Unblown Cases

Outer region similarity of velocity profiles has been the subject of several studies. It led to definition of the equilibrium flows concept of Clauser [79] and to a collection of laws of the wake to express the similitude. Most of these expressions recommended in the literature are generalizations of Coles' [26] law for smooth, impermeable surfaces. He examined a large number of experimental velocity profiles measured on smooth, solid surfaces, both with and without pressure gradients, and found that the velocity profile could be written in the form

$$\frac{U_\infty - U}{U_\tau} = -\frac{1}{.41}\,\ell n\,\frac{y}{\delta} + \frac{\pi}{.41}\left\{1 - w\left(\frac{y}{\delta}\right)\right\} \qquad (6.11)$$

π depends on the pressure gradient, but as in our case for constant pressure boundary layer it has a constant value of 0.55. Some values of the wake function $w(y/\delta)$ are tabulated here:

y/δ	0.0	.10	.20	.30	.40	.50	.60	.70	.80	.90	1.0
$w(y/\delta)$	0.0	.029	.168	.396	.685	.994	1.307	1.600	1.840	1.980	2.0

The wake function, which Coles developed for smooth walls, has been shown to be valid for rough walls by a number of authors, such as Hama [10], Moore [23], and Perry et al. [33]. Figure 6.9 shows some of our velocity profiles, and they are in excellent agreement with Equation (6.11).

These profiles also follow Clauser's equilibrium-defect profiles. For our cases ('equilibrium flows'), Clauser's equilibrium parameter

$$\beta = \frac{\delta_1}{\tau_w}\frac{dp}{dx} = 0 \qquad (6.12)$$

corresponds to the shape factor $G \approx 6.7$. By definition

$$G = \frac{\sqrt{C_f/2}}{\delta_1}\int_o^\infty \left(\frac{U_\infty - U}{U_\tau}\right)^2 dy \qquad (6.13)$$

which is related to the Karman type shape factor, $H = \delta_1/\delta_2$, through

$$H = \frac{1}{1 - G\sqrt{C_f/2}} \qquad (6.14)$$

We have represented in Figure 6.10 the shape factors H measured for the fully rough conditions, and a comparison between the measured values of the friction factors and those calculated using Equation (6.14). Within the uncertainty of the $C_f/2$ measurements (10%), Figure 6.10 shows that the values of H , G and $C_f/2$ reported here are consistent with Equation (6.14).

Smith [77] suggested that the velocity defect law for the non-transpired boundary layer could be used for the transpired boundary layer if the wall shear stress, used by Coles as a scaling velocity, is replaced by the maximum shear stress (τ_{max}/ρ) attained in the boundary layer. He recommended

$$\frac{U_\infty - U}{\sqrt{\tau_{max}/\rho}} = -\frac{1}{.41} \ln \frac{y}{\delta} + \frac{\pi}{.41} \left(2 - w\left(\frac{y}{\delta}\right)\right) \tag{6.15}$$

We have tried to extend this expression to our transpired cases over rough walls. Experiments showed, however, that the measured τ_{max} was lower than the value required to make the measured profiles agree with Equation (6.15). Thus, one would conclude, on this basis, that blowing interacts, differently, with the boundary layer over smooth and rough walls. This must be caused by the fluctuations induced by the jets thru the pores as discussed by Baker [78] or Jayatilleke [48], to which we will refer in the next chapter.

6.5 Mean Velocity Profiles

Mean velocities U/U_∞ profiles plotted against y/δ_2 are shown in Figures 6.11, 6.12, 6.13, 6.14 and 6.15. These correspond to the unblown and blown cases at Station 19. The momentum thickness δ_2 has been chosen as normalizing length because of $C_f/2 = f(\delta_2)$ as concluded in Chapter V, and its determination is more precise than that of δ or δ_1. The coordinate $y^+ = yU_\tau/\nu$ is not used in this work because y^+ implies a dependence of the profiles on the kinematic viscosity. For the fully rough cases there is no dependence on ν, thus the ambiguity is taken care of by avoiding the use of y^+.

In Figure 6.11, for $U_\infty = 89$ ft/sec and $F = 0.0$, we present Schlichting's [5] expression for the fully rough state:

$$\frac{U}{U_\tau} = \frac{1}{\kappa} \ln \frac{y}{k_s} + 8.5 \tag{6.16}$$

As we see, with $k_s = 0.031$ inch as Schlichting recommends for our kind of rough surface, Equation (6.16) represents the logarithmic region when the correct Δy is incorporated to y. In Figures 6.12 and 6.13 profiles are shown for $U_\infty = 52$ and 130 ft/sec with no wall shift. It should be noted that a distinct "buffer region" would appear in the data for 52 ft/sec if the 0.006 inch value of Δy is used.

Figures 6.14 and 6.15 show Equation (6.10) plotted with the proper

z_o determined according to Section 6.3.2. The calculated profile runs through the data points for the two blown cases.

6.6 Temperature - Velocity Profiles

The mean temperature profiles for the unblown cases exhibit a definite logarithmic region when the proper Δy is used in plotting the non-dimensional temperature. This is shown in Figure 6.16. This fact is in accordance with the similarity between velocity and temperature profiles, which can be better appreciated in plots of mean temperature versus mean velocity.

Figures 6.17, 6.18, 6.19, 6.20 and 6.21 show $T - U$ profiles $((T_w - T)/(T_w - T_\infty)$ versus $U/U_\infty)$ for our different conditions. The similarity mentioned above is clearly depicted in these profiles and is even valid for the blown cases.

Figure 6.17 shows a $T - U$ profile for a smooth wall layer from Blackwell's [27] work compared with the rough wall result. The smooth wall profile diverges from the rough wall profile, near the wall. In the region where molecular transport dominates, the smooth wall profile follows the sublayer equation $T^+ = Pr\, U^+$, and is depressed compared to the rough profile. The molecular effects are such that even in the logarithmic region, where turbulent transport overwhelms the molecular transport, the smooth $T - U$ profile is still depressed. It is only in the outer region that both profiles (smooth and rough) follow the same curve.

The procedure used in this work for sequentially measuring velocity and temperature gives an accurate functional relationship between the temperature and the velocity. The determination of the turbulent Prandtl number requires, for instance, the ratio

$$\frac{\partial T/\partial y}{\partial U/\partial y} = \frac{\partial T}{\partial U} \tag{6.17}$$

to be known. A more accurate value of this derivative is therefore obtained with the present technique than with former techniques which required independent measurement of $T(y)$ and $U(y)$, matched and differentiated.

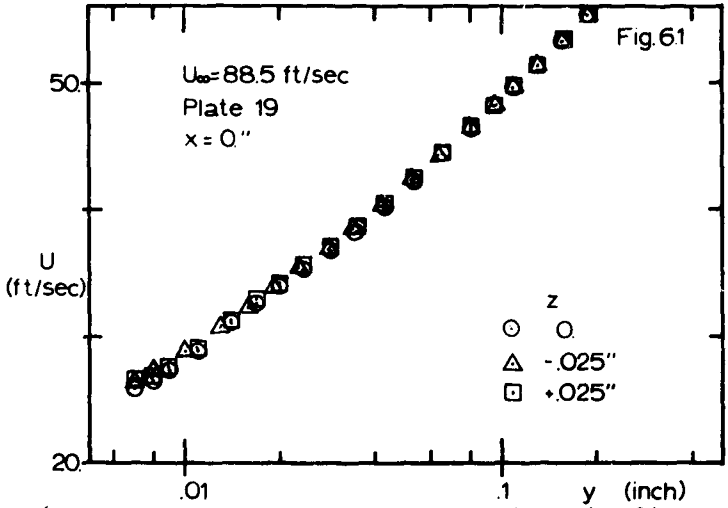

Fig. 6.1 Mean velocity profiles - three dimensionality check in the near wall region.

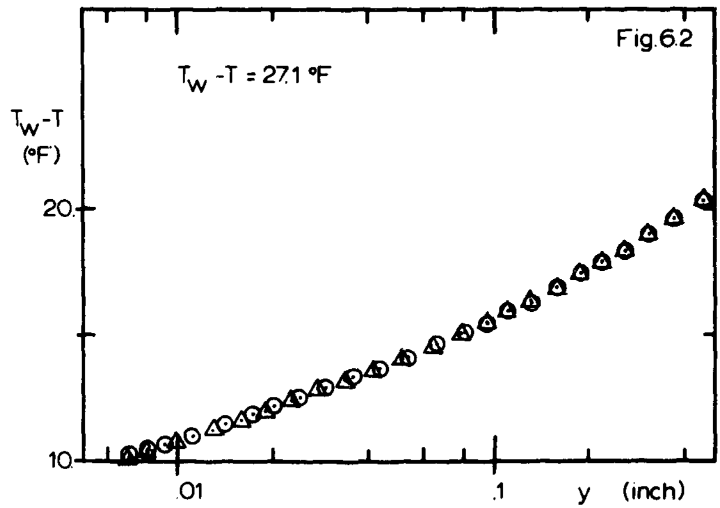

Fig. 6.2 Mean temperature profiles - three dimensionality check in the near wall region.

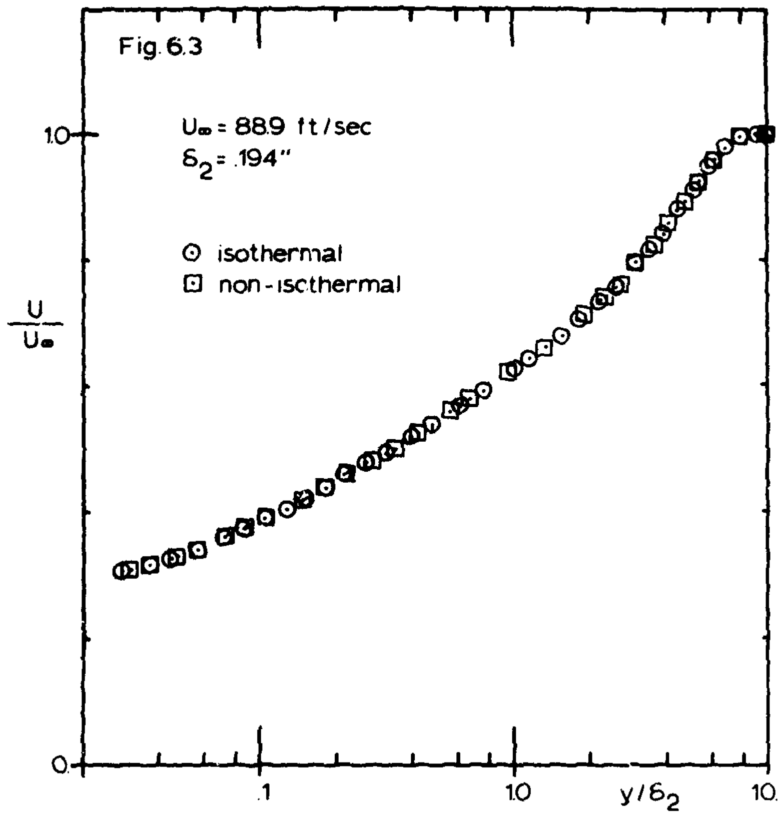

Fig. 6.3 Measurements of mean velocity profiles with hot-wire : isothermal and non-isothermal flows.

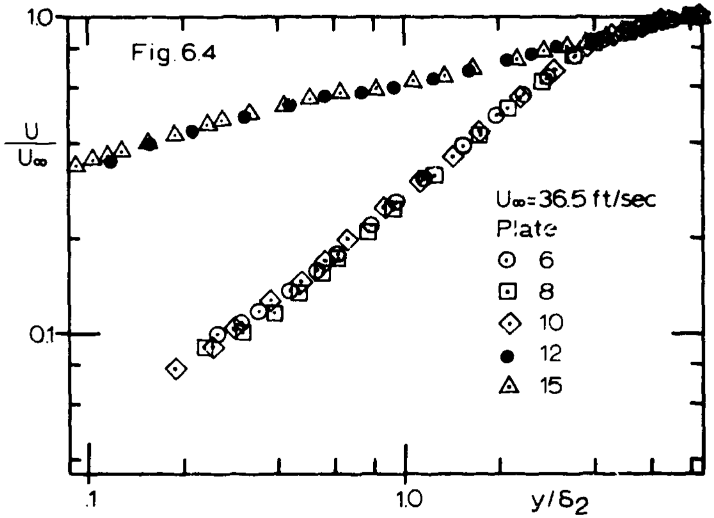

Fig. 6.4 Mean velocity profiles at different x-stations (U_∞ = 36.5 ft/sec).

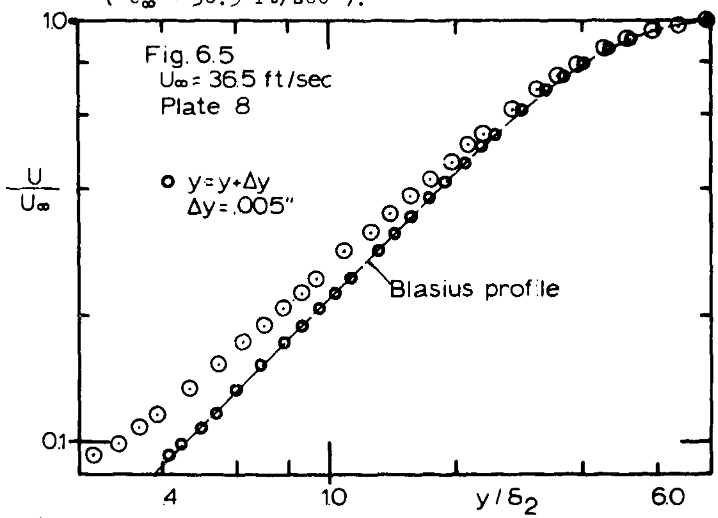

Fig. 6.5 Laminar mean velocity profile on a rough plate.

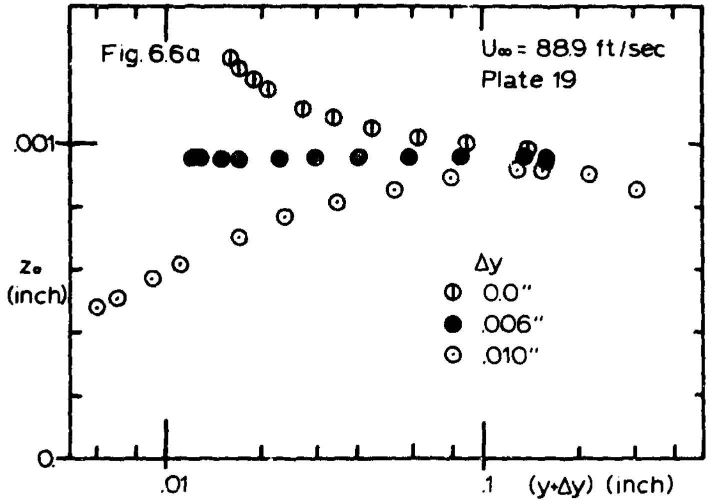

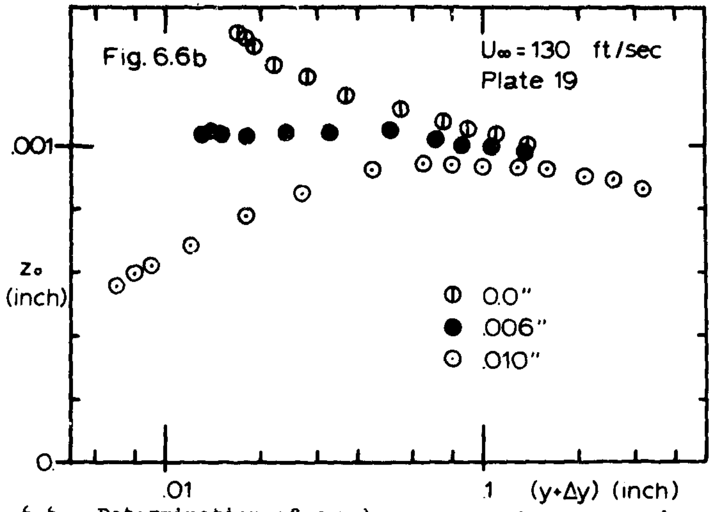

Fig. 6.6 Determination of roughness parameter z_o and wall shift Δy for fully rough velocity profiles with no transpiration.

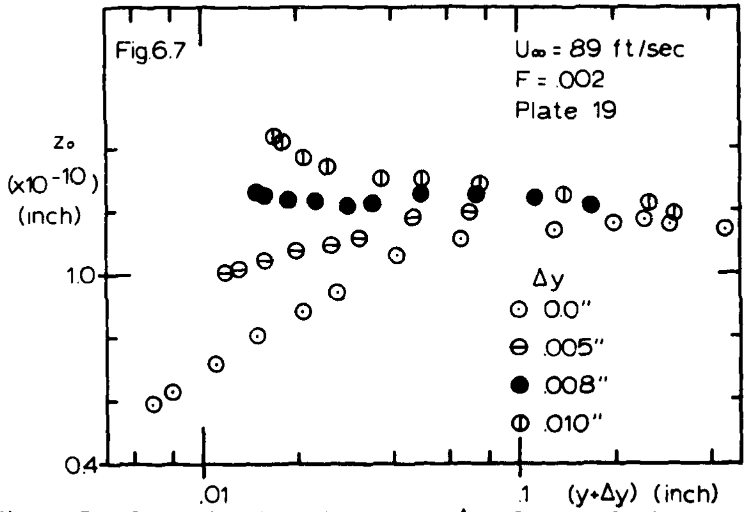

Fig. 6.7 Determination of z_o and Δy for a velocity profile with transpiration - F = 0.002.

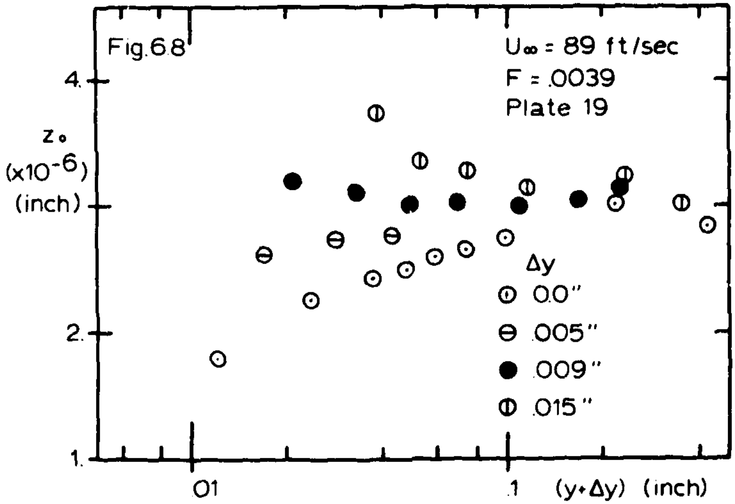

Fig. 6.8 Determination of z_o and Δy for a velocity profile with transpiration - F = 0.004.

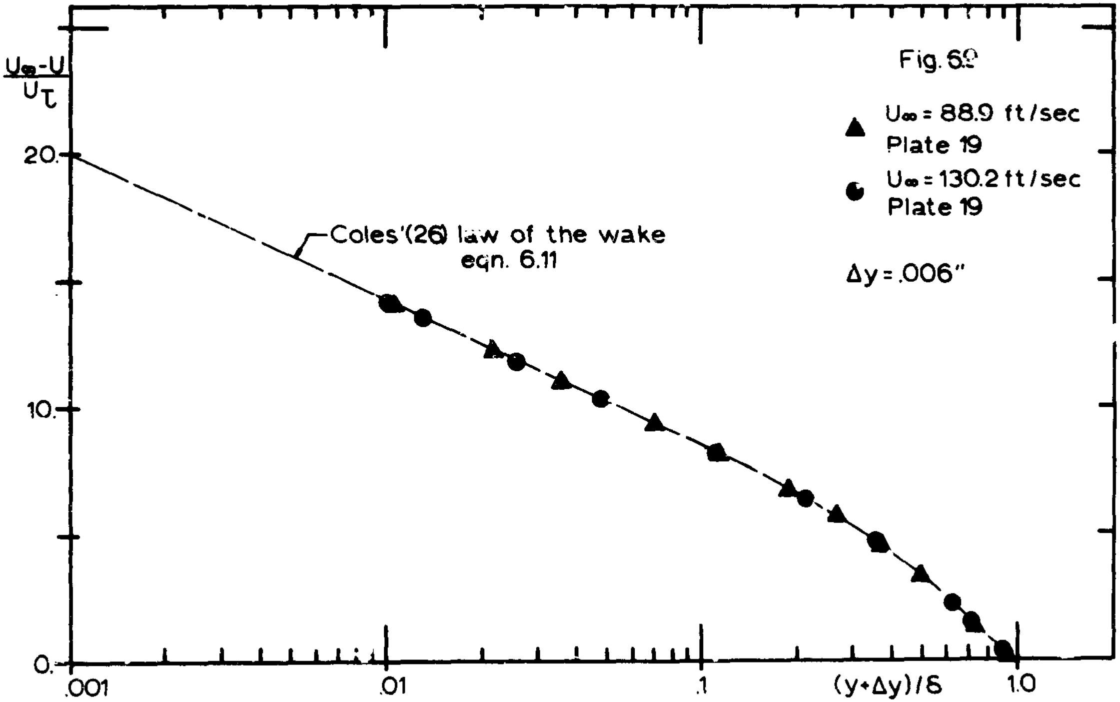

Fig. 6.9 Defect velocity profiles for the fully rough state with wall shift - comparison with Coles' law of the wake.

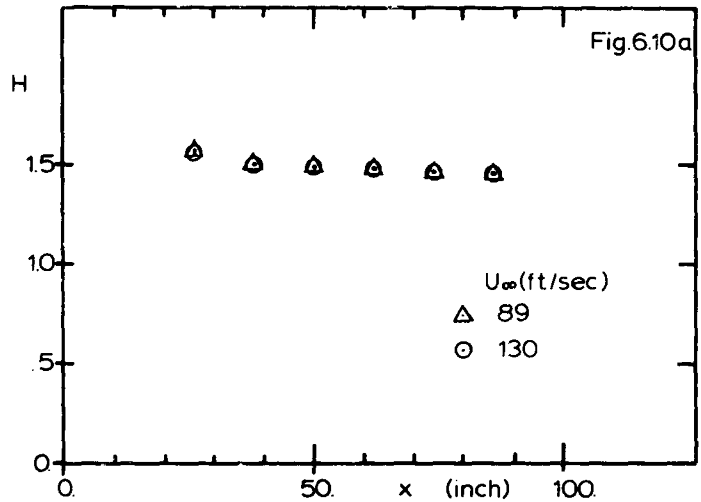

Fig. 6.10a Shape factors $H = \delta_1/\delta_2$ for the fully rough state.

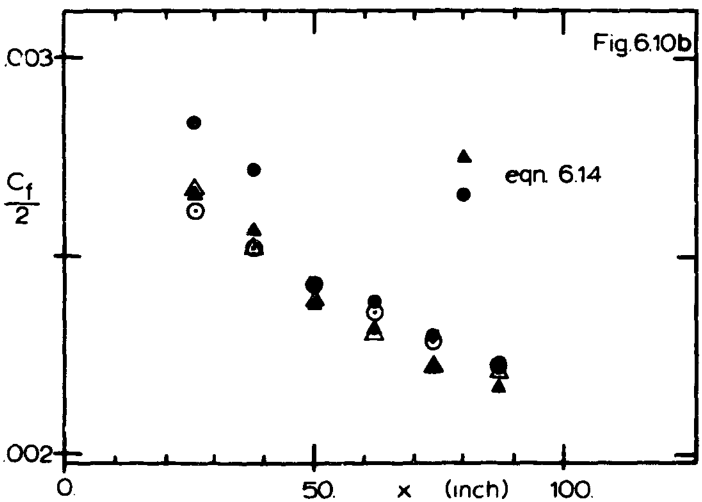

Fig. 6.10b Friction factors for the fully rough state - Hot-wire measurements and calculated values using Eqn. 6.14.

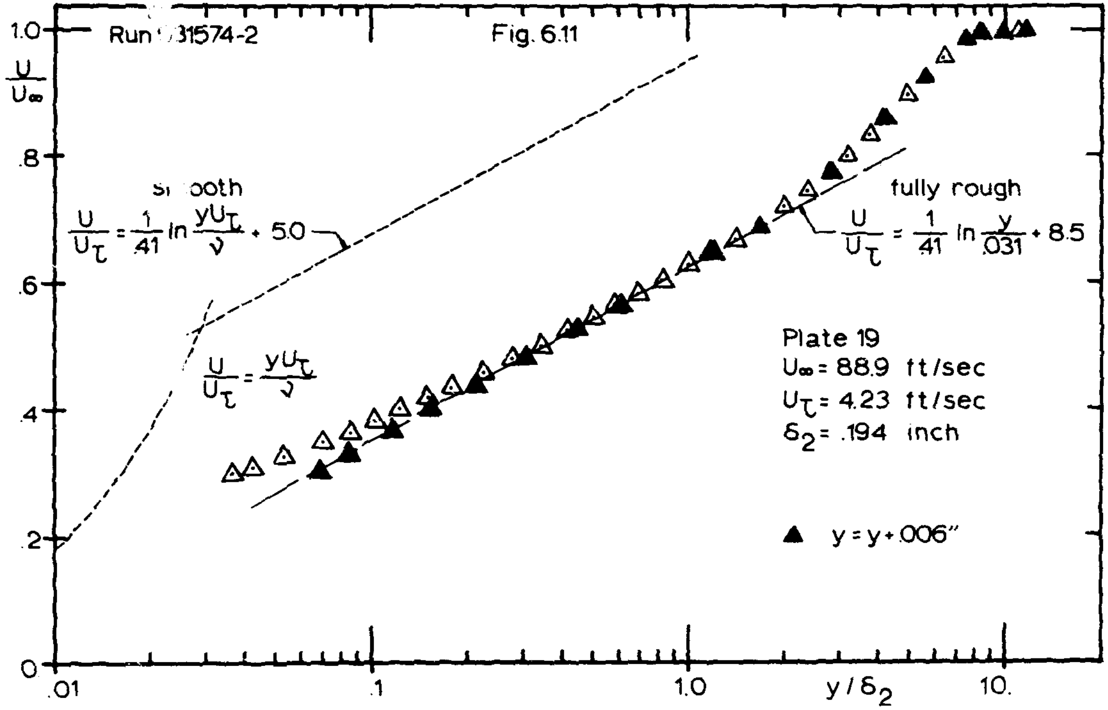

Fig. 6.11 Fully rough velocity profile - shifted and non-shifted y-coordinates.

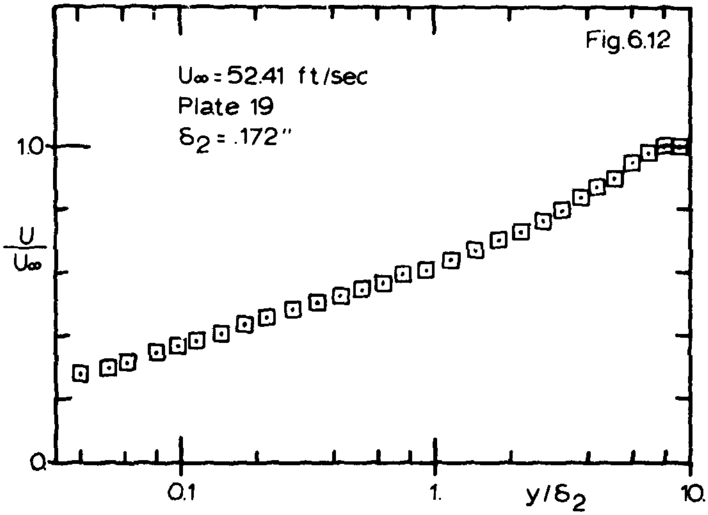

Fig. 6.12 Mean velocity profile - transitionally rough state (U_∞ = 52 ft/sec).

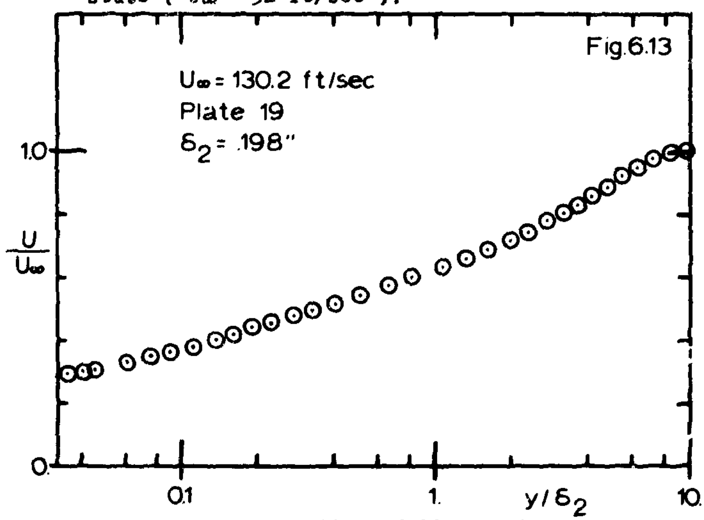

Fig. 6.13 Mean velocity profile - fully rough state (U_∞ = 130 ft/sec).

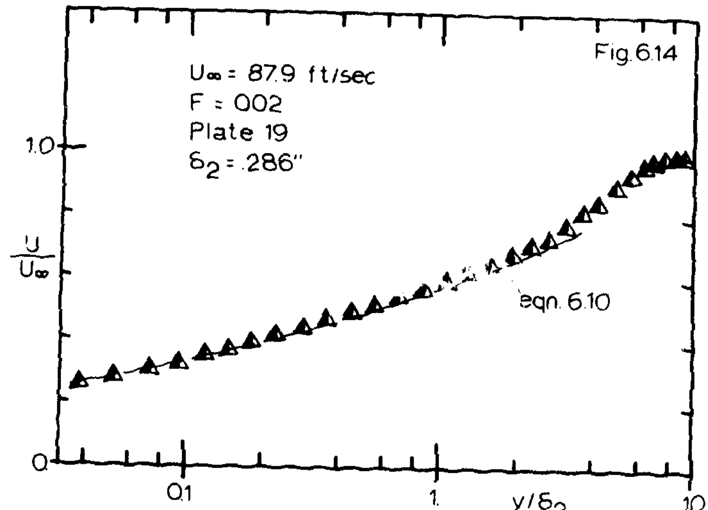

Fig. 6.14 Influence of blowing (F = 0.002) on the mean velocity profile.

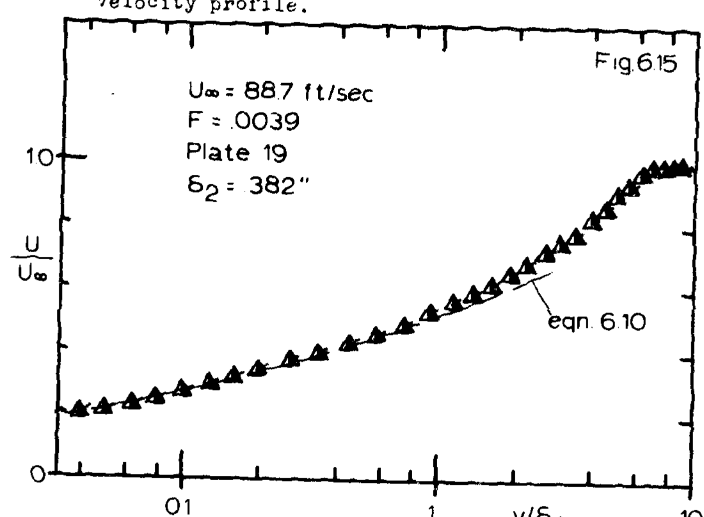

Fig. 6.15 Influence of blowing (F = 0.004) on the mean velocity profile.

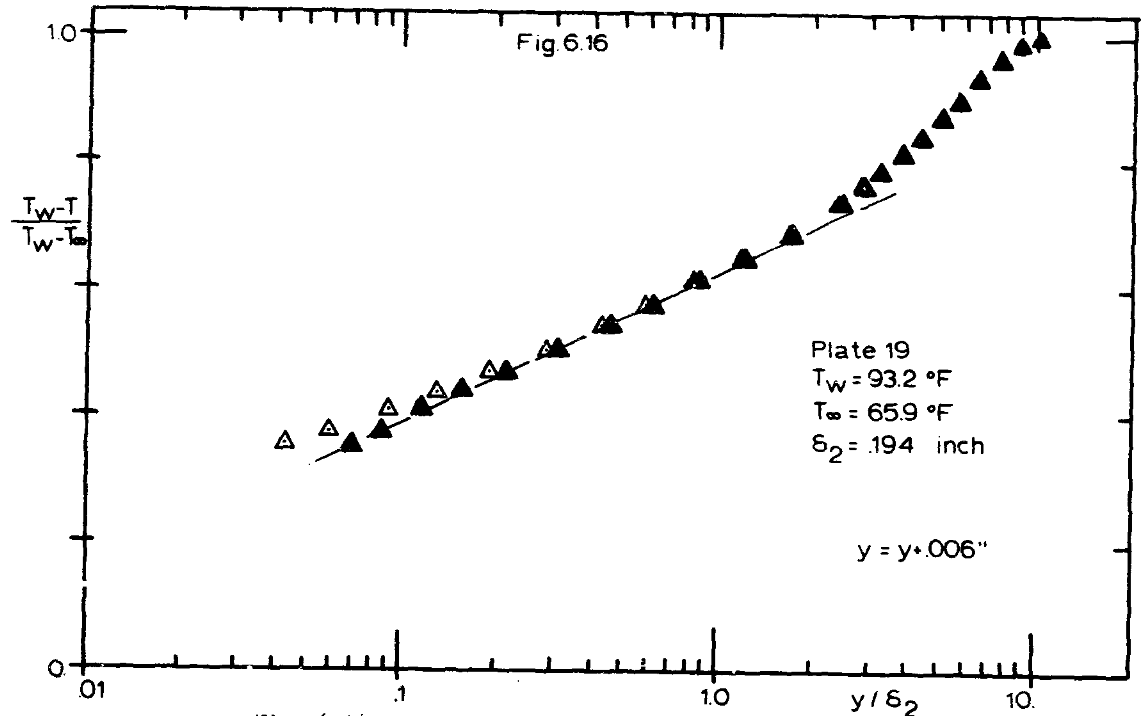

Fig. 6.16 Fully rougn temperature profile - shifted and non-shifted y-coordinates.

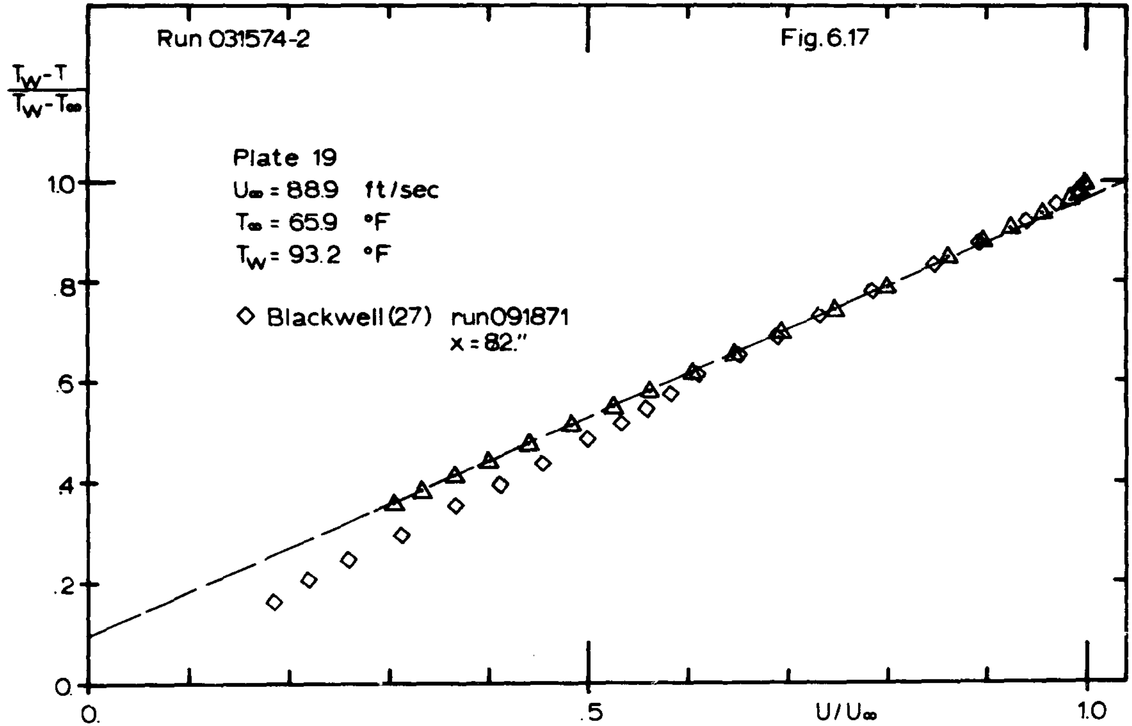

Fig. 6.17 Fully rough T x U profile: mean temperature versus mean velocity - comparison with Blackwell smooth wall data.

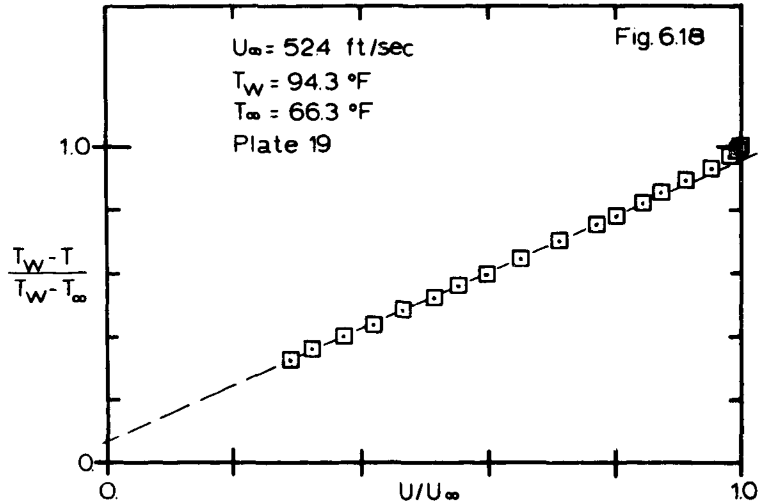

Fig. 6.18 Mean temperature versus mean velocity - T x U - transitionally rough state (U_∞ = 52 ft/sec).

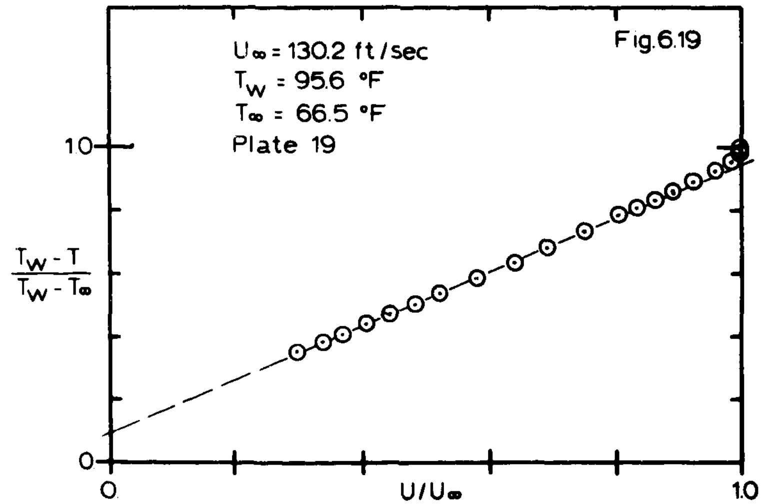

Fig. 6.19 Mean temperature versus mean velocity - T x U - fully rough state (U_∞ = 130 ft/sec).

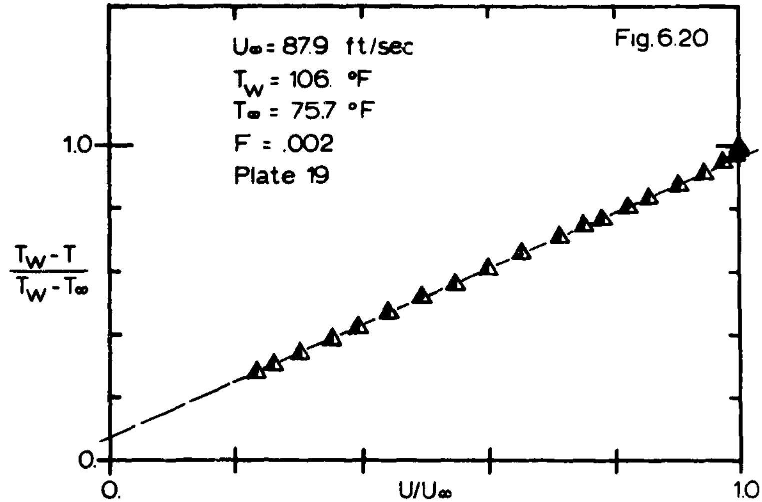

Fig. 6.20 Influence of blowing (F = 0.002) on the T x U profile - mean temperature versus mean velocity.

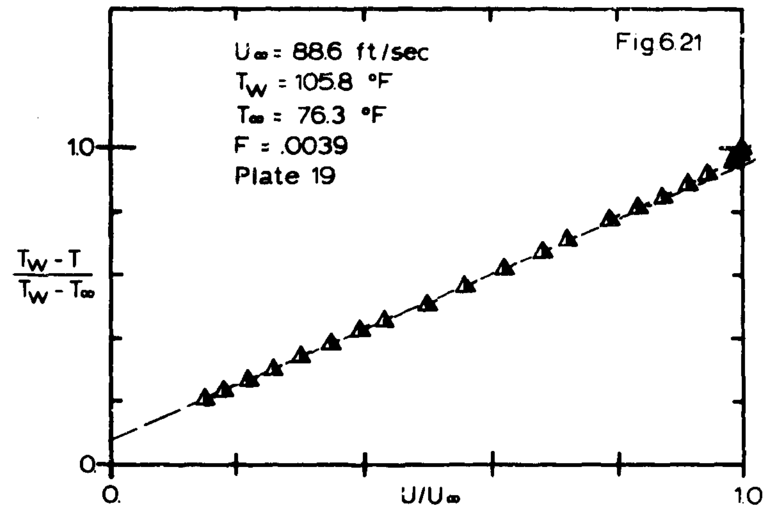

Fig. 6.21 Influence of blowing (F = 0.004) on the T x U profile - mean temperature versus mean velocity.

CHAPTER VII

TURBULENCE MEASUREMENTS

The measurements of the different turbulence quantities were made using the single rotating slant wire and the technique discussed in Chapter IV. Reynolds stress components were measured only for the isothermal cases, while temperature fluctuations and temperature-velocity correlations were determined for the non-isothermal cases.

The knowledge of the distribution of turbulence quantities can tell us a great deal about the turbulence mechanisms, as seen in Chapters II and III. While such knowledge is freely available for smooth walls, the lack of such knowledge for rough wall boundary layers has partly motivated this investigation.

Boundary layer transition is another aspect of rough wall behavior which was investigated during the preliminary runs. Natural transition occurred for all the cases analyzed -- no physical trip was used. As a consequence, the momentum and thermal boundary layers could not be forced to have the same virtual origin. The non-coincidence of these two origins introduces the problem of the unheated starting length, if the characteristics of the layer are analyzed in terms of integral parameters. However, this fact had little effect for the high velocity runs, for which the layer tripped itself very near the beginning of the test section ($x_o \approx 0.0$).

The fully rough state of the unblown boundary layer has been described in Chapters V and VI. The friction factor $C_f/2$ and Stanton number St are independent of Reynolds number and, consequently, independent of viscosity They are, in fact, only functions of local integral parameters δ_2 and Δ_2, the momentum and enthalpy thicknesses, respectively. Furthermore, in the outer region there is mean flow field similarity, as we saw for the variables $(U_\infty-U)/U_\tau$ and y/δ. Therefore, the length scale of the flow is a local layer thickness, say δ, and so we will use the non-dimensional variable y/δ in this chapter. By using similarities arguments it can be expected that the appropriate temperature scale is T_τ.

The data shown in this chapter correspond to measurements taken at plate 19.

7.1 Comments on the Smooth Wall Zero Pressure Gradient Flows

One of our objectives of this investigation was the study of the effects of a rough wall on the turbulence structure of a boundary layer. The ideal way of identifying these effects would have been to measure the turbulence quantities for a smooth wall and a rough wall in the same apparatus and then compare the two cases. The major observable differences in this comparison could, then, in principle, be attributed to roughness effects. Unfortunately, due to the complexity of an apparatus for a rough, permeable wall, we were not able to substitute a smooth wall in our wind tunnel. For the comparisons, therefore, we have to rely on results of other authors.

Measurements of turbulence quantities for smooth wall, zero pressure gradient layers have been reported by several authors. Most of those refer to isothermal flows and, therefore, only to the velocity fluctuations. Very few studies have been reported of turbulent temperature fluctuations.

Klebanoff's [15] isothermal measurements are considered reliable and will be used in this investigation. Figure 7.1 shows some of his results.

There are some observations that are common to most studies of the smooth wall case, and these are used in our comparisons:

··· The turbulence field strongly influences the mean field. In fact, it extracts energy from the mean field through turbulent kinetic energy production, $-\overline{u'v'}\ \partial U/\partial y$. It is the large-scale motions of turbulence (large eddies) that contain most of the turbulent energy and are primarily responsible for the interaction with the mean field.

··· The turbulent field is strongly non-isotropic near the wall, and tends to isotropicity toward the free stream (see Figure 7.1). The distribution of the stream-wise component of the velocity fluctuations has a sharp peak very near the wall, where the eddies are very elongated in the x-direction.

··· The turbulence field extends beyond the edge of the momentum boundary layer, based on mean velocity, to as far as $y/\delta \approx 1.4$. For $y/\delta \gtrsim 0.7$

the flow has an intermittent nature and is not fully turbulent all the time (see Klebanoff [15] or Tennekes [25]).

... The free stream turbulence intensity has a strong influence on the turbulence field, as noted by Orlando [17] and Kearney [40] among others.

... The stream-wise normal velocity correlation, $-\overline{u'v'}/\sqrt{\overline{u'^2}}\sqrt{\overline{v'^2}}$ has the approximately constant value of 0.45 over most of the layer ($0.2 < y/\delta < 0.8$).

... The turbulent shear stress normalized by the turbulent kinetic energy, $-\overline{u'v'}/q^2$ has the approximately constant value of 0.14 over the same region as above (see Bradshaw [38] and Townsend [37]).

As the effects of the free stream turbulence level could overshadow those of the rough wall, we decided to investigate this point further. During the preliminary runs we measured profiles of stream-wise velocity fluctuation $\overline{u'^2}$ for different free stream velocities.

Figures 7.2 and 7.3 show plots of $\sqrt{\overline{u'^2}}$ normalized by U_∞ and U_τ. We have represented a typical profile for our rough wall, when the free-stream velocity was 89 ft/sec. A profile of Klebanoff's [15] work is shown corresponding to the smooth flat plate case with very low free-stream turbulence level ($\approx 0.03\%$). One profile from Orlando's [17] work is shown corresponding to the smooth flat plate case with somewhat higher free-stream turbulence level ($\gtrsim 0.5\%$) than in our Roughness Rig ($= 0.4\%$).

The effect of the free-stream turbulence level in the smooth flat plate case is apparent in the outer region ($y/\delta > 0.3$). The effect of the rough wall, however, is felt throughout the layer in both plots. The higher turbulence intensity in the outer region is evident from the $\sqrt{\overline{u'^2}}/U_\infty$ plot. The near wall region was seen to be strongly dependent on the free-stream velocity, and consequently on the flow regime (fully rough, etc., see Chapter III). These facts go against Hinze's [32] remarks on Corrsin et al. [41] data, which showed U_τ to be a normalizing parameter that would make smooth and rough data look the same outboard of $y/\delta = 0.2$ or so.

The differences in the near wall region can be better appreciated in Figure 7.4. We have represented the smooth, transitionally rough and fully rough profiles. The main feature observed from the fully rough state is the suppression of the peak in $\overline{u'^2}$, near the wall, which is present for the smooth and transitionally rough profiles. The outer region is just slightly affected.

Measurements of the temperature fluctuations and temperature-velocity correlations are not common, and only a few authors have reported them in the literature. Next we will refer to those measurements we used for comparisons.

Figure 7.5 shows a comparison between a typical rough wall measurement of $\overline{t'^2}$ from this study and the smooth, flat plate data of Orlando [17] (corrected data) and Fulachier and Dumas [73]. The rough wall measurements have the same level as those of Fulachier and Dumas, and Orlando, which indicates that $\overline{t'^2}$ is properly non-dimensionalized by T_τ. The data of Orlando has been corrected for the proper conduction loss according to Maye [64]. His $\overline{t'^2}$ data had been undercorrected for this loss, because the length of the hot wire was taken as $\ell = 3$ mm instead of 1.2 mm, which was the real one.

Figure 7.6 shows the turbulent heat flux correlation coefficients for a typical rough wall run. The correlation coefficient distribution is reasonably flat, with values close to 0.6 over most of the layer, and its level compares favorably with Orlando's data [17] (corrected values) for a smooth flat plate case.

7.2 Transition over a Rough Wall

The transition of a boundary layer, developing over a rough wall, from laminar to turbulent behavior is an important aspect considered in design applications of ablative thermal protection of surfaces. This aspect was studied as part of our preliminary runs.

During this investigation, for all cases, the layer had a natural transition. For a very low velocity, in particular, it occurred well down the test section, and a well-defined laminar layer preceded it. We then decided to further analyze a low velocity case. A free-stream velocity around 36 ft/sec was set and turbulence measurements were taken.

As discussed in Section 6.2, transition for the 36 ft/sec run occurred over a distance corresponding to two plate widths, located between plates 10 and 12.

At plate 8 the layer was still laminar. Turbulent fluctuations were essentially those of the free-stream, and no discernible difference on their level from point to point across the layer could be observed.

The transition region was characterized by rather large fluctuations. Their level reached in some places 50 to 60% of the local velocity value. These fluctuations, however, were of intermittent character -- periods of high turbulence intensity were followed by periods of relative quiescence.

Transition is viewed by many as starting in some spots near the wall. This view was supported by the fact that the layer was found not to be turbulent all across its thickness. The free-stream value of turbulence level was reached for $y/\delta < 1.0$. The turbulence in the layer is less intermittent the farther downstream one goes.

A remarkable characteristic of the transition region is in the correlation between the stream-wise u' and normal v' velocity fluctuations. At the beginning of transition, it is only high near the wall. As we follow downstream, the correlation reaches an approximately constant value of 0.45 over most of the layer. This indicates that the turbulent shear stress rapidly reaches its high level near the wall and more slowly in the outer region. This is other evidence that the outer region has a long memory and only slowly reacts to changes in the boundary conditions. This aspect of rough wall behavior is the same as for smooth flat plate layers.

The fast adjustment of the layer to its new condition (fully turbulent) near the wall explains why friction factor and Stanton number distributions for our rough wall show a short transition region. The turbulence field was found to continue evolving for a long distance, even after the mean field had already adjusted itself to the fully turbulent state.

Figures 7.7, 7.8 and 7.9 illustrate some of these points. They refer to our 36 ft/sec run, and show, respectively, $\overline{u'^2}/U_\infty^2$, $-\overline{u'v'}/\sqrt{\overline{u'^2}}\sqrt{\overline{v'^2}}$ and $C_f/2$ distributions.

7.3 Reynolds Stress Components

Systematic measurements of the Reynolds stress components were taken in our investigation for three free-stream velocities and two blowing rates. All profiles shown correspond to plate 19.

Figures 7.10, 7.11, and 7.12 show, respectively, the $\overline{u'^2}$, $\overline{v'^2}$, $\overline{w'^2}$ components for the 52, 89 and 130 ft/sec runs. Major differences between them are in the $\overline{u'^2}$ component.

Figures 7.13 and 7.14 show these components for the blown cases. Now the non-dimensional variable has to be $\overline{u'^2}/U_\infty^2$, because U_τ is diminished with the blowing and is not a good velocity scale.

Figures 7.15 and 7.16 show the correlation coefficients between the longitudinal and normal velocity components. The flows analyzed in this investigation exhibit an approximately constant value of 0.45 for the correlation coefficient. Thus, this characteristic of smooth flat plate layers is, surprisingly, preserved even under the effect of uniform roughness and blowing rate.

These figures also show the ratio between the shear stress and the kinetic energy of turbulence. An approximately constant value of 0.14 is maintained over most of the layer, and again uniform roughness and blowing rate do not alter this characteristic of smooth flat plate layers.

These facts suggest, therefore, similarities in the turbulent transport of momentum in the outer region for smooth and rough wall layers.

7.4 Turbulent Temperature Fluctuations

The measurements of turbulent temperature fluctuations are complicated, not too accurate, and time-consuming. Nonetheless, their distributions and correlations with velocity fluctuations are important to the study of the turbulent transport properties.

Figure 7.17 shows the dimensionless temperature fluctuation profiles for the unblown and blown cases. The extraordinary resemblance to the velocity fluctuation profiles of Figure 7.4 suggests that the turbulent temperature field is governed by the turbulence field.

Figure 7.18 shows the correlation coefficient $-\overline{u't'}/\sqrt{\overline{u'^2}}\sqrt{\overline{t'^2}}$ between the longitudinal velocity and temperature fluctuations. A reasonably constant value of 0.7 to 0.8 is observed for all cases. There is no tendency of the correlation coefficient to be higher near the wall and become 1.0 , an observation reported for smooth walls by Johnson [80] and used by Orlando [17]. In fact, near a rough wall, there is no reason for a higher coherence between t' and any velocity fluctuation.

Figure 7.19 shows the correlation coefficient $\overline{v't'}/\sqrt{\overline{v'^2}}\sqrt{\overline{t'^2}}$ between the normal velocity and temperature fluctuations. $\overline{v't'}$ is the turbulent heat flux, which in our case is at least two orders of magnitude larger than the molecular heat flux, $-k\partial T/\partial y$. This correlation coefficient is reasonably constant for both unblown and blown cases.

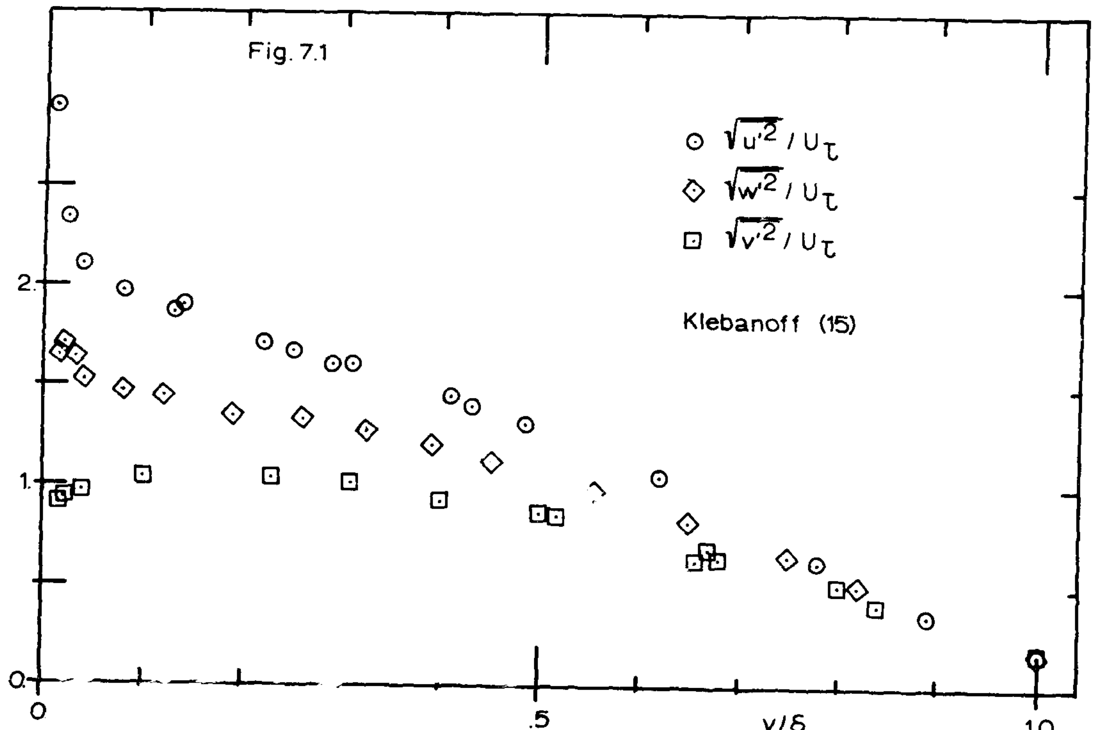

Fig. 7.1 Turbulence intensities profiles - Klebanoff's smooth wall data.

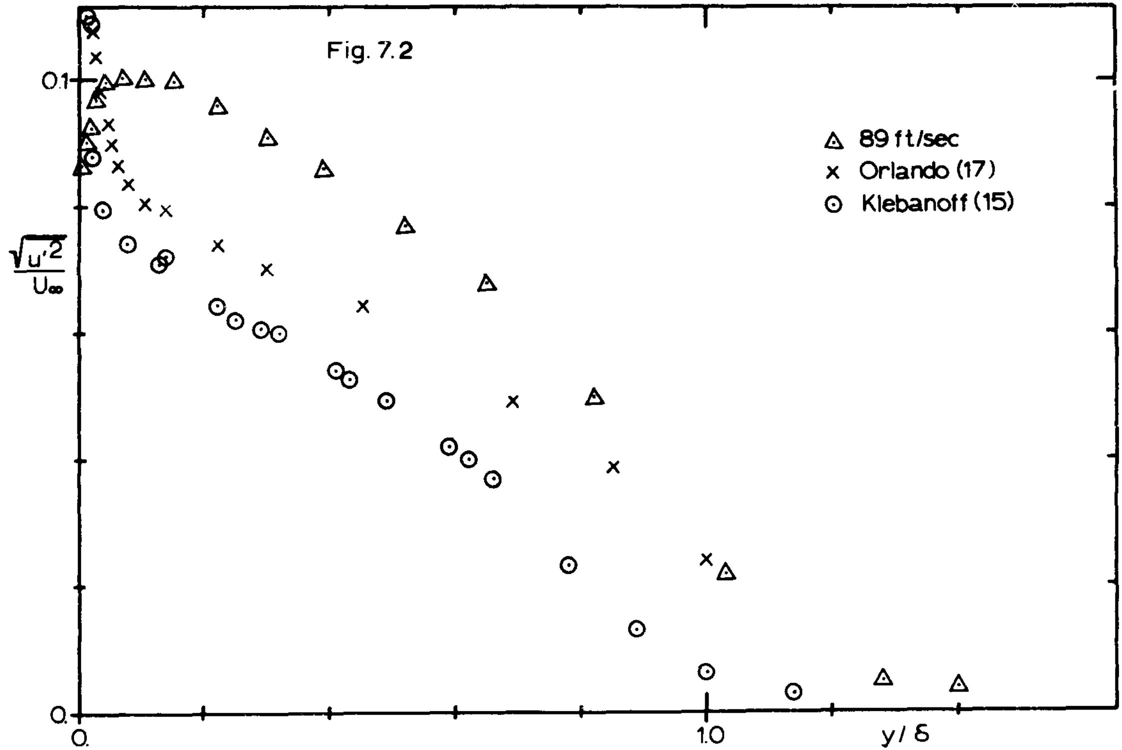

Fig. 7.2 Longitudinal velocity fluctuation profile - fully rough state values normalized by U_∞ compared with smooth wall data.

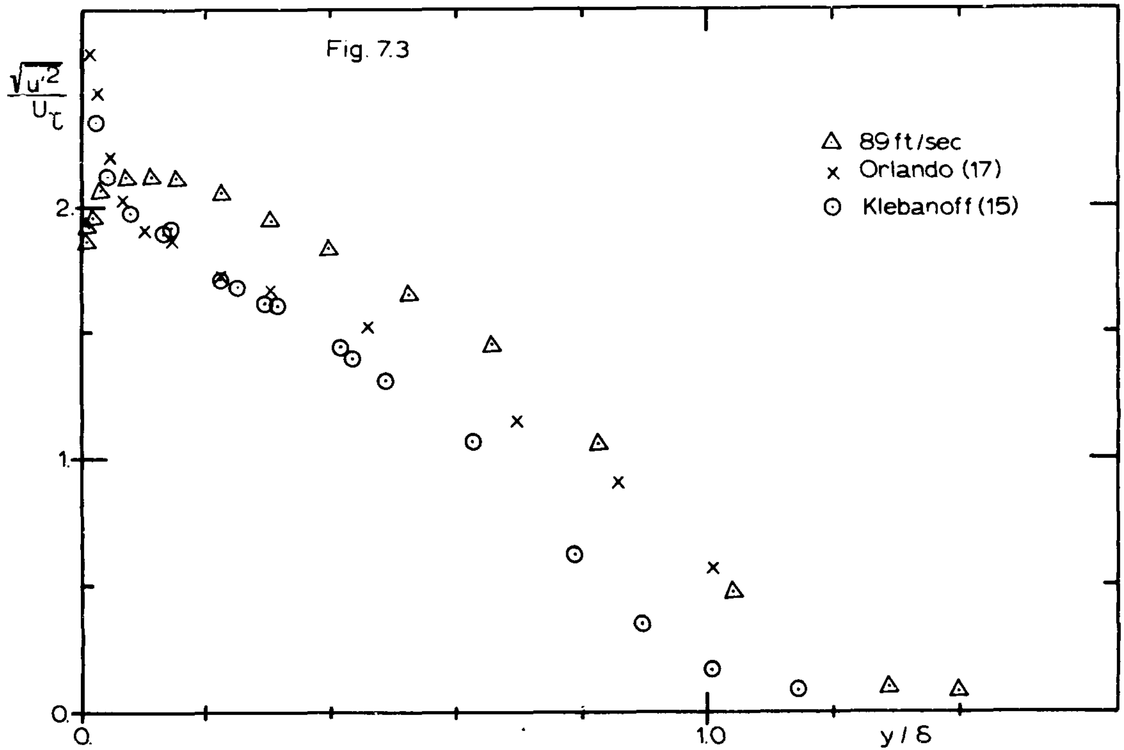

Fig. 7.3 Longitudinal velocity fluctuation profile - fully rough state values normalized by U_τ compared with smooth wall data.

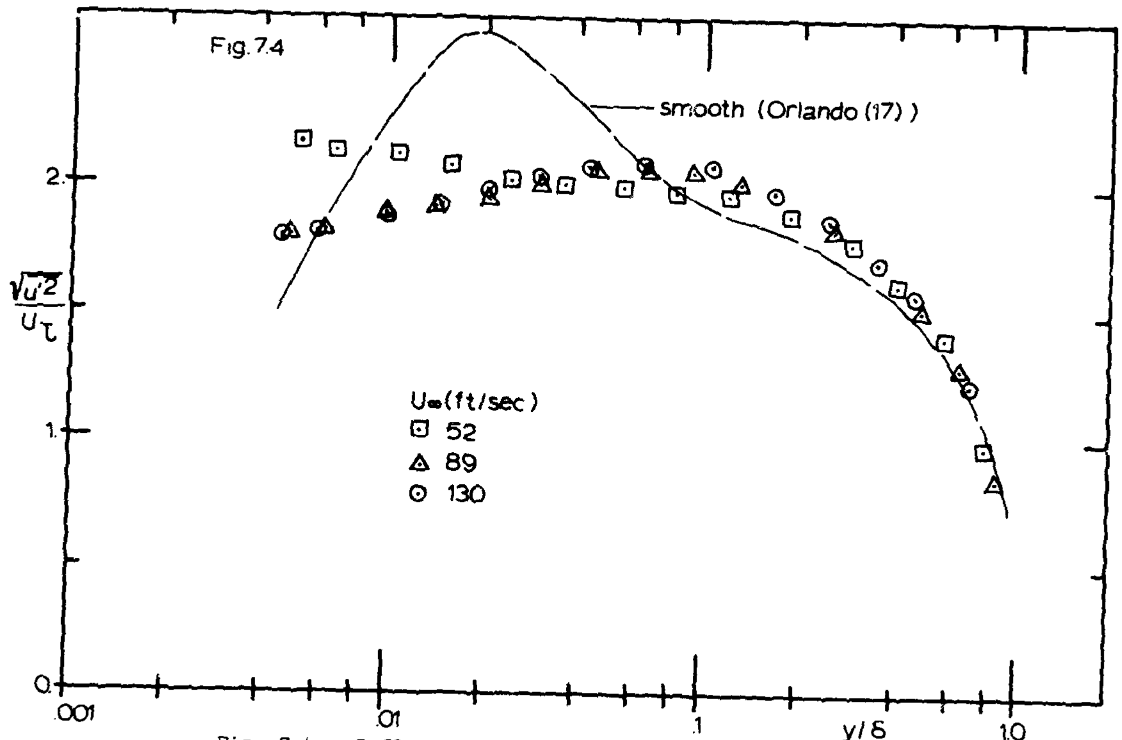

Fig. 7.4 Influence of the rough wall on the longitudinal velocity fluctuation profile in the near wall region.

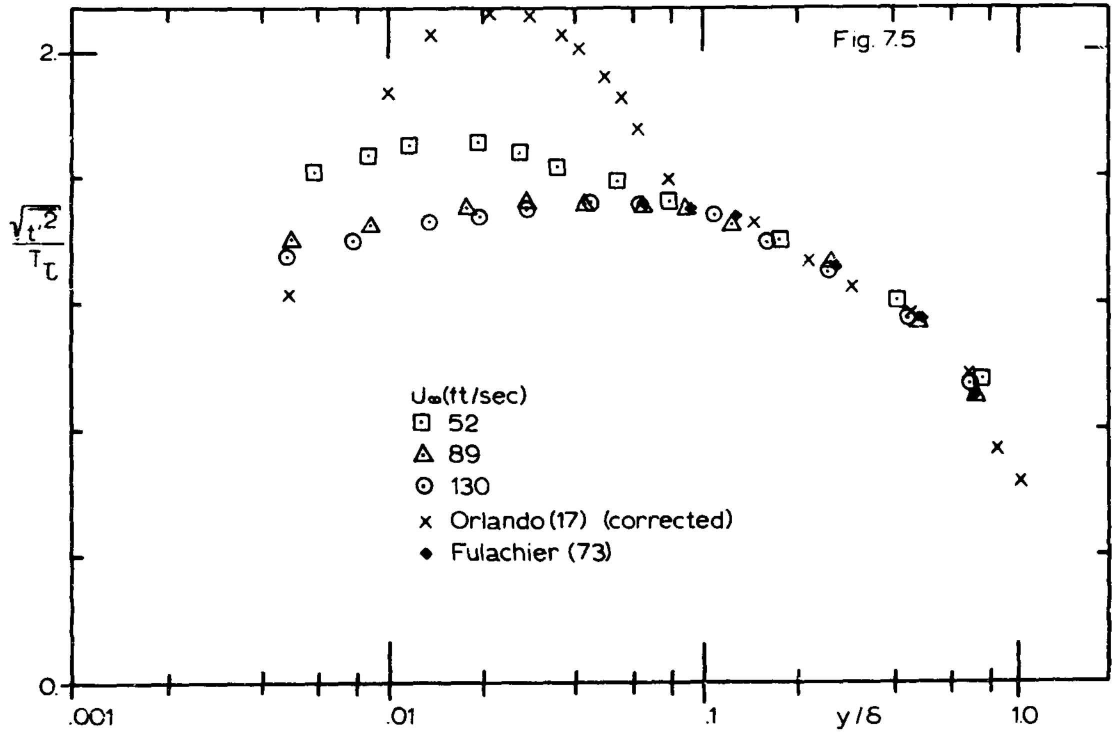

Fig. 7.5 Influence of the rough wall on the temperature fluctuation profile in the near wall region.

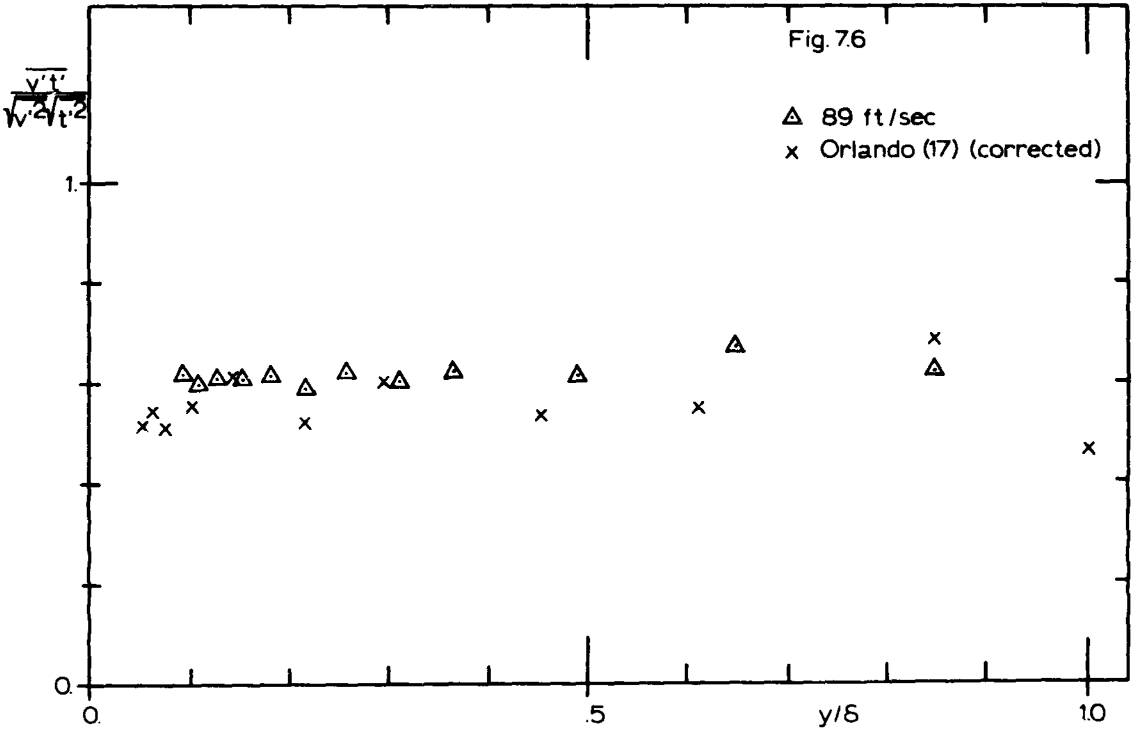

Fig. 7.6 Correlation coefficients between the temperature and normal velocity fluctuations - comparison with smooth wall data.

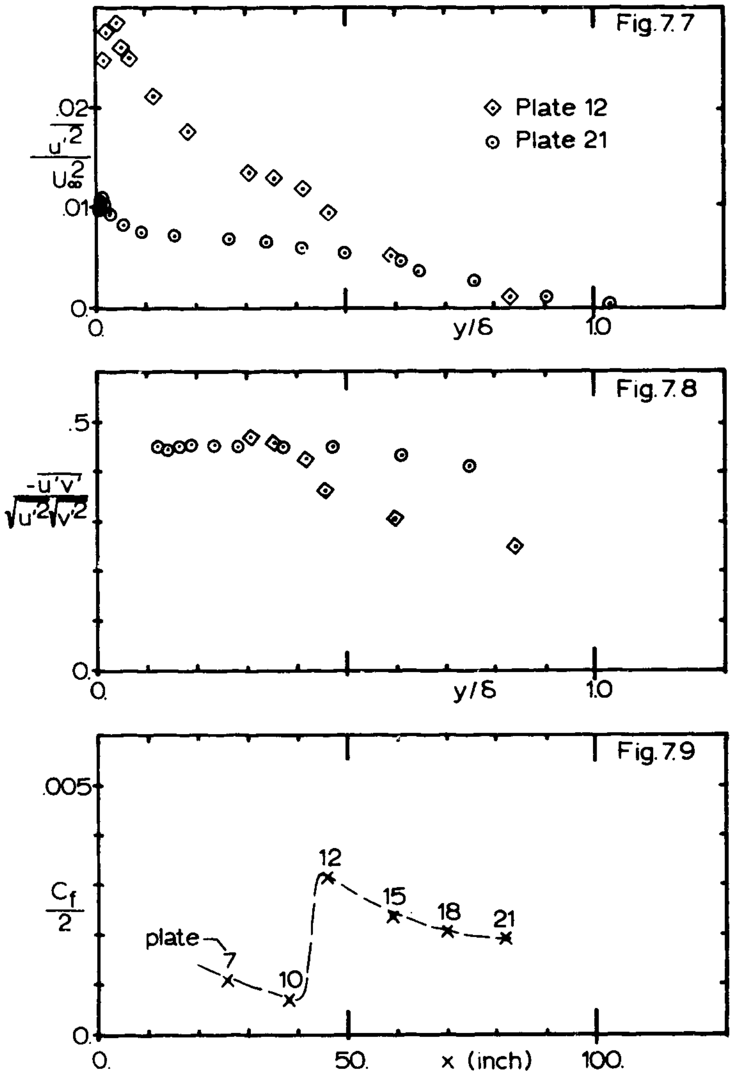

Figs. 7.7-9 Different aspects of transition of a turbulent boundary layer over a rough surface.

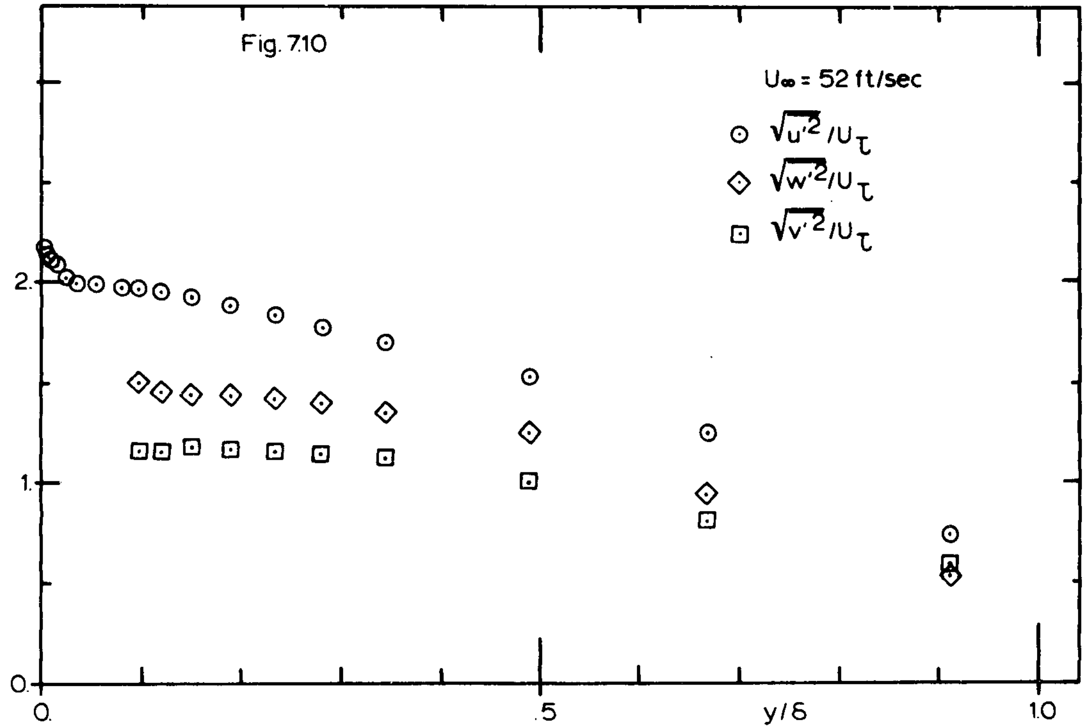

Fig. 7.10 Turbulence intensities profiles - transitionally rough state (U∞ = 52 ft/sec).

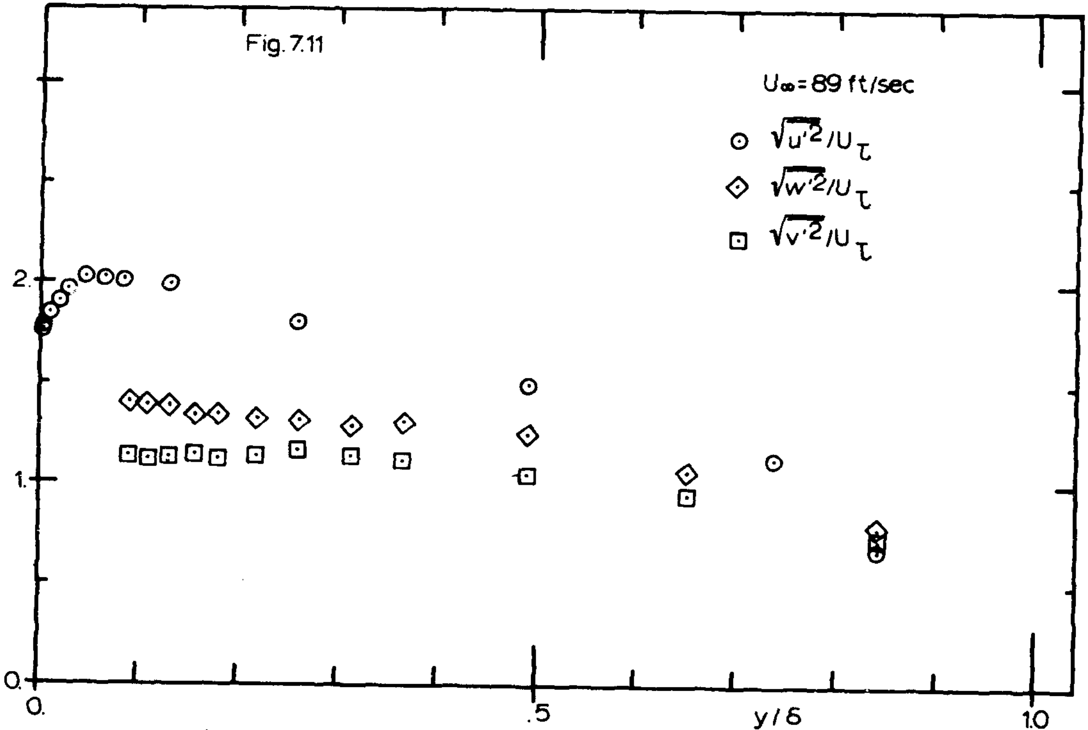

Fig. 7.11 Turbulence intensities profiles - fully rough state (U∞ = 89 ft/sec).

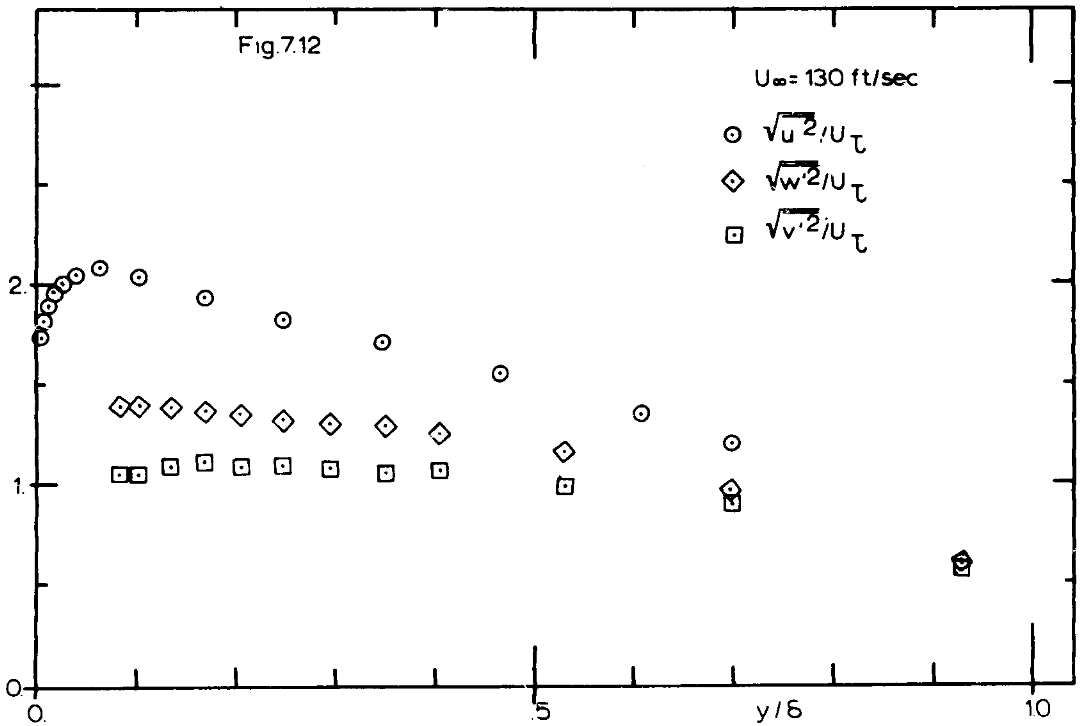

Fig. 7.12 Turbulence intensities profiles - fully rough state (U_∞ = 130 ft/sec).

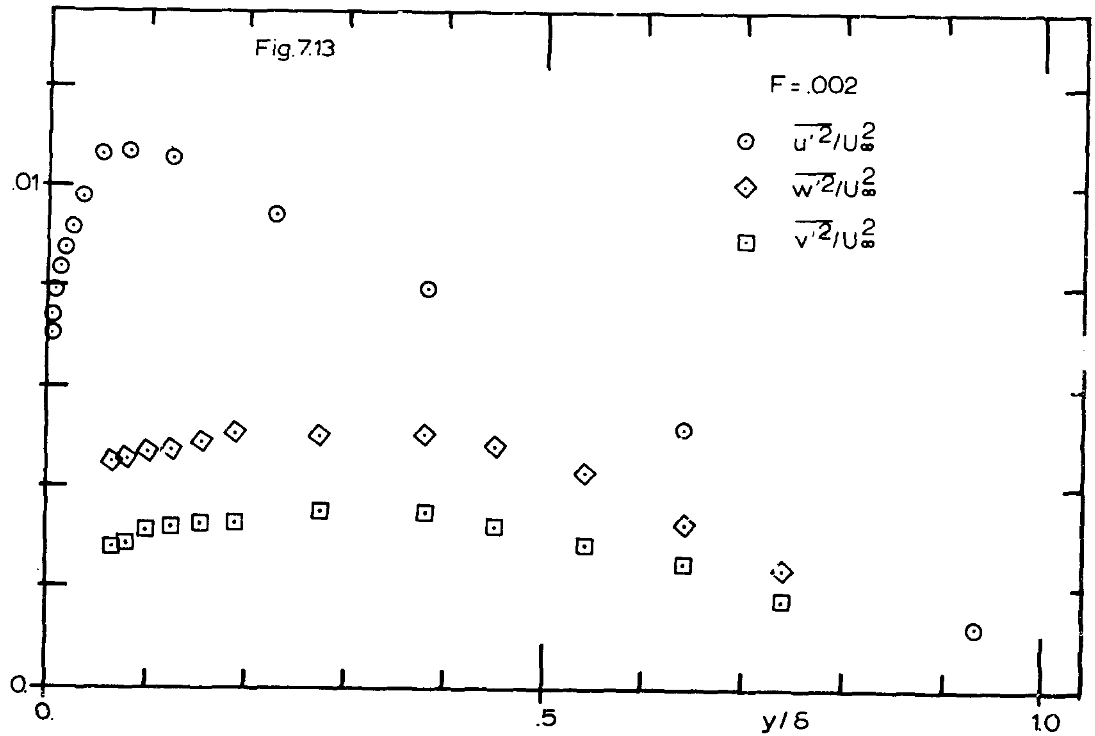

Fig. 7.13 Influence of blowing (F = 0.002) on the turbulence intensities profiles.

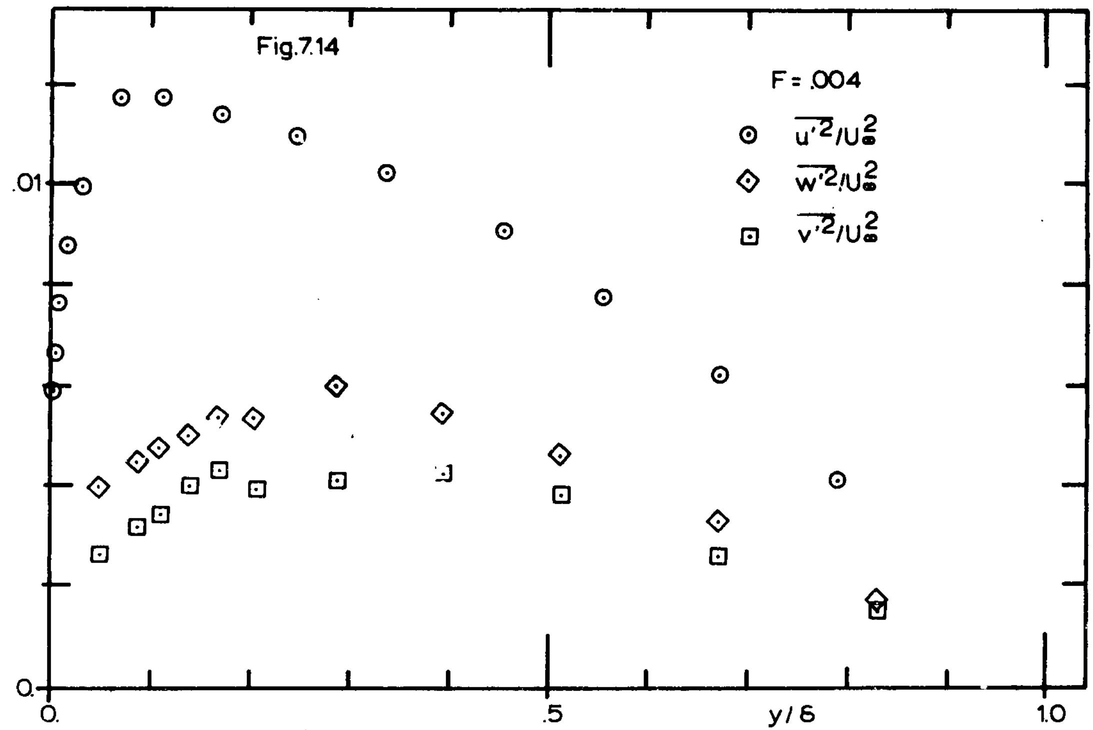

Fig. 7.14 Influence of blowing (F = 0.004) on the turbulence intensities profiles.

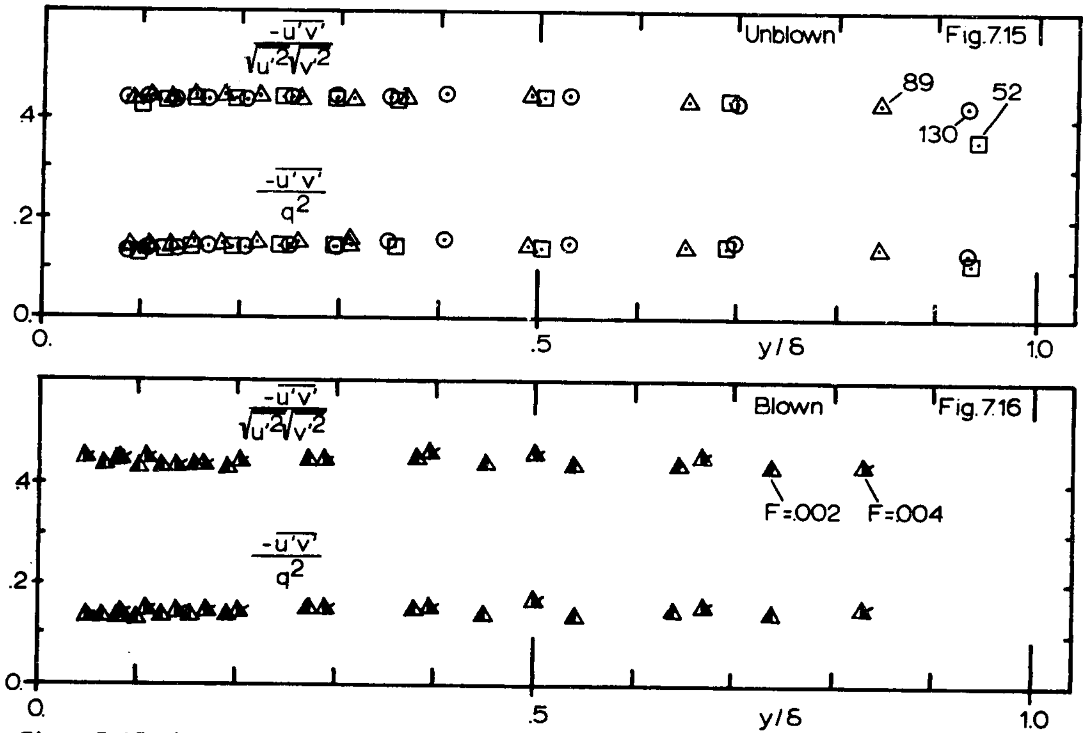

Figs. 7.15-16 Turbulent shear stress distributions - correlation coefficients compared with the values normalized by the turbulent kinetic energy.

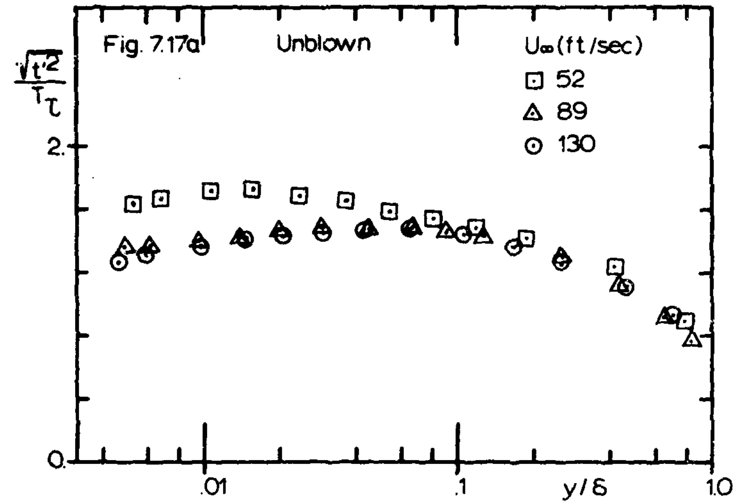

Fig. 7.17a Temperature fluctuation profiles - flows with different free-stream velocities.

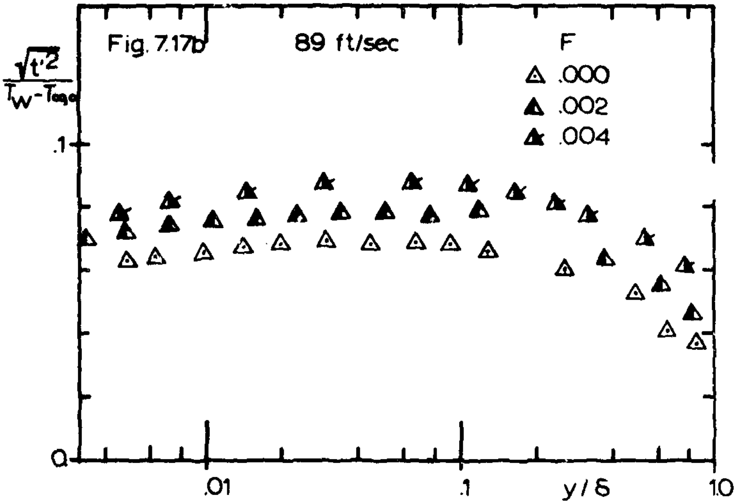

Fig. 7.17b Temperature fluctuation profiles - flows with different blowing rates.

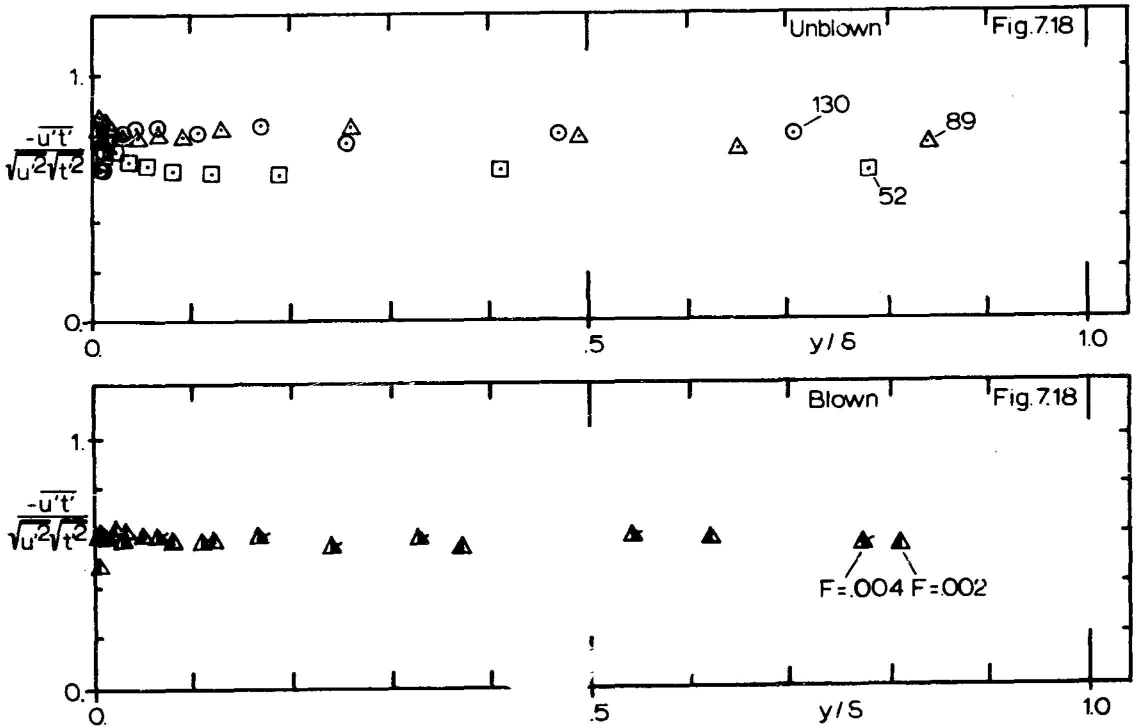

Fig. 7.18 Correlation coefficients between the temperature and longitudinal velocity fluctuations.

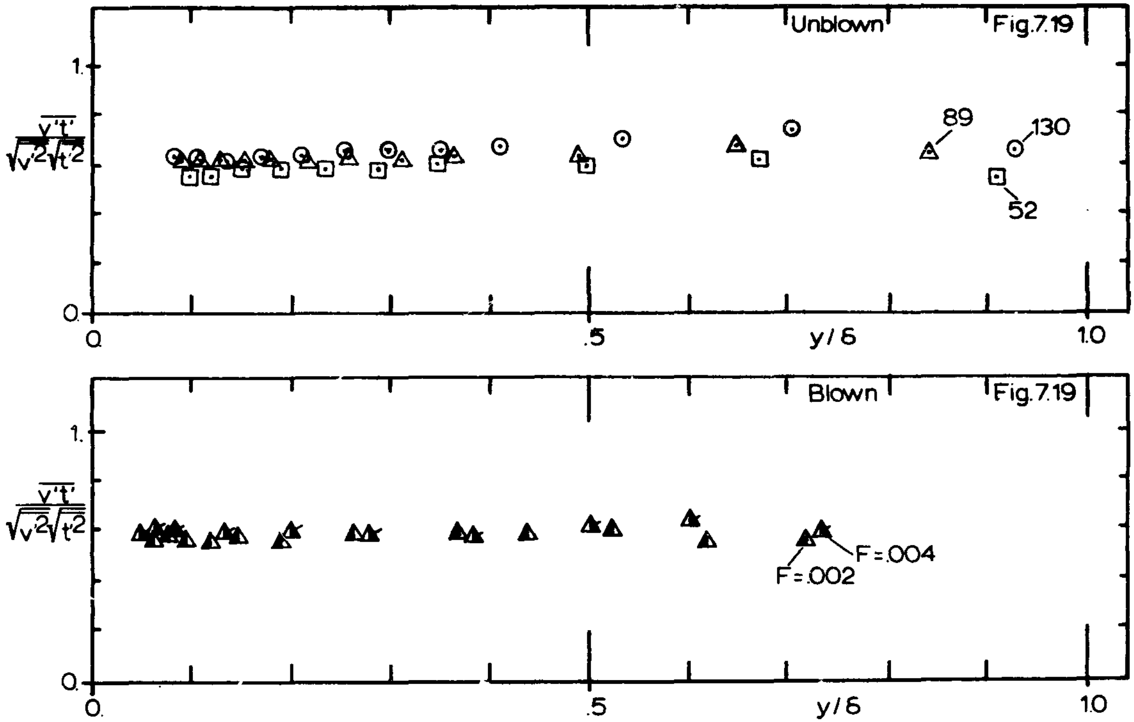

Fig. 7.19 Correlation coefficients between the temperature and normal velocity fluctuations.

CHAPTER VIII

TRANSPORT PROPERTIES OF MOMENTUM AND HEAT

The measurement techniques used in this investigation allow the determination of the turbulent shear stress $-\rho\,\overline{u'v'}$ and turbulent heat flux $\rho\, c_p \overline{v't'}$ distributions. As discussed in Chapter IV, this determination is direct and independent of any information of the mean flow field. The hot-wire probe readings at each position are converted into stress and heat fluxes by means of calibration curves - a definite improvement over methods using the integrated two-dimensional x-momentum and energy boundary layer equations. The latter require parameters such as friction factors $C_f/2$, Stanton numbers St, blowing fractions F and pressure gradient dp/dx to be known and also require x and y - derivatives to be numerically taken. There are several sources of uncertainty which decrease the accuracy of the integrated method, which are not present in the present method.

The correlations $-\overline{u'v'}$ and $\overline{v't'}$ represent local normal fluxes of momentum and heat resulting from the turbulent fluctuations. These fluxes, in fact, are responsible for the direct interaction between the turbulent field and the mean flow field. The study of the turbulent transport of heat and momentum has as one of its objectives the determination of the dependence of $-\overline{u'v'}$ and $\overline{v't'}$ on the fluid flow parameters. This is accomplished in a simple and widely used way by defining the transport properties: eddy diffusivities for momentum and heat, ε_M and ε_H respectively as

$$-\overline{u'v'} = \varepsilon_M \frac{\partial U}{\partial y} \tag{8.1}$$

and

$$-\overline{v't'} = \varepsilon_H \frac{\partial T}{\partial y} \quad . \tag{8.2}$$

The ratio $\varepsilon_M/\varepsilon_H$ between the eddy diffusivities for momentum and heat is the so-called turbulent Prandtl number. Hence, the closure problem of the turbulent boundary layer equations is solved if ε_M and Pr_t are known. It is common practice to devise algebraic expressions to relate

ε_H and ε_M to the flow parameters. Unfortunately, these expressions are destitute of physical content and do not elucidate the turbulence phenomenon. The objective of this study is not, however, determination of such expressions, but rather the documentation and analysis of the distributions of the turbulent shear stress and heat flux.

Direct measurements of $-\overline{u'v'}$ and $\overline{v't'}$ in the same boundary layer are scarcely reported in the literature: Orlando [17], Johnson [80] and Blom [81] show data for smooth wall cases, but no data for rough wall cases were found.

8.1 Turbulent Transport of Momentum - the Mixing-Length

The ratio between the eddy diffusivity for momentum ε_M and the molecular viscosity ν can be taken as a Reynolds number for the turbulence

$$Re_t = \frac{\varepsilon_M}{\nu} \tag{8.3}$$

The present data show that $Re_t \gg 1$ for $y > \xi$ (see Chapter V for ξ definition) for all cases considered in this study. Hence, in the region $(y > \xi)$ where measurements were taken the molecular transport is negligible and

$$\tau = -\rho\, \overline{u'v'} \tag{8.4}$$

This result was expected from the non-dependence of $C_f/2$ on Re_{δ_2} or ν .

If, near the wall, the Couette flow assumption $(\partial/\partial x \approx 0)$ is valid then Equation (5.15) can be written as

$$\frac{C_f}{2} + \frac{UV_o}{U_\infty^2} = -\frac{\overline{u'v'}}{U_\infty^2} \tag{8.5}$$

Let us recall that Equation (5.15) was obtained from the time averaged continuity and x-momentum boundary layer equations for the two-dimensional domain of our layer $(y > \xi)$ (see Chapter V).

Introducing $U_\tau = \sqrt{C_f/2}\, U_\infty$, we obtain

$$1 + \frac{UV_o}{U_\tau^2} = -\frac{\overline{u'v'}}{U_\tau^2} \tag{8.6}$$

which for the unblown case reduces to

$$- \frac{\overline{u'v'}}{U_\tau^2} = 1 \quad . \tag{8.7}$$

The region of validity of Equation (8.7) is the so-called "constant shear stress layer".

Figure 8.1 shows plots of $-\overline{u'v'}/U_\tau^2$, for the unblown and blown cases. Equations (8.7) and (8.6) have been represented in the figure in order to test their validity. Orlando's smooth flat plate data is shown for comparison. One can conclude the Couette flow assumption is reasonable for our rough surface in the near wall region.

Tennekes [25], using dimensional analysis, argued that the above result should hold in a region of the layer where

$$\frac{k_s u_\tau}{\nu} >> 1$$

$$\frac{y}{k_s} > 1 \ , \ \frac{y}{\delta} < 1$$

and

$$\frac{k_s}{\delta} << 1 \quad . \tag{8.8}$$

These constraints define a region where convection by the mean flow is negligible, as well as the effect of the viscosity.

If one defines the mixing-length ℓ by

$$\varepsilon_M = \ell^2 \left| \frac{dU}{dy} \right| \tag{8.9}$$

Equation (8.1) can be re-arranged to give

$$\ell = \frac{\sqrt{-\overline{u'v'}}}{dU/dy} \tag{8.10}$$

ℓ can thus be interpreted as a length scale of the turbulent mixing.

Plots of ℓ are shown in Figures 8.2 (a and b) and 8.3 (a and b) determined using Equation (8.10), the measured turbulent shear stress $-\overline{u'v'}$ when available or calculated from Equations (8.6) and (8.7) for $y/\delta \lesssim 0.1$, and numerically differentiating the mean velocity profile. Its determination has an uncertainty of 8%.

Figure 8.2a shows the mixing-length distributions for an unblown case. A smooth flat plate case of Andersen [17] is also represented. For $y/\delta > 0.1$ the distribution shape is similar for the smooth and rough cases. This suggests that the large eddies, with sizes roughly proportional to ℓ , and the momentum transport mechanisms are similar for these two cases. In this outer region the familiar

$$\ell/\delta \approx \lambda \quad \text{(constant)} \tag{8.11}$$

is a good estimate for the mixing-length.

Figure 8.2b shows the near wall region ($y/\delta < 0.1$) where differences are observed. After the correct y-shifts = Δy (Chapter VI) have been considered for the rough wall data two cases can be seen:

a) for the fully rough state ($U_\infty \geq 89$ ft/sec) we have $\ell = K(y + \Delta y)$, no damping, with $K = 0.41$ as in the smooth wall case.

b) for the transitionally rough state ($U_\infty = 52$ ft/sec) a small amount of damping occurred very near the wall. The traditional van Driest [52] damping is evident for Andersen's data shown in the figure.

Figure 8.3 shows the distribution ℓ for a blown case. Similar distributions are observed as those for the unblown cases.

8.2 Turbulent Transport of Heat - the Turbulent Prandtl Number

The turbulent Prandtl number $Pr_t = \varepsilon_M/\varepsilon_H$, is the ratio between the diffusivities for momentum and heat. It can be verified to be of order 1 for all cases considered in this study. Furthermore, in the region $y > \xi$, where measurements were taken, $Re_t = \varepsilon_M/\nu >> 1$. As a consequence, the contribution of molecular transport is negligible, and the normal heat flux $\dot{q}''$ is given by

$$\dot{q}'' = -\rho\, c_p\, \overline{v't'} \quad . \tag{8.12}$$

The thermal-energy equation for a turbulent boundary layer flow and, in our case, for $y > \xi$ can be written as (White [41])

$$\rho\, c_p \left(U \frac{\partial T}{\partial x} + V \frac{\partial T}{\partial y} \right) = \frac{\partial \dot{q}''}{\partial y} + \frac{\tau}{g_c J} \frac{\partial U}{\partial y} \tag{8.13a}$$

Replacing the expressions for shear stress τ and heat flux $\dot{q}''$ given in Equations (8.4) and (8.12), respectively, one gets

$$U \frac{\partial T}{\partial x} + V \frac{\partial T}{\partial y} = - \frac{\partial \overline{v't'}}{\partial y} + \frac{-\overline{u'v'}}{c_p\, g_c\, J} \frac{\partial U}{\partial y} \tag{8.13}$$

here we are assuming constant properties for the air. The small temperature difference between the wall and the free-stream ($\Delta T \approx 30^{\circ}F$) used in all cases of this investigation makes this assumption reasonable.

Now if, near the wall, the Couette flow assumption ($\partial/\partial x \approx 0$) is valid, Equation (8.13) can be written as

$$\frac{V_o}{U_\tau} \frac{d(T/T_\tau)}{dy} = - \frac{d}{dy} \frac{\overline{v't'}}{U_\tau T_\tau} + Ec\, \frac{(C_f/2)^{3/2}}{St} \frac{-\overline{u'v'}}{U_\tau^2} \frac{d(U/U_\tau)}{dy} \tag{8.14}$$

The last term corresponds to the energy which is dissipated into heat, and is always positive (source). Ec is the non-dimensional Eckert number

$$Ec = \frac{U_\infty^3\, St}{c_p\, g_c\, J\, T_\tau\, U_\tau} \tag{8.15}$$

For $Ec \ll 1$, the "dissipative" source is negligible. In our "worst case", i.e., highest velocity $U_\infty = 130$ ft/sec

$$Ec \approx 0.1 \tag{8.16}$$

and so its contribution is at least an order of magnitude smaller than that of the turbulent heat flux and can be neglected compared to it.

Equation (8.14) can be integrated, following arguments similar to those in Appendix C, to give

$$\frac{V_o}{U_\tau}\ \frac{(T_w - T)}{T_\tau} = \frac{\overline{v't'}}{U_\tau T_\tau} - 1 - S \tag{8.17}$$

where S represents the integrated contribution of the source. S has been retained because it is not negligible compared to the transpiration contribution.

Now, for the unblown case S is negligible and

$$\frac{\overline{v't'}}{U_\tau T_\tau} \approx 1 \tag{8.18}$$

However, for the blown case where $S > 0$ we have

$$\frac{\overline{v't'}}{U_\tau T_\tau} \gtrsim 1 + \frac{V_o}{U_\tau}\left(\frac{T_w - T}{T_\tau}\right) \tag{8.19}$$

Figure 8.4 shows plots of $\overline{v't'}/U_\tau T_\tau$, for the unblown and blown cases. Equations (8.18) and (8.19) have been represented in order to test their validity, the agreement for $y/\delta < 0.1$ is reasonable. A profile from Orlando's smooth flat plate data is also shown for comparison.

The region of validity of Equation (8.18) is the so-called "constant heat flux layer".

The similarity of the curves shown in Figures (8.4) and (8.1) comes as a consequence of $Pr_t \approx 1$.

The definition of the turbulent Prandtl number can be re-arranged to give

$$Pr_t = \frac{\varepsilon_M}{\varepsilon_H} = \frac{-\overline{u'v'}}{\overline{v't'}}\,\frac{\partial T/\partial y}{\partial U/\partial y} \tag{8.20}$$

or

$$Pr_t = \frac{-\overline{u'v'}}{\overline{v't'}}\,\frac{\partial T}{\partial U} \tag{8.21}$$

This last expression was used for determining Pr_t . Measured $-\overline{u'v'}$ and $\overline{v't'}$ values, together with the numerically calculated derivative $\partial T/\partial U$, result in a Pr_t with an uncertainty band of $\pm 18\%$.

The turbulent Prandtl number determined by this technique depends only on local measurements. The derivative $\partial T/\partial U$ is more accurately calculated than with prior techniques because:

- T and U are measured sequentially with the same probe;
- there is no positional error (error in y position);
- T varies rather smoothly and almost linearly with U .

Figures 8.5, 8.6, 8.7, 8.8 and 8.9 show calculated turbulent Prandtl numbers for the blown and unblown cases. Two facts come to attention:

- there is no tendency for Pr_t to go above unity near the rough wall, where it has a smooth distribution, approximately equal to one.
- Pr_t decreases toward the free-stream where it reaches a value around 0.7 to 0.8 .

Recalling Chapter VI, T was observed to be linear with U near the wall so

$$\frac{\partial T}{\partial U} \sim \text{const.} = C_1 \tag{8.22}$$

and for the unblown case we have

$$\frac{-\overline{u'v'}}{U_\tau^2} \approx 1 \quad \text{and} \quad \frac{\overline{v't'}}{U_\tau T_\tau} \approx 1 \tag{8.23}$$

Therefore,

$$Pr_t \approx C_1 \frac{U_\tau}{T_\tau} \tag{8.24}$$

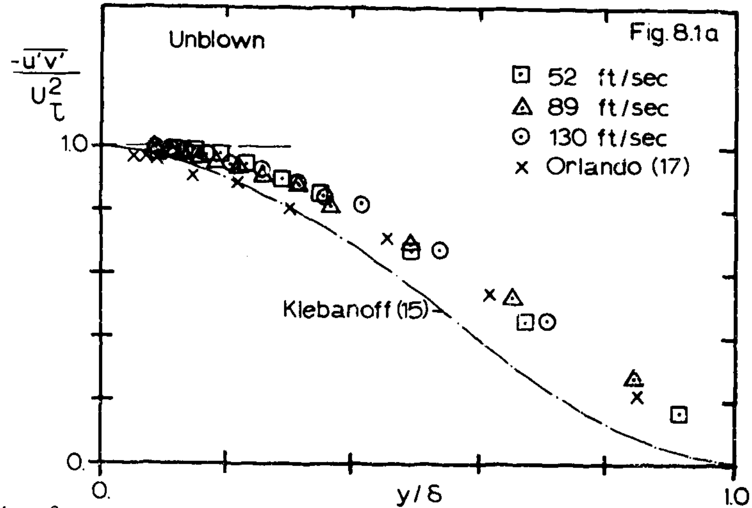

Fig. 8.1a Turbulent shear stress profiles with no transpiration - comparison with smooth wall data

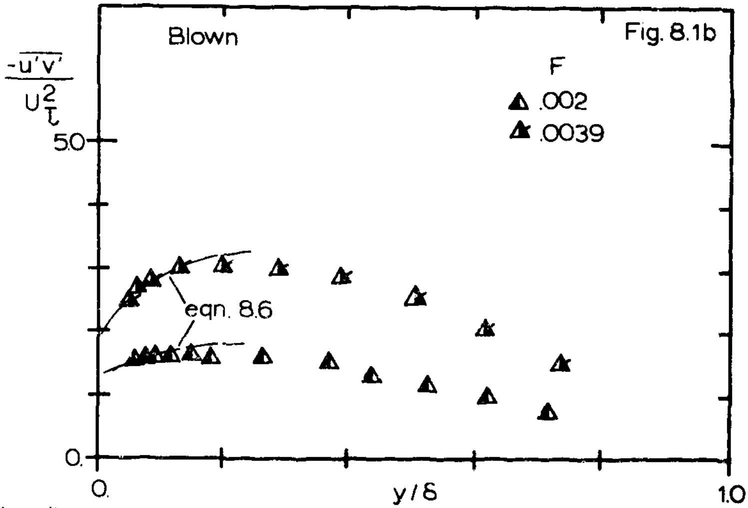

Fig. 8.1b Turbulent shear stress profiles for different blowing rates.

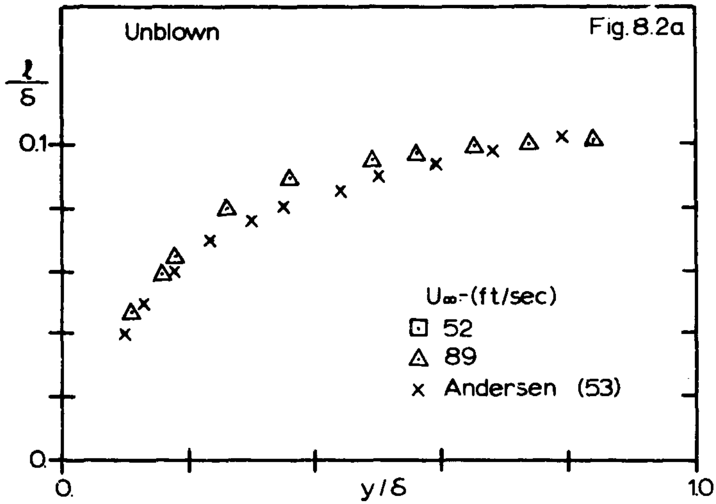

Fig. 8.2a Outer region mixing-length distributions - comparison with smooth wall data.

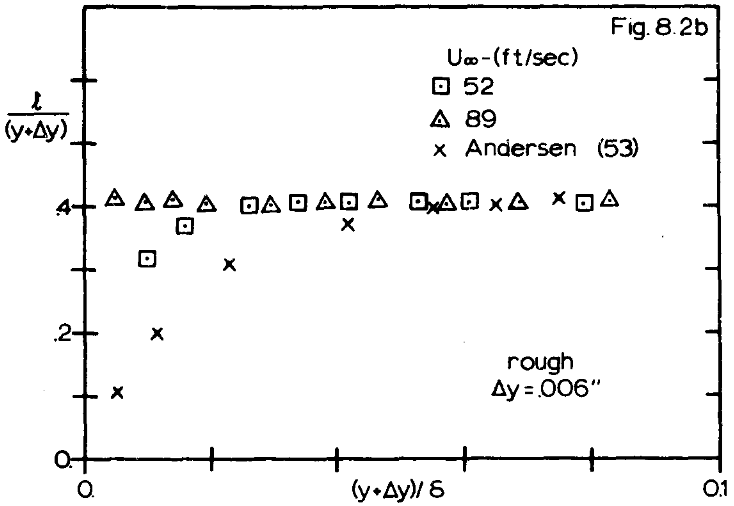

Fig. 8.2b Near wall mixing-length distributions - comparison with smooth wall data.

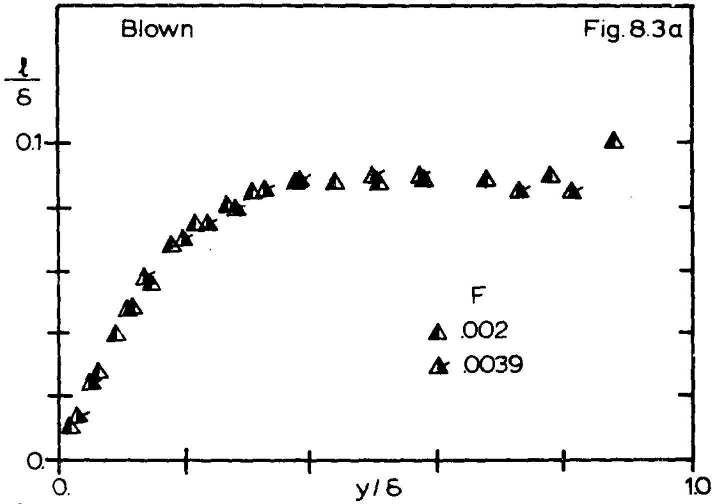

Fig. 8.3a Influence of blowing on the mixing-length distribution in the outer region.

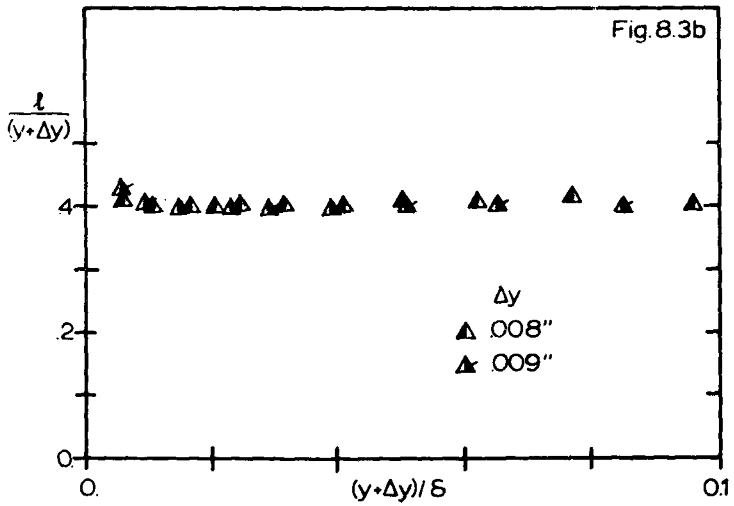

Fig. 8.3b Influence of blowing on the mixing-length distribution in the near wall region.

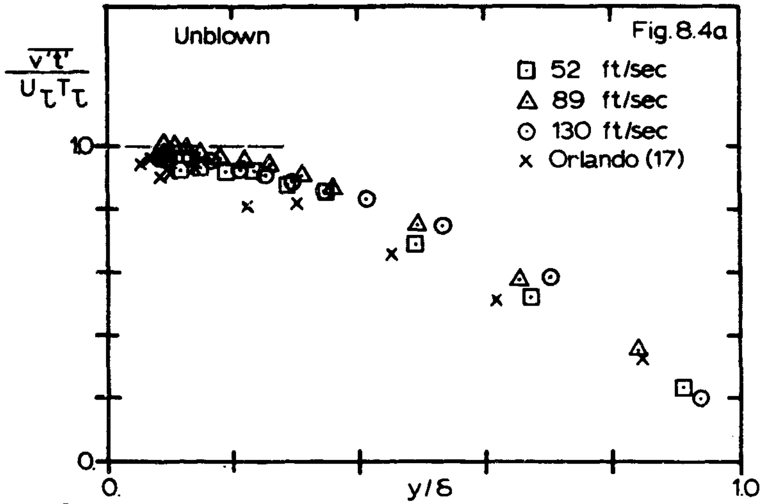

Fig. 8.4a Turbulent heat flux profiles with no transpiration - comparison with smooth wall data

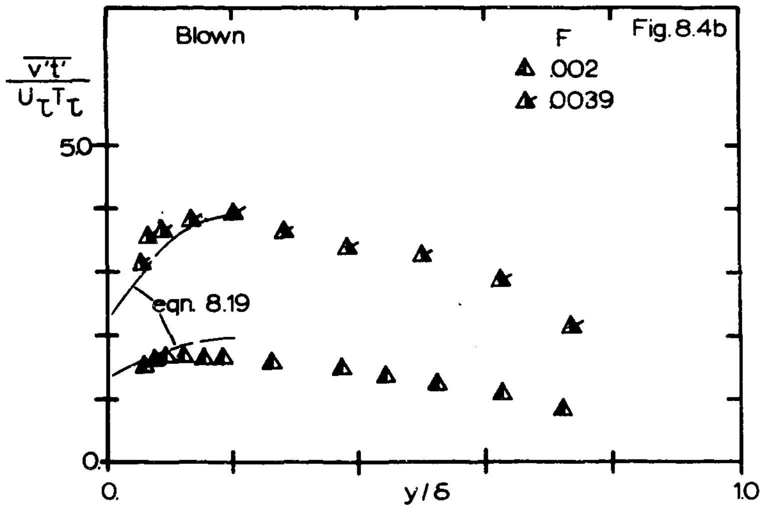

Fig. 8.4b Turbulent heat flux profiles for different blowing rates.

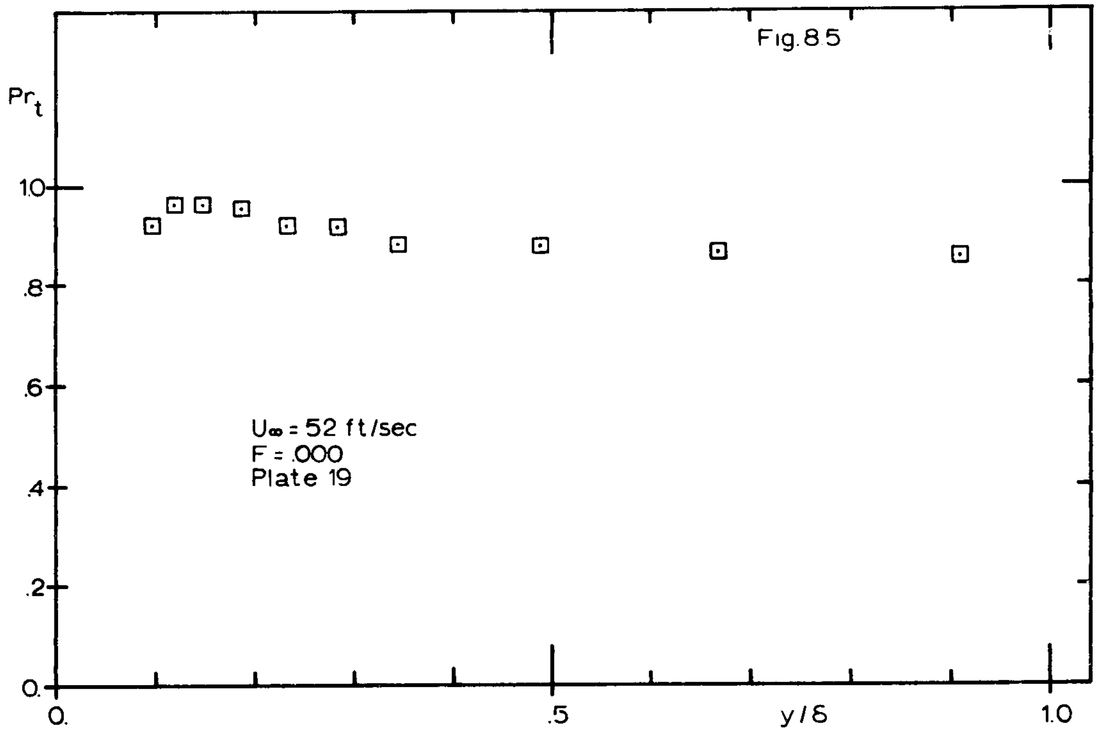

Fig. 8.5 Turbulent Prandtl number distribution - transitionally rough state (U_∞ = 52 ft/sec).

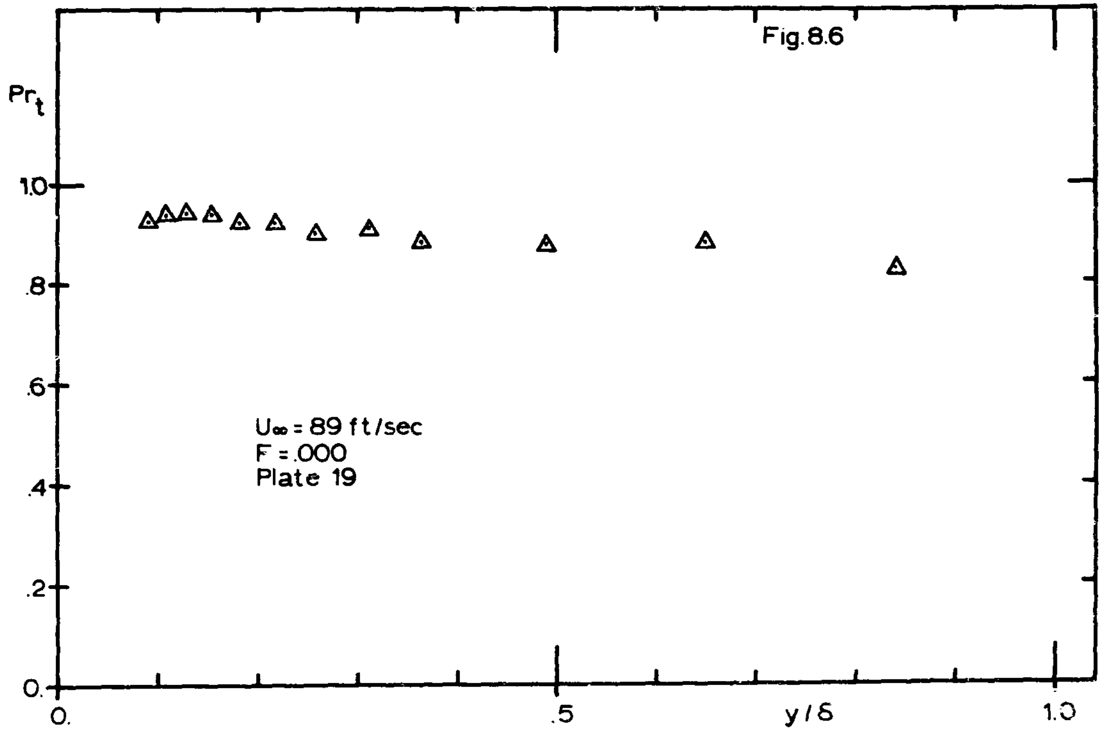

Fig. 8.6 Turbulent Prandtl number distribution - fully rough state (U_∞ = 89 ft/sec).

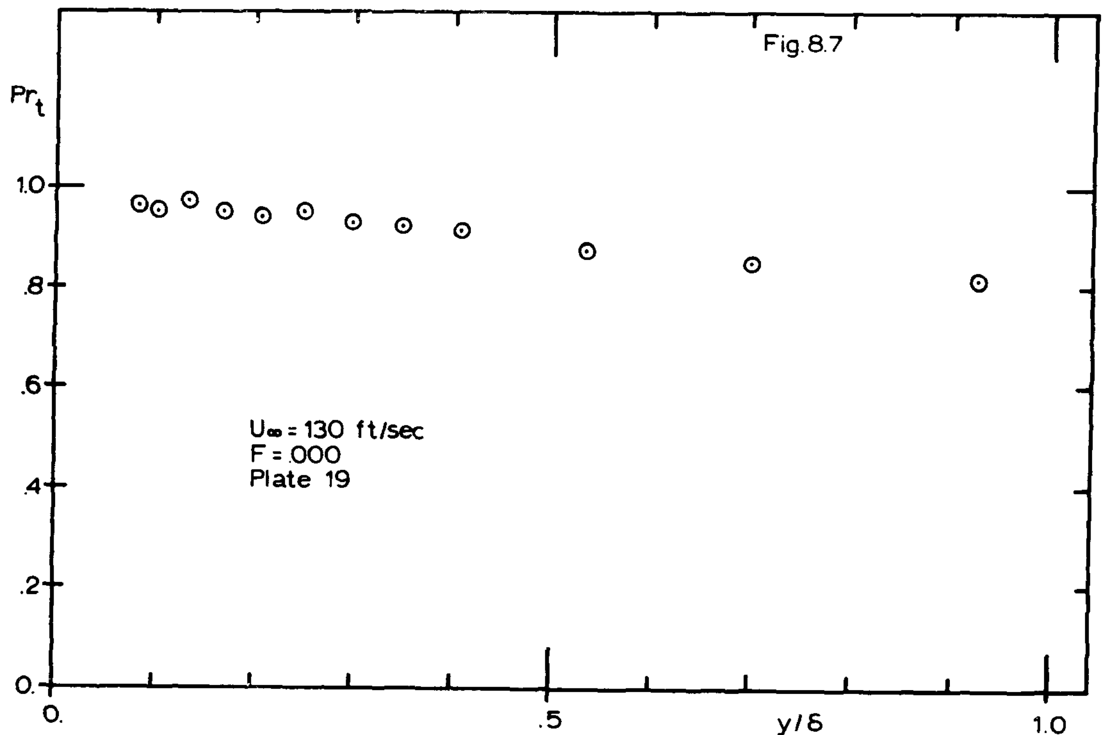

Fig. 8.7 Turbulent Prandtl number distribution - fully rough state (U∞ = 130 ft/sec).

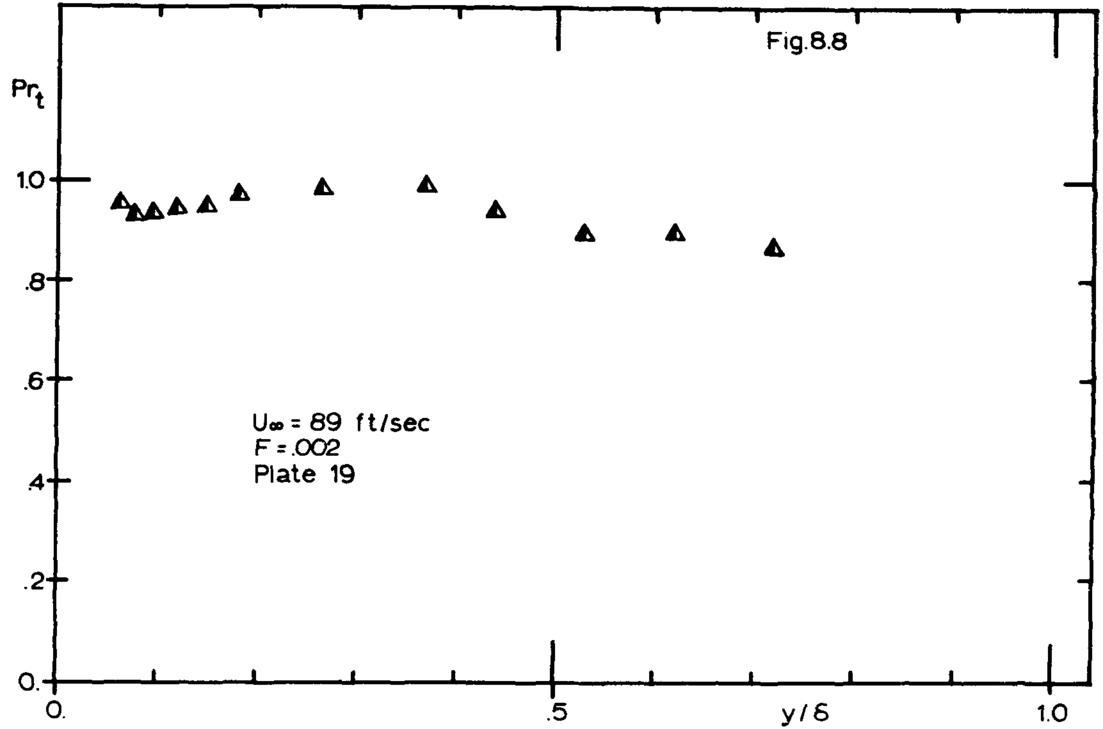

Fig. 8.8 Influence of blowing (F = 0.002) on turbulent Prandtl number distribution.

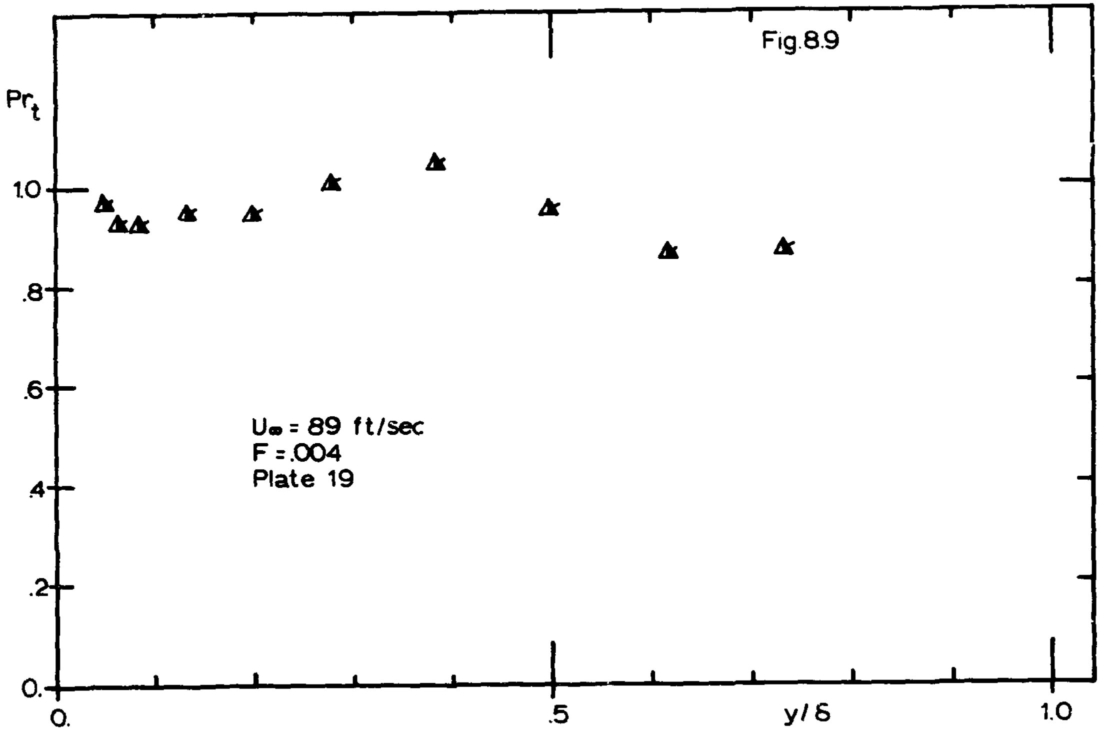

Fig. 8.9 Influence of strong blowing (F = 0.004) on turbulent Prandtl number distribution.

CHAPTER IX

SUMMARY AND CONCLUSIONS

The structure and behavior of a turbulent boundary layer developing over a porcus, deterministically rough, wall under a zero pressure gradient, with and without uniform blowing, have been investigated. The mean and turbulent fields were thoroughly examined for isothermal and non-isothermal boundary conditions.

The important results and conclusions of the present experiments are:

1. The fully rough state can be identified from Stanton number or friction factor, from the mean profiles, or from turbulent fluctuation profiles. Of these, the near wall behavior of the turbulent fluctuations is the most markedly different from smooth wall behavior.

2. The turbulent boundary layer for $U_\infty \geq 89$ ft/sec was in a fully rough state ($Re_k > 65$). The transitionally rough state is identified for the $U_\infty = 52$ ft/sec run ($Re_k \approx 50$).

3. The fully rough state is characterized by the non-dependence of friction factors and Stanton numbers on Reynolds numbers. The friction factors and Stanton numbers are found to be only functions of the local momentum and enthalpy thickness, respectively.

$$\frac{C_f}{2} = f(\delta_2/r) \quad \text{and} \quad St = g(\Delta_2/r) \qquad (9.1)$$

   This suggests that the flow is independent of molecular viscosity and establishes δ or δ_2 as an appropriate length scale of the flow for every position inside the layer.

4. The mean velocity and temperature profiles for the fully rough state are similar near the wall, and when plotted in $U - T$ coordinates they exhibit a linear distribution. However, the virtual origins of these profiles do not coincide: a temperature jump condition seems to exist at the wall.

5. The boundary layer in its fully rough state has no viscous sublayer. The existence, however, of a thin viscous sublayer can be verified from the transitionally rough velocity profiles, as well as from the damping in the mixing-length .

6. The shear velocity U_τ is an appropriate velocity scale throughout the layer either for the mean flow, as well as for the turbulence field, but not with blowing.

7. A virtual origin of a rough wall velocity profile can be unambiguously determined by the method of Monin and Yaglom [24], with respect to the top of the rough elements. The shifts so determined are constant for each blowing fraction F , and as F increases Δy increases.

8. The effect of roughness on the turbulent field structure extends over most of the layer as is particularly shown by the $\overline{u'^2}$ profiles. The fully rough state shows a broad region of nearly uniform intensity, contrasted with the smooth wall which shows a sharp peak near the wall and rapid drop off in the outer region. The transitionally rough state preserves some aspects of smooth wall behavior: a sharp peak in the $\overline{u'^2}$ profile very near the wall.

9. Transpiration (blowing) affects the turbulent fluctuation distribution less than in the smooth wall case.

10. The unblown and blown cases exhibit an approximately constant correlation coefficient between u' and v' ($\cong 0.44$). The same is true for $-\overline{u'v'}$ normalized by the turbulent kinetic energy ($\cong 0.14$).

11. The turbulent Prandtl number is nearly constant close to the wall with a value near unity and monotonically decreases toward the free-stream, where it reaches a value around 0.7 to 0.8 .

12. Transpiration (blowing) makes the layer behave as if the wall had physically larger roughness elements. This behavior can be

observed from either turbulent fluctuations or mixing-length distributions and is attributed to pressure interactions.

13. For very large enthalpy thickness the Stanton number seems to be converging to an asymptotic value. So $St \to$ constant and $\Delta_2 \alpha x$, for large Δ_2 .

REFERENCES

1. Liu, C. K., Kline, S. J., and Johnston, J. P., "An Experimental Study of Turbulent Boundary Layer on Rough Walls," Report No. MD-15, Thermosciences Division, Dept. of Mech. Engrg., Stanford University, July 1966.

2. Dvorak, R. A., "Calculations of Compressible Turbulent Boundary Layers with Roughness and Heat Transfer," AIAA Journal, Vol. 10, No. 11, pp. 1447-1451, November 1972.

3. Gowen, R. A. and Smith, J. W., "Turbulent Heat Transfer from Smooth and Rough Surfaces," Intl. Jn. of Heat and Mass Transfer, Vol. 11, pp. 1657-1673, 1968.

4. Healzer, J. M., Moffat, R. J., and Kays, W. M., "The Turbulent Boundary Layer on a Rough, Porous Plate: Experimental Heat Transfer with Uniform Blowing," Report No. HMT-18, Thermosciences Division, Dept. of Mech. Engrg., Stanford University, 1974.

5. Schlichting, H., Boundary Layer Theory, 6th Edition, McGraw-Hill Book Co., Inc., New York, 1968.

6. Offen, G. R., and Kline, S. J., "Experiments on the Velocity Characteristics of 'Bursts' and on the Interactions between the Inner and Outer Regions of a Turbulent Boundary Layer," Report MD-31, Thermosciences Division, Dept. of Mech. Engrg., Stanford University, 1973.

7. Kim, H. T., Kline, S. J., and Reynolds, W. C., "An Experimental Study of Turbulence Production near a Smooth Wall in a Turbulent Boundary Layer with Zero Pressure Gradient," Report MD-20, Thermosciences Division, Mech. Engrg. Dept., Stanford University, 1968.

8. Grass, A. J., "Structural Features of Turbulent Flow over Smooth and Rough Boundaries," Jn. Fluid Mech., Vol. 50, pp. 233-256, 1971.

9. Laufer, J., private communication, Stanford University, 1974.

10. Hama, F. R., "Boundary Layer Characteristics for Smooth and Rough Surfaces," Trans. Soc. NAME, Vol. 62, pp. 333-354, 1954.

11. Corrsin, S., and Kistler, A. L., "The Free Stream Boundaries of Turbulent Flows," NACA Tech. Note 3133, January 1954.

12. Perry, A. E., Schofield, W. H., and Joubert, P. H., "Rough Wall Turbulent Boundary Layers," Jn. Fluid Mech., Vol. 37, pp. 383-413, 1969.

13. Yaglom, A. M., and Kader, B. A., "Heat and Mass Transfer between a Rough Wall and Turbulent Fluid Flow at High Reynolds and Peclet Number," Jn. Fluid Mech., Vol. 62, Part 3, 11, pp. 601-623, 1974.

14. Powe, R. E., Townes, H. W., Gow, J. L., and Weber, N., "Turbulent Flow in Smooth and Rough Pipes," Jn. Basic Engrg., Trans. ASME, Series D, Vol. 94, No. 2, pp. 353-362, June 1972.

15. Klebanoff, P. S., "Characteristics of Turbulence in a Boundary Layer with Zero Pressure Gradient," NACA Report 1247, 1955.

16. Bradshaw, P., "An Introduction to Turbulence and its Measurements," The Commonwealth and International Library of Science Technology Engineering and Liberal Studies, Pergamon Press, 1971.

17. Orlando, A. F., Moffat, R. J., and Kays, W. M., "Turbulent Transport of Heat and Momentum in a Boundary Layer Subject to Deceleration, Suction and Variable Wall Temperature," Report No. HMT-17, Thermosciences Division, Dept. of Mech. Engrg., Stanford University, 1974.

18. Sharan, V. K., "On the Importance of Turbulence in Boundary Layer Simulation," Int. Jn. Mech. Sci., Vol. 15, pp. 643-649, 1973.

19. Clauser, F. H., "The Turbulent Boundary Layer," Advances in Applied Mechanics, Vol. IV, pp. 1-51, Academic Press, New York, 1956.

20. Nikuradse, J., "Stromugsgestze in rauhen Rohren," VDI Forschungsheft, No. 361, 1950, English Translation, NACA TM 1292.

21. Schlichting, H., and Prandtl, L., "Das Widerstandsgesetz rauher Platten," Werft, Reederei, und Hafen, 1934, p. 1.

22. Kays, W. M., "Convective Heat and Mass Transfer," McGraw-Hill Book Co., New York, 1966.

23. Moore, W. L., "An Experimental Investigation of Boundary Layer Development along a Rough Surface," Ph.D. Dissertation, State University of Iowa, August 1951.

24. Monin, A. S., and Yaglom, A. M., "Statistical Fluid Mechanics," Vol. 1, The MIT Press, 1971.

25. Tennekes, H., and Lumley, J. L., "A First Course in Turbulence," The MIT Press, 1972.

26. Coles, D., "The Law of the Wake in the Turbulent Boundary Layer," Jn. Fluid Mech., Vol. 1, pp. 191, 1956.

27. Blackwell, B. F., Kays, W. M., and Moffat, R. J., "The Turbulent Boundary Layer on a Porous Plate: An Experimental Study of the Heat Transfer Behavior with Adverse Pressure Gradients," Report No. HMT-16, Thermosciences Division, Dept. of Mech. Engrg., Stanford University, 1972.

28. Dipprey, D. F., and Sabersky, R. H., "Heat and Momentum Transfer in Smooth and Rough Tubes at Various Prandtl Numbers," Int. Jn. Heat Mass Transfer, Vol. 6, pp. 329-353, 1963.

29. Owen, P. R., and Thomson, W. R., "Heat Transfer across Rough Surfaces," Jn. Fluid Mech., Vol. 15, pp. 321-334, 1963.

30. Lewis, M. J., "Roughness Functions, the Thermohydraulic Performance of Rough Surfaces and the Hall Transformation - an Overview," Int. Jn. Heat Mass Transfer, Vol. 17, No. 8, pp. 809-815, 1974.

31. Kline, S. J., Reynolds, W. C., Schraub, F. A., and Rundstadler, P. W., "The Structure of Turbulent Boundary Layers," Jn. Fluid Mech., Vol. 30, pp. 741-774, 1967.

32. Hinze, J. O., "Turbulence - An Introduction to its Mechanism and Theory," McGraw-Hill Book Co., 1959.

33. Perry, A. E., and Joubert, P. H., "Rough Wall Boundary Layers in Adverse Pressure Gradients," Jn. Fluid Mech., Vol. 37, pp. 193-211, 1963.

34. Powe, R. E., and Townes, H. W., "Energy Relations for Turbulent Flow in Rough Pipes," Symposium on Turbulence in Liquids, University Missouri, Rolla, Missouri, 1971.

35. Townsend, A. A., "The Structure of the Turbulent Boundary Layer," Proc. Cambridge Phil. Soc., Vol. 47, Part 2, pp. 375-395, April 1951.

36. Laufer, J., "The Structure of Turbulence in Fully Developed Pipe Flow," NACA Report 1174, 1954.

37. Townsend, A. A., The Structure of Turbulent Shear Flow, Cambridge University Press, 1956.

38. Bradshaw, P., "The Turbulence Structure of Equilibrium Boundary Layers," NPL Aero Report 1184, 1966.

39. Simpson, R. L., Kays, W. M., and Moffat, R. J., "The Turbulent Boundary Layer on a Porous Plate: An Experimental Study of the Fluid Dynamics with Injection and Suction," Report No. HMT-2, Thermosciences Division, Dept. of Mech. Engrg., Stanford University, 1967.

40. Kearney, D. W., Moffat, R. J., and Kays, W. M., "The Turbulent Boundary Layer: Experimental Heat Transfer with Strong Favorable Pressure Gradients and Blowing," Report No. HMT-12, Thermosciences Division, Dept. of Mech. Engrg., Stanford University, 1970.

41. White, F. M., Viscous Fluid Flow, McGraw-Hill Book Co., New York, 1974.

42. Reynolds, A. J., Turbulent Flows in Engineering, John Wiley & Sons, London, 1974.

43. Spalding, D. B., and Patankar, S. V., Heat and Mass Transfer in Boundary Layers, 2nd Ed., International Textbook Co. Ltd., London, 1970.

44. Kolar, V., "Heat Transfer in Turbulent Flow of Fluids through Smooth and Rough Tubes," Int. Jn. Heat Mass Transfer, Vol. 8, pp. 639-653, 1965.

45. Nikitin, I. K., "Approximate Calculation of Heat and Mass Transfer in the Turbulent Boundary Layer of a Surface with Arbitrary Roughness Properties," Heat Transfer - Soviet Research, Vol. 5, No. 3, May - June 1973.

46. Nunner, W., "Heat Transfer and Pressure Drop in Rough Tubes," VDI Forschungsheft, No. 455, Series B, Vol. 22, pp. 5-39, 1956, English Translation, A.E.R.E. Library/Transactions 786, 1958.

47. Tillman, W., "Investigations of Some Particularities of Turbulent Boundary Layers on Plates," United Kingdom Interrogation Report, Joint Intelligence Objectives Agency, Washington D.C., File No. B.I.G.S.-19, 1-3-1, June 26, 1946.

48. Jayatilleke, C.L.V., "The Influence of Prandtl Number and Surface Roughness on the Resistance of the Laminar Sub-layer to Momentum and Heat Transfer," Prog. Heat Mass Transfer, Vol. 1, pp. 193-329.

49. Kryukov, V. N., and Solntsev, V. P., "An Investigation of Heat Transfer on a Rough Plate," Heat Transfer - Soviet Research, Vol. 5, No. 2, March-April 1973.

50. Kays, W. M., "Heat Transfer to the Transpired Turbulent Boundary Layer," Report No. HMT-14, Thermosciences Division, Dept. of Mech. Engrg., Stanford University, 1971.

51. Moffat, R. J., and Kays, W. M., "The Turbulent Boundary Layer on a Porous Plate: Experimental Heat Transfer with Uniform Blowing and Suction," Report No. HMT-1, Thermosciences Division, Dept. of Mech. Engrg., Stanford University, 1967.

52. van Driest, E. F., "On Turbulent Flow Near a Wall," Heat Transfer and Fluid Mechanics Institute, 1955.

53. Andersen, P. S., Kays, W. M., and Moffat, R. J., "The Turbulent Boundary Layer on a Porous Plate: An Experimental Study of the Fluid Mechanics for Adverse Free-Stream Pressure Gradients," Report No. HMT-15, Thermosciences Division, Dept. of Mech. Engrg., Stanford University, 1972.

54. Pimenta, M., and Moffat, J., "Stability of Flow through Porous Plates: Coalescent Jets Effects," AIAA Journal, Vol. 12, No. 10, Tech. Note, pp. 1438-1440, 1974.

55. Stevenson, T. N., "A Law of the Wall of Turbulent Boundary Layers with Suction or Injection," The College of Aeronautics, Cranfield, Aero Report No. 166, 1963.

56. Polyayev, V. M., Bashmakov, I. V., Vlasov, D. I., and Cerasimov, I. M., "Hot-Wire Anemometer Investigation of Turbulent Boundary Layers at a Permeable Plate with Injection," Heat Transfer - Soviet Research, Vol. 5, No. 4, July - August, 1973.

57. Eckert, E.R.G., and Drake, Jr., R. M., Analysis of Heat and Mass Transfer, McGraw-Hill Book Co., New York, 1972.

58. Bradshaw, P., Ferris, O. H., and Atwell, N. P., "Calculation of Boundary Layer Development using the Turbulent Energy Equation," Jn. Fluid Mechanics, Vol. 28, Part 3, pp. 593-616, 1967.

59. Whitten, D. G., Kays, W. M., and Moffat, R. J., "The Turbulent Boundary Layer on a Porous Plate: Experimental Heat Transfer with Variable Suction, Blowing, and Surface Temperature," Report No. HMT-3, Thermosciences Division, Dept. of Mech. Engrg., Stanford University, 1967.

60. Julien, H. L., Kays, W. M., and Moffat, R. J., "The Turbulent Layer on a Porous Plate: Experimental Study of the Effects of a Favorable Pressure Gradient," Report No. HMT-4, Thermosciences Division, Dept. of Mech. Engrg., Stanford University, 1969.

61. Thielbahr, W. H., Kays, W. M., and Moffat, R. J., "The Turbulent Boundary Layer: Experimental Heat Transfer with Blowing, Suction and Favorable Pressure Gradient," Report No. HMT-5, Thermosciences Division, Dept. of Mech. Engrg., Stanford University, 1969.

62. Loyd, R. J., Moffat, R. J., and Kays, W. M., "The Turbulent Boundary Layer on a Porous Plate: An Experimental Study of the Fluid Dynamics with Strong Favorable Pressure Gradients and Blowing," Report No. HMT-13, Thermosciences Division, Dept. of Mech. Engrg., Stanford University, 1970.

63. Rasmussen, C. G., and Dahm, M., "Effect of Wire Mounting System on Hot-Wire Probe Characteristics," DISA Information No. 7, pp. 19-24, January 1970.

64. Maye, F. P., "Error Due to Thermal Conduction Between the Sensing Wire and Its Supports when Measuring Temperatures with a Hot-Wire Anemometer Used as a Resistance Thermometer," DISA Information No. 8, pp. 22-26, February 1970.

65. Thinh, N. V., "On Some Measurements Made by Means of a Hot-Wire in a Turbulent Flow Near a Wall," DISA Information No. 7, pp. 13-18, January 1970.

66. Jorgensen, F. E., "Directional Sensitivity of Wire and Hot-film Probes," DISA Information No. 11, 1971.

67. Watts, K. C., "The Development of Asymptotic Turbulent, Transitional and Laminar Boundary Layers Induced by Suction," Ph.D. Thesis, Dept. Mech. Engrg., University of Waterloo, Canada, June 1972.

68. Sandborn, V. A., Resistance Temperature Transducers, Fort Collins, Colorado, Metrology Press, 1972.

69. Fujita, H., and Kovasznay, L.S.G., "Measurements of Reynolds Stress by a Single Rotated Hot-Wire Anemometer," The Review of Scientific Instruments, Vol. 39, No. 9, September 1968.

70. Arya, S.P.S., and Plate, E. J., "Hot-Wire Measurements in Non-isothermal Flow," Instruments & Control Systems, p. 87, March 1969.

71. Corrsin, S., "Extended Applications of the Hot-Wire Anemometer," NACA Tech. Note No. 1864, April 1949.

72. Repik, Y.E.U., and Ponomareva, V. S., "The Effect of Proximity of Walls on the Readings of a Hot-Wire Anemometer in Turbulent Boundary Layers," Heat Transfer - Soviet Research, Vol. 2, No. 4, July 1970.

73. Fulachier, L., and Dumas, R., "Repartitions Spectrales des Fluctuations Thermiques dans une Conche Limite Turbulent," Agard Conference Proceedings No. 93 on Turbulent Shear Flows, Paper 4, 1972.

74. Bremnorst, K., and Walker, T. B., "Spectral Measurements of Turbulent Momentum Transfer in Fully Developed Pipe Flow," Jn. Fluid Mech., Vol. 61, Part 1, pp. 173-186, 1973.

75. Tsuji, Y., and Iida, S., "Velocity Distributions of Rough Wall Turbulent Boundary Layers without Pressure Gradient," Trans. Japan Soc. Aero. Space Sci., Vol. 16, No. 31, pp. 60-70, 1973.

76. Prandtl, L., Z. Angew. Math. Mech., Vol. 5, pp. 136-139.

77. Smith, K. A., "The Transpired Turbulent Boundary Layer," D. Sc. Thesis, Chem. Engrg. Dept., MIT, May 1962.

78. Baker, E., "Influence of Mass Injection on Turbulent Flow Near Walls," Prog. Heat Mass Transfer, Vol. 1, pp. 99-192.

79. Clauser, F. H., "Turbulent Boundary Layers in Adverse Pressure Gradients," Jn. Aero Sci., Vol. 21, p. 91, 1954.

80. Johnson, D. S., "Velocity and Temperature Fluctuation Measurements in a Turbulent Boundary Layer Downstream of a Stepwise Discontinuity in Wall Temperature," Jn. of Applied Mechanics, ASME, p. 325, 1959.

81. Blom, J., "Experimental Determination of the Turbulent Prandtl Number in a Developing Temperature Boundary Layer," Fourth International Heat Transfer Conference, Paris - Versailles, Vol. II, 1970.

82. Kudva, A. K., and Sesonsk, F. A., "Structure of Turbulent Velocity and Temperature Fields in Ethylene Glycol Pipe Flow at Low Reynolds Number," Int. Jn. Heat Mass Transfer, Vol. 15, pp. 127-145, 1972.

83. Roshko, A., NACA TN 3488, 1955.

84. Fox, J., NASA TN D-2501, 1964.

85. Blasius, H., "Grenzschichten in Flüssigkeit mit kleiner Reibung," Z. Math. und Phys., Vol. 56, pp. 1-37, 1908. Engl. transl. in NACA TM 1256.

APPENDICES

APPENDIX A

THE MEASUREMENT OF FLUCTUATING TEMPERATURE

The measurement of $\overline{t'^2}$ was done using the horizontal wire with the probe DISA 55P05. It uses the constant current anemometer and a resistance thermometer approach.

As discussed in Chapter IV the calibration is curved-fitted with a straight line. Thus, Equation (4.1)

$$E^* = AT + B \tag{A.1}$$

Rigorously, we must now assume that instantaneously

$$e^* = At + B \tag{A.2}$$

Therefore, for the fluctuations

$$e^{*'} = \frac{\partial e^*}{\partial t} t' \tag{A.3}$$

so, squaring and time averaging

$$\overline{e^{*'2}} = \left(\frac{\partial e^*}{\partial t}\right)^2 \overline{t'^2} \tag{A.4}$$

or

$$\overline{e^{*'2}} = \left(\frac{\partial E}{\partial T}\right)^2 \overline{t'^2} \tag{A.5}$$

where $\frac{\partial E}{\partial T} = A$ from the calibration curve given by Equation (A.1).

The measurement of $\overline{e^{*'2}}$ (rms output of the anemometer) with the knowledge of A (calibration constant) gives us the temperature fluctuation $\overline{t'^2}$.

A.1 Conduction Error Correction

Heat conduction from wire to the gold plated region and the prongs limits the accuracy and introduces a conduction error. For all our fluctuation measurements this error was estimated and the final results we present were corrected for it. This analysis follows Maye [64] and is presented for the sake of completeness.

It is a reasonable assumption that the prongs and the gold plated part of the wire are isothermal and in an isothermal plane during the measurements.

An energy balance on an element of the sensing wire gives (see Figure A.1)

$$q_x - q_{x+dx} - q_c + I^2 R \frac{dx}{\ell} = \rho \ c_p \ dV \frac{\partial T_w}{\partial \tau} \tag{A.6}$$

or

$$\underbrace{\frac{\pi d^2}{4} \frac{\partial}{\partial x}\left(k \frac{\partial T_w}{\partial x}\right) dx}_{\text{conduction}} - \underbrace{hd\pi(T_w - T_\infty)dx}_{\text{convection}} + \underbrace{I^2 R \frac{dx}{\ell}}_{\text{elect. heat}} =$$

$$= \underbrace{\rho \ c_p \frac{\pi d^2}{4} \frac{\partial T_w}{\partial \tau} dx}_{\text{rate of increase of storage}} \tag{A.7}$$

where T_w - wire temperature

T_∞ - ambient temperature.

This equation, with the assumption of constant properties (good for small temperature differences) reduces for steady state to

$$\frac{d^2 T_w}{dx^2} - \frac{4h}{kd}(T_w - T_\infty) + \frac{4I^2 R}{\pi d^2 k\ell} = 0 \tag{A.8}$$

but $R = AT_w + B$ so

$$\frac{d^2 T_w}{dx^2} - w^2 \ T_w + \lambda = 0 \tag{A.9}$$

where

$$w^2 = \frac{4h}{kd} - \frac{4I^2}{\pi \ell d^2 k} A$$

$$\lambda = \frac{4h}{kd} T_\infty + \frac{4I^2}{\pi \ell d^2 k} B = w^2 T_\infty + \alpha$$

The boundary conditions are:

$$T_w = T_p \quad \text{at} \quad x = \pm \frac{\ell}{2}$$

$$\frac{dT_w}{dx} = 0 \quad \text{at} \quad x = 0 \quad .$$

The solution to (A.9) is:

$$\frac{T_w - \lambda/w^2}{T_p - \lambda/w^2} = \frac{\cosh wx}{\cosh w\ell/2} \tag{A.10}$$

Now, the average wire temperature T_m is defined by

$$T_m = \frac{2}{\ell} \int_o^{\ell/2} T_w \, dx$$

so

$$\frac{T_m - \lambda/w^2}{T_p - \lambda/w^2} = \frac{2}{w\ell} \tanh \frac{w\ell}{2} = \nu \tag{A.11}$$

Following Maye [64], we assume negligible overheating for the very low currents (2mA) used in our measurements and the 5 micron tungsten wires, thus

$$T_\infty = T_m + \frac{\nu}{1-\nu} (T_m - T_p) \tag{A.12}$$

where

$$\nu = \frac{2}{w\ell} \tanh \frac{w\ell}{2}$$

$$w^2 = \frac{4h}{kd} \quad .$$

For mean temperature measurements no corrections were applied to include conduction errors. Orlando [17] also concluded, like Maye [64], that $\overline{T}_m \approx \overline{T}_\infty$.

However, for temperature fluctuations one must use (A.12) or its equivalent to estimate the conduction correction. Assuming the prongs with large thermal inertia, they will go to the average temperature of the gas stream, leaving the driving potential for error $(T_\infty - T_p)$ equal to the entire fluctuation. Following (A.12):

$$t'_\infty = \frac{1}{1-\nu} t'_m \tag{A.13}$$

where

$$\nu = \frac{2}{\ell w} \tanh \frac{w\ell}{2}$$

$$w^2 = \frac{4h}{kd} \quad .$$

Therefore,

$$\overline{t'^2} = \left(\frac{1}{1-\nu}\right)^2 \overline{t'^2_m} \tag{A.14}$$

The expression given in Equation (A.14) was used in this work to correct the rms measurements of the temperature fluctuations.

Different terms were obtained from:

k_{wire} = 96 BTU/hr ft °F (tungsten)

ℓ_{wire} = 1.2 mm (DISA 55P05)

d_{wire} = $5 \times 10^{-0.6}$m

$Nu = 0.32 + 0.56\ Re^{0.5}$

where $Re = \dfrac{U d_{wire}}{\mu/\rho}$

U = local air velocity

μ/ρ local air kinematic viscosity

$$Nu = \frac{hd}{k_{air}} = d^2 \frac{k_{wire}}{4k_{air}} w^2$$

$$k_{air} = 0.015 \text{ BTU/hr ft } ^\circ F$$

As for illustration we show some calculated values for the probe DISA 55P05:

U (ft/sec)	25	50	75	100	125
ν	0.303	0.266	0.245	0.231	0.220
$\overline{t'^2}$ (measured)	1.000	1.000	1.000	1.000	1.000
$\overline{t'^2}$ (corrected)	1.440	1.360	1.320	1.320	1.280

The ratio $\ell/d = 240$ is somewhat low and that is why the corrections are of sizeable magnitudes. The accuracy of $\overline{t'^2}$ measurements, corrected for conduction errors, is estimated to be 15%.

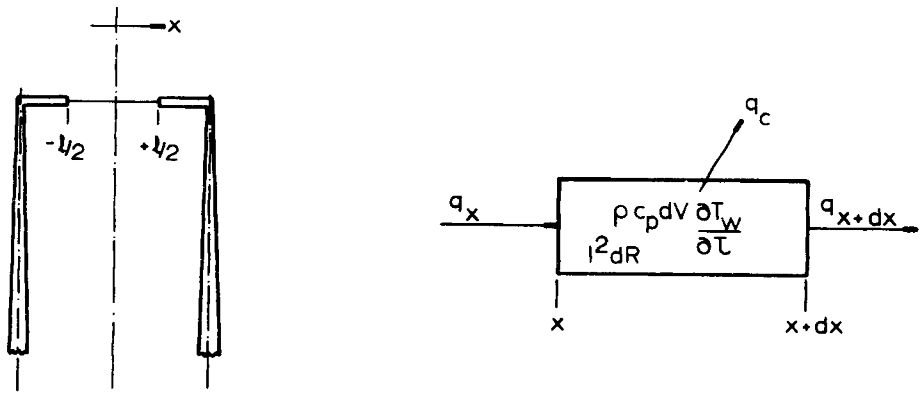

Fig. A.1 Analysis of the wire element.

APPENDIX B

THE MEASUREMENT OF TURBULENT QUANTITIES

This analysis follows from Orlando [17] and is presented here for the sake of completeness. A hot wire in an air stream responds to the air velocity and temperature T. The air velocity that the wire "sees" is the effective velocity u_{eff} which is a function of the actual velocity components u, v, w and is dependent on the directional sensitivity of the wire.

The output e of the anemometer is given by

$$e = e(u_{eff}, t) \tag{B.1}$$

$$de = \frac{\partial e}{\partial u_{eff}} du_{eff} + \frac{\partial e}{\partial t} dt \tag{B.2}$$

which for small fluctuations, $du_{eff} \approx u'_{eff}$ and $dt \approx t'$,

$$e' = \frac{\partial e}{\partial u_{eff}} u'_{eff} + \frac{\partial e}{\partial t} t' \tag{B.3}$$

In our case, the measurements were made under conditions where:

$$U \neq 0$$

$$V \approx 0 \quad (= 0 \text{ at calibration})$$

$$W = 0$$

Thus,

$$e' = \frac{\partial e}{\partial u} \frac{\partial u}{\partial u_{eff}} u'_{eff} + \frac{\partial e}{\partial t} t' \tag{B.4}$$

where $\frac{\partial e}{\partial u}$ and $\frac{\partial e}{\partial t}$ were obtained by differentiating the calibration curve.

B.1 Directional Sensitivity of a Hot Wire

Jorgensen [66] showed that the directional sensitivity of a hot wire is given by:

$$u_{eff}^2 = u_2^2 + k_1^2\, v_2^2 + k_2^2\, w_2^2 \qquad \text{(B.5)}$$

u_2, v_2, w_2 are the velocity components in the wire coordinate system (X_2, Y_2, Z_2). The wire and prongs are contained in the plane X_2, Y_2, (see Figure B.1).

k_1 and k_2 are constants which depend on construction characteristics of the wire. The wire probe DISA 55F02 was chosen because its characteristics are known:

$$k_1 = 0.2$$

$$k_2 = 1.02$$

ϕ is the wire angle and θ is the probe rotation angle. Equation (B.5) can be rewritten in terms of u_1, v_1, w_1, the velocity components in the laboratory coordinates (X_1, Y_1, Z_1):

$$u_{eff}^2 = Au_1^2 + Bv_1^2 + Cw_1^2 + Du_1v_1 + Ev_1w_1 + Fu_1w_1 \qquad \text{(B.6)}$$

where

$$A = \cos^2\phi + k_1^2 \sin^2\phi$$

$$B = (\sin^2\phi + k_1^2 \cos^2\phi)\cos^2\theta + k_2^2 \sin^2\theta$$

$$C = (\sin^2\phi + k_1^2 \cos^2\phi)\sin^2\theta + k_2^2 \cos^2\theta$$

$$D = (1 - k_1^2)\sin 2\phi \cos\theta$$

$$E = (\sin^2\phi + k_1^2 \cos^2\theta - k_2^2)\sin 2\theta$$

$$F = (1 - k_1^2)\sin 2\phi \sin\theta$$

In all our cases the probes were aligned with the mean flow, thus:

$$u_1 = U + u'$$

$$v_1 = v'$$

$$w_1 = w' \quad .$$

The derivation from this point on varies from author to author, but the final result is the same.

Expanding $u_{eff}\ (u_1, v_1, w_1)$ about $u_{eff}\ (\bar{u}, 0, 0)$ like

$$u_{eff} = u_{eff}\ (U, 0, 0) + \frac{\partial u_{eff}}{\partial u_1} u' + \ldots + \frac{\partial^2 u_{eff}}{\partial u_1 \partial v_1} u'v' + \ldots$$

so that,

$$u_{eff} = \sqrt{A}\, U + \sqrt{A}\, u' + \frac{D}{2\sqrt{A}} v' + \frac{F}{2\sqrt{A}} w' + \left(\frac{B}{\sqrt{A}} - \frac{D^2}{4A\sqrt{A}}\right)\frac{v'^2}{2U} +$$

$$\left(\frac{C}{\sqrt{A}} - \frac{F^2}{4A\sqrt{A}}\right)\frac{w'^2}{2U} + \left(\frac{E}{\sqrt{A}} - \frac{DF}{2A\sqrt{A}}\right)\frac{v'w'}{2U} + 0(3) \qquad \text{(B.7)}$$

Now defining u'_{eff} by:

$$u'_{eff} = \sqrt{A}\, u' + \frac{D}{2\sqrt{A}} v' + \frac{F}{2\sqrt{A}} w' + 0\ (2) \qquad \text{(B.8)}$$

thus $U_{eff} = \sqrt{A}\ U + 0(2)$. (B.9)

Squaring Equation (B.8) and taking the time average

$$\overline{u'^2_{eff}} = A\ \overline{u'^2} + \frac{D^2}{4A}\ \overline{v'^2} + \frac{F^2}{4A}\ \overline{w'^2} + D\ \overline{u'v'} + \frac{DF}{2A}\ \overline{v'w'} + F\ \overline{u'w'} + 0(3) \qquad \text{(B.10)}$$

This equation relates the Reynolds stress tensor components to the mean square value of the effective velocity fluctuation.

Measurements with the same wire temperature of $\overline{u'^2_{eff}}$ at six different angles gave us all the six components of the tensor by solving the system of algebraic equations.

For all our runs it was shown that $\overline{v'w'} \approx 0$ and $\overline{u'w'} \approx 0$. Thus, the 2-D hypothesis is valid for our flow field and we used $\overline{v'w'} = \overline{u'w'} = 0$ throughout this study.

B.2 Measurement of $\overline{u'^2}$ in Isothermal Flows

In this case we used the horizontal wire ($\phi = 0^o$, $\theta = 90^o$). Equations (B.3) and (B.10) combined give

$$\overline{e'^2} = \left(\frac{\partial E}{\partial U}\right)^2 \overline{u'^2} + O(3) \qquad \text{(B.11)}$$

Thus the horizontal wire measures $\overline{u'^2}$ to a second order approximation.

B.3 Measurement of the Reynolds Stress Tensor Components in Isothermal Flows

In this case we used the slant wire, with the value $\overline{u'^2}$ known from measurement with horizontal wire.

Equations (B.3) and (B.10) give

$$\overline{e'^2} = \left(\frac{\partial E}{\partial U}\right)^2 \frac{\overline{u'^2_{eff}}}{A} \qquad \text{(B.12)}$$

and

$$\overline{u'^2_{eff}} - A\overline{u'^2} = \frac{D^2}{4A}\overline{v'^2} + \frac{F^2}{4A}\overline{w'^2} + D\,\overline{u'v'} + O(3) \qquad \text{(B.13)}$$

We have three unknowns: $\overline{v'^2}$, $\overline{w'^2}$, $\overline{u'v'}$. Measurements with the same wire temperature for three probe angles ($\theta = 0^o$, 45^o, 135^o) gave a system of algebraic equations that can be solved for the unknowns.

B.4 Measurement of $\overline{u't'}$

In this case we used the horizontal wire ($\phi = 0^o$, $\theta = 90^o$). Equation (B.3) squared and time averaged, using $\partial u/\partial u_{eff} = 1$ and Equation (B.8) and (B.1) give

$$\overline{e'^2} = \left(\frac{\partial E}{\partial U}\right)^2 \overline{u'^2} + \left(\frac{\partial E}{\partial T}\right)^2 \overline{t'^2} + 2\,\frac{\partial E}{\partial U}\,\frac{\partial E}{\partial T}\,\overline{u't'} \tag{B.14}$$

Thus, using $\overline{u'^2}$ from isothermal measurement and $\overline{t'^2}$ from the resistance thermometer approach of Appendix A, one gets $\overline{u't'}$.

According to Corrsin [71] using three wire temperatures, one could, with three measurements, obtain $\overline{u'^2}$, $\overline{t'^2}$, $\overline{u't'}$. But as he discusses, this process is very uncertain and presents a large scatter. This is primarily due to experimental errors in the rms values of the anemometer signal.

In the present investigation, the measured mean velocity profiles for the isothermal and non-isothermal flow fields were the same to within 1 to 2%. The local temperature was at most 15°F above the free-stream, indicating the flow can be considered a constant property flow. This low temperature difference and the invariance of mean velocity field justifies the assumption of the preservation of the hydrodynamics and so of the use of the isothermal $\overline{u'^2}$.

B.5 <u>Measurement of $\overline{v't'}$</u>

In this case we used the slant wire, with the value $\overline{u'v'}$ known from isothermal measurements. Equation (B.3) squared and time averaged, using $\partial u/\partial u_{eff} = 1/\sqrt{A}$, gives

$$\overline{e'^2} = \left(\frac{\partial E}{\partial U}\right)^2 \frac{\overline{u'^2_{eff}}}{A} + \left(\frac{\partial E}{\partial T}\right)^2 \overline{t'^2} + 2\,\frac{\partial E}{\partial U}\,\frac{\partial E}{\partial T}\,\frac{\overline{u'_{eff}t'}}{\sqrt{A}} \tag{B.15}$$

Measuring with the same wire temperature at $\theta = 45^\circ$ and 135° and subtracting the rms values $\overline{e'^2}$ and introducing Equation (B.8)

$$\overline{e'^2}\Big|_{\theta=45^\circ} - \overline{e'^2}\Big|_{\theta=135^\circ} = \overline{e'^2} = \left(\frac{\partial E}{\partial U}\right)^2 \frac{2D}{A}\,\overline{u'v'} + \frac{\partial E}{\partial U}\,\frac{\partial E}{\partial T}\,\frac{2D}{A}\,\overline{v't'} \tag{B.16}$$

Thus, using $\overline{u'v'}$ from isothermal measurement one gets $\overline{v't'}$. The same is valid for $\theta = -45^\circ$ and -135°.

According to Orlando [17], using two wire temperatures one could, with two measurements, obtain $\overline{u'v'}$ and $\overline{v't'}$. But the process is very uncertain and presents a large scatter, because of the experimental errors in the rms values of the anemometer signal.

Several authors like Johnson [80], and Kudva et al. [82] report measurements of both isothermal and non-isothermal $\overline{u'v'}$, with very small differences between the two, and certainly well within the uncertainty of the measurements. Based on this evidence and the arguments of previous sections concerning isothermal $\overline{u'^2}$, it is justified to use the isothermal $\overline{u'v'}$.

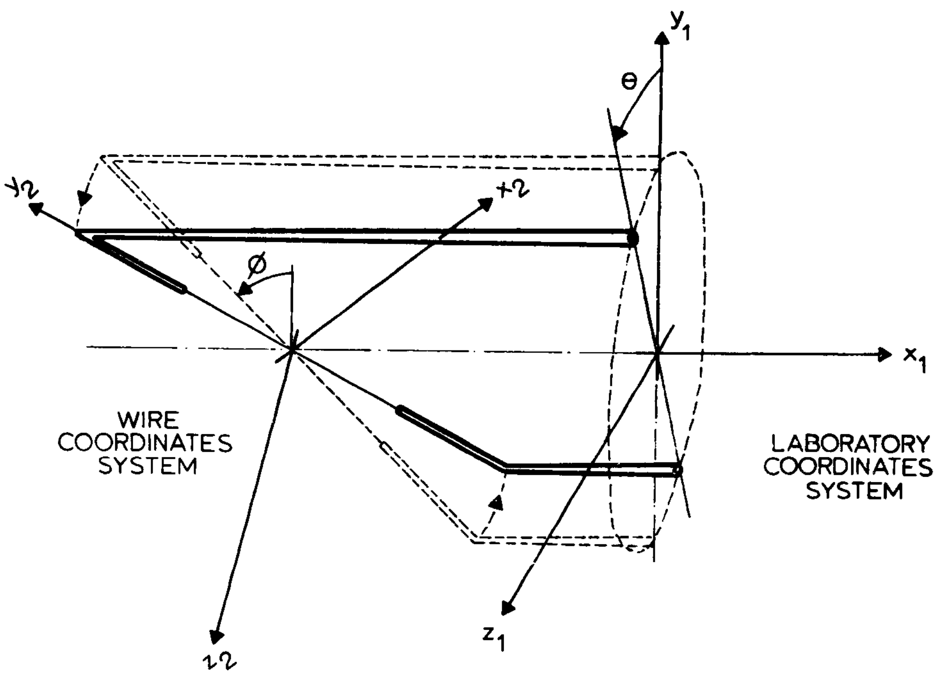

Fig. B.1 Slant wire: geometry and coordinates.

APPENDIX C

ON THE DETERMINATION OF FRICTION FACTORS

Very near the wall the flow is three-dimensional. For $y > \xi$, however, the flow is two-dimensional and we are faced with the problem of matching these two regions. Different ways of relating the two regions have been proposed, but most of them, if not all, neglect the near wall region: the "apparent" wall conditions are directly related to the outer-flow ($y > \xi$). The procedure proposed here is an attempt to perform a more rigorous matching, which could, perhaps, be extended to large roughness cases. It is our intention to clearly point out where the major assumptions are introduced.

The flow field is assumed to be two-dimensional for $y > \xi$. The time averaged continuity equation and x-momentum boundary layer equation for constant properties and zero pressure gradient are

$$\frac{\partial U}{\partial x} + \frac{\partial V}{\partial y} = 0 \qquad \text{(C.1)}$$

$$U\frac{\partial U}{\partial x} + V\frac{\partial U}{\partial y} = \frac{\partial}{\partial y}\frac{\tau}{\rho} \qquad \text{(C.2)}$$

where, for $y > \xi$, $\quad \dfrac{\tau}{\rho} = \nu\dfrac{\partial U}{\partial y} - \overline{u'v'}$.

Equation (C.2) can be rearranged to:

$$\frac{1}{\rho}\frac{\partial \tau}{\partial y} = \frac{\partial}{\partial y} UV + \frac{\partial U^2}{\partial x} \qquad \text{(C.3)}$$

Integrating from ξ to y one gets:

$$\frac{\tau(y)}{\rho} = \frac{\tau(\xi)}{\rho} + U(y)\ V(y) - U(\xi)\ V(\xi) + \frac{\partial}{\partial x}\int_{\xi}^{y} U^2 dy \qquad \text{(C.4)}$$

Using Equation (C.1):

$$V(y) = V(\xi) - \frac{\partial}{\partial x}\int_{\xi}^{y} U dy \qquad (C.5)$$

and substituting the definition for $\frac{\tau}{\rho}$, Equation (C.4) becomes

$$\frac{\tau(\xi)}{\rho} + \left(U(y) - U(\xi)\right) V(\xi) = \nu \frac{\partial U}{\partial y}\bigg|_{y} - \overline{u'v'}(y) + U \frac{\partial}{\partial x}\int_{\xi}^{y} U dy - \frac{\partial}{\partial x}\int_{\xi}^{y} U^2 dy \qquad (C.6)$$

Now let us turn our attention to the left hand side of the equation. For the boundary layer where $y < \xi$ the flow is three-dimensional and we will follow analogous considerations as those of Perry et al. [13], Roshko [83], and Fox [84].

Our rough surface is represented in Figure C.1. λ_x and λ_z are respectively the periods for our deterministic surface in the x direction (downstream) and in the z direction (cross-stream).

Let us introduce a new velocity decomposition. The mean velocity components can be throught as

$$U_i(x, y, z) = U_i^*(x, y) + \tilde{U}_i(x, y, z) \qquad (C.7)$$

for $y < \xi$.

The part U_i^* corresponds to the velocity resultant from the boundary layer evolving in the x-direction. We will refer to it as the basic flow. The part $\tilde{U}_i$ corresponds to the perturbation on the velocity field imposed by the roughness elements. We will refer to it as the perturbed flow.

Our surface given by $f(x, y, z) = 0$ is periodic with periods λ_x and λ_z. Therefore, it is reasonable to think that $\tilde{U}_i(x, y, z)$ is also periodic, with periods λ_x and λ_z.

From the properties of $\tilde{U}_i$, one can introduce the concept of spatial average

$$U_i^*(x, y) = \frac{1}{\lambda_x \lambda_z}\iint U_i(x, y, z) dx\, dz \qquad (C.8)$$

The time and spatially averaged continuity equation now reads:

$$\frac{\partial U^*}{\partial x} + \frac{\partial V^*}{\partial y} = 0 \tag{C.9}$$

It is reasonable to assume for the basic flow in the region considered here that $\partial/\partial x = 0$ (Couette flow) so

$$V^*(\xi) = V_o$$

but from our hypothesis

$$U_i(x, \xi, z) = U_i^*(x, y)$$

thus

$$V(\xi) = V_o \tag{C.10}$$

V_o is the transpiration flow rate per plate divided by the area of the plate, i.e., it is the area-averaged normal velocity to the wall.

The time and spatially averaged x-momentum equation can be cast in the following form (tensorial notation) with decompositions of p and τ made in analogous form to Equation (C.7)

$$U_i^* \frac{\partial}{\partial x_i} U_j^* = -\frac{1}{\rho} \frac{\partial}{\partial x_j} p^* + \frac{1}{\rho} \frac{\partial}{\partial x_i} \tau_{ij}^* \tag{C.11}$$

where τ_{ij}^* contains terms of the kind $\tilde{U}_i \tilde{U}_j$ as well as $\overline{u_i' u_j'}$.

Let us consider a control volume enclosed by the plane $y = \xi$, the surface of the balls $f(x, y, z) = 0$, and a cylindrical surface normal to the plane $y = \xi$ and intercepting it in a rectangle of sides λ_x and λ_y .

Integrating Equation (C.11) over this control volume and using the divergence theorem of calculus, we write

$$\int_V U_i^* \frac{\partial}{\partial x_i} U_j^* \, dV \cong U(\xi)\ V(\xi) \tag{C.12}$$

$$\int_V \frac{1}{\rho}\frac{\partial}{\partial x_j} p^* \, dV \cong F_D^* \text{ (drag)} \tag{C.13}$$

$$\int_V \frac{1}{\rho}\frac{\partial}{\partial x_i} \tau_{ij}^* \, dV \cong \frac{\tau(\xi)}{\rho} + \iint_{S_1} \frac{1}{\rho} \tau_{ij}^* \eta_i \, dS \tag{C.14}$$

where S_1 is the $f(x, y, z) = 0$ surface and η_i is the normal unit vector. For the fully rough case (neglecting the contribution of the surface integral):

$$U(\xi)\, V(\xi) = -F_D^* + \frac{\tau(\xi)}{\rho} \tag{C.15}$$

In Equations (C.12) and (C.14) we used the same assumptions made by Perry et al. [13], which we mentioned before. Having in mind the magnitude of the different terms of the integrated Equation (C.11), we are basically neglecting:

- the contribution of convection of momentum by the basic flow (Couette flow) compared to $U(\xi)\, V(\xi)$ and to the drag (pressure forces);
- the contribution of other shear forces compared to $\tau(\xi)$ (shear at plane $y = \xi$) and to the drag (pressure forces);
- the contribution of pressure forces at surfaces other than fluid wall interface, where the drag F_D is effectively generated.

Further, it is our belief that terms containing $U_i U_j$ when integrated over their periods of variation will not give contribution to the basic flow.

These assumptions are liable to criticism by Powe et al. [34] who, for a non-uniform artificially roughened pipe flow, included those contributions. It is these effects with which he proposed to explain the excursions of the $-\overline{u'v'}$ profile from the theoretical straight line profile. We did not have a sufficiently small probe available for testing our assumptions, but the observed two-dimensionality of the flow field partially support them.

Note that the shear stress contribution, over the surface S_1, given by the surface integral in Equation (C.14) $\iint_{S_1} \frac{1}{\rho} \tau^*_{ij} n_i \, dS$, should be retained for the smooth and transitionally rough cases. This contribution in both cases is not negligible.

Now, defining (fully rough case)

$$\frac{C_f}{2} = \frac{F^*_D}{U^2_\infty} \tag{C.16}$$

we finally have

$$\frac{C_f}{2} U^2_\infty = \tau(\xi) - U(\xi)\, V(\xi) \tag{C.17}$$

This last result and $V(\xi) = V_o$ (Equation C.10)) substituted into Equation (C.6) give

$$\frac{C_f}{2} = \frac{\nu}{U^2_\infty} \frac{\partial U}{\partial y}\bigg|_y - \frac{\overline{u'v'}}{U^2_\infty} - UV_o + \frac{U}{U^2_\infty} \frac{\partial}{\partial x} \int_\xi^y U \, dy - \frac{1}{U^2_\infty} \frac{\partial}{\partial x} \int_\xi^y U^2 \, dy \tag{C.18}$$

Friction factors $\frac{C_f}{2}$ in this study were determined from Equation (C.18) by means of measuring $-\overline{u'v'}$ and mean velocity profiles. This analysis is made necessary because $y = 0$ does not represent the wall in our case, neither the flow is 2-D in the neighborhood of the wall.

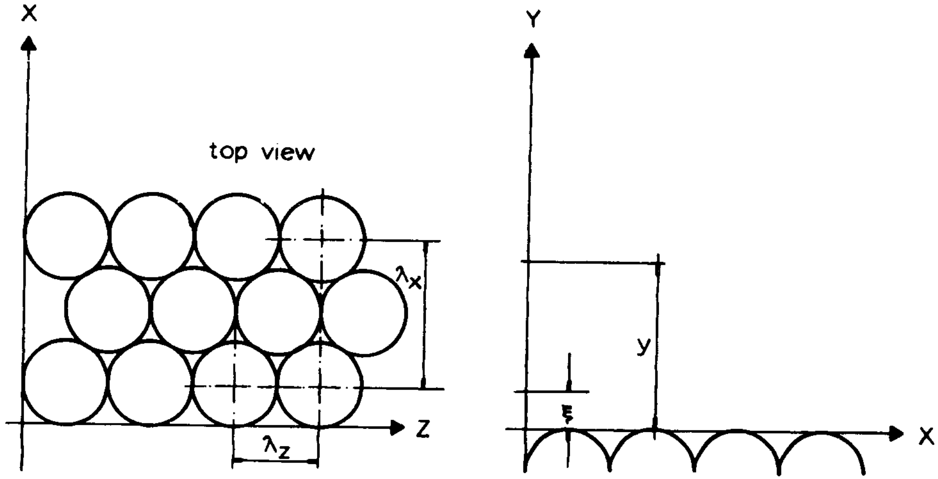

Fig. C.1 Rough wall: periodicity and coordinates.

APPENDIX D

TABULATION OF EXPERIMENTAL DATA

D.1 Stanton Number Data: Uniformly Blown and Unblown Cases

This section contains the Stanton number data for the uniformly blown and unblown cases. The following is a summary of the test cases and abbreviations used in the data listings.

U (ft/sec)	F
30	0.000
52	0.000
9	0.000
130	0.000
89	0.002
89	0.004

UINF	Free-stream velocity	(ft/sec)
F	Blowing fraction	-
TINF	Free-stream static temperature	(°F)
TINFO	Free-stream total temperature	(°F)
PAMB	Ambient pressure	(in Hg)
P	Free-stream static pressure	(psia)
TDB	Dry bulb temperature	(°F)
TWB	Wet bulb temperature	(°F)
PL	Plate number	-
X	Distance along test section, from inlet	(inch)
ST	Stanton number	-
REH	Enthalpy thickness Reynolds number	-
DELH2	Enthalpy thickness	(inch)
REX	x - Reynolds number	-
BH	F / St	-

TPL	Plate temperature	(^{o}F)
TAIR	Transpiration air temperature	(^{o}F)
QWALL	Heat flux from each 0.5 ft^2 plate to mainstream	(BTU/sec)

STANTON NUMBER RUN - UINF= 30 FT/SEC , F=0.000

UINF = 29.58
TINF = 67.50
TINFO = 67.60
PAMB = 29.82
P = 14.68
TDB = 77.0
TWB = 66.0

PL	X	ST	REH	DELH2	REX	F	BH	TPL	TAIR	QWALL
1	2	0.00231	70.1	0.005	30356.	0.0000	0.000	96.7	91.2	0.01802
2	6	0.00117	175.6	0.012	91069.	0.0000	0.000	96.8	91.0	0.00916
3	10	0.00099	241.1	0.016	151781.	0.0000	0.000	96.8	91.0	0.00775
4	14	0.00093	299.2	0.020	212493.	0.0000	0.000	96.8	90.3	0.00728
5	18	0.00092	355.4	0.023	273206.	0.0000	0.000	96.9	90.8	0.00723
6	22	0.00089	410.4	0.027	333918.	0.0000	0.000	96.6	90.1	0.00692
7	26	0.00164	487.2	0.032	394630.	0.0000	0.000	96.4	90.8	0.01266
8	30	0.00256	614.8	0.040	455342.	0.0000	0.000	96.5	92.6	0.01983
9	34	0.00301	783.9	0.052	516055.	0.0000	0.000	96.5	89.4	0.02332
10	38	0.00296	965.3	0.063	576767.	0.0000	0.000	96.5	89.5	0.02293
11	42	0.00289	1142.9	0.075	637479.	0.0000	0.000	96.8	90.9	0.02262
12	46	0.00277	1314.8	0.086	698192.	0.0000	0.000	97.0	92.8	0.02183
13	50	0.00260	1477.8	0.097	758904.	0.0000	0.000	96.8	92.1	0.02035
14	54	0.00245	1631.0	0.107	819616.	0.0000	0.000	96.7	93.0	0.01911
15	58	0.00243	1779.1	0.117	880329.	0.0000	0.000	96.7	92.0	0.01895
16	68	0.00238	1925.1	0.127	941041.	0.0000	0.000	96.8	91.0	0.01863
17	66	0.00239	2069.9	0.136	1001753.	0.0000	0.000	96.8	90.5	0.01871
18	70	0.00231	2212.7	0.145	1062465.	0.0000	0.000	96.8	90.9	0.01808
19	74	0.00228	2352.2	0.155	1123177.	0.0000	0.000	96.7	89.4	0.01778
20	78	0.00221	2488.6	0.164	1183890.	0.0000	0.000	96.7	91.8	0.01724
21	82	0.00216	2612.3	0.172	1244602.	0.0000	0.000	96.7	91.8	0.01685
22	86	0.00213	2751.3	0.181	1305314.	0.0000	0.000	96.7	91.8	0.01661
23	90	0.00213	2880.4	0.189	1366027.	0.0000	0.000	96.7	91.6	0.01661
24	94	0.00210	3008.7	0.198	1426739.	0.0000	0.000	96.7	91.8	0.01638

STANTON NUMBER RUN - UINF= 52 FT/SEC , F=0.000

UINF = 52.96
TINF = 66.10
TINFO = 66.30
PAMB = 29.82
P = 14.68
TDB = 78.0
TWB = 64.0

PL	X	ST	REH	DELH2	REX	F	BH	TPL	TAIR	QWALL
1	2	0.00170	92.9	0.003	54619.	0.0000	0.000	94.5	90.2	0.02301
2	6	0.00090	234.8	0.009	163858.	0.0000	0.000	94.5	89.4	0.01218
3	10	0.00109	343.3	0.013	273096.	0.0000	0.000	94.4	89.1	0.01470
4	14	0.00343	590.1	0.022	382334.	0.0000	0.000	94.3	90.3	0.04609
5	18	0.00379	964.6	0.036	491573.	0.0000	0.000	94.3	90.5	0.05093
6	22	0.00314	1363.1	0.050	600811.	0.0000	0.000	94.3	89.3	0.04219
7	26	0.00298	1697.4	0.062	710050.	0.0000	0.000	94.3	90.3	0.04004
8	30	0.00271	2008.6	0.074	819288.	0.0000	0.000	94.3	91.3	0.03641
9	34	0.00260	2299.0	0.084	928526.	0.0000	0.000	94.2	88.4	0.03481
10	38	0.00251	2578.4	0.095	1037765.	0.0000	0.000	94.3	88.3	0.03373
11	42	0.00249	2851.4	0.105	1147003.	0.0000	0.000	94.4	89.7	0.03358
12	46	0.00240	3118.4	0.114	1256241.	0.0000	0.000	94.3	91.3	0.03225
13	50	0.00236	3378.1	0.124	1365479.	0.0000	0.000	94.4	90.5	0.03183
14	54	0.00225	3629.8	0.133	1474718.	0.0000	0.000	94.3	91.6	0.03023
15	58	0.00222	3874.3	0.142	1583956.	0.0000	0.000	94.3	90.6	0.02983
16	62	0.00219	4115.5	0.151	1693194.	0.0000	0.000	94.3	89.7	0.02943
17	66	0.00218	4354.6	0.160	1802433.	0.0000	0.000	94.3	89.3	0.02929
18	70	0.00217	4597.3	0.169	1911671.	0.0000	0.000	94.3	89.7	0.02916
19	74	0.00215	4828.2	0.177	2020910.	0.0000	0.000	94.4	89.0	0.02899
20	78	0.00213	5061.9	0.186	2130148.	0.0000	0.000	94.5	86.1	0.02883
21	82	0.00207	5291.2	0.194	2239386.	0.0000	0.000	94.4	90.2	0.02791
22	86	0.00206	5516.7	0.203	2348625.	0.0000	0.000	94.4	90.7	0.02778
23	90	0.00206	5741.6	0.211	2457863.	0.0000	0.000	94.4	90.7	0.02778
24	94	0.00204	5965.4	0.219	2567101.	0.0000	0.000	94.3	92.5	0.02741

STANTON NUMBER RUN - UINF= 89 FT/SEC , F=0.000

UINF = 89.01
TINF = 65.80
TINFO = 66.50
PAMB = 29.93
P = 14.73
TDB = 77.0
TWB = 61.5

PL	X	ST	REH	DELH2	REX	F	BH	TPL	TAIR	QWALL
1	2	0.00143	131.6	0.003	92132.	0.0000	0.000	92.8	90.7	0.03058
2	6	0.00446	674.2	0.015	276397.	0.0000	0.000	92.6	94.8	0.09464
3	10	0.00375	1431.1	0.031	460662.	0.0000	0.000	92.6	90.7	0.07957
4	14	0.00324	2075.6	0.045	644927.	0.0000	0.000	92.5	89.8	0.06849
5	18	0.00297	2648.4	0.057	829192.	0.0000	0.000	92.6	89.8	0.06302
6	22	0.00276	3177.6	0.069	1013457.	0.0000	0.000	92.5	88.7	0.05834
7	26	0.00272	3683.4	0.080	1197722.	0.0000	0.000	92.5	89.7	0.05750
8	30	0.00255	4169.8	0.091	1381987.	0.0000	0.000	92.5	90.6	0.0[illegible]390
9	34	0.00250	4635.7	0.101	1566252.	0.0000	0.000	92.4	88.9	0.05264
10	38	0.00244	5091.1	0.111	1750517.	0.0000	0.000	92.4	88.4	0.05138
11	42	0.00242	5539.2	0.120	1934782.	0.0000	0.000	92.3	86.5	0.05076
12	46	0.00239	5982.8	0.130	2119047.	0.0000	0.000	92.3	90.6	0.05013
13	50	0.00237	6421.8	0.139	2303312.	0.0000	0.000	92.5	89.8	0.05010
14	54	0.00228	6850.9	0.149	2487577.	0.0000	0.000	92.3	91.1	0.04782
15	58	0.00226	7269.5	0.158	2671842.	0.0000	0.000	92.3	90.1	0.04740
16	62	0.00223	7683.3	0.167	2856107.	0.0000	0.000	92.2	89.1	0.04659
17	66	0.00222	8094.0	0.176	3040372.	0.0000	0.000	92.4	88.9	0.04675
18	70	0.00223	8504.9	0.185	3224637.	0.0000	0.000	92.4	89.1	0.0469[illegible]
19	74	0.00221	8914.2	0.193	3408902.	0.0000	0.000	92.5	87.9	0.04672
20	78	0.00218	9319.1	0.202	3593167.	0.0000	0.000	92.6	89.7	0.04626
21	82	0.00213	9717.1	0.211	3777432.	0.0000	0.000	92.5	89.6	0.04502
22	86	0.00213	10110.6	0.219	3961697.	0.0000	0.000	92.5	90.4	0.04502
23	90	0.00214	10504.7	0.228	4145962.	0.0000	0.000	92.6	90.6	0.04541
24	94	0.00214	10899.3	0.237	4330227.	0.0000	0.000	92.5	93.1	0.04524

STANTON NUMBER RUN - UINF= 89 FT/SEC , F=0.002

UINF = 89.69
TINF = 75.60
TINFO = 76.20
PAMB = 29.98
P = 14.75
TDB = 86.0
TWB = 75.0

PL	X	ST	REH	DELH2	REX	F	BH	TPL	TAIR	QWALL
1	2	0.00171	326.5	0.007	89894.	0.0019	1.122	106.8	79.5	0.04196
2	6	0.00372	1154.6	0.025	269682.	0.0019	0.560	105.9	80.7	0.08860
3	10	0.00262	2066.8	0.045	449470.	0.0019	0.741	105.9	80.3	0.06240
4	14	0.00228	2844.1	0.062	629258.	0.0018	0.792	105.9	80.6	0.05430
5	18	0.00193	3557.1	0.078	809046.	0.0019	1.000	106.2	78.5	0.04643
6	22	0.00187	4240.7	0.093	988834.	0.0019	1.012	106.3	80.2	0.04514
7	26	0.00180	4913.4	0.108	1168622.	0.0019	1.074	106.3	80.4	0.04345
8	30	0.00165	5570.0	0.122	1348410.	0.0019	1.171	106.2	80.9	0.03970
9	34	0.00160	6209.7	0.136	1528198.	0.0019	1.213	106.2	79.9	0.03849
10	38	0.00152	6841.6	0.150	1707986.	0.0020	1.292	106.1	79.8	0.03645
11	42	0.00151	7468.2	0.164	1887773.	0.0020	1.309	106.1	79.9	0.03621
12	46	0.00149	8090.1	0.178	2067561.	0.0019	1.300	106.0	80.9	0.03561
13	50	0.00143	8705.1	0.191	2247349.	0.0020	1.377	106.0	79.7	0.03417
14	54	0.00143	9307.0	0.204	2427137.	0.0018	1.293	106.0	80.6	0.03417
15	58	0.00139	9910.3	0.217	2606925.	0.0020	1.460	106.1	79.8	0.03333
16	62	0.00140	10510.5	0.231	2768713.	0.0019	1.334	106.3	81.0	0.03379
17	66	0.00141	11101.1	0.244	2966501.	0.0019	1.355	106.3	80.4	0.03403
18	70	0.00140	11684.0	0.256	3146289.	0.0018	1.273	106.3	80.7	0.03379
19	74	0.00143	12275.0	0.269	3326077.	0.0020	1.373	106.2	81.0	0.03440
20	78	0.00130	12874.8	0.283	3505865.	0.0020	1.518	106.7	81.1	0.03180
21	82	0.00123	13457.6	0.295	3685653.	0.0020	1.615	106.8	81.4	0.03018
22	86	0.00124	14034.2	0.308	3865441.	0.0020	1.590	107.0	82.0	0.03063
23	90	0.00136	14618.6	0.321	4045229.	0.0019	1.433	106.9	82.6	0.03348
24	94	0.00123	15200.3	0.334	4225017.	0.0019	1.588	106.8	82.7	0.03018

STANTON NUMBER RUN - UINF= 89 FT/SEC , F=0.004

UINF = 88.76
TINF = 75.50
TINFO = 76.10
PAMB = 29.84
P = 14.70
TDB = 83.0
TWB = 69.0

PL	X	ST	REH	DELH2	REX	F	BH	TPL	TAIR	QWALL
1	2	0.00187	508.9	0.011	88802.	0.0039	2.068	104.8	78.1	0.04248
2	6	0.00307	1629.0	0.037	266406.	0.0038	1.241	104.7	77.5	0.06949
3	10	0.00200	2757.2	0.062	444011.	0.0038	1.907	104.7	76.6	0.04527
4	14	0.00169	3765.8	0.085	621615.	0.0038	2.281	104.6	77.2	0.03812
5	18	0.00155	4737.1	0.107	799219.	0.0038	2.482	104.7	77.7	0.03509
6	22	0.00132	5674.1	0.128	976823.	0.0038	2.905	104.7	77.5	0.02988
7	26	0.00123	6579.0	0.148	1154427.	0.0038	3.090	104.5	77.5	0.02765
8	30	0.00113	7458.7	0.168	1332031.	0.0037	3.321	104.4	77.6	0.02531
9	34	0.00112	8333.6	0.188	1509635.	0.0039	3.456	104.4	76.7	0.02505
10	38	0.00103	9211.5	0.208	1687239.	0.0039	3.758	104.4	76.8	0.02307
11	42	0.00108	10076.1	0.227	1864843.	0.0037	3.458	104.3	77.2	0.02411
12	46	0.00104	10953.6	0.247	2042448.	0.0040	3.872	104.4	77.9	0.02329
13	50	0.00101	11832.1	0.267	2220052.	0.0038	3.780	104.6	77.6	0.02278
14	54	0.00091	12674.0	0.286	2397656.	0.0037	4.069	104.6	78.1	0.02053
15	58	0.00093	13511.1	0.305	2575260.	0.0039	4.156	104.8	77.6	0.02113
16	62	0.00093	14368.0	0.324	2752864.	0.0039	4.222	104.8	78.3	0.02113
17	66	0.00089	15231.0	0.343	2930468.	0.0040	4.434	104.6	77.9	0.02008
18	70	0.00083	16074.7	0.362	3108073.	0.0038	4.601	104.6	77.7	0.01872
19	74	0.00082	16904.3	0.381	3285677.	0.0039	4.762	104.7	77.8	0.01856
20	78	0.00086	17740.3	0.400	3463281.	0.0039	4.496	104.7	77.3	0.01947
21	82	0.00078	18577.8	0.419	3640885.	0.0039	5.028	104.8	77.3	0.01772
22	86	0.00071	19406.2	0.437	3818489.	0.0039	5.510	104.8	78.0	0.0[illegible]613
23	90	0.00081	20225.7	0.456	3996093.	0.0039	4.718	104.7	78.7	0.01834
24	94	0.00071	21041.9	0.474	4173698.	0.0039	5.473	104.8	78.8	0.01613

STANTON NUMBER RUN - UINF=130 FT/SEC , F=0.000

UINF = 130.63
TINF = 66.10
TINFO = 67.50
PAMB = 29.89
P = 14.72
TDB = 80.0
TWB = 67.5

PL	X	ST	REH	DELH2	REX	F	BH	TPL	TAIR	QWALL
1	2	0.00340	458.3	0.007	134974.	0.0000	0.000	95.9	97.0	0.11460
2	6	0.00399	1455.2	0.022	404922.	0.0000	0.000	95.3	98.1	0.13165
3	10	0.00326	2434.1	0.036	674871.	0.0000	0.000	95.2	94.7	0.10718
4	14	0.00297	3276.0	0.048	944819.	0.0000	0.000	95.3	94.0	0.09799
5	18	0.00279	4054.3	0.060	1214766.	0.0000	0.000	95.4	93.8	0.09239
6	22	0.00266	4791.1	0.071	1484714.	0.0000	0.000	95.3	92.4	0.08777
7	26	0.00264	5507.6	0.081	1754662.	0.0000	0.000	95.5	93.7	0.08773
8	30	0.00251	6202.7	0.092	2024610.	0.0000	0.000	95.5	94.6	0.08341
9	34	0.00243	6869.4	0.102	2294558.	0.0000	0.000	95.1	93.8	0.07960
10	38	0.00240	7521.9	0.111	2564506.	0.0000	0.000	95.1	94.5	0.07862
11	42	0.00236	8164.9	0.121	2834454.	0.0000	0.000	95.1	88.2	0.07731
12	46	0.00234	8799.6	0.130	3104402.	0.0000	0.000	95.3	91.6	0.07721
13	50	0.00233	9430.4	0.139	3374350.	0.0000	0.000	95.3	94.6	0.07688
14	54	0.00227	10052.2	0.149	3644298.	0.0000	0.000	95.3	94.8	0.07490
15	58	0.00224	10661.4	0.158	3914246.	0.0000	0.000	95.1	93.7	0.07338
16	62	0.00223	11264.9	0.167	4184194.	0.0000	0.000	95.2	92.7	0.07331
17	66	0.00222	11865.4	0.175	4454142.	0.0000	0.000	95.3	92.6	0.07325
18	70	0.00225	12468.0	0.184	4724090.	0.0000	0.000	95.1	92.5	0.07370
19	74	0.00222	13071.3	0.193	4994039.	0.0000	0.000	95.2	91.8	0.07298
20	78	0.00220	13667.7	0.202	5263987.	0.0000	0.000	95.1	92.5	0.07207
21	82	0.00216	14256.0	0.211	5533935.	0.0000	0.000	95.1	92.8	0.07076
22	86	0.00215	14838.2	0.219	5803883.	0.0000	0.000	95.1	94.3	0.07043
23	90	0.00218	15423.1	0.228	6073831.	0.0000	0.000	95.0	95.0	0.07115
24	94	0.00215	16007.3	0.237	6343779.	0.0000	0.000	95.0	97.3	0.07017

D.2 Stanton Number Data: Step in Blowing Cases

This section contains the Stanton number data listings for the cases with a step in blowing. Air was uniformly transpired through a certain number of plates in the beginning of the test section, and the rest was kept unblown. These tests were performed with the objective of allowing the analysis of the unblown Stanton number behavior for enlarged Re ranges. The following is a summary of the test cases.

U (ft/sec)	F	
89	0.002	plates 1 thru 6
	0.000	plates 7 thru 24
89	0.004	plates 1 thru 9
	0.000	plates 10 thru 24
89	0.004	plates 1 thru 12
	0.000	plates 13 thru 24

UINF	Free-stream velocity	(ft/sec)
F	Blowing fraction	-
TINF	Free-stream static temperature	(°F)
PAMB	Ambient pressure	(in Hg)
X	Distance along test section, from inlet	(inch)
ST	Stanton number	-
REH	Enthalpy thickness Reynolds number	-
DELH2	Enthalpy thickness	(inch)
REX	x - Reynolds number	-
TPL	Plate temperature	(°F)

STANTON NUMBER RUN - UINF= 90 FT/SEC , (1-6)F=0.002,(7-24)F=0.000

UINF = 90.10
TINF = 66.10
TINFC = 66.80
PAMB = 29.93
P = 14.73
TDB = 77.0
TWB = 62.0

PL	X	ST	REH	DELH2	REX	F	BH	TPL	TAIR	QWALL
1	2	0.00192	371.2	0.008	92695.	0.0021	1.083	92.2	67.1	0.03987
2	6	0.00369	1264.8	0.027	278086.	0.0019	0.529	92.3	67.3	0.07693
3	10	0.00264	2220.5	0.048	463477.	0.0020	0.769	92.5	67.5	0.05547
4	14	0.00223	3048.3	0.066	648868.	0.0020	0.910	92.4	67.2	0.04667
5	18	0.00206	3824.2	0.083	834259.	0.0020	0.995	92.4	67.2	0.04311
6	22	0.00189	4567.6	0.099	1019650.	0.0020	1.065	92.4	67.7	0.03956
7	26	0.00220	4946.7	0.107	1205041.	0.0000	0.000	92.3	76.7	0.04586
8	30	0.00221	5355.5	0.116	1390432.	0.0000	0.000	92.2	82.3	0.04589
9	34	0.00222	5766.2	0.124	1575823.	0.0000	0.000	92.1	85.4	0.04592
10	38	0.00221	6176.8	0.133	1761214.	0.0000	0.000	92.7	86.4	0.04679
11	42	0.00223	6588.4	0.142	1946605.	0.0000	0.000	92.6	87.5	0.04704
12	46	0.00223	7001.8	0.151	2131996.	0.0000	0.000	92.5	89.3	0.04685
13	50	0.00223	7415.2	0.160	2317387.	0.0000	0.000	92.5	88.2	0.04685
14	54	0.00217	7823.1	0.169	2502778.	0.0000	0.000	92.4	87.2	0.04542
15	58	0.00216	8224.4	0.177	2688169.	0.0000	0.000	92.2	87.6	0.04485
16	62	0.00211	8620.2	0.186	2873560.	0.0000	0.000	92.7	88.1	0.04468
17	66	0.00214	9014.2	0.194	3058951.	0.0000	0.000	92.1	89.1	0.04426
18	70	0.00212	9409.1	0.203	3244342.	0.0000	0.000	92.3	87.2	0.04420
19	74	0.00213	9807.7	0.212	3429733.	0.0000	0.000	92.4	88.0	0.04458
20	78	0.00205	10195.1	0.220	3615123.	0.0000	0.000	92.5	87.5	0.04307
21	82	0.00204	10574.3	0.228	3800514.	0.0000	0.000	92.7	88.7	0.04320
22	86	0.00204	10952.5	0.236	3985905.	0.0000	0.000	92.2	89.6	0.04236
23	90	0.00207	11333.4	0.245	4171296.	0.0000	0.000	92.3	90.3	0.04315
24	94	0.00203	11713.5	0.253	4356687.	0.0000	0.000	92.1	90.3	0.04199

STANTON NUMBER RUN - UINF= 90 FT/SEC , (1-9)F=0.004,(10-24)F=0.000

UINF = 90.55
TINF = 65.50
TINFO = 66.20
PAMB = 29.99
P = 14.77
TDB = 69.5
TWB = 56.0

PL	X	ST	REH	DELH2	REX	F	BH	TPL	TAIR	QWALL
1	2	0.00191	595.6	0.013	93737.	0.0044	2.308	92.7	67.8	0.04175
2	6	0.00288	1878.9	0.040	252800.	0.0044	1.531	92.9	67.4	0.06343
3	10	0.00189	3166.3	0.067	471335.	0.0045	2.341	92.7	67.5	0.04131
4	14	0.00147	4323.5	0.092	659868.	0.0044	3.020	92.8	67.3	0.03225
5	18	0.00136	5447.4	0.116	848402.	0.0046	3.375	92.8	67.4	0.02984
6	22	0.00115	6552.6	0.139	1036936.	0.0046	4.006	92.8	67.1	0.02523
7	26	0.00110	7587.0	0.161	1225470.	0.0042	3.751	93.0	66.2	0.02432
8	30	0.00101	8600.9	0.182	1414004.	0.0045	4.481	92.9	66.1	0.02224
9	34	0.00095	9641.9	0.204	1602538.	0.0046	4.768	92.9	65.3	0.02092
10	38	0.00162	10310.2	0.219	1791071.	0.0000	0.000	93.0	77.7	0.03581
11	42	0.00179	10631.7	0.225	1979605.	0.0000	0.000	93.5	81.6	0.04031
12	46	0.00189	10978.6	0.233	2168139.	0.0000	0.000	92.9	85.7	0.04163
13	50	0.00196	11341.5	0.240	2356673.	0.0000	0.000	92.9	87.3	0.04317
14	54	0.00198	11712.9	0.248	2545207.	0.0000	0.000	93.0	89.8	0.04377
15	58	0.00198	12086.2	0.256	2733740.	0.0000	0.000	93.0	88.9	0.04377
16	62	0.00201	12462.4	0.264	2922275.	0.0000	0.000	93.1	88.0	0.04460
17	66	0.00203	12843.2	0.272	3110808.	0.0000	0.000	93.0	87.7	0.04488
18	70	0.00206	13228.8	0.281	3299342.	0.0000	0.000	93.0	88.4	0.04554
19	74	0.00206	13617.1	0.289	3487876.	0.0000	0.000	93.2	87.3	0.04588
20	78	0.00204	14003.6	0.297	3676410.	0.0000	0.000	93.1	88.7	0.04527
21	82	0.00200	14384.5	0.305	3864944.	0.0000	0.000	93.2	89.2	0.04454
22	86	0.00201	14762.5	0.313	4053478.	0.0000	0.000	93.2	90.2	0.04477
23	90	0.00204	15144.3	0.321	4242012.	0.0000	0.000	93.1	90.3	0.04527
24	94	0.00205	15529.8	0.329	4430545.	0.0000	0.000	93.1	93.3	0.04549

STANTON NUMBER RUN - UINF= 90 FT/SEC , (1-12)F=0.004,(12-24)F=0.000

UINF = 90.41
TINF = 67.20
TINFO = 67.90
PAMB = 29.97
P = 14.77
TDB = 77.0
TWB = 62.0

PL	X	ST	REH	DELH2	REX	F	BH	TPL	TAIR	QWALL
1	2	0.00188	585.1	0.013	93014.	0.0044	2.335	92.5	67.1	0.03794
2	6	0.00283	1841.2	0.040	279043.	0.0044	1.555	92.8	67.3	0.05781
3	10	0.00187	3098.9	0.067	465072.	0.0044	2.364	92.1	67.8	0.03712
4	14	0.00148	4233.7	0.091	651100.	0.0044	2.973	92.2	67.5	0.02950
5	18	0.00127	5309.9	0.114	837129.	0.0046	3.457	92.3	67.3	0.02542
6	22	0.00110	6352.6	0.137	1023158.	0.0045	4.045	92.1	67.2	0.02184
7	26	0.00101	7379.5	0.159	1209187.	0.0045	4.436	92.7	66.8	0.02055
8	30	0.00094	8391.5	0.180	1395216.	0.0044	4.734	92.9	66.2	0.01928
9	34	0.00097	9403.5	0.202	1581245.	0.0045	4.660	92.9	65.6	0.01989
10	38	0.00093	10412.7	0.224	1767273.	0.0044	4.763	92.2	67.3	0.01854
11	42	0.00092	11406.1	0.245	1953302.	0.0044	4.783	92.2	67.9	0.01834
12	46	0.00094	12396.7	0.267	2139331.	0.0044	4.670	92.3	68.1	0.01882
13	50	0.00152	13033.8	0.280	2325360.	0.0000	0.000	92.5	77.2	0.03067
14	54	0.00169	13332.4	0.287	2511388.	0.0000	0.000	92.3	86.1	0.03383
15	58	0.00173	13650.5	0.294	2697417.	0.0000	0.000	92.7	88.3	0.03520
16	62	0.00180	13978.8	0.301	2883446.	0.0000	0.000	92.5	88.0	0.03632
17	66	0.00185	14318.3	0.308	3069475.	0.0000	0.000	92.7	87.1	0.03764
18	70	0.00192	14669.0	0.315	3255504.	0.0000	0.000	92.9	88.8	0.03938
19	74	0.00198	15031.7	0.323	3441533.	0.0000	0.000	93.0	87.4	0.04077
20	78	0.00203	15404.7	0.331	3627561.	0.0000	0.000	93.0	88.7	0.04180
21	82	0.00201	15775.9	0.339	3813591.	0.0000	0.000	93.1	89.5	0.04155
22	86	0.00204	16152.6	0.347	3999619.	0.0000	0.000	93.2	90.3	0.04234
23	90	0.00203	16531.1	0.355	4185648.	0.0000	0.000	93.2	90.1	0.04213
24	94	0.00202	16907.8	0.364	4371677.	0.0000	0.000	93.1	92.8	0.04176

D.3 Mean Velocity and Temperature Profiles Data

This section contains the mean velocity and temperature profiles data for the uniformly blown and unblown cases. The following is a summary of the test cases and abbreviations used in the data listings.

U_∞ (ft/sec)	F
52	0.000
89	0.000
130	0.000
89	0.002
89	0.004

UINF	Free-stream velocity	(ft/sec)
F	Blowing fraction	-
RUN	Run number	-
PLATE	Plate number	-
X(IN)	x - wise coordinate, from inlet	(inch)
$x-x_o$ (IN)	Distance from virtual origin	(inch)
Z (IN)	z - wise coordinate, from center line	(inch)
POINTS	Number of data points	-
TWALL	Wall temperature	(^{o}F)
TINF	Free-stream static temperature	(^{o}F)
CF/2	Friction factor	-
ST	Stanton number	-
DELM	Momentum boundary layer thickness	(inch)
DELM1	Displacement thickness, δ_1	(inch)
DELM2	Momentum thickness, δ_2	(inch)

H	Shape factor, δ_1/δ_2	-
DELH	Thermal boundary layer thickness, δ_T	(inch)
DELH2	Enthalpy thickness, Δ_2	(inch)
REX	x - Reynolds number	-
REM	Momentum thickness Reynolds number	-
REK	Roughness Reynolds number, (k_s = 0.031 in)	-
UTAU	Friction velocity, $U_\infty\sqrt{C_f/2} = U_\tau$	(ft/sec)
TTAU	$(T_w - T_{\infty,o})\ St/\sqrt{C_f/2} = T_\tau$	(^oF)
I	Profile point number	-
Y	Normal to the wall coordinate, from the crests of the rough surface balls	(inch)
YS	y - coordinate from velocity profile virtual origin, $(y + \Delta y)$	(inch)
U	Local velocity	(ft/sec)
UDE	Defect velocity, $(U_\infty - U)/U_\tau$	-
T	Local static temperature	(^oF)
TBAR	$(T_w - T)/(T_w - T_\infty)$	-
TDE	$(T - T_\infty)/T_\tau$	-

MEAN VELOCITY AND TEMPERATURE PROFILE - UINF= 52 FT/SEC F=0.000

RUN	= 070974-3	UINF	= 52.29	DELM	= 0.184	REX	= 0.380E 06
PLATE	= 4	TWALL	= 93.75	DELM1	= 0.035	REM	= 595.40
X(IN)	= 14.	TINF	= 66.31	DELM2	= 0.022	REH	= 541.30
X-XO(IN)	= 14.0	F	= C.000	H	= 1.596	REK	= 48.10
Z(IN)	= 0.000	CF/2	= 0.00328	DELH	= 0.208	UTAU	= 2.99
PCINTS	= 33	ST	= 0.00343	DELH2	= 0.020	TTAU	= 1.630

I	Y	YS	Y/DELM	YS/DELM	Y/DELM2	YS/DELM2	U	U/UINF	UDE	Y/DELH2	YS/DELH2	T	TBAR	TDE
1	0.007	0.013	0.0380	0.0707	0.3182	0.5909	23.19	0.443	9.732	0.3500	0.6500	79.80	0.508	8.28
2	0.008	0.014	0.0435	0.0761	0.3636	0.6364	23.95	0.458	9.478	0.4000	0.7000	79.47	0.520	8.07
3	0.009	0.015	0.0489	0.0815	0.4091	0.6818	24.77	0.474	9.204	C.4500	0.7500	79.21	0.530	7.91
4	0.011	0.017	0.0598	0.0924	0.5000	0.7727	25.61	0.490	8.923	0.5500	0.8500	78.61	0.552	7.55
5	0.013	0.015	0.0707	0.1033	0.5909	0.8636	26.59	0.509	8.595	0.6500	0.9500	78.15	0.569	7.26
6	0.015	0.021	0.0815	0.1141	0.6818	0.9545	27.79	0.531	8.194	0.7500	1.0500	77.61	0.588	6.93
7	0.018	0.024	0.0978	0.1304	0.8182	1.0909	28.86	0.552	7.836	0.9000	1.2000	77.11	0.606	6.63
8	0.021	0.027	0.1141	0.1467	0.9545	1.2273	29.97	0.573	7.465	1.0500	1.3500	76.44	0.631	6.21
9	0.024	0.030	0.1304	0.1630	1.0909	1.3636	31.03	0.593	7.110	1.2000	1.5000	76.08	0.644	5.99
10	0.028	0.034	0.1522	0.1848	1.2727	1.5455	32.08	0.614	6.759	1.4000	1.7000	75.49	0.665	5.63
11	0.032	0.038	0.1739	0.2065	1.4545	1.7273	33.09	0.633	6.421	1.6000	1.9000	75.03	0.682	5.35
12	0.037	0.043	0.2011	0.2337	1.6818	1.9545	34.68	0.663	5.890	1.8500	2.1500	74.38	0.706	4.95
13	0.043	0.049	0.2337	0.2663	1.9545	2.2273	36.17	0.692	5.391	2.1500	2.4500	73.68	0.731	4.52
14	0.049	0.055	0.2663	0.2989	2.2273	2.5000	37.73	0.722	4.870	2.4500	2.7500	73.07	0.754	4.15
15	0.056	0.062	0.3043	0.3370	2.5455	2.8182	38.87	0.743	4.488	2.8000	3.1000	72.42	0.777	3.75
16	0.063	0.069	0.3424	0.3750	2.8636	3.1364	40.39	0.772	3.980	3.1500	3.4500	71.78	0.801	3.36
17	0.071	0.077	0.3859	0.4185	3.2273	3.5000	42.05	0.804	3.425	3.5500	3.8500	71.05	0.827	2.91
18	0.078	0.084	0.4239	0.4565	3.5455	3.8182	43.25	0.827	3.023	3.9000	4.2000	70.52	0.847	2.58
19	0.086	0.092	0.4674	0.5000	3.9091	4.1818	44.50	0.851	2.605	4.3000	4.6000	70.01	0.865	2.27
20	0.095	0.101	0.5163	0.5489	4.3182	4.5905	46.04	0.880	2.090	4.7500	5.0500	69.47	0.885	1.94
21	0.105	0.111	0.5707	0.6033	4.7727	5.0455	47.14	0.902	1.722	5.2500	5.5500	68.94	0.904	1.61
22	0.115	0.121	0.6250	0.6576	5.2273	5.5000	48.27	0.923	1.344	5.7500	6.0500	68.48	0.921	1.33
23	0.13C	0.136	0.7065	0.7391	5.9091	6.1818	49.41	G.945	0.963	6.5000	6.8000	68.01	0.938	1.04
24	0.150	0.156	0.8152	0.8478	6.8182	7.0909	50.81	0.972	0.495	7.5000	7.8000	67.39	0.961	0.66
25	0.170	0.176	0.9239	0.9565	7.7273	8.0000	51.43	0.984	0.288	8.5000	8.8000	67.03	0.974	0.44
26	0.190	0.196	1.0325	1.0652	8.6364	8.9091	51.89	0.992	0.134	9.5000	9.8000	66.75	0.984	0.27
27	0.215	0.221	1.1685	1.2011	9.7727	10.0455	52.06	0.996	0.077	10.7500	11.0500	66.55	0.991	0.15
28	0.240	0.246	1.3043	1.3370	10.9091	11.1818	52.33	1.001	-0.013	12.0000	12.3000	66.44	0.995	0.08
29	0.270	0.276	1.4674	1.5000	12.2727	12.5455	52.33	1.001	-0.013	13.5000	13.8000	66.39	0.997	0.05
30	0.300	0.306	1.6304	1.6630	13.6364	13.9091	52.31	1.000	-0.007	15.0000	15.3000	66.36	0.998	0.03
31	0.350	0.356	1.9022	1.9348	15.9091	16.1818	52.30	1.000	-0.003	17.5000	17.8000	66.34	0.999	0.02
32	0.45C	0.456	2.4457	2.4783	20.4545	20.7273	52.29	1.000	0.000	22.5000	22.8000	66.31	1.000	0.00
33	0.550	0.556	2.9891	3.0217	25.0000	25.2727	52.29	1.000	0.000	27.5000	27.8000	66.31	1.000	0.00

MEAN VELOCITY AND TEMPERATURE PROFILE - UINF= 52 FT/SEC F=0.000

RUN = 070974-2		UINF = 52.25		DELM = 0.452		REX = 0.700E 06	
PLATE = 7		TWALL = 93.80		DELM1 = 0.090		REM = 1595.60	
X(IN) = 26.		TINF = 66.37		DELM2 = 0.059		REH = 1649.70	
X-XO(IN) = 26.0		F = 0.000		H = 1.520		REK = 43.60	
Z(IN) = 0.000		CF/2 = 0.00270		DELH = 0.495		UTAU = 2.71	
POINTS = 31		ST = 0.00298		DELH2 = 0.061		TTAU = 1.560	

I	Y	YS	Y/DELM	YS/DELM	Y/DELM2	YS/DELM2	U	U/UINF	UDE	Y/DELH2	YS/DELH2	T	TBAR	TDE
1	0.007	0.013	0.0155	0.0288	0.1186	0.2203	18.91	0.362	12.303	0.1148	0.2131	82.45	0.414	10.31
2	0.008	0.014	0.0177	0.0310	0.1356	0.2373	19.46	0.372	12.100	0.1311	0.2295	82.25	0.421	10.18
3	0.009	0.015	0.0199	0.0332	0.1525	0.2542	19.87	0.380	11.948	0.1475	0.2459	82.07	0.428	10.06
4	0.011	0.017	0.0243	0.0376	0.1864	0.2881	21.00	0.402	11.531	0.1803	0.2787	81.59	0.445	9.76
5	0.014	0.020	0.0310	0.0442	0.2373	0.3390	22.41	0.429	11.011	0.2295	0.3279	80.95	0.468	9.35
6	0.017	0.023	0.0376	0.0509	0.2881	0.3898	23.70	0.454	10.535	0.2787	0.3770	80.40	0.489	8.99
7	0.021	0.027	0.0465	0.0597	0.3559	0.4576	24.59	0.478	10.059	0.3443	0.4426	79.75	0.512	8.58
8	0.025	0.031	0.0553	0.0686	0.4237	0.5254	26.31	0.504	9.572	0.4098	0.5082	79.21	0.532	8.23
9	0.030	0.036	0.0664	0.0796	0.5085	0.6102	27.38	0.524	9.177	0.4918	0.5902	78.71	0.550	7.91
10	0.037	0.043	0.0819	0.0951	0.6271	0.7288	28.62	0.548	8.720	0.6066	0.7049	78.10	0.572	7.52
11	0.045	0.051	0.0996	0.1128	0.7627	0.8644	29.86	0.571	8.262	0.7377	0.8361	77.46	0.596	7.11
12	0.053	0.059	0.1173	0.1305	0.8983	1.0000	30.94	0.592	7.863	0.8689	0.9672	76.96	0.614	6.79
13	0.063	0.069	0.1394	0.1527	1.0678	1.1695	32.16	0.616	7.413	1.0328	1.1311	76.45	0.633	6.46
14	0.075	0.081	0.1659	0.1792	1.2712	1.3729	33.43	0.640	6.945	1.2295	1.3279	75.82	0.655	6.06
15	0.090	0.096	0.1991	0.2124	1.5254	1.6271	34.72	0.664	6.469	1.4754	1.5738	75.12	0.681	5.61
16	0.110	0.116	0.2434	0.2566	1.8644	1.9661	36.35	0.696	5.867	1.8033	1.9016	74.48	0.704	5.20
17	0.130	0.136	0.2876	0.3009	2.2034	2.3051	37.78	0.723	5.339	2.1311	2.2295	73.73	0.732	4.72
18	0.150	0.156	0.3319	0.3451	2.5424	2.6441	39.30	0.752	4.779	2.4590	2.5574	73.15	0.753	4.35
19	0.175	0.181	0.3872	0.4004	2.9661	3.0678	40.89	0.783	4.192	2.8689	2.9672	72.42	0.779	3.88
20	0.200	0.206	0.4425	0.4558	3.3898	3.4915	42.36	0.811	3.649	3.2787	3.3770	71.41	0.816	3.23
21	0.225	0.231	0.4978	0.5111	3.8136	3.9153	43.89	0.840	3.085	3.6885	3.7869	71.07	0.829	3.01
22	0.255	0.261	0.5642	0.5774	4.3220	4.4237	45.33	0.868	2.554	4.1803	4.2787	70.39	0.653	2.58
23	0.290	0.296	0.6416	0.6549	4.9153	5.0169	46.88	0.897	1.982	4.7541	4.8525	69.57	0.883	2.05
24	0.325	0.331	0.7190	0.7323	5.5085	5.6102	48.32	0.925	1.450	5.3279	5.4262	68.90	0.908	1.62
25	0.375	0.381	0.8296	0.8429	6.3559	6.4576	50.13	0.959	0.782	6.1475	6.2459	68.04	0.939	1.07
26	0.425	0.431	0.9403	0.9535	7.2034	7.3051	51.34	0.983	0.336	6.9672	7.0656	67.26	0.968	0.57
27	0.475	0.481	1.0509	1.0642	8.0508	8.1525	51.93	0.994	0.118	7.7869	7.8852	66.78	0.985	0.26
28	0.525	0.531	1.1615	1.1748	8.8983	9.0000	52.26	1.000	-0.004	8.6066	8.7049	66.53	0.994	10
29	0.600	0.606	1.3274	1.3407	10.1695	10.2712	52.25	1.000	0.000	9.8361	9.9344	66.41	0.999	0.03
30	0.700	0.706	1.5487	1.5619	11.8644	11.9661	52.25	1.000	0.000	11.4754	11.5738	66.37	1.000	0.00
31	0.850	0.856	1.8805	1.8938	14.4068	14.5085	52.25	1.000	0.000	13.9344	14.0328	66.37	1.000	0.00

MEAN VELOCITY AND TEMPERATURE PROFILE - UINF= 52 FT/SEC F=0.000

RUN	= 070974-1	UINF	= 52.29	DELM	= 0.700	REX	= 0.103E 07
PLATE	= 10	TWALL	= 93.65	DELM1	= 0.140	REM	= 2517.10
X(IN)	= 38.	TINF	= 66.27	DELM2	= 0.093	REH	= 2571.20
X-XO(IN)	= 38.0	F	= 0.000	H	= 1.506	REK	= 41.80
Z(IN)	= 0.000	CF/2	= 0.00247	DELH	= 0.731	UTAU	= 2.61
POINTS	= 30	ST	= 0.00251	DELH2	= 0.095	TTAU	= 1.366

I	Y	YS	Y/DELM	YS/DELM	Y/DELM2	YS/DELM2	U	U/UINF	UDE	Y/DELH2	YS/DELH2	T	TBAR	TDE
1	0.007	0.013	0.0100	0.0186	0.0753	0.1358	16.85	0.322	13.594	0.0737	0.1368	83.42	0.374	12.55
2	0.008	0.014	0.0114	0.0200	0.0860	0.1505	17.37	0.332	13.395	0.0842	0.1474	83.21	0.381	12.40
3	0.009	0.015	0.0129	0.0214	0.0968	0.1613	17.90	0.342	13.191	0.0947	0.1579	82.86	0.394	12.14
4	0.011	0.017	0.0157	0.0243	0.1183	0.1828	19.20	0.367	12.693	0.1158	0.1789	82.39	0.411	11.80
5	0.014	0.020	0.0200	0.0286	0.1505	0.2151	20.47	0.391	12.206	0.1474	0.2105	81.74	0.435	11.33
6	0.017	0.023	0.0243	0.0329	0.1828	0.2473	21.81	0.417	11.692	0.1789	0.2421	81.22	0.454	10.94
7	0.020	0.026	0.0286	0.0371	0.2151	0.2796	22.65	0.433	11.369	0.2105	0.2737	80.81	0.469	10.64
8	0.025	0.031	0.0357	0.0443	0.2688	0.3333	23.73	0.454	10.955	0.2632	0.3263	80.24	0.490	10.23
9	0.030	0.036	0.0429	0.0514	0.3226	0.3871	24.70	0.472	10.583	0.3158	0.3789	79.75	0.508	9.87
10	0.036	0.042	0.0514	0.0600	0.3871	0.4516	26.10	0.499	10.046	0.3789	0.4421	79.29	0.524	9.53
11	0.043	0.049	0.0614	0.0700	0.4624	0.5269	27.12	0.519	9.655	0.4526	0.5158	78.76	0.544	9.14
12	0.051	0.057	0.0729	0.0814	0.5484	0.6129	28.23	0.540	9.229	0.5368	0.6000	78.29	0.561	8.80
13	0.062	0.068	0.0886	0.0971	0.6667	0.7312	29.47	0.564	8.753	0.6526	0.7158	77.71	0.582	8.37
14	0.076	0.082	0.1086	0.1171	0.8172	0.8817	30.80	0.589	8.243	0.8000	0.8632	77.15	0.603	7.96
15	0.094	0.100	0.1343	0.1429	1.0108	1.0753	31.98	0.612	7.791	0.9895	1.0526	76.50	0.626	7.49
16	0.112	0.118	0.1600	0.1686	1.2043	1.2688	33.29	0.637	7.288	1.1789	1.2421	75.95	0.646	7.09
17	0.130	0.136	0.1857	0.1943	1.3978	1.4624	34.26	0.655	6.916	1.3684	1.4316	75.50	0.663	6.76
18	0.155	0.161	0.2214	0.2300	1.6667	1.7312	35.73	0.683	6.352	1.6316	1.6947	74.80	0.688	6.24
19	0.185	0.191	0.2643	0.2729	1.9892	2.0538	37.11	0.710	5.823	1.9474	2.0105	74.16	0.712	5.78
20	0.215	0.221	0.3071	0.3157	2.3118	2.3763	38.48	0.736	5.297	2.2632	2.3263	73.54	0.734	5.32
21	0.250	0.256	0.3571	0.3657	2.6882	2.7527	39.89	0.763	4.756	.6316	2.6947	72.86	0.759	4.82
22	0.300	0.306	0.4286	0.4371	3.2258	3.2903	41.86	0.801	4.001	3.1579	3.2211	71.99	0.791	4.19
23	0.350	0.356	0.5000	0.5086	3.7634	3.8280	43.65	0.836	3.299	3.6842	3.7474	71.07	0.825	3.51
24	0.425	0.431	0.6071	0.6157	4.5699	4.6344	46.19	0.883	2.340	4.4737	4.5368	69.95	0.866	2.69
25	0.500	0.506	0.7143	0.7229	5.3763	5.4409	48.25	0.923	1.550	5.2632	5.3263	68.89	0.904	1.92
26	0.600	0.606	0.8571	0.8657	6.4516	6.5161	50.57	0.967	0.660	6.3158	6.3789	67.62	0.951	0.99
27	0.700	0.706	1.0000	1.0086	7.5269	7.5914	51.77	0.990	0.199	7.3684	7.4316	66.73	0.983	0.34
28	0.850	0.856	1.2143	1.2229	9.1398	9.2043	52.29	1.000	0.000	8.9474	9.0105	66.27	1.000	0.00
29	1.000	1.006	1.4286	1.4371	10.7527	10.8172	52.29	1.000	0.000	10.5263	10.5895	66.27	1.000	0.00
30	1.150	1.156	1.6429	1.6514	12.3656	12.4301	52.29	1.000	0.000	12.1053	12.1684	66.27	1.000	0.00

MEAN VELOCITY AND TEMPERATURE PROFILE - UINF= 52 FT/SEC F=0.000

RUN	= 070974-4	UINF	=	52.30	DELM	= 0.905	REX	=	0.135E 07
PLATE	= 13	TWALL	=	94.19	DELM1	= 0.181	REM	=	3275.50
X(IN)	= 50.	TINF	=	66.37	DELM2	= 0.121	REH	=	3383.80
X-XO(IN)	= 50.0	F	=	0.000	H	= 1.494	REK	=	40.85
Z(IN)	= 0.000	CF/2	=	0.00237	DELH	= 0.957	UTAU	=	2.55
POINTS	= 32	ST	=	0.00236	DELH2	= 0.125	TTAU	=	1.328

I	Y	YS	Y/DELM	YS/DELM	Y/DELM2	YS/DELM2	U	U/UINF	UCE	Y/DELH2	YS/DELH2	T	TBAR	TOE
1	0.007	0.013	0.0077	0.0144	0.0579	0.1074	16.53	0.318	13.988	0.0560	0.1040	84.04	0.365	13.21
2	0.008	0.014	0.0088	0.0155	0.0661	0.1157	17.17	0.328	13.776	0.0640	0.1120	83.79	0.374	13.02
3	0.009	0.015	0.0099	0.0166	0.0744	0.1240	17.77	0.340	13.541	0.0720	0.1200	83.53	0.383	12.83
4	0.011	0.017	0.0122	0.0188	0.0909	0.1405	18.82	0.360	13.129	0.0880	0.1360	83.05	0.400	12.47
5	0.014	0.020	0.0155	0.0221	0.1157	0.1653	20.06	0.384	12.643	0.1120	0.1600	82.41	0.423	11.99
6	0.017	0.023	0.0188	0.0254	0.1405	0.1901	21.22	0.406	12.188	0.1360	0.1840	81.98	0.439	11.67
7	0.020	0.026	0.0221	0.0287	0.1653	0.2149	22.03	0.421	11.871	0.1600	0.2080	81.53	0.455	11.33
8	0.025	0.031	0.0276	0.0343	0.2066	0.2562	23.35	0.446	11.353	0.2000	0.2480	80.97	0.475	10.91
9	0.030	0.036	0.0331	0.0398	0.2479	0.2975	24.13	0.461	11.047	0.2400	0.2880	80.58	0.489	10.62
10	0.037	0.043	0.0409	0.0475	0.3058	0.3554	25.33	0.484	10.576	0.2960	0.3440	79.99	0.510	10.18
11	0.045	0.051	0.0497	0.0564	0.3719	0.4215	26.33	0.503	10.184	0.3600	0.4080	79.45	0.530	9.78
12	0.053	0.059	0.0586	0.0652	0.4380	0.4876	27.35	0.523	9.784	0.4240	0.4720	79.07	0.543	9.49
13	0.063	0.069	0.0696	0.0762	0.5207	0.5702	28.24	0.540	9.435	0.5040	0.5520	78.64	0.559	9.17
14	0.076	0.082	0.0840	0.0906	0.6281	0.6777	29.26	0.559	9.035	0.6080	0.6560	78.08	0.579	8.75
15	0.092	0.098	0.1017	0.1083	0.7603	0.8099	30.51	0.583	8.545	0.7360	0.7840	77.66	0.594	8.44
16	0.110	0.116	0.1215	0.1282	0.9091	0.9587	31.55	0.603	8.137	0.8800	0.9280	77.09	0.615	8.01
17	0.130	0.136	0.1436	0.1503	1.0744	1.1240	32.60	0.623	7.725	1.0400	1.0880	76.57	0.633	7.62
18	0.155	0.161	0.1713	0.1779	1.2810	1.3306	33.89	0.648	7.220	1.2400	1.2880	75.99	0.654	7.19
19	0.185	0.191	0.2044	0.2110	1.5289	1.5785	35.03	0.670	6.773	1.4800	1.5280	75.34	0.678	6.70
20	0.225	0.231	0.2486	0.2552	1.8595	1.9091	36.52	0.698	6.188	1.8000	1.8480	74.59	0.705	6.14
21	0.275	0.281	0.3039	0.3105	2.2727	2.3223	38.20	0.730	5.529	2.2000	2.2480	73.79	0.733	5.55
22	0.335	0.341	0.3702	0.3768	2.7686	2.8182	40.25	0.770	4.725	2.6800	2.7280	72.97	0.763	4.93
23	0.400	0.406	0.4420	0.4486	3.3058	3.3554	42.10	0.805	4.000	3.2000	3.2480	71.97	0.799	4.19
24	0.475	0.481	0.5249	0.5315	3.9256	3.9752	44.26	0.846	3.153	3.8000	3.8480	71.07	0.831	3.51
25	0.550	0.556	0.6077	0.6144	4.5455	4.5950	46.01	0.880	2.467	4.4000	4.4480	70.15	0.864	2.83
26	0.625	0.631	0.6906	0.6972	5.1653	5.2149	47.70	0.912	1.804	5.0000	5.0480	69.31	0.894	2.20
27	0.700	0.706	0.7735	0.7801	5.7851	5.8347	49.12	0.939	1.247	5.6000	5.6480	68.56	0.921	1.64
28	0.800	0.806	0.8840	0.8906	6.6116	6.6612	50.90	0.973	0.549	6.4000	6.4480	67.63	0.955	0.94
29	0.900	0.906	0.9945	1.0011	7.4380	7.4876	51.77	0.990	0.208	7.2000	7.2480	66.93	0.980	0.42
30	1.050	1.056	1.1602	1.1669	8.6777	8.7273	52.32	1.000	-0.008	8.4000	8.4480	66.43	0.998	0.04
31	1.200	1.206	1.3260	1.3326	9.917[illegible]	9.9669	52.30	1.000	0.000	9.6000	9.6480	66.37	1.000	0.00
32	1.400	1.406	1.5470	1.5536	11.5702	11.6198	52.30	1.000	0.000	11.2000	11.2480	66.37	1.000	0.00

MEAN VELOCITY AND TEMPERATURE PROFILE - UINF= 52 FT/SEC F=0.000

RUN	= 070974 5	UINF	= 52.41	DELM	= 1.102	REX	= 0.168E 07
PLATE	= 16	TWALL	= 94.10	DELM1	= 0.220	REM	= 4014.80
X(IN)	= 62.	TINF	= 66.37	DELM2	= 0.148	REH	= 4177.60
X-XO(IN)	= 62.0	F	= 0.000	H	= 1.485	REK	= 39.90
Z(IN)	= 0.000	CF/2	= 0.00222	DELH	= 1.194	UTAU	= 2.47
POINTS	= 34	ST	= 0.00219	DELH2	= 0.154	TTAU	= 1.288

I	Y	YS	Y/DELM	YS/DELM	Y/DELM2	YS/DELM2	U	U/UINF	UDE	Y/DELH2	YS/DELH2	T	TBAR	TDE
1	0.007	0.013	0.0064	0.0118	0.0473	0.0878	15.65	0.299	14.883	0.0455	0.0844	84.77	0.336	14.29
2	0.008	0.014	0.0073	0.0127	0.0541	0.0946	16.10	0.307	14.700	0.0519	0.0909	84.45	0.348	14.04
3	0.009	0.015	0.0082	0.0136	0.0608	0.1014	16.66	0.318	14.474	0.0584	0.0974	84.26	0.355	13.89
4	0.011	0.017	0.0100	0.0154	0.0743	0.1149	17.71	0.338	14.049	0.0714	0.1104	83.70	0.375	13.45
5	0.013	0.019	0.0118	0.0172	0.0878	0.1284	18.63	0.355	13.676	0.0844	0.1234	83.27	0.391	13.12
6	0.016	0.022	0.0145	0.0200	0.1081	0.1486	19.98	0.381	13.130	0.1039	0.1429	82.71	0.411	12.69
7	0.020	0.026	0.0181	0.0236	0.1351	0.1757	21.29	0.406	12.599	0.1299	0.1688	82.18	0.430	12.27
8	0.024	0.030	0.0218	0.0272	0.1622	0.2027	21.98	0.419	12.320	0.1558	0.1948	81.59	0.451	11.82
9	0.030	0.036	0.0272	0.0327	0.2027	0.2432	23.38	0.446	11.753	0.1948	0.2338	81.08	0.470	11.42
10	0.038	0.044	0.0345	0.0399	0.2568	0.2973	24.86	0.474	11.154	0.2468	0.2857	80.42	0.493	10.91
11	0.048	0.054	0.0436	0.0490	0.3243	0.3649	25.96	0.495	10.708	0.3117	0.3506	79.83	0.515	10.45
12	0.060	0.066	0.0544	0.0599	0.4054	0.4459	27.25	0.520	10.186	0.3896	0.4286	79.27	0.535	10.02
13	0.074	0.080	0.0672	0.0726	0.5000	0.5405	28.30	0.540	9.761	0.4805	0.5195	78.74	0.554	9.60
14	0.090	0.096	0.0817	0.0871	0.6081	0.6486	29.65	0.566	9.215	0.5844	0.6234	78.20	0.573	9.18
15	0.108	0.114	0.0980	0.1034	0.7297	0.7703	30.55	0.583	8.850	0.7013	0.7403	77.72	0.591	8.81
16	0.130	0.136	0.1180	0.1234	0.8784	0.9189	31.63	0.604	8.413	0.8442	0.8831	77.08	0.614	8.32
17	0.155	0.161	0.1407	0.1461	1.0473	1.0878	32.61	0.622	8.016	1.0065	1.0455	76.57	0.632	7.92
18	0.185	0.191	0.1679	0.1733	1.2500	1.2905	33.99	0.649	7.457	1.2013	1.2403	76.08	0.650	7.54
19	0.220	0.226	0.1996	0.2051	1.4865	1.5270	35.12	0.670	7.000	1.4286	1.4675	75.47	0.672	7.07
20	0.260	0.266	0.2359	0.2414	1.7568	1.7973	36.45	0.695	6.462	1.6883	1.7273	74.83	0.695	6.57
21	0.310	0.316	0.2813	0.2868	2.0946	2.1351	37.81	0.721	5.911	2.0130	2.0519	74.17	0.719	6.06
22	0.370	0.376	0.3358	0.3412	2.5000	2.5405	39.34	0.751	5.292	2.4026	2.4416	73.28	0.751	5.36
23	0.440	0.446	0.3993	0.4047	2.9730	3.0135	41.17	0.786	4.551	2.8571	2.8961	72.57	0.776	4.81
24	0.510	0.516	0.4628	0.4682	3.4459	3.4865	42.75	0.816	3.911	3.3117	3.3506	71.71	0.807	4.15
25	0.580	0.586	0.5263	0.5318	3.9189	3.9595	44.26	0.844	3.300	3.7662	3.8052	71.07	0.831	3.65
26	0.660	0.666	0.5989	0.6044	4.4595	4.5000	45.83	0.874	2.664	4.2857	4.3247	70.27	0.859	3.03
27	0.740	0.746	0.6715	0.6770	5.0000	5.0405	47.32	0.903	2.061	4.8052	4.8442	69.53	0.886	2.45
28	0.840	0.846	0.7623	0.7677	5.6757	5.7162	49.00	0.935	1.381	5.4545	5.4935	68.72	0.915	1.82
29	0.940	0.946	0.8530	0.8584	6.3514	6.3919	50.32	0.960	0.846	6.1039	6.1429	67.93	0.944	1.21
30	1.090	1.096	0.9891	0.9946	7.3649	7.4054	51.81	0.989	0.243	7.0779	7.1169	67.01	0.977	0.50
31	1.240	1.246	1.1252	1.1307	8.3784	8.4189	52.25	0.997	0.065	8.0519	8.0909	66.54	0.994	0.13
32	1.440	1.446	1.3067	1.3122	9.7297	9.7703	52.41	1.000	0.000	9.3506	9.3896	66.37	1.000	0.00
33	1.640	1.646	1.4882	1.4936	11.0811	11.1216	52.41	1.000	0.000	10.6494	10.6883	66.37	1.000	0.00
34	1.840	1.846	1.6697	1.6751	12.4324	12.4730	52.41	1.000	0.000	11.9481	11.9870	66.37	1.000	0.00

MEAN VELOCITY AND TEMPERATURE PROFILE - UINF= 52 FT/SEC F=0.000

RUN	= U70974-6	UINF =	52.41	DELM = 1.325		REX =	0.200E 07
PLATE	= 19	TWALL =	94.27	DELM1 = 0.253		REM =	4665.90
X(IN)	= 74.	TINF =	66.30	DELM2 = 0.172		REH =	4964.30
XVO(IN)	= 74.0	F =	0.000	H = 1.473		REK =	38.20
Z(IN)	= 0.000	CF/2 =	0.00213	DELH = 1.402		UTAU =	2.42
POINTS	= 32	ST =	0.00215	DELH2 = 0.183		TTAU =	1.289

I	Y	YS	Y/DELM	YS/DELM	Y/DELM2	YS/DELM2	U	U/UINF	LCE	Y/DELH2	YS/DELH2	T	TBAR	TOE
1	0.007	0.013	[illegible]	0.0098	0.0407	0.0756	15.03	0.287	15.459	0.0383	0.0710	84.99	0.332	14.50
2	0.008	0.014	[illegible]	0.0106	0.0465	0.0814	15.30	0.292	15.347	0.0437	0.0765	84.83	0.338	14.38
3	0.009	0.015	[illegible]	0.0113	0.0523	0.0872	15.69	0.299	15.186	0.0492	0.0820	84.63	0.345	14.22
4	0.011	0.017	[illegible]	0.0128	0.0640	0.0988	16.85	0.322	14.706	0.0601	0.0929	84.19	0.360	13.88
5	0.014	0.020	[illegible]	0.0151	0.0814	0.1163	18.23	0.348	14.136	0.0765	0.1093	83.60	0.381	13.42
6	0.017	0.023	[illegible]	0.0174	0.0988	0.1337	19.47	0.371	13.623	0.0929	0.1257	83.08	0.400	13.02
7	0.020	0.026	[illegible]	0.0196	0.1163	0.1512	20.39	0.389	13.242	0.1093	0.1421	82.60	0.417	12.65
8	0.025	0.031	[illegible]	0.0234	0.1453	0.1802	21.85	0.417	12.639	0.1366	0.1694	82.02	0.438	12.20
9	0.031	0.037	0.0234	0.0279	0.1802	0.2151	23.23	0.443	12.068	0.1694	0.2022	81.47	0.458	11.77
10	0.039	0.045	0.0294	0.0340	0.2267	0.2616	24.41	0.466	11.580	0.2131	0.2459	80.76	0.483	11.22
11	0.048	0.054	0.0362	0.0408	0.2791	0.3140	25.55	0.488	11.108	0.2623	0.2951	80.15	0.505	10.74
12	0.060	0.066	0.0453	0.0498	0.3488	0.3837	26.67	0.509	10.645	0.3279	0.3607	79.65	0.521	10.39
13	0.074	[illegible]	[illegible]	0.0604	0.4302	0.4651	27.82	0.531	10.170	0.4044	0.4372	79.09	0.543	9.92
14	0.090	0.096	[illegible]	0.0725	0.5233	0.5581	28.87	0.551	9.735	0.4918	0.5246	78.56	0.562	9.51
15	0.108	[illegible]	[illegible]	0.0860	0.6279	0.6628	29.93	0.571	9.297	0.5902	0.6230	78.04	0.580	9.11
16	0.130	[illegible]	[illegible]	0.1026	0.7558	0.7907	31.16	0.595	8.788	0.7104	0.7432	77.61	0.596	8.77
17	0.160	[illegible]	[illegible]	0.1253	0.9302	0.9651	32.29	0.616	8.321	0.8743	0.9071	76.97	0.619	8.28
18	0.200	0.206	[illegible]	0.1555	1.1628	1.1977	33.91	0.647	7.651	1.0929	1.1257	76.22	0.645	7.70
19	0.250	0.256	0.1887	0.1932	1.4535	1.4884	35.27	0.673	7.089	1.3661	1.3989	75.51	0.671	7.15
20	0.310	0.316	0.2340	0.2385	1.8023	1.8372	37.08	0.707	6.340	1.6940	1.7268	74.76	0.698	6.56
21	0.380	0.386	0.2868	0.2913	2.2093	2.2442	38.44	0.733	5.778	2.0765	2.1093	73.93	0.727	5.92
22	0.460	0.466	0.3472	0.3517	2.6744	2.7093	40.40	0.771	4.967	2.5137	2.5464	73.08	0.758	5.26
23	0.550	0.556	0.4151	0.4196	3.1977	3.2326	42.06	0.803	4.280	3.0055	3.0382	72.14	0.791	4.53
24	0.650	0.656	0.4906	0.4951	3.7791	3.8140	44.12	0.842	3.428	3.5519	3.5847	71.32	0.821	3.89
25	0.760	0.766	0.5736	0.5781	4.4186	4.4535	45.82	0.874	2.725	4.1530	4.1858	70.37	0.854	3.16
26	0.890	0.896	0.6717	0.6762	5.1744	5.2093	47.81	0.912	1.902	4.8634	4.8962	69.38	0.890	2.39
27	1.040	1.046	0.7849	0.7894	6.0465	6.0814	49.66	0.948	1.137	5.6831	5.7158	68.33	0.927	1.57
28	1.210	1.216	0.9132	0.9177	7.0349	7.0698	51.26	0.978	0.476	6.6120	6.6448	67.31	0.964	0.78
29	1.400	1.406	1.0566	1.0611	8.1395	8.1744	52.07	0.994	0.141	7.6503	7.6831	66.60	0.989	0.23
30	1.600	1.606	1.2075	1.2121	9.3023	9.3372	52.42	1.000	-0.004	8.7432	8.7760	66.32	0.999	0.02
31	1.800	1.806	1.3585	1.3630	10.4651	10.5000	52.41	1.000	0.000	9.8361	9.8688	66.30	1.000	0.00
32	2.000	2.006	1.5094	1.5140	11.6279	11.6628	52.41	1.000	0.000	10.9290	10.9617	66.30	1.000	0.00

MEAN VELOCITY AND TEMPERATURE PROFILE - UINF= 52 FT/SEC F=0.000

RUN	= 070974-7	UINF	= 52.41	DELM	= 1.510	REX	= 0.233E 07
PLATE	= 22	TWALL	= 94.17	DELM1	= 0.289	REM	= 5344.10
X(IN)	= 86.	TINF	= 66.27	DELM2	= 0.197	REH	= 6049.40
X-XO(IN)	= 86.0	F	= C.000	H	= 1.461	REK	= 38.41
Z(IN)	= 0.000	CF/2	= 0.00209	DELH	= 1.716	UTAU	= 2.40
POINTS	= 35	ST	= 0.00206	DELH2	= 0.223	TTAU	= 1.247

I	Y	YS	Y/DELM	YS/DELM	Y/DELM2	YS/DELM2	U	U/UINF	UDE	Y/DELH2	YS/DELH2	T	TBAR	TDE
1	0.007	0.013	0.0046	0.0086	0.0355	0.0660	15.31	0.292	15.458	0.0314	0.0583	84.91	0.332	14.95
2	0.008	0.014	0.0053	0.0093	0.0406	0.0711	15.40	0.294	15.421	0.0359	0.0628	84.84	0.334	14.89
3	0.009	0.015	0.0060	0.0099	0.0457	0.0761	15.84	0.302	15.237	0.0404	0.0673	84.56	0.344	14.67
4	0.011	0.017	0.0073	0.0113	0.0558	0.0863	17.28	0.330	14.638	0.0493	0.0762	84.09	0.361	14.29
5	0.014	0.020	0.0093	0.0132	0.0711	0.1015	18.30	0.349	14.213	0.0628	0.0897	83.49	0.383	13.81
6	0.017	0.023	0.0113	0.0152	0.0863	0.1168	19.74	0.377	13.613	0.0762	0.1031	83.03	0.399	13.44
7	0.021	0.027	0.0139	0.0179	0.1066	0.1371	20.82	0.397	13.163	0.0942	0.1211	82.50	0.418	13.02
8	0.025	0.031	0.0166	0.0205	0.1269	0.1574	22.05	0.421	12.650	0.1121	0.1390	82.11	0.432	12.70
9	0.030	0.036	0.0199	0.0238	0.1523	0.1827	22.90	0.437	12.296	0.1345	0.1614	81.59	0.451	12.29
10	0.036	0.042	0.0238	0.0278	0.1827	0.2132	23.77	0.454	11.933	0.1614	0.1883	81.14	0.467	11.92
11	0.044	0.050	0.0291	0.0331	0.2234	0.2538	24.95	0.476	11.442	0.1973	0.2242	80.64	0.485	11.52
12	0.053	0.059	0.0351	0.0391	0.2690	0.2995	25.75	0.491	11.108	0.2377	0.2646	80.18	0.501	11.15
13	0.065	0.071	0.0430	0.0470	0.3299	0.3604	26.72	0.510	10.704	0.2915	0.3184	79.74	0.517	10.80
14	0.079	0.085	0.0523	0.0563	0.4010	0.4315	27.95	0.533	10.192	0.3543	0.3812	79.17	0.538	10.34
15	0.094	0.100	0.0623	0.0662	0.4772	0.5076	28.79	0.549	9.842	0.4215	0.4484	78.65	0.556	9.93
16	0.110	0.116	0.0728	0.0768	0.5584	0.5888	29.52	0.563	9.538	0.4933	0.5202	78.33	0.568	9.67
17	0.130	0.136	0.0861	0.0901	0.6599	0.6904	30.50	0.582	9.129	0.5830	0.6099	77.95	0.581	9.37
18	0.155	0.161	0.1026	0.1066	0.7868	0.8173	31.90	0.609	8.546	0.6951	0.7220	77.36	0.603	8.89
19	0.185	0.191	0.1225	0.1265	0.9391	0.9695	32.66	0.623	8.229	0.8296	0.8565	76.96	0.617	8.57
20	0.225	0.231	0.1490	0.1530	1.1421	1.1726	33.83	0.645	7.742	1.0090	1.0359	76.26	0.642	8.01
21	0.275	0.281	0.1821	0.1861	1.3959	1.4264	35.53	0.678	7.033	1.2332	1.2601	75.55	0.666	7.47
22	0.350	0.356	0.2318	0.2358	1.7766	1.8071	37.11	0.708	6.375	1.5695	1.5964	74.73	0.697	6.78
23	0.425	0.431	0.2815	0.2854	2.1574	2.1878	38.66	0.738	5.729	1.9058	1.9327	74.07	0.720	6.26
24	0.500	0.506	0.3311	0.3351	2.5381	2.5685	40.13	0.766	5.117	2.2422	2.2691	73.39	0.745	5.71
25	0.600	0.606	0.3974	0.4013	3.0457	3.0761	41.66	0.795	4.479	2.6906	2.7175	72.55	0.775	5.04
26	0.726	0.732	0.4808	0.4848	3.6853	3.7157	43.81	0.836	3.583	3.2556	3.2825	71.60	0.809	4.27
27	0.875	0.881	0.5795	0.5834	4.4416	4.4721	45.81	0.874	2.750	3.9238	3.9507	70.50	0.848	3.39
28	1.025	1.031	0.6788	0.6828	5.2030	5.2335	47.84	0.913	1.904	4.5964	4.6233	69.58	0.881	2.65
29	1.200	1.206	0.7947	0.7987	6.0914	6.1218	49.76	0.949	1.104	5.3812	5.4081	68.45	0.920	1.78
30	1.400	1.406	0.9272	0.9311	7.1066	7.1371	51.39	0.981	0.425	6.2780	6.3049	67.46	0.957	0.95
31	1.600	1.606	1.0596	1.0636	8.1218	8.1523	52.04	0.993	0.154	7.1749	7.2018	66.76	0.982	0.39
32	1.800	1.806	1.1921	1.1960	9.1371	9.1675	52.23	0.997	0.075	8.0717	8.0907	66.50	0.992	0.18
33	2.000	2.006	1.3245	1.3285	10.1523	10.1827	52.30	0.998	0.046	8.9686	8.9955	66.46	0.993	0.15
34	2.200	2.206	1.4570	1.4609	11.1675	11.1980	52.37	0.999	0.017	9.8655	9.8924	66.38	0.996	0.09
35	2.400	2.406	1.5894	1.5934	12.1827	12.2132	52.41	1.000	0.000	10.7623	10.7892	66.27	1.000	0.00

MEAN VELOCITY AND TEMPERATURE PROFILE - UINF= 89 FT/SEC F=0.000

RUN	= 031574-6	UINF	= 89.00	DELM	= 0.586	REX	= 0.118E 07
PLATE	= 7	TWALL	= 92.97	DELM1	= 0.123	REM	= 3617.89
X(IN)	= 26.	TINF	= 65.90	DELM2	= 0.080	REH	= 3844.00
X-XC(IN)	= 23.5	F	= 0.000	H	= 1.528	REK	= 72.50
Z(IN)	= 0.000	CF/2	= 0.00267	DELH	= 0.623	UTAU	= 4.60
POINTS	= 33	ST	= 0.00272	DELH2	= 0.085	TTAU	= 1.391

I	Y	YS	Y/DELM	YS/DELM	Y/DELM2	YS/DELM2	U	U/UINF	LDE	Y/DELH2	YS/DELH2	T	TBAR	TDE
1	0.006	0.012	0.0102	0.0205	0.0750	0.1500	31.93	0.359	12.407	0.0706	0.1412	81.91	0.409	11.51
2	0.007	0.013	0.0119	0.0222	0.0875	0.1625	32.21	0.362	12.346	0.0824	0.1529	81.75	0.414	11.39
3	0.009	0.015	0.0154	0.0256	0.1125	0.1875	33.51	0.377	12.063	0.1059	0.1765	81.41	0.427	11.15
4	0.011	0.017	0.0188	0.0290	0.1375	0.2125	34.96	0.393	11.748	0.1294	0.2000	81.04	0.441	10.88
5	0.013	0.019	0.0222	0.0324	0.1625	0.2375	36.32	0.408	11.452	0.1529	0.2235	80.68	0.454	10.63
6	0.016	0.022	0.0273	0.0375	0.2000	0.2750	37.87	0.426	11.115	0.1882	0.2588	80.26	0.470	10.32
7	0.019	0.025	0.0324	0.0427	0.2375	0.3125	39.11	0.439	10.846	0.2235	0.2941	79.88	0.484	10.05
8	0.023	0.029	0.0392	0.0495	0.2875	0.3625	40.67	0.457	10.507	0.2706	0.3412	79.49	0.498	9.77
9	0.027	0.033	0.0461	0.0563	0.3375	0.4125	41.88	0.471	10.243	0.3176	0.3882	79.14	0.511	9.52
10	0.032	0.038	0.0546	0.0648	0.4000	0.4750	43.26	0.486	9.943	0.3765	0.4471	78.75	0.525	9.24
11	0.039	0.045	0.0666	0.0766	0.4875	0.5625	45.38	0.510	9.483	0.4588	0.5294	78.21	0.545	8.85
12	0.046	0.052	0.0785	0.0887	0.5750	0.6500	46.76	0.525	9.183	0.5412	0.6118	77.80	0.560	8.56
13	0.054	0.060	0.0922	0.1024	0.6750	0.7580	48.20	0.542	8.870	0.6353	0.7059	77.45	0.573	8.30
14	0.064	0.070	0.1092	0.1195	0.8000	0.8750	50.00	0.562	8.478	0.7529	0.8235	76.92	0.593	7.92
15	0.076	0.082	0.1297	0.1399	0.9500	1.0250	52.16	0.586	8.009	0.8941	0.9647	76.45	0.610	7.58
16	0.088	0.094	0.1502	0.1604	1.1000	1.1750	53.78	0.604	7.657	1.0353	1.1059	[illegible]5.93	0.628	7.23
17	0.102	0.108	0.1741	0.1843	1.2750	1.3500	55.45	0.623	7.293	1.2000	1.2706	[illegible].51	0.645	6.91
18	0.116	0.122	0.1980	0.2082	1.4500	1.5250	57.13	0.642	6.928	1.3647	1.435[illegible]	[illegible]3	0.663	6.56
19	0.130	0.136	0.2210	0.2321	1.6250	1.7000	58.50	0.657	6.630	1.5294	1.60[illegible]	[illegible]5	0.677	6.29
20	0.15[illegible]	0.156	0.2560	0.2662	1.8750	1.9500	60.88	0.684	6.113	1.7647	1.835[illegible]	[illegible]4.09	0.697	5.89
21	0.170	0.176	0.2901	0.3003	2.1250	2.2000	62.70	0.704	5.717	2.[illegible]0	2.0[illegible]6	73.51	0.717	5.51
22	0.200	0.206	0.3413	0.3515	2.5000	2.5750	65.51	0.736	5.107	2.[illegible]	[illegible]5	72.86	0.743	5.00
23	0.240	0.246	0.4096	0.4198	3.0000	3.0750	68.69	0.772	4.415	2.[illegible]	[illegible]	71.97	0.776	4.36
24	0.280	0.286	0.4778	0.4881	3.5000	3.5750	71.83	0.807	3.733	3.2[illegible]	[illegible]4[illegible]	71.18	0.805	3.80
25	0.320	0.326	0.5461	0.5563	4.0000	4.0750	74.98	0.842	3.048	3.7[illegible]	[illegible]353	70.38	0.835	3.22
26	0.360	0.366	0.6142	0.6246	4.5000	4.5750	77.67	0.873	2.463	4.2353	[illegible].3059	69.66	0.861	2.70
27	0.400	0.406	0.6826	0.6928	5.0000	5.0750	80.27	0.902	1.898	4.7059	4.7765	68.95	0.887	2.19
28	0.450	0.456	0.7679	0.7782	5.6250	5.7000	83.23	0.935	1.254	5.2941	5.3647	68.15	0.917	1.62
29	0.500	0.506	0.8532	0.8635	6.2500	6.3250	85.59	0.962	0.741	5.8824	5.9529	67.40	0.945	1.08
30	0.575	0.581	0.9812	0.9915	7.1875	7.2625	87.87	0.987	0.246	6.7647	6.8353	66.52	0.977	0.45
31	0.650	0.656	1.1092	1.1195	8.1250	8.2000	88.81	0.998	0.041	7.6471	7.7176	66.06	0.994	0.12
32	0.750	0.756	1.2799	1.2901	9.3750	9.4500	89.00	1.000	0.000	8.8235	8.8941	65.90	1.000	0.00
33	0.850	0.856	1.4505	1.4608	10.6250	10.7000	89.00	1.000	0.000	10.0000	10.0706	65.90	1.000	0.00

MEAN VELOCITY AND TEMPERATURE PROFILE - UINF= 89 FT/SEC F=0.000

RUN	= 031574-5	UINF	= 88.60	DELM	= 0.824	REX	= 0.171E 07
PLATE	= 10	TWALL	= 52.94	DELM1	= 0.171	REM	= 5087.30
X(IN)	= 38.	TINF	= 65.80	DELM2	= 0.113	REH	= 5222.36
X-XO(IN)	= 35.5	F	= 0.000	H	= 1.515	REK	= 70.00
Z(IN)	= 0.000	CF/2	= 0.00252	DELH	= 0.900	UTAU	= 4.45
POINTS	= 31	ST	= 0.00244	DELH2	= 0.116	TTAU	= 1.288

I	Y	YS	Y/DELM	YS/DELM	Y/DELM2	YS/DELM2	U	U/UINF	UDE	Y/DELH2	YS/DELH2	T	TBAR	TDE
1	0.006	0.012	0.0073	0.0146	0.0531	0.1062	28.74	0.324	13.452	0.0517	0.1034	82.66	0.379	13.09
2	0.007	0.013	0.0085	0.0158	0.0619	0.1150	29.57	0.334	13.265	0.0603	0.1121	82.54	0.383	13.00
3	0.009	0.015	0.0109	0.0182	0.0796	0.1327	31.08	0.351	12.926	0.0776	0.1293	82.10	0.399	12.66
4	0.012	0.018	0.0146	0.0218	0.1062	0.1593	33.00	0.372	12.494	0.1034	0.1552	81.51	0.421	12.20
5	0.015	0.021	0.0182	0.0255	0.1327	0.1858	34.63	0.391	12.128	0.1293	0.1810	81.06	0.438	11.85
6	0.019	0.025	0.0231	0.0303	0.1681	0.2212	36.48	0.412	11.712	0.1638	0.2155	80.56	0.456	11.46
7	0.024	0.030	0.0291	0.0364	0.2124	0.2655	38.43	0.434	11.274	0.2069	0.2586	80.04	0.475	11.06
8	0.030	0.036	0.0364	0.0437	0.2655	0.3186	40.37	0.456	10.838	0.2586	0.3103	79.68	0.492	10.71
9	0.038	0.044	0.0461	0.0534	0.3363	0.3894	42.52	0.480	10.355	0.3276	0.3793	79.08	0.511	10.31
10	0.046	0.052	0.0558	0.0631	0.4071	0.4602	44.32	0.500	9.951	0.3966	0.4483	78.68	0.528	9.94
11	0.056	0.062	0.0680	0.0752	0.4956	0.5487	46.21	0.522	9.526	0.4828	0.5345	78.13	0.546	9.57
12	0.068	0.074	0.0825	0.0898	0.6018	0.6549	48.11	0.543	9.099	0.5862	0.6379	77.64	0.564	9.19
13	0.082	0.088	0.0995	0.1068	0.7257	0.7788	49.99	0.564	8.676	0.7069	0.7586	77.11	0.583	8.78
14	0.102	0.108	0.1238	0.1311	0.9027	0.9558	52.20	0.589	8.180	0.8793	0.9310	76.50	0.606	8.31
15	0.130	0.136	0.1578	0.1650	1.1504	1.2035	54.69	0.617	7.620	1.1207	1.1724	75.75	0.633	7.73
16	0.160	0.166	0.1942	0.2015	1.4159	1.4690	57.08	0.644	7.083	1.3793	1.4310	75.10	0.657	7.22
17	0.200	0.206	0.2427	0.2500	1.7699	1.8230	59.86	0.676	6.458	1.7241	1.7759	74.36	0.685	6.65
18	0.240	0.246	0.2913	0.2985	2.1239	2.1770	62.86	0.709	5.784	2.0690	2.1207	73.61	0.712	6.06
19	0.280	0.286	0.3398	0.3471	2.4779	2.5310	65.35	0.738	5.225	2.4138	2.4655	72.96	0.736	5.56
20	0.330	0.336	0.4005	0.4078	2.9204	2.9735	68.30	0.771	4.562	2.8448	2.8966	72.13	0.767	4.91
21	0.380	0.386	0.4612	0.4684	3.3628	3.4159	71.01	0.801	3.953	3.2759	3.3276	71.32	0.797	4.29
22	0.440	0.446	0.5340	0.5413	3.8938	3.9469	74.32	0.839	3.209	3.7931	3.8448	70.55	0.825	3.69
23	0.500	0.506	0.6068	0.6141	4.4248	4.4779	77.36	0.873	2.526	4.3103	4.3621	69.73	0.855	3.05
24	0.575	0.581	0.6978	0.7051	5.0885	5.1416	80.39	0.907	1.845	4.9569	5.0086	68.78	0.890	2.31
25	0.650	0.656	0.7888	0.7961	5.7522	5.8053	83.65	0.944	1.112	5.6034	5.6552	67.91	0.922	1.64
26	0.727	0.733	0.8823	0.8896	6.4336	6.4867	85.98	0.970	0.589	6.2672	6.3190	67.12	0.951	1.02
27	0.800	0.806	0.9709	0.9782	7.0796	7.1327	87.52	0.988	0.243	6.8966	6.9483	66.51	0.974	0.55
28	0.900	0.906	1.0922	1.0995	7.9646	8.0177	88.33	0.997	0.061	7.7586	7.8103	66.03	0.992	0.18
29	1.000	1.006	1.2136	1.2209	8.8496	8.9027	88.60	1.000	0.000	8.6207	8.6724	65.87	0.997	0.05
30	1.100	1.106	1.3350	1.3422	9.7345	9.7876	88.60	1.000	0.000	9.4828	9.5345	65.80	1.000	0.00
31	1.200	1.206	1.4563	1.4636	10.6195	10.6726	88.60	1.000	0.000	10.3448	10.3965	65.80	1.000	0.00

MEAN VELOCITY AND TEMPERATURE PROFILE - UINF= 89 FT/SEC F=0.000

RUN.	= 031574-4	UINF	= 88.87	DELM	= 1.024	REX	= 0.226E 07
PLATE	= 13	TWALL	= 93.19	DELM1	= 0.208	REM	= 6322.05
X(IN)	= 50.	TINF	= 65.94	DELM2	= 0.140	REH	= 6276.90
X-XO(IN)	= 47.5	F	= 0.000	H	= 1.487	REK	= 68.42
Z(IN)	= 0.000	CF/2	= 0.00239	DELH	= 1.091	UTAU	= 4.34
POINTS	= 31	ST	= 0.00237	DELH2	= 0.139	TTAU	= 1.290

I	Y	YS	Y/DELM	YS/DELM	Y/DELM2	YS/DELM2	U	U/UINF	UDE	Y/DELH2	YS/DELH2	T	TBAR	TDE
1	0.006	0.012	0.0059	0.0117	0.0429	0.0857	28.25	0.318	13.968	0.0432	0.0863	82.81	0.381	13.08
2	0.007	0.013	0.0068	0.0127	0.0500	0.0929	29.07	0.327	13.779	0.0504	0.0935	82.57	0.390	12.89
3	0.009	0.015	0.0088	0.0146	0.0643	0.1071	30.53	0.344	13.442	0.0647	0.1079	82.16	0.405	12.57
4	0.012	0.018	0.0117	0.0176	0.0857	0.1286	32.40	0.365	13.012	0.0863	0.1295	81.67	0.423	12.19
5	0.015	0.021	0.0146	0.0205	0.1071	0.1500	34.00	0.383	12.643	0.1079	0.1511	81.31	0.436	11.91
6	0.019	0.025	0.0186	0.0244	0.1357	0.1786	35.80	0.403	12.228	0.1367	0.1799	80.90	0.451	11.60
7	0.024	0.030	0.0234	0.0293	0.1714	0.2143	37.70	0.424	11.790	0.1727	0.2158	80.39	0.470	11.20
8	0.030	0.036	0.0293	0.0352	0.2143	0.2571	39.60	0.446	11.353	0.2158	0.2590	80.02	0.483	10.91
9	0.038	0.044	0.0371	0.0430	0.2714	0.3143	41.70	0.469	10.869	0.2734	0.3165	79.44	0.505	10.47
10	0.046	0.052	0.0449	0.0508	0.3286	0.3714	43.45	0.489	10.465	0.3309	0.3741	79.03	0.520	10.15
11	0.056	0.062	0.0547	0.0605	0.4000	0.4429	45.24	0.509	10.053	0.4029	0.4460	78.45	0.541	9.70
12	0.068	0.074	0.0664	0.0723	0.4857	0.5286	47.15	0.531	9.613	0.4892	0.5324	78.02	0.557	9.36
13	0.082	0.088	0.0801	0.0859	0.5857	0.6286	48.97	0.551	9.194	0.5899	0.6331	77.56	0.574	9.01
14	0.102	0.108	0.0996	0.1055	0.7286	0.7714	51.13	0.575	8.696	0.7338	0.7770	77.00	0.594	8.57
15	0.130	0.136	0.1270	0.1328	0.9286	0.9714	53.56	0.603	8.136	0.9353	0.9784	76.27	0.621	8.01
16	0.160	0.166	0.1563	0.1621	1.1429	1.1857	55.88	0.629	7.601	1.1511	1.1942	75.63	0.644	7.51
17	0.195	0.201	0.1904	0.1963	1.3929	1.4357	58.33	0.656	7.037	1.4029	1.4460	75.06	0.665	7.07
18	0.230	0.236	0.2246	0.2305	1.6429	1.6857	60.26	0.678	6.592	1.6547	1.6978	74.41	0.689	6.57
19	0.270	0.276	0.2637	0.2695	1.9286	1.9714	62.40	0.702	6.099	1.9424	1.9856	73.85	0.710	6.13
20	0.320	0.326	0.3125	0.3184	2.2857	2.3286	64.97	0.731	5.507	2.3022	2.3453	73.13	0.736	5.57
21	0.370	0.376	0.3613	0.3672	2.6429	2.6857	67.32	0.758	4.965	2.6619	2.7050	72.51	0.759	5.09
22	0.430	0.436	0.4199	0.4258	3.0714	3.1143	70.08	0.789	4.329	3.0935	3.1367	71.80	0.785	4.54
23	0.500	0.506	0.4883	0.4941	3.5714	3.6143	72.95	0.821	3.668	3.5971	3.6403	70.99	0.815	3.91
24	0.575	0.581	0.5615	0.5674	4.1071	4.1500	75.80	0.853	3.012	4.1367	4.1799	70.21	0.843	3.31
25	0.650	0.656	0.6348	0.6406	4.6429	4.6857	78.60	0.884	2.366	4.6763	4.7194	69.45	0.871	2.72
26	0.750	0.756	0.7324	0.7383	5.3571	5.4000	82.09	0.924	1.562	5.3957	5.4388	68.48	0.907	1.97
27	0.850	0.856	0.8301	0.8359	6.0714	6.1143	84.80	0.954	0.938	6.1151	6.1583	67.62	0.938	1.30
28	0.975	0.981	0.9521	0.9580	6.9643	7.0071	87.34	0.983	0.353	7.0144	7.0576	66.73	0.971	0.61
29	1.125	1.131	1.0986	1.1045	8.0357	8.0786	88.66	0.998	0.048	8.0935	8.1367	66.12	0.993	0.14
30	1.300	1.306	1.2695	1.2754	9.2857	9.3286	88.87	1.000	0.000	9.3525	9.3957	65.94	1.000	0.00
31	1.500	1.506	1.4648	1.4707	10.7143	10.7571	88.87	1.000	0.000	10.7914	10.8345	65.94	1.000	0.00

MEAN VELOCITY AND TEMPERATURE PROFILE - UINF= 89 FT/SEC F=0.000

RUN	= 031574-3	UINF	= 89.03	DELM	= 1.241	REX	= 0.280E 07
PLATE	= 16	TWALL	= 93.04	DELM1	= 0.247	REM	= 7554.88
X(IN)	= 62.	TINF	= 65.83	DELM2	= 0.167	REH	= 7600.12
X-XO(IN)	= 59.5	F	= 0.000	H	= 1.475	REK	= 67.38
Z(IN)	= 0.000	CF/2	= 0.00231	DELH	= 1.343	UTAU	= 4.28
POINTS	= 35	ST	= 0.00223	DELH2	= 0.168	TTAU	= 1.232

I	Y	YS	Y/DELM	YS/DELM	Y/DELM2	YS/DELM2	U	U/UINF	UDE	Y/DELH2	YS/DELH2	T	TBAR	TDE
1	0.006	0.012	0.0048	0.0097	0.0359	0.0719	27.03	0.304	14.486	0.0357	0.0714	83.30	0.358	14.18
2	0.007	0.013	0.0056	0.0105	0.0419	0.0778	27.88	0.313	14.287	0.0417	0.0774	83.07	0.366	13.99
3	0.009	0.015	0.0073	0.0121	0.0539	0.0898	29.35	0.330	13.944	0.0536	0.0893	82.68	0.381	13.68
4	0.011	0.017	0.0089	0.0137	0.0659	0.1018	30.63	0.344	13.645	0.0655	0.1012	82.30	0.395	13.37
5	0.014	0.020	0.0113	0.0161	0.0838	0.1158	32.30	0.363	13.255	0.0833	0.1190	81.86	0.411	13.01
6	0.017	0.023	0.0137	0.0185	0.1018	0.1377	33.74	0.379	12.918	0.1012	0.1369	81.49	0.424	12.71
7	0.021	0.027	0.0169	0.0218	0.1257	0.1617	35.39	0.398	12.533	0.1250	0.1607	81.08	0.440	12.38
8	0.025	0.031	0.0201	0.0250	0.1497	0.1856	36.82	0.414	12.199	0.1488	0.1845	80.72	0.453	12.09
9	0.030	0.036	0.0242	0.0290	0.1796	0.2156	38.37	0.431	11.836	0.1786	0.2143	80.32	0.467	11.76
10	0.037	0.043	0.0298	0.0346	0.2216	0.2575	40.21	0.452	11.407	0.2202	0.2560	79.88	0.484	11.40
11	0.045	0.051	0.0363	0.0411	0.2695	0.3054	41.91	0.471	11.009	0.2679	0.3035	79.45	0.499	11.06
12	0.055	0.061	0.0443	0.0492	0.3293	0.3653	43.84	0.492	10.558	0.3274	0.3631	78.93	0.519	10.63
13	0.065	0.071	0.0524	0.0572	0.3892	0.4251	45.41	0.510	10.192	0.3869	0.4226	78.56	0.532	10.33
14	0.077	0.083	0.0620	0.0665	0.4611	0.4970	47.04	0.528	9.811	0.4583	0.4940	78.11	0.549	9.97
15	0.090	0.096	0.0725	0.0774	0.5389	0.5749	48.52	0.545	9.465	0.5357	0.5714	77.69	0.564	9.63
16	0.105	0.111	0.0846	0.0894	0.6287	0.6647	50.14	0.563	9.086	0.6250	0.6607	77.27	0.580	9.29
17	0.120	0.126	0.0967	0.1015	0.7186	0.7545	51.38	0.577	8.797	0.7143	0.7500	76.82	0.596	8.92
18	0.130	0.136	0.1048	0.1096	0.7784	0.8144	52.18	0.586	8.610	0.7738	0.8095	76.42	0.611	8.60
19	0.155	0.161	0.1249	0.1297	0.9281	0.9641	53.94	0.606	8.199	0.9226	0.9583	75.95	0.628	8.21
20	0.180	0.186	0.1450	0.1499	1.0778	1.1138	56.26	0.632	7.657	1.0714	1.1071	75.68	0.638	8.00
21	0.220	0.226	0.1773	0.1821	1.3174	1.3533	58.29	0.655	7.182	1.3095	1.3452	75.22	0.655	7.62
22	0.260	0.266	0.2095	0.2143	1.5569	1.5928	60.18	0.676	6.741	1.5476	1.5833	74.63	0.677	7.14
23	0.310	0.316	0.2498	0.2546	1.8563	1.8922	62.56	0.703	6.185	1.8452	1.8810	73.95	0.700	6.62
24	0.370	0.376	0.2981	0.3030	2.2156	2.2515	64.84	0.728	5.652	2.2024	2.2381	73.31	0.725	6.07
25	0.445	0.451	0.3586	0.3634	2.6647	2.7006	67.64	0.760	4.998	2.6488	2.6845	72.51	0.755	5.42
26	0.545	0.551	0.4392	0.4440	3.2635	3.2954	71.31	0.801	4.140	3.2440	3.2798	71.51	0.791	4.61
27	0.645	0.651	0.5197	0.5246	3.8623	3.8982	74.85	0.841	3.313	3.8393	3.8750	70.58	0.825	3.86
28	0.745	0.751	0.6003	0.6052	4.4611	4.4970	77.61	0.872	2.668	4.4345	4.4702	69.65	0.858	3.13
29	0.850	0.856	0.6849	0.6898	5.0898	5.1257	80.83	0.908	1.516	5.0595	5.0952	68.84	0.889	2.44
30	0.975	0.981	0.7857	0.7905	5.8383	5.8743	83.85	0.942	1.210	5.8036	5.8393	67.93	0.923	1.70
31	1.100	1.106	0.8864	0.8912	6.5868	6.6228	86.35	0.970	0.626	6.5476	6.5833	67.07	0.954	1.01
32	1.250	1.256	1.0073	1.0121	7.4850	7.5210	88.22	0.991	0.189	7.4405	7.4762	66.37	0.980	0.44
33	1.450	1.456	1.1684	1.1732	8.6826	8.7186	89.02	1.000	0.002	8.6310	8.6667	65.96	0.995	0.11
34	1.650	1.656	1.3296	1.3344	9.8802	9.9162	89.03	1.000	0.000	9.8214	9.8571	65.83	1.000	0.00
35	1.850	1.856	1.4907	1.4956	11.0778	11.1138	89.03	1.000	0.000	11.0119	11.0476	65.83	1.000	0.00

MEAN VELOCITY AND TEMPERATURE PROFILE - UINF= 89 FT/SEC F=0.000

RUN = 031574-2		UINF = 88.89		DELM = 1.453		REX = 0.334E 07	
PLATE = 19		TWALL = 93.22		DELM1 = 0.285		REM = 8762.53	
X(IN) = 74.		TINF = 65.89		DELM2 = 0.194		REH = 8852.87	
X-XO(IN) = 71.5		F = 0.000		H = 1.467		REK = 66.66	
Z(IN) = 0.000		CF/2 = 0.00226		DELH = 1.548		UTAU = 4.23	
POINTS = 35		ST = 0.00221		DELH2 = 0.196		TTAU = 1.237	

I	Y	YS	Y/DELM	YS/DELM	Y/DELM2	YS/DELM2	U	U/UINF	UDE	Y/DELH2	YS/DELH2	T	TBAR	TDE
1	0.006	0.012	0.0041	0.0083	0.0309	0.0619	26.14	0.294	14.835	0.0306	0.0612	83.56	0.353	14.28
2	0.007	0.013	0.0048	0.0089	0.0361	0.0670	26.97	0.303	14.638	0.0357	0.0663	83.33	0.362	14.10
3	0.009	0.015	0.0062	0.0103	0.0464	0.0773	28.45	0.320	14.288	0.0459	0.0765	82.76	0.383	13.64
4	0.011	0.017	0.0076	0.0117	0.0567	0.0876	29.74	0.335	13.983	0.0561	0.0867	82.39	0.396	13.34
5	0.014	0.020	0.0096	0.0138	0.0722	0.1031	31.41	0.353	13.589	0.0714	0.1020	82.10	0.407	13.10
6	0.017	0.023	0.0117	0.0158	0.0876	0.1186	32.85	0.370	13.248	0.0867	0.1173	81.66	0.423	12.75
7	0.020	0.026	0.0138	0.0179	0.1031	0.1340	34.11	0.384	12.950	0.1020	0.1327	81.32	0.435	12.47
8	0.024	0.030	0.0165	0.0206	0.1237	0.1546	35.59	0.400	12.600	0.1224	0.1531	80.94	0.449	12.17
9	0.029	0.035	0.0200	0.0241	0.1495	0.1804	37.18	0.418	12.225	0.1480	0.1786	80.48	0.466	11.79
10	0.035	0.041	0.0241	0.0282	0.1804	0.2113	38.81	0.437	11.839	0.1786	0.2092	80.13	0.479	11.51
11	0.043	0.049	0.0296	0.0337	0.2216	0.2526	40.65	0.457	11.404	0.2194	0.2500	79.69	0.495	11.16
12	0.053	0.059	0.0365	0.0406	0.2732	0.3041	42.56	0.479	10.953	0.2704	0.3010	79.21	0.513	10.77
13	0.065	0.071	0.0447	0.0489	0.3351	0.3660	44.44	0.500	10.508	0.3316	0.3622	78.70	0.531	10.36
14	0.080	0.086	0.0551	0.0592	0.4124	0.4433	46.59	0.524	10.000	0.4082	0.4388	78.18	0.550	9.94
15	0.095	0.101	0.0654	0.0695	0.4897	0.5206	48.10	0.541	9.643	0.4847	0.5153	77.82	0.563	9.64
16	0.110	0.116	0.0757	0.0798	0.5670	0.5979	49.57	0.558	9.296	0.5612	0.5918	77.40	0.579	9.30
17	0.130	0.136	0.0895	0.0936	0.6701	0.7010	51.17	0.576	8.917	0.6633	0.6939	76.92	0.596	8.92
18	0.155	0.161	0.1067	0.1108	0.7990	0.8299	53.04	0.597	8.475	0.7908	0.8214	76.44	0.614	8.53
19	0.185	0.191	0.1273	0.1315	0.9536	0.9845	54.92	0.618	8.031	0.9439	0.9745	76.06	0.628	8.22
20	0.220	0.226	0.1514	0.1555	1.1340	1.1649	56.70	0.638	7.610	1.1224	1.1531	75.50	0.648	7.77
21	0.260	0.266	0.1789	0.1831	1.3402	1.3711	58.66	0.660	7.147	1.3265	1.3571	74.92	0.670	7.30
22	0.310	0.316	0.2134	0.2175	1.5979	1.6289	60.84	0.684	6.631	1.5816	1.6122	74.35	0.690	6.84
23	0.370	0.376	0.2546	0.2588	1.9072	1.9381	62.98	0.709	6.125	1.8878	1.9184	73.73	0.713	6.34
24	0.445	0.451	0.3063	0.3104	2.2938	2.3247	65.44	0.736	5.544	2.2704	2.3010	72.97	0.741	5.72
25	0.520	0.526	0.3579	0.3620	2.6804	2.7113	68.07	0.766	4.922	2.6531	2.6837	72.27	0.767	5.16
26	0.600	0.606	0.4129	0.4171	3.0928	3.1237	70.59	0.794	4.326	3.0612	3.0918	71.61	0.791	4.62
27	0.700	0.706	0.4818	0.4859	3.6082	3.6392	73.30	0.825	3.686	3.5714	3.6020	70.89	0.817	4.04
28	0.800	0.806	0.5506	0.5547	4.1237	4.1546	76.01	0.855	3.045	4.0816	4.1122	70.09	0.846	3.40
29	0.925	0.931	0.6366	0.6407	4.7680	4.7990	79.31	0.892	2.265	4.7194	4.7500	69.24	0.877	2.71
30	1.050	1.056	0.7226	0.7268	5.4124	5.4433	82.01	0.923	1.626	5.3571	5.3878	68.46	0.906	2.08
31	1.200	1.206	0.8259	0.8300	6.1856	6.2165	84.90	0.955	0.943	6.1224	6.1531	67.56	0.939	1.35
32	1.350	1.356	0.9291	0.9332	6.9588	6.9897	86.96	0.978	0.456	6.8878	6.9184	67.53	0.940	1.33
33	1.550	1.556	1.0668	1.0709	7.9897	8.0206	88.61	0.997	0.066	7.9082	7.9388	66.15	0.990	0.21
34	1.750	1.756	1.2044	1.2085	9.0206	9.0515	88.81	0.999	0.019	8.9286	8.9592	65.92	0.999	0.02
35	1.950	1.956	1.3421	1.3462	10.0515	10.0825	88.89	1.000	0.000	9.9490	9.9796	65.89	1.000	0.00

MEAN VELOCITY AND TEMPERATURE PROFILE - UINF= 89 FT/SEC F=0.000

RUN	=	031574-1	UINF	=	89.12	DELM	= 1.757	REX	=	0.389E 07
PLATE	=	22	TWALL	=	93.15	DELM1	= 0.332	REM	=	10324.90
X(IN)	=	86.	TINF	=	65.85	DELM2	= 0.228	REH	=	10143.70
X-XO(IN)	=	83.5	F	=	0.000	H	= 1.454	REK	=	66.17
Z(IN)	=	0.000	CF/2	=	0.00222	DELH	= 1.736	UTAU	=	4.19
POINTS	=	34	ST	=	0.00213	DELH2	= 0.224	TTAU	=	1.204

I	Y	YS	Y/DELM	YS/DELM	Y/DELM2	YS/DELM2	U	U/UINF	UDE	Y/DELH2	YS/DELH2	T	TBAR	TDE
1	0.006	0.012	0.0034	0.0068	0.0263	0.0526	25.63	0.288	15.153	0.0268	0.0536	83.05	0.370	14.29
2	0.007	0.013	0.0040	0.0074	0.0307	0.0570	26.42	0.296	14.964	0.0313	0.0580	82.90	0.375	14.16
3	0.008	0.014	0.0046	0.0080	0.0351	0.0614	27.15	0.305	14.790	0.0357	0.0625	82.62	0.386	13.93
4	0.010	0.016	0.0057	0.0091	0.0439	0.0702	28.48	0.320	14.473	0.0446	0.0714	82.42	0.393	13.76
5	0.013	0.019	0.0074	0.0108	0.0570	0.0833	30.19	0.339	14.064	0.0580	0.0848	81.92	0.411	13.35
6	0.016	0.022	0.0091	0.0125	0.0702	0.0965	31.65	0.355	13.716	0.0714	0.0982	81.60	0.423	13.08
7	0.019	0.025	0.0108	0.0142	0.0833	0.1096	32.93	0.370	13.411	0.0848	0.1116	81.29	0.434	12.82
8	0.023	0.029	0.0131	0.0165	0.1009	0.1272	34.43	0.386	13.053	0.1027	0.1295	80.90	0.449	12.50
9	0.031	0.037	0.0176	0.0211	0.1360	0.1623	36.89	0.414	12.465	0.1384	0.1652	80.32	0.470	12.02
10	0.042	0.048	0.0239	0.0273	0.1842	0.2105	39.52	0.443	11.838	0.1875	0.2143	79.76	0.490	11.55
11	0.056	0.062	0.0319	0.0353	0.2456	0.2719	42.12	0.473	11.217	0.2500	0.2768	79.11	0.514	11.01
12	0.066	0.072	0.0376	0.0410	0.2895	0.3158	43.64	0.490	10.854	0.2946	0.3214	78.73	0.528	10.70
13	0.088	0.094	0.0501	0.0535	0.3860	0.4123	46.38	0.520	10.200	0.3929	0.4196	78.10	0.551	10.17
14	0.115	0.121	0.0655	0.0689	0.5044	0.5307	48.95	0.549	9.587	0.5134	0.5402	77.46	0.575	9.64
15	0.130	0.136	0.0740	0.0774	0.5702	0.5965	50.12	0.562	9.308	0.5804	0.6071	77.14	0.586	9.38
16	0.175	0.181	0.0996	0.1030	0.7675	0.7939	53.03	0.595	8.613	0.7813	0.8080	76.46	0.611	8.81
17	0.230	0.236	0.1309	0.1343	1.0088	1.0351	55.85	0.627	7.940	1.0268	1.0536	75.72	0.638	8.20
18	0.265	0.271	0.1508	0.1542	1.1623	1.1886	57.24	0.642	7.609	1.1830	1.2098	75.29	0.654	7.84
19	0.345	0.351	0.1964	0.1998	1.5132	1.5395	60.48	0.679	6.835	1.5402	1.5670	74.33	0.689	7.04
20	0.390	0.396	0.2220	0.2254	1.7105	1.7368	61.95	0.695	6.484	1.7411	1.7679	73.63	0.708	6.63
21	0.440	0.446	0.2504	0.2538	1.9298	1.9561	3.63	0.714	6.084	1.9643	1.9911	73.31	0.727	6.20
22	0.500	0.506	0.2846	0.2880	2.1930	2.2193	65.33	0.733	5.678	2.2321	2.2589	72.82	0.745	5.79
23	0.570	0.576	0.3244	0.3278	2.5000	2.5263	67.35	0.756	5.196	2.5446	2 714	72.31	0.763	5.37
24	0.640	0.646	0.3643	0.3677	2.8070	2.8333	69.41	0.779	4.704	2.8571	2.8839	71.76	0.784	4.91
25	0.720	0.726	0.4098	0.4132	3.1579	3.1842	71.33	0.800	4.246	3.2143	3.2411	71.24	0.803	4.48
26	0.820	0.826	0.4667	0.4701	3.5965	3.6228	73.89	0.829	3.635	3.6607	3.6875	70.56	0.827	3.91
27	0.920	0.926	0.5236	0.5270	4.0351	4.0614	76.24	0.855	3.074	4.1071	4.1339	69.92	0.851	3.38
28	1.020	1.026	0.5805	0.5839	4.4737	4.5000	78.24	0.878	2.597	4.5536	4.5804	69.31	0.873	2.87
29	1.145	1.151	0.6517	0.6551	5.0219	5.0482	80.74	0.906	2.000	5.1116	5.1384	68.57	0.900	2.26
30	1.270	1.276	0.7228	0.7262	5.5702	5.5965	83.13	0.933	1.430	5.6696	5.6964	67.92	0.924	1.72
31	1.395	1.401	0.7940	0.7974	6.1184	6.1447	84.96	0.953	0.993	6.2277	6.2545	67.31	0.947	1.21
32	1.545	1.551	0.8793	0.8828	6.7763	6.8026	86.90	0.975	0.530	6.8973	6.9241	66.70	0.969	0.71
33	1.920	1.926	1.0928	1.0962	8.4211	8.4474	88.67	0.995	0.107	8.5714	8.5982	65.91	0.998	0.05
34	2.220	2.226	1.2635	1.2665	9.7368	9.7632	89.12	1.000	0.000	9.9107	9.9375	65.85	1.000	0.00

MEAN VELOCITY AND TEMPERATURE PROFILE - UINF= 89 FT/SEC F=0.002

RUN	= 080174-1		UINF	= 87.98		DELM	= 0.871		REX	= 0.118E 07
PLATE	= 7		TWALL	= 105.01		DELM1	= 0.197		REM	= 5373.50
X(IN)	= 26.		TINF	= 75.62		DELM2	= 0.118		REH	= 4918.10
X-XO(IN)	= 26.0		F	= 0.002		H	= 1.672		REK	= 61.20
Z(IN)	= 0.000		CF/2	= 0.00188		DELH	= 0.834		UTAU	= 3.81
POINTS	= 35		ST	= 0.00180		DELH2	= 0.108		TTAU	= 1.193

I	Y	YS	Y/DELM	YS/DELM	Y/DELM2	YS/DELM2	L	U/UINF	UDE	Y/DELH2	YS/DELH2	T	TBAR	TDE
1	0.007	0.015	0.0080	0.0172	0.0593	0.1271	23.94	0.272	16.808	0.0648	0.1389	94.67	0.352	15.97
2	0.009	0.017	0.0103	0.0195	0.0763	0.1441	24.71	0.281	16.606	0.0833	0.1574	94.34	0.363	15.69
3	0.012	0.020	0.0138	0.0230	0.1017	0.1695	26.87	0.305	16.039	0.1111	0.1852	93.98	0.375	15.39
4	0.016	0.024	0.0184	0.0276	0.1356	0.2034	29.60	0.336	15.323	0.1481	0.2222	93.35	0.397	14.86
5	0.020	0.028	0.0230	0.0321	0.1695	0.2373	31.41	0.357	14.848	0.1852	0.2593	92.80	0.415	14.40
6	0.025	0.033	0.0287	0.0379	0.2119	0.2797	33.39	0.380	14.328	0.2315	0.3056	92.21	0.436	13.91
7	0.031	0.039	0.0356	0.0448	0.2627	0.3305	34.70	0.394	13.984	0.2870	0.3611	91.71	0.453	13.49
8	0.038	0.046	0.0436	0.0528	0.3220	0.3898	36.42	0.414	13.533	0.3519	0.4259	91.27	0.468	13.12
9	0.047	0.055	0.0540	0.0631	0.3983	0.4661	38.69	0.440	12.937	0.4352	0.5093	90.58	0.491	12.54
10	0.057	0.065	0.0654	0.0746	0.4831	0.5508	40.33	0.458	12.507	0.5278	0.6019	90.24	0.503	12.2
11	0.069	0.077	0.0792	0.0884	0.5847	0.6525	42.79	0.486	11.861	0.6389	0.7130	89.60	0.524	11.72
12	0.082	0.090	0.0941	0.1033	0.6949	0.7627	44.34	0.504	11.454	0.7593	0.8333	88.90	0.548	11.13
13	0.096	0.104	0.1102	0.1194	0.8136	0.8814	46.37	0.527	10.921	0.8889	0.9630	88.45	0.563	10.75
14	0.112	0.120	0.1286	0.1378	0.9492	1.0169	48.08	0.546	10.472	1.0370	1.1111	87.92	0.581	10.31
15	0.130	0.138	0.1493	0.1584	1.1017	1.1695	50.04	0.569	9.958	1.2037	1.2778	87.36	0.601	9.84
16	0.155	0.163	0.1780	0.1871	1.3136	1.3814	52.55	0.597	9.299	1.4352	1.5093	86.66	0.624	9.25
17	0.185	0.193	0.2124	0.2216	1.5678	1.6356	55.24	0.628	8.593	1.7130	1.7870	85.87	0.651	8.59
18	0.220	0.228	0.2526	0.2618	1.8644	1.9322	58.09	0.660	7.845	2.0370	2.1111	85.03	0.680	7.89
19	0.260	0.268	0.2985	0.3077	2.2034	2.2712	61.35	0.697	6.989	2.4074	2.4815	84.17	0.709	7.17
20	0.300	0.308	0.3444	0.3536	2.5424	2.6102	64.12	0.729	6.262	2.7778	2.8519	83.35	0.737	6.48
21	0.340	0.348	0.3904	0.3995	2.8814	2.9492	66.78	0.759	5.564	3.1481	3.2222	82.56	0.764	5.82
22	0.390	0.398	0.4478	0.4569	3.3051	3.3729	70.25	0.798	4.654	3.6111	3.6852	81.67	0.794	5.07
23	0.440	0.448	0.5052	0.5144	3.7288	3.7966	73.07	0.831	3.913	4.0741	4.1481	80.88	0.824	4.34
24	0.490	0.498	0.5626	0.5718	4.1525	4.2203	75.91	0.863	3.168	4.5370	4.6111	79.93	0.853	3.61
25	0.540	0.548	0.6200	0.6292	4.5763	4.6441	78.64	0.894	2.451	5.0000	5.0741	79.17	0.879	2.98
26	0.600	0.608	0.6889	0.6980	5.0847	5.1525	81.63	0.928	1.667	5.5556	5.6296	78.31	0.908	2.25
27	0.660	0.668	0.7577	0.7669	5.5932	5.6610	83.98	0.955	1.050	6.1111	6.1852	77.49	0.936	1.57
28	0.730	0.738	0.8381	0.8473	6.1864	6.2542	84.91	0.965	0.806	6.7593	6.8333	76.70	0.963	0.91
29	0.800	0.808	0.9185	0.9277	6.7797	6.8475	86.25	0.980	0.454	7.4074	7.4815	76.14	0.982	0.44
30	0.875	0.883	1.0046	1.0138	7.4153	7.4831	87.15	0.991	0.218	8.1019	8.1759	75.81	0.994	0.16
31	0.950	0.958	1.0907	1.0999	8.0508	8.1186	87.20	0.991	0.205	8.7963	8.8704	75.68	0.998	0.05
32	1.025	1.033	1.1768	1.1860	8.6864	8.7542	87.71	0.997	0.071	9.4907	9.5648	75.63	1.000	0.01
33	1.100	1.108	1.2629	1.2721	9.3220	9.3898	87.63	0.996	0.092	10.1852	10.2593	75.56	1.002	-0.05
34	1.200	1.208	1.3777	1.3869	10.1695	10.2373	87.96	1.000	0.005	11.1111	11.1852	75.59	1.001	-0.03
35	1.300	1.308	1.4925	1.5017	11.0170	11.0847	87.98	1.000	0.000	12.0370	12.1111	75.62	1.000	0.00

MEAN VELOCITY AND TEMPERATURE PROFILE - UINF= 89 FT/SEC F=0.002

RUN	= 080174-2	UINF	=	87.45	DELM	=	1.126	REX	=	0.169E 07
PLATE	=	10	TWALL	=	105.24	DELM1	=	0.267	REM	=	7109.70
X(IN)	=	38.	TINF	=	75.76	DELM2	=	0.160	REH	=	6754.30
X-XO(IN)	=	38.0	F	=	0.002	H	=	1.662	REK	=	57.50
Z(IN)	=	0.000	CF/2	=	0.00174	DELH	=	1.142	UTAU	=	3.65
POINTS	=	35	ST	=	0.00152	DELH2	=	0.152	TTAU	=	1.051

I	Y	YS	Y/DELM	YS/DELM	Y/DELM2	YS/DELM2	U	U/UINF	UDE	Y/DELH2	YS/DELH2	T	TBAR	TDE
1	0.007	0.015	0.0062	0.0133	0.0437	0.0937	22.34	0.255	17.830	0.0461	0.0987	95.84	0.319	19.11
2	0.009	0.017	0.0080	0.0151	0.0562	0.1062	23.88	0.273	17.416	0.0592	0.1118	95.42	0.333	18.71
3	0.012	0.020	0.0107	0.0178	0.0750	0.1250	25.54	0.292	16.962	0.0789	0.1316	94.97	0.348	18.28
4	0.016	0.024	0.0142	0.0213	0.1000	0.1500	27.58	0.315	16.403	0.1053	0.1579	94.42	0.367	17.75
5	0.020	0.028	0.0178	0.0249	0.1250	0.1750	29.24	0.334	15.948	0.1316	0.1842	94.01	0.381	17.36
6	0.025	0.033	0.0222	0.0293	0.1562	0.2062	31.02	0.355	15.460	0.1645	0.2171	93.50	0.398	16.88
7	0.031	0.039	0.0275	0.0346	0.1937	0.2437	32.71	0.374	14.997	0.2039	0.2566	92.91	0.418	16.32
8	0.038	0.046	0.0337	0.0409	0.2375	0.2875	34.43	0.394	14.526	0.2500	0.3026	92.36	0.437	15.79
9	0.047	0.055	0.0417	0.0488	0.2937	0.3437	36.18	0.414	14.047	0.3092	0.3618	91.87	0.454	15.33
10	0.057	0.065	0.0506	0.0577	0.3562	0.4062	38.26	0.438	13.477	0.3750	0.4276	91.29	0.473	14.78
11	0.065	0.077	0.0613	0.0684	0.4312	0.4812	39.84	0.456	13.044	0.4539	0.5066	90.79	0.490	14.30
12	0.082	0.090	0.0728	0.0799	0.5125	0.5625	41.82	0.478	12.501	0.5395	0.5921	90.15	0.512	13.69
13	0.096	0.104	0.0853	0.0924	0.6000	0.6500	43.60	0.499	12.014	0.6316	0.6842	89.73	0.526	13.29
14	0.112	0.120	0.0995	0.1066	0.7000	0.7500	44.99	0.514	11.633	0.7368	0.7895	89.15	0.546	12.74
15	0.130	0.138	0.1155	0.1226	0.8125	0.8625	46.83	0.536	11.129	0.8553	0.9079	88.65	0.563	12.26
16	0.155	0.163	0.1377	0.1448	0.9687	1.0187	48.63	0.556	10.636	1.0197	1.0724	88.05	0.583	11.69
17	0.185	0.193	0.1643	0.1714	1.1562	1.2062	50.85	0.581	10.027	1.2171	1.2697	87.38	0.606	11.06
18	0.220	0.228	0.1954	0.2025	1.3750	1.4250	53.64	0.613	9.263	1.4474	1.5000	86.77	0.627	10.48
19	0.260	0.268	0.2309	0.2380	1.6250	1.6750	55.91	0.639	8.641	1.7105	1.7632	85.97	0.654	9.71
20	0.300	0.308	0.2664	0.2735	1.8750	1.9250	57.92	0.662	8.090	1.9737	2.0263	85.35	0.675	9.12
21	0.340	0.348	0.3020	0.3091	2.1250	2.1750	59.87	0.685	7.556	2.2368	2.2895	84.59	0.700	8.40
22	0.390	0.398	0.3464	0.3535	2.4375	2.4875	62.71	0.717	6.778	2.5658	2.6184	83.90	0.724	7.75
23	0.440	0.448	0.3908	0.3979	2.7500	2.8000	65.09	0.744	6.126	2.8947	2.9474	83.13	0.750	7.01
24	0.490	0.498	0.4352	0.4423	3.0625	3.1125	67.56	0.773	5.449	3.2237	3.2763	82.52	0.771	6.43
25	0.540	0.548	0.4796	0.4867	3.3750	3.4250	69.66	0.797	4.874	3.5526	3.6053	81.82	0.794	5.77
26	0.600	0.608	0.5329	0.5400	3.7500	3.8000	72.34	0.827	4.140	3.9474	4.0000	81.07	0.820	5.05
27	0.675	0.683	0.5995	0.6066	4.2187	4.2687	75.14	0.859	3.373	4.4408	4.4934	80.15	0.851	4.18
28	0.750	0.758	0.6661	0.6732	4.6875	4.7375	78.26	0.895	2.518	4.9342	4.9868	79.30	0.880	3.37
29	0.850	0.858	0.7549	0.7620	5.3125	5.3625	81.49	0.932	1.633	5.5921	5.6447	78.22	0.917	2.34
30	0.950	0.958	0.8437	0.8508	5.9375	5.9875	83.60	0.956	1.055	6.2500	6.3026	77.23	0.950	1.40
31	1.050	1.058	0.9325	0.9396	6.5625	6.6125	85.52	0.978	0.529	6.9079	6.9605	76.54	0.974	0.74
32	1.150	1.158	1.0213	1.0284	7.1875	7.2375	86.83	0.993	0.170	7.5658	7.6184	76.02	0.991	0.25
33	1.300	1.308	1.1545	1.1616	8.1250	8.1750	87.18	0.997	0.074	8.5526	8.6053	75.82	0.998	0.05
34	1.450	1.459	1.2877	1.2946	9.0625	9.1125	87.45	1.000	0.000	9.5395	9.5921	75.76	1.000	0.00
35	1.600	1.608	1.4210	1.4281	10.0000	10.0500	87.45	1.000	0.000	10.5263	10.5789	75.76	1.000	0.00

MEAN VELOCITY AND TEMPERATURE PROFILE - UINF= 89 FT/SEC F=0.002

RUN	=	080174-3	UINF	=	87.89	DELM	=	1.425	REX	=	0.223E 07
PLATE	=	13	TWALL	=	105.44	DELM1	=	0.334	REM	=	9110.50
X(IN)	=	50.	TINF	=	75.69	DELM2	=	0.204	REH	=	9333.80
X-XO(IN)	=	50.0	F	=	0.002	H	=	1.636	REK	=	56.60
Z(IN)	=	0.000	CF/2	=	0.00167	DELH	=	1.596	UTAU	=	3.59
POINTS	=	35	ST	=	0.00143	DELH2	=	0.209	TTAU	=	1.019

I	Y	YS	Y/DELM	YS/DELM	Y/DELM2	YS/DELM2	U	U/UINF	UDE	Y/DELH2	YS/DELH2	T	TBAR	TDE
1	0.007	0.015	0.0049	0.0105	0.0343	0.0733	21.84	0.248	18.398	0.0335	0.0718	96.67	0.295	20.59
2	0.009	0.017	0.0063	0.0119	0.0441	0.0833	23.29	0.265	17.994	0.0431	0.0813	96.31	0.307	20.24
3	0.012	0.020	0.0084	0.0140	0.0588	0.0980	24.93	0.284	17.538	0.0574	0.0957	95.81	0.324	19.74
4	0.016	0.024	0.0112	0.0168	0.0784	0.1176	26.68	0.304	17.050	0.0766	0.1148	95.18	0.345	19.13
5	0.020	0.028	0.0140	0.0196	0.0980	0.1373	28.59	0.325	16.518	0.0957	0.1340	94.67	0.362	18.63
6	0.025	0.033	0.0175	0.0232	0.1225	0.1618	29.87	0.340	16.162	0.1196	0.1579	94.14	0.380	18.11
7	0.031	0.039	0.0218	0.0274	0.1520	0.1912	32.00	0.364	15.568	0.1483	0.1866	93.61	0.398	17.59
8	0.038	0.046	0.0267	0.0323	0.1863	0.2255	33.57	0.382	15.131	0.1818	0.2201	93.18	0.412	17.16
9	0.047	0.055	0.0330	0.0386	0.2304	0.2696	35.57	0.405	14.574	0.2249	0.2632	92.54	0.434	16.54
10	0.057	0.065	0.0400	0.0456	0.2794	0.3186	37.55	0.427	14.022	0.2727	0.3110	92.00	0.452	16.01
11	0.069	0.077	0.0484	0.0540	0.3382	0.3775	39.28	0.447	13.540	0.3301	0.3684	91.45	0.470	15.47
12	0.082	0.090	0.0575	0.0632	0.4020	0.4412	41.14	0.468	13.022	0.3923	0.4306	90.93	0.488	14.96
13	0.096	0.104	0.0674	0.0730	0.4706	0.5098	42.64	0.485	12.604	0.4593	0.4976	90.44	0.504	14.47
14	0.112	0.120	0.0786	0.0842	0.5490	0.5882	44.43	0.506	12.106	0.5359	0.5742	89.95	0.521	13.99
15	0.130	0.138	0.0912	0.0968	0.6373	0.6765	45.88	0.522	11.702	0.6220	0.6603	89.40	0.539	13.45
16	0.155	0.163	0.1088	0.1144	0.7598	0.7990	47.76	0.543	11.178	0.7416	0.7799	88.81	0.559	12.88
17	0.185	0.193	0.1298	0.1354	0.9069	0.9461	49.57	0.564	10.674	0.8852	0.9234	88.24	0.578	12.32
18	0.220	0.228	0.1544	0.1600	1.0784	1.1176	51.81	0.589	10.050	1.0526	1.0909	87.66	0.598	11.75
19	0.260	0.268	0.1825	0.1881	1.2745	1.3137	53.80	0.612	9.496	1.2440	1.2823	87.02	0.619	11.12
20	0.300	0.308	0.2105	0.2161	1.4706	1.5098	55.99	0.637	8.886	1.4354	1.4737	86.35	0.640	10.50
21	0.350	0.358	0.2456	0.2512	1.7157	1.7549	57.88	0.659	8.359	1.6746	1.7129	85.72	0.663	9.84
22	0.400	0.408	0.2807	0.2863	1.9608	2.0000	60.22	0.685	7.708	1.9139	1.9522	85.13	0.683	9.26
23	0.475	0.483	0.3333	0.3389	2.3284	2.3676	62.88	0.715	6.967	2.2727	2.3110	84.37	0.708	8.52
24	0.550	0.558	0.3860	0.3916	2.6961	2.7353	65.30	0.743	6.292	2.6316	2.6699	83.52	0.737	7.68
25	0.650	0.658	0.4561	0.4618	3.1863	3.2255	68.81	0.783	5.315	3.1100	3.1483	82.44	0.773	6.62
26	0.750	0.758	0.5263	0.5319	3.6765	3.7157	72.28	0.822	4.348	3.5885	3.6268	81.48	0.805	5.68
27	0.900	0.908	0.6316	0.6372	4.4118	4.4510	76.57	0.871	3.153	4.3062	4.3445	80.06	0.853	4.29
28	1.050	1.058	0.7368	0.7425	5.1471	5.1863	80.83	0.920	1.967	5.0239	5.0622	78.81	0.895	3.06
29	1.250	1.258	0.8772	0.8828	6.1275	6.1667	84.95	0.967	0.819	5.9809	6.0191	77.31	0.946	1.59
30	1.450	1.458	1.0175	1.0232	7.1078	7.1471	87.17	0.992	0.201	6.9378	6.9761	76.31	0.979	0.61
31	1.650	1.658	1.1579	1.1635	8.0882	8.1274	87.56	0.996	0.092	7.8947	7.9330	75.96	0.991	0.26
32	1.850	1.858	1.2982	1.3035	9.0686	9.1078	87.71	0.998	0.050	8.8517	8.8900	75.83	0.995	0.14
33	2.050	2.058	1.4386	1.4442	10.0490	10.0882	87.75	0.998	0.039	9.8086	9.8469	75.73	0.999	0.04
34	2.250	2.258	1.5789	1.5846	11.0294	11.0686	87.89	1.000	0.000	10.7656	10.8038	75.69	1.000	0.00
35	2.450	2.458	1.7193	1.7249	12.0098	12.0490	87.89	1.000	0.000	11.7225	11.7608	75.69	1.000	0.00

MEAN VELOCITY AND TEMPERATURE PROFILE - UINF= 89 FT/SEC F=0.002

RUN	= 081174-4	UINF	= 87.65	DELM	= 1.713	REX	= 0.276E 07
PLATE	= 16	TWALL	= 105.70	DELM1	= 0.401	REM	= 10956.30
X(IN)	= 62.	TINF	= 75.59	DELM2	= 0.246	REH	= 10778.10
X-XO(IN)	= 62.0	F	= 0.002	H	= 1.631	REK	= 35.40
Z(IN)	= 0.000	CF/2	= 0.00161	DELH	= 1.796	UTAU	= 3.52
POINTS	= 33	ST	= 0.00140	DELH2	= 0.242	TTAL	= 1.028

I	Y	YS	Y/DELM	YS/DELM	Y/DELM2	YS/DELM2	U	U/UINF	UDE	Y/DELH2	YS/DELH2	T	TBAR	TDE
1	0.007	0.015	0.0041	0.0088	0.0285	0.0610	20.36	0.232	19.116	0.0289	0.0620	97.21	0.282	21.03
2	0.009	0.017	0.0053	0.0099	0.0366	0.0691	21.56	0.246	18.776	0.0372	0.0702	96.84	0.294	20.67
3	0.012	0.020	0.0070	0.0117	0.0488	0.0813	23.41	0.267	18.250	0.0496	0.0826	96.13	0.318	19.98
4	0.016	0.024	0.0093	0.0140	0.0650	0.0976	25.53	0.291	17.648	0.0661	0.0992	95.57	0.336	19.44
5	0.020	0.028	0.0117	0.0163	0.0813	0.1138	27.11	0.309	17.199	0.0826	0.1157	95.11	0.352	18.99
6	0.025	0.033	0.0146	0.0193	0.1016	0.1341	28.85	0.329	16.705	0.1033	0.1364	94.43	0.374	18.33
7	0.031	0.039	0.0181	0.0228	0.1260	0.1585	30.82	0.352	16.145	0.1281	0.1612	93.87	0.393	17.78
8	0.038	0.046	0.0222	0.0269	0.1545	0.1870	31.93	0.364	15.830	0.1570	0.1901	93.44	0.407	17.36
9	0.047	0.055	0.0274	0.0321	0.1911	0.2236	34.00	0.388	15.241	0.1942	0.2277	92.89	0.425	16.83
10	0.057	0.065	0.0333	0.0379	0.2317	0.2642	36.40	0.415	14.560	0.2355	0.2686	92.27	0.446	16.23
11	0.069	0.077	0.0403	0.0450	0.2805	0.3130	37.70	0.430	14.190	0.2851	0.3182	91.82	0.461	15.79
12	0.082	0.090	0.0479	0.0525	0.3333	0.3659	39.35	0.449	13.722	0.3388	0.3719	91.24	0.480	15.22
13	0.096	0.104	0.0560	0.0607	0.3902	0.4228	40.90	0.467	13.281	0.3967	0.4298	90.85	0.493	14.84
14	0.112	0.120	0.0654	0.0701	0.4553	0.4878	42.62	0.486	12.793	0.4628	0.4959	90.38	0.509	14.39
15	0.130	0.138	0.0759	0.0806	0.5285	0.5610	44.27	0.505	12.324	0.5372	0.5702	89.80	0.528	13.82
16	0.155	0.163	0.0905	0.0952	0.6301	0.6626	45.99	0.525	11.835	0.6405	0.6736	89.31	0.544	13.35
17	0.185	0.193	0.1080	0.1127	0.7520	0.7846	48.10	0.549	11.236	0.7645	0.7975	88.82	0.561	12.87
18	0.225	0.233	0.1313	0.1360	0.9146	0.9472	50.04	0.571	10.685	0.9298	0.9628	88.08	0.585	12.15
19	0.275	0.283	0.1605	0.1652	1.1179	1.1504	52.28	0.596	10.048	1.1364	1.1694	87.27	0.612	11.36
20	0.325	0.333	0.1897	0.1944	1.3211	1.3537	54.44	0.621	9.435	1.3430	1.3760	86.65	0.633	10.76
21	0.400	0.408	0.2335	0.2382	1.6260	1.6585	56.77	0.648	8.773	1.6529	1.6859	85.80	0.661	9.93
22	0.475	0.483	0.2773	0.2820	1.9309	1.9634	59.77	0.682	7.920	1.9628	1.9959	85.12	0.683	9.27
23	0.575	0.583	0.3357	0.3403	2.3374	2.3699	62.70	0.715	7.088	2.3760	2.4091	84.14	0.716	8.32
24	0.675	0.683	0.3940	0.3987	2.7439	2.7764	65.70	0.750	6.236	2.7893	2.8223	83.23	0.746	7.43
25	0.800	0.808	0.4670	0.4717	3.2520	3.2846	68.91	0.786	5.324	3.3058	3.3388	82.16	0.782	6.39
26	0.925	0.933	0.5400	0.5447	3.7602	3.7927	72.43	0.826	4.324	3.8223	3.8554	81.17	0.815	5.43
27	1.075	1.083	0.6276	0.6322	4.3699	4.4024	75.94	0.866	3.327	4.4421	4.4752	80.02	0.853	4.31
28	1.225	1.233	0.7151	0.7198	4.9797	5.0122	79.69	0.909	2.261	5.0620	5.0950	78.92	0.885	3.24
29	1.425	1.433	0.8319	0.8365	5.7927	5.8252	83.20	0.949	1.264	5.8884	5.9215	77.58	0.934	1.94
30	1.625	1.633	0.9486	0.9533	6.6057	6.6382	86.09	0.982	0.443	6.7149	6.7479	76.49	0.970	0.88
31	1.825	1.833	1.0654	1.0701	7.4187	7.4512	87.14	0.994	0.145	7.5413	7.5744	75.83	0.992	0.23
32	2.025	2.033	1.1821	1.1868	8.2317	8.2642	87.65	1.000	0.000	8.3678	8.4008	70.59	1.166	-4.86
33	2.225	2.233	1.2989	1.3036	9.0447	9.0772	87.65	1.000	0.000	9.1942	9.2273	75.59	1.000	0.00

MEAN VELOCITY AND TEMPERATURE PROFILE - UINF= 89 FT/SEC F=0.002

RUN = 080174-4	UINF = 87.65	DELM = 1.713	REX = 0.276E 07
PLATE = 16	TWALL = 105.70	DELM1 = 0.401	REM = 10956.30
X(IN) = 62.	TINF = 75.59	DELM2 = 0.246	REH = 10778.10
X-XO(IN) = 62.0	F = 0.002	H = 1.631	REK = 55.40
Z(IN) = 0.000	CF/2 = 0.00161	DELH = 1.796	UTAU = 3.52
POINTS = 33	ST = 0.00140	DELH2 = 0.242	TTAL = 1.028

I	Y	YS	Y/DELM	YS/DELM	Y/DELM2	YS/DELM2	U	U/UINF	UDE	Y/DELH2	YS/DELH2	T	TBAR	TDE
1	0.007	0.015	0.0041	0.0088	0.0285	0.0610	20.36	0.232	19.116	0.0289	0.0620	97.21	0.282	21.03
2	0.009	0.017	0.0053	0.0099	0.0366	0.0691	21.56	0.246	18.776	0.0372	0.0702	96.84	0.294	20.67
3	0.012	0.020	0.0070	0.0117	0.0488	0.0813	23.41	0.267	18.250	0.0496	0.0826	96.13	0.318	19.98
4	0.016	0.024	0.0093	0.0140	0.0650	0.0976	25.53	0.291	17.648	0.0661	0.0992	95.57	0.336	19.44
5	0.020	0.028	0.0117	0.0163	0.0813	0.1138	27.11	0.309	17.199	0.0826	0.1157	95.11	0.352	18.99
6	0.025	0.033	0.0146	0.0193	0.1016	0.1341	28.85	0.329	16.705	0.1033	0.1364	94.43	0.374	18.33
7	0.031	0.039	0.0181	0.0228	0.1260	0.1585	30.82	0.352	16.145	0.1281	0.1612	93.87	0.393	17.78
8	0.038	0.046	0.0222	0.0269	0.1545	0.1870	31.93	0.364	15.830	0.1570	0.1901	93.44	0.407	17.36
9	0.047	0.055	0.0274	0.0321	0.1911	0.2236	34.00	0.388	15.241	0.1942	0.2273	[illegible]	0.425	16.83
10	0.057	0.065	0.0333	0.0379	0.2317	0.2642	36.40	0.415	14.560	0.2355	0.2686	92.27	0.446	16.23
11	0.069	0.077	0.0403	0.0450	0.2805	0.3130	37.70	0.430	14.190	0.2851	0.3182	91.82	0.461	15.79
12	0.082	0.090	0.0479	0.0525	0.3333	0.3659	39.35	0.449	13.722	0.3388	0.3719	91.24	0.480	15.22
13	0.096	0.104	0.0560	0.0607	0.3902	0.4228	40.90	0.467	13.281	0.3967	0.4298	90.85	0.493	14.84
14	0.112	0.120	0.0654	0.0701	0.4553	0.4878	42.62	0.486	12.793	0.4628	0.4959	90.38	0.509	14.39
15	0.130	0.138	0.0759	0.0806	0.5285	0.5610	44.27	0.505	12.324	0.5372	0.5702	89.80	0.528	13.82
16	0.155	0.163	0.0905	0.0952	0.6301	0.6626	45.99	0.525	11.835	0.6405	0.6736	89.31	0.544	13.35
17	0.185	0.193	0.1080	0.1127	0.7520	0.7846	48.10	0.549	11.236	0.7645	0.7975	88.82	0.561	12.87
18	0.225	0.233	0.1313	0.1360	0.9146	0.9472	50.04	0.571	10.685	0.9298	0.9628	88.08	0.585	12.15
19	0.275	0.283	0.1605	0.1652	1.1179	1.1504	52.28	0.596	10.048	1.1364	1.1694	87.27	0.612	11.36
20	0.325	0.333	0.1897	0.1944	1.3211	1.3537	54.44	0.621	9.435	1.3430	1.3760	86.65	0.633	10.76
21	0.400	0.408	0.2335	0.2382	1.6260	1.6585	56.77	0.648	8.773	1.6529	1.6859	85.80	0.661	9.93
22	0.475	0.483	0.2773	0.2820	1.9309	1.9634	59.77	0.682	7.920	1.9628	1.9959	85.12	0.683	9.27
23	0.575	0.583	0.3357	0.3403	2.3374	2.3699	62.70	0.715	7.088	2.3760	2.4091	84.14	0.716	8.32
24	0.675	0.683	0.3940	0.3987	2.7439	2.7764	65.70	0.750	6.236	2.7893	2.8223	83.23	0.746	7.43
25	0.800	0.808	0.4670	0.4717	3.2520	3.2846	68.91	0.786	5.324	3.3058	3.3388	82.16	0.782	6.39
26	0.925	0.933	0.5400	0.5447	3.7602	3.7927	72.43	0.826	4.324	3.8223	3.8554	81.17	0.815	5.43
27	1.075	1.083	0.6276	0.6322	4.3699	4.4024	75.94	0.866	3.327	4.4421	4.4752	80.02	0.853	4.31
28	1.225	1.233	0.7151	0.7198	4.9797	5.0122	79.69	0.909	2.261	5.0620	5.0950	78.92	0.889	3.24
29	1.425	1.433	0.8319	0.8365	5.7927	5.8252	83.20	0.949	1.264	5.8884	5.9215	77.58	0.934	1.94
30	1.625	1.633	0.9486	0.9533	6.6057	6.6382	86.09	0.982	0.443	6.7149	6.7479	76.49	0.970	0.88
31	1.825	1.833	1.0654	1.0701	7.4187	7.4512	87.14	0.994	0.145	7.5413	7.5744	75.83	0.992	0.23
32	2.025	2.033	1.1821	1.1868	8.2317	8.2642	87.65	1.000	0.000	8.3678	8.4008	70.59	1.166	-4.86
33	2.225	2.233	1.2989	1.3036	9.0447	9.0772	87.65	1.000	0.000	9.1942	9.227[illegible]	75.59	1.000	0.00

MEAN VELOCITY AND TEMPERATURE PROFILE - UINF= 85 FT/SEC F=0.002

RUN	= 080174-5	UINF	=	87.85	DELM	= 2.074	REX	=	0.330E 07
PLATE	= 19	TWALL	=	105.98	DELM1	= 0.464	REM	=	12766.80
X(IN)	= 74.	TINF	=	75.65	DELM2	= 0.286	REH	=	13034.70
X-XC(IN)	= 74.0	F	=	0.002	H	= 1.623	REK	=	55.00
Z(IN)	= 0.000	CF/2	=	0.00158	DELH	= 2.264	UTAU	=	3.49
POINTS	= 35	ST	=	0.00143	DELH2	= 0.292	TTAU	=	1.071

I	Y	YS	Y/DELM	YS/DELM	Y/DELM2	YS/DELM2	U	U/UINF	UDE	Y/DELH2	YS/DELH2	T	TBAR	TDE
1	0.007	0.015	0.0034	0.0072	0.0245	0.0524	20.07	0.228	19.421	0.0240	0.0514	97.42	0.282	20.33
2	0.008	0.016	0.0039	0.0077	0.0280	0.0559	20.68	0.235	19.246	0.0274	0.0548	97.27	0.287	20.19
3	0.011	0.019	0.0053	0.0092	0.0385	0.0664	22.52	0.256	18.719	0.0377	0.0651	96.84	0.301	19.79
4	0.015	0.023	0.0072	0.0111	0.0524	0.0804	24.45	0.278	18.166	0.0514	0.0788	96.15	0.324	19.14
5	0.021	0.029	0.0101	0.0140	0.0734	0.1014	26.94	0.307	17.453	0.0719	0.0993	95.58	0.343	[illegible]
6	0.027	0.035	0.0130	0.0169	0.0944	0.1224	28.77	0.327	16.928	0.0925	0.1199	94.82	0.368	17.90
7	0.034	0.042	0.0164	0.0203	0.1189	0.1469	30.75	0.350	16.361	0.1164	0.1438	94.25	0.387	17.37
8	0.042	0.050	0.0203	0.0241	0.1469	0.1748	32.23	0.367	15.937	0.1438	0.1712	93.78	0.402	16.93
9	0.052	0.060	0.0251	0.0289	0.1818	0.2098	34.33	0.391	15.335	0.1781	0.2055	93.04	0.427	16.24
10	0.066	0.074	0.0318	0.0357	0.2308	0.2587	36.35	0.414	14.756	0.2260	0.2534	92.35	0.449	15.59
11	0.084	0.092	0.0405	0.0444	0.2937	0.3217	38.78	0.441	14.060	0.2877	0.3151	91.67	0.472	14.96
12	0.104	0.112	0.0501	0.0540	0.3636	0.3916	41.11	0.468	13.393	0.3562	0.3836	91.15	0.489	14.47
13	0.130	0.138	0.0627	0.0665	0.4545	0.4825	43.35	0.493	12.751	0.4452	0.4726	90.34	0.516	13.72
14	0.150	0.168	0.0771	0.0810	0.5594	0.5874	45.44	0.517	12.152	0.5479	0.5753	89.63	0.539	13.05
15	0.200	0.208	0.0964	0.1003	0.6993	[illegible]	47.89	0.545	11.450	0.6849	0.7123	88.97	0.561	12.44
16	0.250	0.258	0.1205	0.1244	0.8741	[illegible]	50.25	0.572	10.774	0.8562	0.8836	88.22	0.586	11.74
17	0.300	0.308	0.1446	0.1485	1.0490	1.0769	52.53	0.598	10.120	1.0274	1.0548	87.57	0.607	11.13
18	0.375	0.383	0.1808	0.1847	1.3112	1.3392	55.02	0.626	9.407	1.2842	1.3116	86.71	0.635	10.33
19	0.450	0.458	0.2170	0.2208	1.5734	1.6014	57.28	0.652	8.759	1.5411	1.5685	86.02	0.658	9.68
20	0.550	0.558	0.2652	0.2690	1.9231	1.9510	59.98	0.683	7.986	1.8836	1.9110	85.14	0.687	8.86
21	0.650	0.658	0.3134	0.3173	2.2727	2.3007	62.53	0.712	7.255	2.2260	2.2534	84.35	0.713	8.12
22	0.775	0.783	0.3737	0.3775	2.7098	2.7378	65.83	0.749	6.309	2.6541	2.6815	83.45	0.743	7.28
23	0.900	0.908	0.4339	0.4378	3.1469	3.1748	68.32	0.778	5.596	3.0822	3.1096	82.59	0.771	6.48
24	1.050	1.058	0.5063	0.5101	3.6713	3.6993	72.09	0.821	4.516	3.5959	3.6233	81.55	0.805	5.51
25	1.200	1.208	0.5786	0.5824	4.1958	4.2238	74.89	0.852	3.713	4.1096	4.1370	80.55	0.838	4.58
26	1.400	1.408	0.6750	0.6789	4.8951	4.9231	78.95	0.899	2.550	4.7945	4.8219	79.37	0.877	3.47
27	1.600	1.608	0.7715	0.7753	5.5944	5.6224	82.36	0.938	1.573	5.4795	5.5068	78.29	0.913	2.46
28	1.800	1.808	0.8679	0.8717	6.2937	6.3217	85.25	0.970	0.745	6.1644	6.1918	77.26	0.947	1.50
29	2.000	2.008	0.9643	0.9682	6.9930	7.0210	86.62	0.986	0.352	6.8493	6.8767	76.50	0.972	0.79
30	2.200	2.208	1.0608	1.0646	7.6923	7.7203	87.56	0.997	[illegible]	7.5342	7.5616	76.08	0.986	0.40
31	2.400	2.408	1.1572	1.1610	8.3916	8.4196	[illegible]	0.999	0.029	8.2192	8.2466	75.71	0.998	0.06
32	2.600	2.608	1.2536	1.2575	9.0909	9.1189	87.85	1.000	0.000	8.9041	8.9315	75.65	1.000	0.00
33	2.800	2.808	1.3500	1.3539	9.7902	9.8182	87.85	1.000	0.000	9.5890	9.6164	75.65	1.000	0.00

MEAN VELOCITY AND TEMPERATURE PROFILE - UINF= 89 FT/SEC F=0.002

RUN	= 080174-6	UINF	= 87.50	DELM	= 2.365	REX	= 0.382E 07
PLATE	= 22	TWALL	= 106.06	DELM1	= 0.534	REM	= 14716.70
X(IN)	= 86.	TINF	= 75.76	DELM2	= 0.331	REH	= 14627.80
X-XO(IN)	= 86.0	F	= 0.002	H	= 1.610	REK	= 53.50
Z(IN)	= 0.000	CF/2	= 0.00151	DELH	= 2.497	UTAU	= 3.40
POINTS	= 33	ST	= 0.00124	DELH2	= 0.329	TYAL	= 0.497

I	Y	YS	Y/DELM	YS/DELM	Y/DELM2	YS/DELM2	U	U/UINF	UDE	Y/DELH2	YS/DELH2	T	TBAR	TDE
1	0.007	0.015	0.0030	0.0063	0.0211	0.0453	19.72	0.225	19.935	0.0213	0.0456	98.00	0.266	44.75
2	0.009	0.017	0.0038	0.0072	0.0272	0.0514	20.89	0.239	19.591	0.0274	0.0517	97.67	0.277	44.08
3	0.012	0.020	0.0051	0.0085	0.0363	0.0604	22.55	0.258	19.103	0.0365	0.0608	97.18	0.293	43.10
4	0.016	0.024	0.0068	0.0101	0.0483	0.0725	24.54	0.280	18.518	0.0486	0.0729	96.67	0.310	42.07
5	0.021	0.029	0.0089	0.0123	0.0634	0.0876	26.65	0.305	17.897	0.0638	0.0881	96.05	0.330	40.82
6	0.027	0.035	0.0114	0.0148	0.0816	0.1057	28.58	0.327	17.329	0.0821	0.1064	95.42	0.351	39.56
7	0.034	0.042	0.0144	0.0178	0.1027	0.1269	30.[illegible]	0.346	16.824	0.1033	0.1277	94.87	0.369	38.45
8	0.043	0.051	0.0182	0.0216	0.1299	0.1541	32[illegible]	0.368	16.265	0.1307	0.1550	94.28	0.389	37.26
9	0.055	0.063	0.0233	0.0266	0.1662	0.1903	34.[illegible]	0.390	15.703	0.1672	0.1915	93.67	0.409	36.04
10	0.070	0.078	0.0296	0.0330	0.2115	0.2356	36.[illegible]	0.413	15.106	0.2128	0.2371	92.90	0.434	34.49
11	0.090	0.098	0.0381	0.0414	0.2719	0.2961	38.04	0.435	14.547	0.2736	0.2979	92.19	0.458	33.06
12	0.130	0.138	0.0550	0.0584	0.3927	0.4169	42.14	0.482	13.341	0.3951	0.4195	91.14	0.492	30.95
13	0.180	0.188	0.0761	0.0795	0.5438	0.5680	45.42	0.519	12.376	0.5471	0.5714	90.18	0.524	29.01
14	0.240	0.248	0.1015	0.1049	0.7251	0.7492	48.28	0.552	11.535	0.7295	0.7538	89.26	0.554	27.16
15	0.300	0.308	0.1268	0.1302	0.9063	0.9305	50.43	0.576	10.903	0.9119	0.9362	88.37	0.584	25.37
16	[illegible]	0.[illegible]	[illegible]586	0.167	1.132[illegible]	1.15[illegible]	53.41	0.610	10.026	1.1398	1.1641	87.61	0.609	23.84
17	[illegible]	0.4[illegible]	[illegible].1903	0.19[illegible]	1.3595	1.383[illegible]	55.58	0.635	9.388	1.3678	1.3921	86.92	0.632	22.45
18	0.550	0.558	0.2326	0.2359	1.6616	1.6858	57.89	0.562	8.709	1.6717	1.6960	86.04	0.661	20.68
19	0.650	0.658	0.2748	0.2782	1.9637	1.9879	60.57	0.692	7.921	1.9757	2.0000	85.26	0.686	19.11
20	0.775	0.783	0.3277	0.3311	2.3414	2.3656	63.28	0.723	7.124	2.3556	2.3799	84.32	0.717	17.22
21	0.900	0.908	0.3805	0.3839	2.7190	2.7432	65.55	0.749	6.456	2.7356	2.7599	83.50	0.745	15.57
22	1.050	1.058	0.4440	0.4474	3.1722	3.1964	68.26	0.780	5.659	3.1915	3.2158	82.55	0.776	13.66
23	1.200	1.208	0.5074	0.5108	3.6254	3.6495	71.29	0.815	4.768	3.6474	3.6717	81.66	0.805	11.87
24	1.400	1.408	0.5920	0.5953	4.2296	4.2538	75.06	0.858	3.659	4.2553	4.2796	80.54	0.842	9.62
25	1.600	1.608	0.6765	0.6799	4.8338	4.8580	78.23	0.894	2.726	4.8632	4.8875	79.46	0.878	7.44
26	1.800	1.808	0.7611	0.7645	5.4381	5.4622	81.52	0.932	1.759	5.4711	5.4954	78.39	0.913	5.29
27	2.000	2.008	0.8457	0.8490	6.0423	6.0665	83.77	0.957	1.097	6.0790	6.1033	77.46	0.944	3.42
28	2.250	2.258	0.9514	0.9548	6.7976	6.8218	86.07	0.984	0.421	6.8389	6.8632	76.58	0.973	1.65
29	2.500	2.508	1.0571	1.0605	7.5529	7.5770	87.27	0.997	0.068	7.5988	7.6231	76.06	0.990	0.60
30	2.750	2.758	1.1628	1.1662	8.3082	8.3323	87.44	0.999	0.018	8.3587	8.3830	75.83	0.998	0.14
31	3.000	3.008	1.2665	1.2719	9.0634	9.0876	87.46	1.000	0.012	9.1185	9.1429	75.78	0.999	0.04
32	3.200	3.208	1.3531	1.3564	9.6677	9.6918	87.50	1.000	0.000	9.7264	9.7508	75.76	1.000	0.00
33	3.400	3.408	1.4376	1.4410	10.2719	10.2961	87.50	1.000	0.000	10.3343	10.3587	75.76	1.000	0.00

MEAN VELOCITY AND TEMPERATURE PROFILE - UINF= 89 FT/SEC F=0.004

RUN	=	080874-1	UINF	=	88.84	DELM	= 1.010	REX	=	0.117E 07
PLATE	=	7	TWALL	=	105.44	DELM1	= 0.269	REM	=	6861.60
X(IN)	=	26.	TINF	=	76.26	DELM2	= 0.152	REH	=	6635.90
X-XO(IN)	=	26.0	F	=	0.004	H	= 1.773	REK	=	48.70
Z(IN)	=	0.000	CF/2	=	0.00121	DELH	= 1.045	UTAU	=	3.09
PCINTS	=	33	ST	=	0.00123	DELH2	= 0.147	TTAL	=	1.009

I	Y	YS	Y/DELM	YS/DELM	Y/DELM2	YS/DELM2	U	U/UINF	LDE	Y/DELH2	YS/DELH2	T	TBAR	TDE
1	0.007	0.016	0.0069	0.0158	0.0461	0.1053	18.31	0.206	22.825	0.0476	0.1086	97.78	0.263	21.33
2	0.009	0.018	0.0089	0.0178	0.0592	0.1184	19.58	0.220	22.414	0.0612	0.1224	97.37	0.277	20.92
3	0.012	0.021	0.0119	0.0208	0.0789	0.1382	21.20	0.239	21.890	0.0816	0.1429	96.99	0.290	20.55
4	0.015	0.024	0.0149	0.0238	0.0987	0.1579	22.87	0.257	21.350	0.1020	0.1633	96.55	0.305	20.11
5	0.019	0.028	0.0188	0.0277	0.1250	0.1842	24.57	0.277	20.799	0.1293	0.1905	96.04	0.322	19.60
6	0.023	0.032	0.0228	0.0317	0.1513	0.2105	26.49	0.298	20.178	0.1565	0.2177	95.58	0.338	19.15
7	0.028	0.037	0.0277	0.0366	0.1842	0.2434	27.87	0.314	19.731	0.1905	0.2517	94.99	0.358	18.56
8	0.034	0.043	0.0337	0.0426	0.2237	0.2829	29.56	0.333	19.184	0.2313	0.2925	94.53	0.374	18.11
9	0.042	0.051	0.0416	0.0505	0.2763	0.3355	31.73	0.357	18.482	0.2857	0.3469	93.97	0.393	17.55
10	0.050	0.059	0.0495	0.0584	0.3289	0.3882	33.29	0.375	17.977	0.3401	0.4014	93.49	0.410	17.08
11	0.060	0.069	0.0594	0.0683	0.3947	0.4539	34.82	0.392	17.482	0.4082	0.4694	92.86	0.431	16.45
12	0.072	0.081	0.0713	0.0802	0.4737	0.5329	36.93	0.416	16.795	0.4898	0.5510	92.34	0.449	15.94
13	0.086	0.095	0.0851	0.0941	0.5658	0.6250	38.87	0.438	16.172	0.5850	0.6463	91.78	0.468	15.38
14	0.102	0.111	0.1010	0.1099	0.6711	0.7303	41.03	0.462	15.472	0.6939	0.7551	91.18	0.489	14.79
15	0.116	0.125	0.1149	0.1238	0.7632	0.8224	42.59	0.479	14.968	0.7891	0.8503	90.69	0.505	14.30
16	0.130	0.139	0.1287	0.1376	0.8553	0.9145	44.20	0.498	14.447	0.8844	0.9456	90.31	0.519	13.92
17	0.155	0.164	0.1535	0.1624	1.0197	1.0789	46.29	0.521	13.770	1.0544	1.1156	89.57	0.544	13.19
18	0.185	0.194	0.1832	0.1921	1.2171	1.2763	48.67	0.548	13.000	1.2585	1.3197	88.98	0.564	12.61
19	0.225	0.234	0.2228	0.2317	1.4803	1.5395	51.96	0.585	11.935	1.5306	1.5918	88.02	0.597	11.66
20	0.275	0.284	0.2723	0.2812	1.8092	1.8684	55.61	0.626	10.754	1.8707	1.9320	87.02	0.631	10.66
21	0.325	0.334	0.3218	0.3307	2.1382	2.1974	58.55	0.659	9.803	2.2109	2.27.1	86.00	0.666	9.65
22	0.400	0.409	0.3960	0.4050	2.6316	2.6908	63.46	0.714	8.214	2.7211	2.7823	84.69	0.711	8.35
23	0.475	0.484	0.4703	0.4792	3.1250	3.1842	67.60	0.761	6.874	3.2313	3.2925	83.42	0.755	7.10
24	0.550	0.559	0.5446	0.5535	3.6184	3.6776	71.70	0.807	5.547	3.7415	3.8027	82.22	0.796	5.91
25	0.625	0.634	0.6188	0.6277	4.1118	4.1711	75.33	0.848	4.372	4.2517	4.3129	81.07	0.835	4.77
26	0.700	0.709	0.6931	0.7020	4.6053	4.6645	78.85	0.888	3.233	4.7619	4.8231	80.00	0.872	3.71
27	0.775	0.784	0.7673	0.7762	5.0987	5.1579	82.00	0.923	2.214	5.2721	5.3333	79.01	0.906	2.73
28	0.850	0.859	0.8416	0.8505	5.5921	5.6513	84.70	0.953	1.340	5.7823	5.8435	78.19	0.934	1.91
29	0.925	0.934	0.9158	0.9248	6.0855	6.1447	86.40	0.973	0.790	6.2925	6.3537	77.29	0.965	1.02
30	1.000	1.009	0.9901	0.9990	6.5789	6.6382	87.80	0.988	0.337	6.8027	6.8639	76.76	0.983	0.50
31	1.100	1.109	1.0891	1.0980	7.2368	7.2961	88.55	0.997	0.094	7.4830	7.5442	76.43	0.995	0.16
32	1.200	1.209	1.1881	1.1970	7.8947	7.9539	88.84	1.000	0.000	8.1633	8.2245	76.26	1.000	0.00
33	1.300	1.309	1.2871	1.2960	8.5526	8.6118	88.84	1.000	0.000	8.8435	8.9048	76.26	1.000	0.00

MEAN VELOCITY AND TEMPERATURE PROFILE - UINF= 89 FT/SEC F=0.004

RUN	= 080874-2	UINF	= 88.67	DELM	= 1.375	REX	= 0.171E 07
PLATE	= 10	TWALL	= 105.46	DELM1	= 0.369	REM	= 9416.70
X(IN)	= 38.	TINF	= 76.19	DELM2	= 0.209	REH	= 9506.80
X-XO(IN)	= 38.0	F	= 0.004	H	= 1.767	REK	= 46.50
Z(IN)	= 0.000	CF/2	= 0.00111	DELH	= 1.479	UTAU	= 2.95
POINTS	= 33	ST	= 0.00103	DELH2	= 0.211	TTAU	= 0.885

I	Y	YS	Y/DELM	YS/DELM	Y/DELM2	YS/DELM2	U	U/UINF	UDE	Y/DELH2	YS/DELH2	T	TBAR	TDE
1	0.007	0.016	0.0051	0.0116	0.0335	0.0766	16.80	0.189	24.363	0.0332	0.0758	98.33	0.244	25.02
2	0.009	0.018	0.0065	0.0131	0.0431	0.0861	17.71	0.200	24.054	0.0427	0.0853	98.04	0.254	24.69
3	0.012	0.021	0.0087	0.0153	0.0574	0.1005	19.29	0.218	23.519	0.0569	0.0995	97.43	0.274	24.00
4	0.016	0.025	0.0116	0.0182	0.0766	0.1156	21.00	0.237	22.939	0.0758	0.1185	97.00	0.289	23.51
5	0.021	0.030	0.0153	0.0218	0.1005	0.1435	23.42	0.264	22.119	0.0995	0.1422	96.43	0.309	22.87
6	0.026	0.035	0.0189	0.0255	0.1244	0.1675	25.43	0.287	21.437	0.1232	0.1659	95.83	0.329	22.19
7	0.032	0.041	0.0233	0.0298	0.1531	0.1962	26.51	0.299	21.071	0.1517	0.1943	94.49	0.375	20.68
8	0.040	0.049	0.0291	0.0356	0.1914	0.2344	28.58	0.322	20.369	0.1896	0.2322	94.98	0.358	21.23
9	0.050	0.059	0.0364	0.0429	0.2392	0.2823	30.89	0.348	19.586	0.2370	0.2796	94.29	0.382	20.45
10	0.062	0.071	0.0451	0.0516	0.2967	0.3397	32.49	0.366	19.044	0.2938	0.3365	93.66	0.403	19.74
11	0.076	0.085	0.0553	0.0618	0.3636	0.4067	34.55	0.390	18.346	0.3602	0.4028	93.11	0.422	19.12
12	0.092	0.101	0.0669	0.0735	0.4402	0.4833	36.25	0.409	17.769	0.4360	0.4787	92.63	0.438	18.58
13	0.110	0.119	0.0800	0.0865	0.5263	0.5654	38.21	0.431	17.105	0.5213	0.5640	91.53	0.476	17.33
14	0.130	0.139	0.0945	0.1011	0.6220	0.6651	40.41	0.456	16.359	0.6161	0.6588	91.49	0.477	17.29
15	0.155	0.164	0.1127	0.1193	0.7416	0.7847	42.35	0.478	15.702	0.7346	0.7773	90.74	0.503	16.44
16	0.185	0.194	0.1345	0.1411	0.8852	0.9282	44.74	0.505	14.892	0.8768	0.9194	90.28	0.519	15.92
17	0.225	0.234	0.1636	0.1702	1.0766	1.1196	47.77	0.539	13.864	1.0663	1.1090	89.53	0.544	15.07
18	0.265	0.274	0.1927	0.1993	1.2679	1.3110	49.62	0.560	13.237	1.2559	1.2986	88.72	0.572	14.16
19	0.315	0.324	0.2291	0.2356	1.5072	1.5502	52.38	0.591	12.302	1.4929	1.5355	88.02	0.596	13.37
20	0.375	0.384	0.2727	0.2793	1.7943	1.8373	55.30	0.624	11.312	1.7773	1.8199	87.05	0.629	12.27
21	0.450	0.459	0.3273	0.3338	2.1531	2.1962	59.25	0.668	9.973	2.1327	2.1754	86.13	0.660	11.23
22	0.525	0.534	0.3818	0.3884	2.5120	2.5550	61.79	0.697	9.112	2.4882	2.5308	85.07	0.697	10.03
23	0.625	0.634	0.4545	0.4611	2.9904	3.0335	66.08	0.745	7.658	2.9621	3.0047	83.92	0.736	8.73
24	0.725	0.734	0.5273	0.5338	3.4689	3.5120	70.06	0.790	6.308	3.4360	3.4787	82.73	0.777	7.39
25	0.825	0.834	0.6000	0.6065	3.9474	3.9904	74.04	0.835	4.959	3.9100	3.9526	81.65	0.813	6.17
26	0.925	0.934	0.6727	0.6793	4.4258	4.4689	77.22	0.871	3.881	4.3839	4.4265	80.62	0.849	5.01
27	1.050	1.059	0.7636	0.7702	5.0239	5.0670	81.43	0.918	2.454	4.9763	5.0190	79.35	0.892	3.57
28	1.200	1.209	0.8727	0.8793	5.7416	5.7847	85.13	0.960	1.200	5.6872	5.7299	78.05	0.936	2.10
29	1.350	1.359	0.9818	0.9884	6.4593	6.5024	87.55	0.987	0.380	6.3981	6.4408	77.04	0.971	0.96
30	1.500	1.509	1.0909	1.0975	7.1770	7.2201	88.39	0.997	0.095	7.1090	7.1517	76.43	0.992	0.27
31	1.650	1.659	1.2000	1.2065	7.8947	7.9378	88.70	1.000	-0.010	7.8199	7.8626	76.23	0.999	0.05
32	1.800	1.809	1.3091	1.3156	8.6124	8.6555	88.67	1.000	0.000	8.5308	8.5735	76.19	1.000	0.00
33	2.000	2.009	1.4545	1.4611	5.5694	9.6124	88.67	1.000	0.000	9.4787	9.5213	76.19	1.000	0.00

MEAN VELOCITY AND TEMPERATURE PROFILE - UINF= 89 FT/SEC F=0.004

RUN	= 080874-3	UINF	= 88.82	DELM	= 1.784	REX	= 0.226E 07
PLATE	= 13	TWALL	= 105.41	DELM1	= 0.468	REM	= 12140.50
X(IN)	= 50.	TINF	= 76.37	DELM2	= 0.269	REH	= 12456.40
X-X3(IN)	= 50.0	F	= 0.004	H	= 1.742	REK	= 46.00
Z(IN)	= 0.000	CF/2	= 0.00108	DELH	= 1.909	UTAU	= 2.92
POINTS	= 35	ST	= 0.00101	DELH2	= 0.276	TTAU	= 0.872

I	Y	YS	Y/DELM	YS/DELM	Y/DELM2	YS/DELM2	U	U/UINF	UDE	Y/DELH2	YS/DELH2	T	TBAR	TDE
1	0.007	0.016	0.0039	0.0090	0.0260	0.0595	15.06	0.170	25.260	0.0254	0.0580	98.83	0.227	25.76
2	0.009	0.018	0.0050	0.0101	0.0335	0.0669	16.36	0.184	24.815	0.0326	0.0652	98.59	0.235	25.48
3	0.012	0.021	0.0067	0.0118	0.0446	0.0781	18.05	0.203	24.236	0.0435	0.0761	98.09	0.252	24.91
4	0.016	0.025	0.0090	0.0140	0.0595	0.0929	19.83	0.223	23.627	0.0580	0.0966	97.59	0.269	24.33
5	0.021	0.030	0.0118	0.0168	0.0781	0.1115	21.93	0.247	22.908	0.0761	0.1087	96.98	0.290	23.64
6	0.027	0.036	0.0151	0.0202	0.1004	0.1338	23.86	0.269	22.247	0.0978	0.1304	96.45	0.309	23.03
7	0.034	0.043	0.0191	0.0241	0.1264	0.1599	25.36	0.286	21.733	0.1232	0.1558	95.93	0.326	22.43
8	0.043	0.052	0.0241	0.0291	0.1599	0.1933	27.47	0.309	21.010	0.1558	0.1884	95.38	0.345	21.80
9	0.053	0.062	0.0297	0.0348	0.1970	0.2305	29.70	0.334	20.247	0.1920	0.2246	94.79	0.366	21.12
10	0.065	0.074	0.0364	0.0415	0.2416	0.2751	31.77	0.358	19.536	0.2355	0.2681	94.24	0.385	20.49
11	0.077	0.086	0.0432	0.0482	0.2862	0.3197	33.49	0.377	18.949	0.2790	0.3116	93.81	0.399	20.00
12	0.092	0.101	0.0516	0.0566	0.3420	0.3755	35.06	0.395	18.411	0.3333	0.3659	93.35	0.415	19.47
13	0.110	0.119	0.0617	0.0667	0.4089	0.4424	37.04	0.417	17.733	0.3986	0.4312	92.74	0.436	18.77
14	0.130	0.139	0.0729	0.0779	0.4833	0.5167	38.75	0.436	17.147	0.4710	0.5036	92.28	0.452	18.25
15	0.155	0.164	0.0869	0.0919	0.5762	0.6097	40.93	0.461	16.401	0.5616	0.5942	91.65	0.472	17.57
16	0.190	0.199	0.1065	0.1115	0.7063	0.7398	43.24	0.487	15.610	0.6884	0.7210	91.09	0.493	16.88
17	0.230	0.239	0.1289	0.1340	0.8550	0.8885	45.21	0.509	14.935	0.8333	0.8659	90.50	0.513	16.20
18	0.280	0.289	0.1570	0.1620	1.0409	1.0743	48.05	0.541	13.962	1.0145	1.0471	89.65	0.543	15.23
19	0.350	0.359	0.1962	0.2012	1.3011	1.3346	51.15	0.576	12.901	1.2681	1.3007	88.78	0.573	14.23
20	0.425	0.434	0.2382	0.2433	1.5799	1.6134	53.95	0.607	11.942	1.5399	1.5725	87.89	0.603	13.21
21	0.500	0.509	0.2803	0.2853	1.8587	1.8922	56.77	0.639	10.976	1.8116	1.8442	87.00	0.634	12.19
22	0.575	0.584	0.3223	0.3274	2.1375	2.1710	59.41	0.669	10.072	2.0833	2.1159	86.16	0.663	11.23
23	0.675	0.684	0.3784	0.3834	2.5093	2.5428	62.35	0.702	9.065	2.4457	2.4783	85.24	0.695	10.17
24	0.775	0.784	0.4344	0.4395	2.8810	2.9145	64.62	0.728	8.288	2.8080	2.8406	84.37	0.725	9.17
25	0.900	0.909	0.5045	0.5095	3.3457	3.3792	69.48	0.782	6.623	3.2609	3.2935	83.20	0.765	7.83
26	1.050	1.059	0.5886	0.5936	3.9033	3.9368	73.79	0.831	5.147	3.8043	3.8370	81.98	0.817	6.43
27	1.200	1.209	0.6726	0.6777	4.4610	4.4944	77.84	0.876	3.760	4.3478	4.3804	80.73	0.850	5.00
28	1.400	1.409	0.7848	0.7898	5.2045	5.2379	82.64	0.930	2.116	5.0725	5.1051	79.21	0.902	3.26
29	1.600	1.609	0.8969	0.9019	5.9480	5.9814	86.09	0.969	0.935	5.7971	5.8297	77.80	0.951	1.64
30	1.800	1.809	1.0090	1.0140	6.6915	6.7249	88.04	0.991	0.267	6.5217	6.5543	76.94	0.980	0.65
31	2.000	2.009	1.1211	1.1261	7.4349	7.4684	88.56	0.997	0.089	7.2464	7.2790	76.57	0.993	0.23
32	2.200	2.209	1.2332	1.2382	8.1784	8.2119	88.73	0.999	0.031	7.9710	8.0036	76.42	0.998	0.06
33	2.400	2.409	1.3453	1.3503	8.9219	8.9554	88.78	1.000	0.014	8.6956	8.7283	76.40	0.999	0.03
34	2.600	2.609	1.4574	1.4624	9.6654	9.6989	88.82	1.000	0.000	9.4203	9.4529	76.37	1.000	0.00
35	2.800	2.809	1.5695	1.5746	10.4089	10.4424	88.82	1.000	0.000	10.1449	10.1775	76.37	1.000	0.00

MEAN VELOCITY AND TEMPERATURE PROFILE - UINF= 89 FT/SEC F=0.004

RUN	= 080874-4	UINF	= 88.66	DELM	= 2.129	REX	= 0.279E 07
PLATE	= 16	TWALL	= 105.41	DELM1	= 0.563	REM	= 14551.40
X(IN)	= 62.	TINF	= 76.26	DELM2	= 0.323	REH	= 15001.90
X-XO(IN)	= 62.0	F	= C.004	H	= 1.744	REK	= 45.50
Z(IN)	= 0.000	CF/2	= 0.00106	DELH	= 2.318	UTAU	= 2.89
POINTS	= 34	ST	= 0.00093	DELH2	= 0.333	TTAU	= 0.814

I	Y	YS	Y/DELM	YS/DELM	Y/DELM2	YS/DELM2	U	U/UINF	UDE	Y/DELH2	YS/DELH2	T	TBAR	TDE
1	0.007	0.016	0.0033	0.0075	0.0217	0.0495	13.58	0.153	25.979	0.0210	0.0480	99.76	0.194	28.87
2	0.009	0.018	0.0042	0.0085	0.0279	0.0557	14.43	0.163	25.685	0.0270	0.0541	99.49	0.203	28.54
3	0.012	0.021	0.0056	0.0099	0.0372	0.0650	16.35	0.184	25.021	0.0360	0.0631	98.94	0.222	27.86
4	0.016	0.025	0.0075	0.0117	0.0495	0.0774	18.19	0.205	24.384	0.0480	0.0751	98.41	0.240	27.21
5	0.021	C.030	0.0099	0.0141	0.0650	0.0929	20.16	0.227	23.702	0.0631	0.0901	97.90	0.258	26.58
6	0.027	0.036	0.0127	0.0169	0.0836	0.1115	22.04	0.249	23.052	0.0811	0.1081	97.22	0.281	25.75
7	0.034	0.043	0.0160	0.0202	0.1053	0.1331	23.52	0.265	22.540	0.1021	0.1291	96.64	0.301	25.04
8	0.043	0.052	0.0202	0.0244	0.1331	0.1610	25.51	0.288	21.851	0.1291	0.1562	96.18	0.317	24.47
9	0.053	0.062	0.0249	0.0291	0.1641	0.1920	27.54	0.311	21.149	0.1592	0.1862	95.51	0.340	23.65
10	0.065	0.074	0.0305	0.0348	0.2012	0.2291	29.43	0.332	20.495	0.1952	0.2222	95.06	0.355	23.10
11	0.077	0.086	0.0362	0.0404	0.2384	0.2663	31.52	0.356	19.772	0.2312	0.2583	94.48	0.375	22.38
12	0.092	0.101	0.0432	0.0474	0.2848	0.3127	33.41	0.377	19.118	0.2763	0.3033	94.04	0.390	21.84
13	0.110	0.119	0.0517	0.0559	0.3406	0.3684	34.94	0.394	18.588	0.3303	0.3574	93.39	0.412	21.04
14	0.130	0.139	0.0611	0.0653	0.4025	0.4303	36.69	0.414	17.983	0.3904	0.4174	92.87	0.430	20.41
15	0.155	0.164	0.0728	0.0770	0.4799	0.5077	38.34	0.432	17.412	0.4655	0.4925	92.40	0.446	19.83
16	0.190	0.199	0.0892	0.0935	0.5882	0.6161	40.86	0.461	16.540	0.5706	0.5976	91.75	0.469	19.03
17	0.240	0.249	0.1127	0.1170	0.7430	0.7709	43.91	0.495	15.484	0.7207	0.7477	90.87	0.499	17.95
18	0.290	0.299	0.1362	0.1404	0.8978	0.9257	46.12	0.520	14.720	0.8709	0.8979	90.19	0.522	17.11
19	0.350	0.359	0.1644	0.1686	1.0836	1.1115	48.58	0.548	13.869	1.0511	1.0781	89.45	0.548	16.20
20	0.425	0.434	0.1996	0.2039	1.3158	1.3437	51.43	0.580	12.882	1.2763	1.3033	88.66	0.575	15.23
21	0.500	0.509	0.2349	0.2391	1.5480	1.5759	53.88	0.608	12.035	1.5015	1.5285	87.90	0.601	14.30
22	0.600	0.609	0.2818	0.2860	1.8576	1.8854	56.75	0.640	11.042	1.8018	1.8288	87.00	0.632	13.19
23	0.700	0.709	0.3288	0.3330	2.1672	2.1950	59.58	0.672	10.062	2.1021	2.1291	86.17	0.660	12.17
24	0.825	0.834	0.3875	0.3917	2.5542	2.5820	62.85	0.709	8.931	2.4775	2.5045	85.19	0.694	10.97
25	0.950	0.959	0.4462	0.4504	2.9412	2.9650	66.31	0.748	7.734	2.8529	2.8799	84.16	0.729	9.71
26	1.100	1.109	0.5167	0.5209	3.4056	3.4334	69.52	0.784	6.623	3.3033	3.3303	83.04	0.767	8.33
27	1.300	1.309	0.6106	0.6148	4.0248	4.0526	74.38	0.839	4.941	3.9039	3.9309	81.72	0.813	6.71
28	1.500	1.509	0.7046	0.7088	4.6440	4.6718	78.65	0.887	3.464	4.5045	4.5315	80.33	0.860	5.00
29	1.750	1.759	0.8220	0.8262	5.4180	5.4458	83.16	0.938	1.903	5.2553	5.2823	78.75	0.915	3.04
30	2.000	2.009	0.9394	0.9436	6.1919	6.2198	86.75	0.978	0.661	6.0060	6.0330	77.47	0.958	1.49
31	2.250	2.259	1.0568	1.0611	6.9659	6.9938	88.24	0.995	0.145	6.7568	6.7838	76.73	0.984	0.58
32	2.500	2.509	1.1743	1.1785	7.7399	7.7678	88.73	1.001	-0.024	7.5075	7.5345	76.38	0.996	0.15
33	2.750	2.759	1.2917	1.2959	8.5139	8.5418	88.66	1.000	0.000	8.2583	8.2853	76.38	0.996	0.15
34	3.000	3.009	1.4091	1.4133	9.2879	9.3158	88.66	1.000	0.000	9.0090	9.0360	76.38	0.996	0.15

MEAN VELOCITY AND TEMPERATURE PROFILE - UINF= 89 FT/SEC F=0.004

RUN	= 080874-5	UINF	=	88.74	DELM	= 2.586	REX	=	0.333E 07
PLATE	= 19	TWALL	=	105.82	DELM1	= 0.660	REM	=	17224.90
X(IN)	= 74.	TINF	=	76.30	DELM2	= 0.382	REH	=	17495.50
X-XO(IN)	= 74.0	F	=	0.004	H	= 1.728	REK	=	44.20
Z(IN)	= 0.000	CF/2	=	0.00100	DELH	= 2.697	UTAU	=	2.81
POINTS	= 35	ST	=	0.00082	DELH2	= 0.388	TTAU	=	0.749

I	Y	YS	Y/DELM	YS/DELM	Y/DELM2	YS/DELM2	U	U/UINF	LOE	Y/DELH2	YS/DELH2	T	TBAR	TOE
1	0.007	0.016	0.0027	0.0062	0.0183	0.0419	13.37	0.151	26.822	0.0180	0.0412	99.70	0.207	31.24
2	0.009	0.018	0.0035	0.0070	0.0236	0.0471	14.32	0.161	26.484	0.0232	0.0464	99.41	0.217	30.85
3	0.012	0.021	0.0046	0.0081	0.0314	0.0550	16.16	0.182	25.829	0.0309	0.0541	99.01	0.231	30.32
4	0.015	0.024	0.0058	0.0093	0.0393	0.0628	17.94	0.202	25.196	0.0387	0.0619	98.62	0.244	29.80
5	0.019	0.028	0.0073	0.0108	0.0497	0.0733	19.12	0.215	24.776	0.0490	0.0722	98.15	0.260	29.17
6	0.024	0.033	0.0093	0.0128	0.0628	0.0864	20.76	0.234	24.192	0.0619	0.0851	97.57	0.279	28.40
7	0.030	0.039	0.0116	0.0151	0.0785	0.1021	22.68	0.256	23.509	0.0773	0.1005	97.05	0.297	27.70
8	0.038	0.047	0.0147	0.0182	0.0995	0.1230	24.79	0.279	22.758	0.0979	0.1211	96.51	0.315	26.98
9	0.048	0.057	0.0186	0.0220	0.1257	0.1492	26.73	0.301	22.068	0.1237	0.1469	95.80	0.339	26.03
10	0.060	0.069	0.0232	0.0267	0.1571	0.1806	28.47	0.321	21.448	0.1546	0.1778	95.38	0.354	25.47
11	0.075	0.084	0.0290	0.0325	0.1963	0.2199	30.68	0.346	20.662	0.1933	0.2165	94.64	0.379	24.49
12	0.100	0.109	0.0387	0.0422	0.2618	0.2853	33.47	0.377	19.669	0.2577	0.2809	94.00	0.400	23.63
13	0.130	0.139	0.0503	0.0538	0.3403	0.3639	35.03	0.395	19.114	0.3351	0.3582	93.23	0.426	22.60
14	0.170	0.179	0.0657	0.0692	0.4450	0.4686	38.11	0.429	18.018	0.4381	0.4613	92.47	0.452	21.59
15	0.220	0.229	0.0851	0.0886	0.5759	0.5995	41.12	0.463	16.947	0.5670	0.5902	91.59	0.482	20.41
16	0.280	0.289	0.1083	0.1118	0.7330	0.7565	43.66	0.492	16 .43	0.7216	0.7448	90.83	0.508	19.40
17	0.350	0.359	0.1353	0.1388	0.9162	0.9358	47.02	0.530	14.847	0.9021	0.9253	89.95	0.538	18.22
18	0.430	0.439	0.1663	0.1698	1.1257	1.1492	49.72	0.560	13.686	1.1082	1.1314	89.14	0.565	17.14
19	0.520	0.529	0.2011	0.2046	1.3613	1.3848	52.21	0.588	13.000	1.3402	1.3634	88.44	0.589	16.21
20	0.620	0.629	0.2398	0.2432	1.6230	1.6466	55.13	0.621	11.961	1.5979	1.6211	87.47	0.622	14.91
21	0.730	0.739	0.2823	0.2858	1.9110	1.9346	57.58	0.649	11.089	1.8814	1.9046	86.68	0.648	13.86
22	0.850	0.859	0.3287	0.3322	2.2251	2.2487	60.75	0.685	9.961	2.1907	2.2139	85.85	0.676	12.75
23	1.000	1.009	0.3867	0.3902	2.6178	2.6414	63.88	0.720	8.847	2.5773	2.6005	84.82	0.711	11.38
24	1.150	1.159	0.4447	0.4482	3.0105	3.0340	66.93	0.754	7.762	2.9639	2.9871	83.81	0.746	10.03
25	1.300	1.309	0.5027	0.5062	3.4031	3.4267	69.77	0.786	6.751	3.3505	3.3737	82.97	0.774	8.91
26	1.500	1.509	0.5800	0.5835	3.9267	3.9503	73.75	0.831	5.335	3.8660	3.8892	81.87	0.811	7.44
27	1.700	1.709	0.6574	0.6609	4.4503	4.4738	77.24	0.870	4.093	4.3814	4.4046	80.71	0.851	5.89
28	1.900	1.909	0.7347	0.7382	4.9738	4.9974	80.89	0.912	2.794	4.8969	4.9201	79.68	0.886	4.51
29	2.100	2.109	0.8121	0.8155	5.4974	5.5209	83.76	0.944	1.772	5.4124	5.4356	78.68	0.919	3.18
30	2.350	2.359	0.9087	0.9122	6.1518	6.1754	86.65	0.976	0.744	6.0567	6.0799	77.59	0.956	1.72
31	2.600	2.609	1.0054	1.0089	6.8063	6.8298	88.00	0.992	0.263	6.7010	6.7242	76.80	0.983	0.67
32	2.850	2.859	1.1021	1.1056	7.4607	7.4843	88.73	1.000	0.004	7.3454	7.3686	76.43	0.996	0.17
33	3.100	3.109	1.1988	1.2022	8.1152	0.1387	88.72	1.000	0.007	7.9897	8.0129	76.28	1.001	-0.03
34	3.350	3.359	1.2954	1.2989	8.7696	8.7932	88.74	1.000	0.000	8.6340	8.6572	76.30	1.000	0.00
35	3.600	3.609	1.3921	1.3956	9.4241	9.4476	88.74	1.000	0.000	9.2784	9.3015	76.30	1.000	0.00

MEAN VELOCITY AND TEMPERATURE PROFILE - UINF= 89 FT/SEC F=0.004

RUN	= 080874-6	UINF	= 88.85	DELM	= 2.954	REX	= 0.388E 07
PLATE	= 22	TWALL	= 106.22	DELM1	= 0.759	REM	= 20135.70
X(IN)	= 86.	TINF	= 76.26	DELM2	= 0.446	REH	= 19864.80
X-XO(IN)	= 86.0	F	= 0.004	H	= 1.702	REK	= 42.50
Z(IN)	= 0.000	CF/2	= 0.00092	DELH	= 3.141	UTAU	= 2.69
POINTS	= 34	ST	= 0.00071	DELH2	= 0.440	TTAU	= 0.686

I	Y	YS	Y/DELM	YS/DELM	Y/DELM2	YS/DELM2	U	U/UINF	UDE	Y/DELH2	YS/DELH2	T	TBAR	TDE
1	0.007	0.016	0.0024	0.0054	0.0157	0.0359	14.00	0.158	27.825	0.0159	0.0364	99.91	0.211	34.48
2	0.009	0.018	0.0030	0.0061	0.0202	0.0404	15.27	0.172	27.353	0.0205	0.0409	99.66	0.219	34.11
3	0.012	0.021	0.0041	0.0071	0.0269	0.0471	17.03	0.192	26.699	0.0273	0.0477	99.18	0.235	33.41
4	0.016	0.025	0.0054	0.0085	0.0359	0.0561	18.45	0.208	26.171	0.0364	0.0568	98.77	0.249	32.81
5	0.022	0.031	0.0074	0.0105	0.0493	0.0695	20.57	0.232	25.383	0.0500	0.0705	98.07	0.272	31.79
6	0.028	0.037	0.0095	0.0125	0.0628	0.0830	22.59	0.254	24.632	0.0636	0.0841	97.50	0.291	30.96
7	0.036	0.045	0.0122	0.0152	0.0807	0.1009	24.85	0.280	23.792	0.0818	0.1023	96.85	0.313	30.01
8	0.044	0.053	0.0149	0.0179	0.0987	0.1188	25.66	0.289	23.491	0.1000	0.1205	96.38	0.328	29.33
9	0.054	0.063	0.0183	0.0213	0.1211	0.1413	27.62	0.311	22.762	0.1227	0.1432	95.93	0.343	28.67
10	0.068	0.077	0.0230	0.0261	0.1525	0.1726	29.16	0.328	22.190	0.1545	0.1750	95.41	0.361	27.92
11	0.085	0.094	0.0288	0.0318	0.1906	0.2108	31.76	0.357	21.223	0.1932	0.2136	94.76	0.383	26.97
12	0.105	0.114	0.0355	0.0386	0.2354	0.2556	33.62	0.378	20.532	0.2386	0.2591	94.15	0.403	26.08
13	0.130	0.139	0.0440	0.0471	0.2915	0.3117	35.56	0.400	19.810	0.2955	0.3159	93.53	0.424	25.17
14	0.170	0.179	0.0575	0.0606	0.3812	0.4013	38.09	0.429	18.870	0.3864	0.4068	92.62	0.454	23.85
15	0.220	0.229	0.0745	0.0775	0.4933	0.5135	40.50	0.456	17.974	0.5000	0.5205	91.92	0.477	22.83
16	0.295	0.304	0.0999	0.1029	0.6614	0.6816	44.01	0.495	16.669	0.6705	0.6909	90.95	0.510	21.41
17	0.370	0.379	0.1253	0.1283	0.8296	0.8498	46.46	0.523	15.758	0.8409	0.8614	90.13	0.537	20.22
18	0.470	0.479	0.1591	0.1622	1.0538	1.0740	50.22	0.565	14.361	1.0682	1.0886	89.25	0.566	18.94
19	0.570	0.579	0.1930	0.1960	1.2780	1.2982	52.57	0.592	13.487	1.2955	1.3159	88.45	0.593	17.77
20	0.695	0.704	0.2353	0.2383	1.5583	1.5785	55.55	0.625	12.379	1.5795	1.6000	87.59	0.622	16.52
21	0.854	0.863	0.2891	0.2921	1.9148	1.9350	57.83	0.651	11.532	1.9409	1.9614	86.77	0.649	15.32
22	1.020	1.029	0.3453	0.3483	2.2870	2.3072	61.25	0.689	10.260	2.3182	2.3386	85.69	0.685	13.75
23	1.200	1.209	0.4062	0.4093	2.6906	2.7108	64.51	0.726	9.048	2.7273	2.7477	84.74	0.717	12.36
24	1.400	1.409	0.4739	0.4770	3.1390	3.1592	68.14	0.767	7.699	3.1818	3.2023	83.62	0.754	10.73
25	1.600	1.609	0.5416	0.5447	3.5874	3.6076	71.57	0.806	6.424	3.6364	3.6568	82.62	0.788	9.27
26	1.800	1.809	0.6093	0.6124	4.0359	4.0561	74.70	0.841	5.260	4.0909	4.1114	81.58	0.822	7.76
27	2.050	2.059	0.6940	0.6970	4.5964	4.6166	78.66	0.885	3.788	4.6591	4.6795	80.43	0.861	6.08
28	2.300	2.309	0.7786	0.7817	5.1570	5.1771	81.93	0.922	2.572	5.2273	5.2477	79.33	0.898	4.48
29	2.550	2.559	0.8632	0.8663	5.7175	5.7377	85.02	0.957	1.424	5.7955	5.8159	78.24	0.934	2.89
30	2.800	2.809	0.9479	0.9509	6.2780	6.2982	87.06	0.980	0.665	6.3636	6.3841	77.34	0.964	1.57
31	3.050	3.059	1.0325	1.0355	6.8386	6.8587	88.27	0.993	0.216	6.9318	6.9523	76.72	0.985	0.67
32	3.300	3.309	1.1171	1.1202	7.3991	7.4193	88.48	0.996	0.138	7.5000	7.5205	76.42	0.995	0.23
33	3.550	3.559	1.2018	1.2048	7.9596	7.9798	88.86	1.000	-0.004	8.0682	8.0886	76.27	1.000	0.01
34	3.700	3.709	1.2525	1.2556	8.2960	8.3161	88.85	1.000	0.000	8.4091	8.4295	76.26	1.000	0.00

MEAN VELOCITY AND TEMPERATURE PROFILE - UINF=130 FT/SEC F=0.000

RUN	= 071374-1	UINF	= 130.30	DELM	= 0.628	REX	= 0.175E 07
PLATE	= 7	TWALL	= 95.44	DELM1	= 0.137	REM	= 5935.00
X(IN)	= 26.	TINF	= 66.44	DELM2	= 0.082	REH	= 5530.00
X-XC(IN)	= 26.0	F	= 0.000	H	= 1.556	REK	= 106.80
Z(IN)	= 0.000	CF/2	= 0.00261	DELH	= 0.673	UTAU	= 6.66
POINTS	= 32	ST	= 0.00264	DELH2	= 0.082	TTAU	= 1.425

I	Y	YS	Y/DELM	YS/DELM	Y/DELM2	YS/DELM2	U	U/UINF	UDE	Y/DELH2	YS/DELH2	T	TBAR	TDE
1	0.007	0.013	0.0111	0.0207	0.0854	0.1585	43.64	0.335	13.012	0.0854	0.1585	83.49	0.412	11.96
2	0.008	0.014	0.0127	0.0223	0.0976	0.1707	44.64	0.343	12.862	0.0976	0.1707	83.31	0.410	11.84
3	0.009	0.015	0.0143	0.0239	0.1098	0.1829	45.74	0.351	12.697	0.1098	0.1829	83.22	0.421	11.78
4	0.011	0.017	0.0175	0.0271	0.1341	0.2073	47.83	0.367	12.383	0.1341	0.2073	82.76	0.437	11.45
5	0.013	0.019	0.0207	0.0303	0.1585	0.2317	49.37	0.379	12.152	0.1585	0.2317	82.52	0.446	11.28
6	0.016	0.022	0.0255	0.0350	0.1951	0.2683	51.65	0.396	11.809	0.1951	0.2683	82.04	0.462	10.95
7	0.019	0.025	0.0303	0.0398	0.2317	0.3049	53.65	0.412	11.509	0.2317	0.3049	81.66	0.475	10.68
8	0.023	0.029	0.0366	0.0462	0.2805	0.3537	56.08	0.430	11.144	0.2805	0.3537	81.27	0.489	10.41
9	0.027	0.033	0.0430	0.0525	0.3293	0.4024	58.24	0.447	10.820	0.3293	0.4024	80.86	0.503	10.12
10	0.032	0.038	0.0510	0.0605	0.3902	0.4634	60.13	0.461	10.536	0.3902	0.4634	80.41	0.518	9.80
11	0.040	0.046	0.0637	0.0732	0.4878	0.5610	63.41	0.487	10.044	0.4878	0.5610	79.94	0.534	9.47
12	0.048	0.054	0.0764	0.0860	0.5854	0.6585	66.07	0.507	9.644	0.5854	0.6585	79.46	0.551	9.14
13	0.058	0.064	0.0924	0.1019	0.7073	0.7805	68.84	0.528	9.228	0.7073	0.7805	78.97	0.568	8.79
14	0.070	0.076	0.1115	0.1210	0.8537	0.9268	71.60	0.550	8.814	0.8537	0.9268	78.36	0.589	8.36
15	0.084	0.090	0.1338	0.1433	1.0244	1.0976	74.84	0.574	8.327	1.0244	1.0976	77.89	0.605	8.04
16	0.100	0.106	0.1592	0.1688	1.2195	1.2927	77.94	0.598	7.862	1.2195	1.2927	77.28	0.626	7.61
17	0.118	0.124	0.1879	0.1975	1.4390	1.5122	81.05	0.622	7.389	1.4390	1.5122	76.76	0.644	7.24
18	0.130	0.136	0.2070	0.2166	1.5854	1.6585	83.00	0.637	7.102	1.5854	1.6585	76.36	0.658	6.96
19	0.140	0.146	0.2229	0.2325	1.7073	1.7805	84.56	0.649	6.868	1.7073	1.7805	76.02	0.670	6.72
20	0.165	0.171	0.2627	0.2723	2.0122	2.0854	88.47	0.679	6.281	2.0122	2.0854	75.35	0.693	6.25
21	0.195	0.201	0.3105	0.3201	2.3780	2.4512	92.37	0.709	5.695	2.3780	2.4512	74.75	0.713	5.83
22	0.235	0.241	0.3742	0.3838	2.8659	2.9390	97.03	0.745	4.995	2.8659	2.9390	73.93	0.742	5.26
23	0.275	0.281	0.4379	0.4475	3.3537	3.4268	101.82	0.781	4.276	3.3537	3.4268	73.04	0.772	4.63
24	0.315	0.321	0.5016	0.5111	3.8415	3.9146	106.11	0.814	3.632	3.8415	3.9146	72.22	0.801	4.06
25	0.360	0.366	0.5732	0.5828	4.3902	4.4634	110.83	0.851	2.923	4.3902	4.4634	71.40	0.829	3.48
26	0.410	0.416	0.6529	0.6624	5.0000	5.0732	115.44	0.886	2.231	5.0000	5.0732	70.47	0.861	2.83
27	0.460	0.466	0.7325	0.7420	5.6098	5.6829	120.16	0.922	1.523	5.6098	5.6829	69.53	0.893	2.17
28	0.510	0.516	0.8121	0.8217	6.2195	6.2927	123.37	0.947	1.041	6.2195	6.2927	69.70	0.922	1.59
29	0.560	0.566	0.8917	0.9013	6.8293	6.9024	126.72	0.973	0.538	6.8293	6.9024	67.90	0.950	1.02
30	0.635	0.641	1.0111	1.0207	7.7439	7.8171	129.08	0.991	0.183	7.7439	7.8171	67.03	0.980	0.41
31	0.710	0.716	1.1306	1.1401	8.6585	8.7317	130.28	1.000	0.003	8.6585	8.7317	66.56	0.996	0.08
32	0.810	0.816	1.2898	1.2994	9.8780	9.9512	130.27	1.000	0.005	9.8780	9.9512	66.44	1.000	0.00

MEAN VELOCITY AND TEMPERATURE PROFILE - UINF=130 FT/SEC F=0.000

RUN = 071374-2	UINF = 130.30	DELM = 0.857	REX = 0.256E 07
PLATE = 10	TWALL = 55.31	DELM1 = 0.184	REM = 8093.10
X(IN) = 38.	TINF = 66.45	DELM2 = 0.120	REH = 7351.30
X-XO(IN) = 38.0	F = 0.000	H = 1.537	REK = 104.90
Z(IN) = 0.000	CF/2 = 0.00252	DELH = 0.923	UTAU = 5.53
POINTS = 28	ST = 0.00240	DELH2 = 0.109	TTAU = 1.313

I	Y	YS	Y/DELM	YS/DELM	Y/DELM2	YS/DELM2	U	U/UINF	UDE	Y/DELH2	YS/DELH2	T	TBAR	TDE
1	0.007	0.013	0.0082	0.0152	0.0583	0.1083	40.17	0.308	13.802	0.0642	0.1193	84.20	0.385	13.52
2	0.008	0.014	0.0093	0.0163	0.0667	0.1167	40.60	0.312	13.737	0.0734	0.1284	84.04	0.391	13.40
3	0.009	0.015	0.0105	0.0175	0.0750	0.1250	42.31	0.325	13.475	0.0826	0.1376	83.84	0.397	13.24
4	0.012	0.018	0.0140	0.0210	0.1000	0.1500	45.34	0.348	13.011	0.1101	0.1651	83.31	0.416	12.84
5	0.016	0.022	0.0187	0.0257	0.1333	0.1833	48.85	0.375	12.473	0.1468	0.2018	82.67	0.438	12.35
6	0.020	0.026	0.0233	0.0303	0.1667	0.2167	51.24	0.393	12.107	0.1835	0.2385	82.21	0.454	12.00
7	0.025	0.031	0.0292	0.0362	0.2083	0.2583	53.85	0.413	11.708	0.2294	0.2844	81.80	0.468	11.69
8	0.031	0.037	0.0362	0.0432	0.2583	0.3083	56.40	0.433	11.317	0.2844	0.3394	81.32	0.485	11.33
9	0.038	0.044	0.0443	0.0513	0.3167	0.3667	58.99	0.453	10.920	0.3486	0.4037	80.82	0.502	10.94
10	0.046	0.052	0.0537	0.0607	0.3833	0.4333	62.02	0.476	10.456	0.4220	0.4771	80.32	0.519	10.56
11	0.056	0.062	0.0653	0.0723	0.4667	0.5167	64.36	0.494	10.098	0.5138	0.5688	79.84	0.536	10.20
12	0.068	0.074	0.0793	0.0863	0.5667	0.6167	67.86	0.521	9.562	0.6239	0.6789	79.32	0.554	9.80
13	0.084	0.090	0.0980	0.1050	0.7000	0.7500	70.78	0.543	9.115	0.7706	0.8257	78.73	0.574	9.35
14	0.104	0.110	0.1214	0.1284	0.8667	0.9167	73.93	0.567	8.632	0.9541	1.0092	78.10	0.596	8.87
15	0.130	0.136	0.1517	0.1587	1.0833	1.1333	78.22	0.600	7.975	1.1927	1.2477	77.41	0.620	8.35
16	0.160	0.166	0.1867	0.1937	1.3333	1.3833	81.98	0.629	7.400	1.4679	1.5229	76.69	0.645	7.80
17	0.195	0.201	0.2275	0.2345	1.6250	1.6750	85.71	0.658	6.828	1.7890	1.8440	75.93	0.672	7.22
18	0.235	0.241	0.2742	0.2812	1.9583	2.0083	89.87	0.690	6.191	2.1560	2.2110	75.16	0.698	6.63
19	0.275	0.281	0.3209	0.3279	2.2917	2.3417	93.78	0.720	5.593	2.5229	2.5780	74.44	0.723	6.09
20	0.325	0.331	0.3792	0.3862	2.7083	2.7583	98.57	0.756	4.859	2.9817	3.0367	73.62	0.752	5.46
21	0.400	0.406	0.4667	0.4737	3.3333	3.3833	104.41	0.801	3.965	3.6697	3.7248	72.36	0.795	4.50
22	0.475	0.481	0.5543	0.5613	3.9583	4.0083	110.38	0.847	3.051	4.3578	4.4128	71.29	0.832	3.69
23	0.550	0.556	0.6418	0.6488	4.5833	4.6333	115.24	0.884	2.305	5.0459	5.1009	70.26	0.868	2.90
24	0.625	0.631	0.7293	0.7363	5.2083	5.2583	119.94	0.920	1.587	5.7339	5.7890	69.34	0.900	2.20
25	0.725	0.731	0.8460	0.8530	6.0417	6.0917	124.79	0.958	0.844	6.6514	6.7064	68.20	0.939	1.33
26	0.825	0.831	0.9627	0.9697	6.8750	6.9250	128.34	0.985	0.300	7.5688	7.6239	67.27	0.972	0.62
27	0.975	0.981	1.1377	1.1447	8.1250	8.1750	129.81	0.996	0.075	8.9450	9.0000	66.64	0.993	0.14
28	1.125	1.131	1.3127	1.3197	9.3750	9.4250	130.29	1.000	0.002	10.3211	10.3761	66.45	1.000	0.00

MEAN VELOCITY AND TEMPERATURE PROFILE - UINF=130 FT/SEC F=0.000

RUN	= 071374-3	UINF	= 130.20	DELM	= 1.094	REX	= 0.337E 07
PLATE	= 13	TWALL	= 95.39	DELM1	= 0.222	REM	= 9973.90
X(IN)	= 50.	TINF	= 66.48	DELM2	= 0.148	REH	= 9434.80
X-XC(IN)	= 50.0	F	= 0.000	H	= 1.495	REK	= 102.90
Z(IN)	= 0.000	CF/2	= 0.00243	DELH	= 1.177	UTAU	= 6.41
POINTS	= 28	ST	= 0.00233	DELH2	= 0.140	TTAU	= 1.300

I	Y	YS	Y/DELM	YS/DELM	Y/DELM2	YS/DELM2	U	U/UINF	UDE	Y/DELH2	YS/DELH2	T	TBAR	TDE
1	0.007	0.013	0.0064	0.0119	0.0473	0.0878	41.27	0.317	13.874	0.0500	0.0929	84.42	0.379	13.80
2	0.008	0.014	0.0073	0.0128	0.0541	0.0946	42.45	0.326	13.690	0.0571	0.1000	84.23	0.386	13.55
3	0.009	0.015	0.0082	0.0137	0.0608	0.1014	43.57	0.335	13.515	0.0643	0.1071	84.03	0.393	13.50
4	0.012	0.018	0.0110	0.0165	0.0811	0.1216	46.20	0.355	13.105	0.0857	0.1286	83.55	0.410	13.13
5	0.015	0.021	0.0137	0.0192	0.1014	0.1419	48.03	0.369	12.819	0.1071	0.1500	83.12	0.424	12.80
6	0.020	0.026	0.0183	0.0238	0.1351	0.1757	51.42	0.395	12.290	0.1429	0.1857	82.65	0.441	12.44
7	0.025	0.031	0.0229	0.0283	0.1689	0.2095	53.90	0.414	11.903	0.1786	0.2214	82.20	0.456	12.09
8	0.032	0.038	0.0293	0.0347	0.2162	0.2568	56.81	0.436	11.449	0.2286	0.2714	81.62	0.476	11.65
9	0.040	0.046	0.0366	0.0420	0.2703	0.3108	59.89	0.460	10.969	0.2857	0.3286	81.06	0.496	11.22
10	0.050	0.056	0.0457	0.0512	0.3378	0.3784	63.12	0.485	10.465	0.3571	0.4000	80.54	0.514	10.82
11	0.060	0.066	0.0548	0.0603	0.4054	0.4459	65.41	0.502	10.108	0.4286	0.4714	80.05	0.531	10.44
12	0.075	0.081	0.0686	0.0740	0.5068	0.5473	68.47	0.526	9.630	0.5357	0.5786	79.44	0.552	9.97
13	0.090	0.096	0.0823	0.0878	0.6081	0.6486	71.30	0.548	9.189	0.6429	0.6857	79.03	0.566	9.65
14	0.110	0.116	0.1005	0.1060	0.7432	0.7838	74.41	0.572	8.704	0.7857	0.8286	78.36	0.589	9.14
15	0.130	0.136	0.1188	0.1243	0.8784	0.9189	77.30	0.594	8.253	0.9286	0.9714	77.92	0.604	8.80
16	0.160	0.166	0.1463	0.1517	1.0811	1.1216	80.52	0.618	7.750	1.1429	1.1857	77.24	0.628	8.28
17	0.210	0.216	0.1920	0.1974	1.4189	1.4595	85.42	0.656	6.986	1.5000	1.5429	76.30	0.660	7.55
18	0.260	0.266	0.2377	0.2431	1.7568	1.7973	89.82	0.690	6.300	1.8571	1.9000	75.50	0.688	6.94
19	0.335	0.341	0.3062	0.3117	2.2635	2.3041	95.19	0.731	5.462	2.3929	2.4357	74.40	0.726	6.09
20	0.435	0.441	0.3976	0.4031	2.9392	2.9797	102.04	0.784	4.393	3.1071	3.1500	73.12	0.770	5.11
21	0.535	0.541	0.4890	0.4945	3.6149	3.6554	107.92	0.825	3.476	3.8214	3.8643	71.95	0.811	4.21
22	0.635	0.641	0.5804	0.5859	4.2905	4.3311	112.03	0.860	2.835	4.5357	4.5786	70.91	0.847	3.41
23	0.735	0.741	0.6718	0.6773	4.9662	5.0068	117.05	0.899	2.051	5.2500	5.2929	69.88	0.882	2.62
24	0.835	0.841	0.7633	0.7687	5.6419	5.6824	122.07	0.938	1.268	5.9643	6.0071	68.45	0.925	1.67
25	0.960	0.966	0.8775	0.8830	6.4865	6.5270	125.85	0.967	0.679	6.8571	6.9000	67.91	0.951	1.10
26	1.110	1.116	1.0146	1.0201	7.5000	7.5405	129.16	0.992	0.162	7.9286	7.9714	67.02	0.981	0.42
27	1.260	1.266	1.1517	1.1572	8.5135	8.5541	129.62	0.996	0.090	9.0000	9.0429	66.63	0.995	0.12
28	1.410	1.416	1.2888	1.2943	9.5270	9.5676	130.19	1.000	0.002	10.0714	10.1143	66.48	1.000	0.00

MEAN VELOCITY AND TEMPERATURE PROFILE - UINF=130 FT/SEC F=0.000

RUN	=	071374-4	UINF	=	130.10	DELM	=	1.284	REX	=	0.417E 07
PLATE	=	16	TWALL	=	95.35	DELM1	=	0.256	REM	=	11582.40
X(IN)	=	62.	TINF	=	66.38	DELM2	=	0.172	REH	=	11851.80
X-XC(IN)	=	62.0	F	=	0.000	H	=	1.488	REK	=	101.50
Z(IN)	=	0.000	CF/2	=	0.00236	DELH	=	1.480	UTAU	=	6.32
POINTS	=	34	ST	=	0.00273	DELH2	=	0.176	TTAU	=	1.264

I	Y	YS	Y/DELM	YS/DELM	Y/DELM2	YS/DELM2	U	U/UINF	UDE	Y/DELH2	YS/DELH2	T	TBAR	DE
1	0.007	0.013	0.0055	0.0101	0.0407	0.0756	40.19	0.309	14.226	0.0398	0.0739	85.03	0.356	14.75
2	0.008	0.014	0.0062	0.0109	0.0465	0.0814	41.16	0.316	14.073	0.0455	0.0795	84.83	0.363	14.60
3	0.009	0.015	0.0070	0.0117	0.0523	0.0872	42.05	0.323	13.932	0.0511	0.0852	84.65	0.369	14.45
4	0.012	0.018	0.0093	0.0140	0.0698	0.1047	44.91	0.345	13.479	0.0682	0.1023	84.08	0.389	14.00
5	0.015	0.021	0.0117	0.0164	0.0872	0.1221	47.38	0.364	13.089	0.0852	0.1193	83.53	0.408	13.57
6	0.020	0.026	0.0156	0.0202	0.1163	0.1512	50.17	0.386	12.647	0.1136	0.1477	82.99	0.427	13.14
7	0.025	0.031	0.0195	0.0241	0.1453	0.1802	52.71	0.405	12.245	0.1420	0.1761	82.54	0.442	12.78
8	0.032	0.038	0.0249	0.0296	0.1860	0.2209	55.42	0.426	11.816	0.1813	0.2159	81.98	0.462	12.34
9	0.040	0.046	0.0312	0.0358	0.2326	0.2674	58.66	0.451	11.304	0.2273	0.2614	81.46	0.479	11.93
10	0.050	0.056	0.0389	0.0436	0.2907	0.3256	61.93	0.476	10.786	0.2841	0.3182	80.95	0.497	11.53
11	0.060	0.066	0.0467	0.0514	0.3488	0.3837	64.43	0.495	10.391	0.3409	0.3750	80.46	0.514	11.14
12	0.075	0.081	0.0584	0.0631	0.4360	0.4709	67.05	0.515	9.976	0.4261	0.4602	79.88	0.534	10.68
13	0.090	0.096	0.0701	0.0748	0.5233	0.5581	70.16	0.539	9.484	0.5114	0.5455	79.35	0.552	10.26
14	0.110	0.116	0.0857	0.0903	0.6395	0.6744	73.22	0.563	9.000	0.6250	0.6591	78.60	0.571	9.83
15	0.130	0.136	0.1012	0.1059	0.7558	0.7907	76.06	0.585	8.551	0.7386	0.7[illegible]27	78.34	0.587	9.46
16	0.160	0.166	0.1246	0.1293	0.9302	0.9651	78.69	0.605	8.134	0.909[illegible]	0.9432	77.72	0.609	8.97
17	0.210	0.216	0.1636	0.1682	1.2209	1.2558	83.95	0.645	7.302	1.1932	1.2273	76.83	0.639	8.27
18	0.260	0.266	0.2025	0.2072	1.5116	1.5465	87.44	0.672	6.750	1.4773	1.5114	76.02	0.667	7.63
19	0.335	0.341	0.2609	0.2656	1.9477	1.9826	92.53	0.711	[illegible].945	1.9034	1.9375	75.05	0.701	6.86
20	0.435	0.441	0.3388	0.3435	2.5291	2.5640	98.03	0.753	5.074	2.4716	2.5057	73.95	0.739	5.99
21	0.535	0.541	0.4167	0.4213	3.1105	3.1453	103.39	0.795	4.226	3.0398	3.0739	72.97	0.773	5.21
22	0.635	0.641	0.4945	0.4992	3.6919	3.7267	108.01	0.830	3.495	3.[illegible]080	3.6420	71.93	0.808	4.39
23	0.735	0.741	0.5724	0.5771	4.2733	4.3081	112.67	0.866	2.758	4.1761	4.2102	71.05	0.837	3.73
24	0.835	0.841	0.6503	0.6550	4.8547	4.8895	116.52	0.896	2.149	4.7443	4.77[illegible]	70.24	0.867	3.05
25	0.960	0.966	0.7477	0.7523	5.5814	5.6[illegible]63	121.01	0.930	1.438	5.4545	5.488[illegible]	69.25	0.900	2.30
26	1.110	1.116	0.8645	0.8692	6.4535	6.4884	125.19	0.962	0.777	6.3068	6.3409	68.19	0.938	1.43
27	1.260	1.266	0.9813	0.9860	7.3256	7.3605	128.48	0.988	0.256	7.1591	7.1932	67.35	0.967	0.77
28	1.410	1.416	1.0981	1.1028	8.1977	8.2326	129.68	0.997	0.066	8.0114	8.0455	66.83	0.984	0.36
29	1.560	1.566	1.2150	1.2196	9.0698	9.1047	130.10	1.000	0.000	8.8636	8.8977	66.59	0.993	0.17
30	1.710	1.716	1.3318	1.3364	9.9419	9.9767	130.22	1.001	-0.019	9.7159	9.7500	66.51	0.996	0.10
31	1.860	1.866	1.4486	1.4533	10.8140	10.8488	130.20	1.001	-0.016	10.5682	10.6023	66.45	0.998	0.06
32	2.010	2.016	1.5654	1.5701	11.6860	11.7209	130.16	1.000	-0.009	11.4205	11.4545	66.41	0.999	0.02
33	2.160	2.166	1.6822	1.6869	12.5581	12.5930	130.12	1.000	-0.003	12.2727	12.3068	66.38	1.000	0.00
34	2.310	2.316	1.7991	1.8037	13.4302	13.4651	130.12	1.000	-0.003	13.1250	13.1591	66.38	1.000	0.00

MEAN VELOCITY AND TEMPERATURE PROFILE - UINF=130 FT/SEC F=0.000

RUN	= 071374-5	UINF	=	130.20	DELM	=	1.535	REX	=	0.490E 07
PLATE	=	19	TWALL	=	95.55	DEL1	=	0.292	REM	=	13343.50
X(IN)	=	74.	TINF	=	66.45	DELM2	=	0.198	REH	=	13613.00
X-XO(IN)	=	74.0	F	=	0.000	H	=	1.474	REK	=	99.90
Z(IN)	=	0.000	CF/2	=	0.00229	DELH	=	1.946	UTAU	=	6.23
POINTS	=	35	ST	=	0.00222	DELH2	=	0.202	TTAU	=	1.286

I	Y	YS	Y/DELM	YS/DELM	Y/DELM2	YS/DELM2	U	U/UINF	UCE	Y/DELH2	YS/DELH2	T	TBAR	TDE
1	0.007	0.013	0.0046	0.0085	0.0354	0.0657	38.40	0.295	14.735	0.0347	0.0644	85.20	0.356	14.58
2	0.008	0.014	0.0052	0.0091	0.0404	0.0707	39.44	0.303	14.568	0.0396	0.0693	85.00	0.363	14.42
3	0.009	0.015	0.0059	0.0098	0.0455	0.0758	40.56	0.312	14.388	0.0446	0.0743	84.80	0.369	14.27
4	0.012	0.018	0.0078	0.0117	0.0606	0.0909	43.49	0.334	13.918	0.0594	0.0891	84.32	0.386	13.90
5	0.015	0.021	0.0098	0.0137	0.0758	0.106[illegible]	5.56	0.350	13.586	0.0743	0.1040	83.92	0.400	13.58
6	0.018	0.024	0.0117	0.0156	0.0909	0.1212	47.66	0.366	13.249	0.0891	0.1188	83.61	0.410	13.34
7	0.022	0.028	0.0143	0.0182	0.1111	0.1414	49.50	0.380	12.953	0.1089	0.1386	83.17	0.425	13.00
8	0.027	0.033	0.0176	0.0215	0.1364	0.1667	52.55	0.404	12.464	0.1337	0.1634	82.71	0.441	12.64
9	0.032	0.038	0.0208	0.0248	0.1616	0.1919	54.64	0.420	12.128	0.1584	0.1881	82.31	0.455	12.33
10	0.038	0.044	0.0248	0.0287	0.1919	0.2222	57.55	0.442	11.661	0.1881	0.2178	81.84	0.471	11.97
11	0.045	0.051	0.0293	0.0332	0.2273	0.2576	59.01	0.453	11.427	0.2228	0.2525	81.42	0.486	11.64
12	0.055	0.061	0.0358	0.0397	0.2778	0.3081	62.41	0.479	10.881	0.2723	0.3020	80.98	0.501	11.30
13	0.065	0.071	0.0423	0.0463	0.3283	0.3586	64.53	0.496	10.541	0.3218	0.3515	80.48	0.518	10.91
14	0.080	0.086	0.0521	0.0560	0.4040	0.4343	67.57	0.519	10.053	0.3960	0.4257	79.95	0.536	10.50
15	0.100	0.106	0.0651	0.0691	0.5051	0.5354	70.97	0.545	9.507	0.4950	0.5248	79.35	0.557	10.03
16	0.130	0.136	0.0847	0.0886	0.6566	0.6869	75.06	0.576	8.851	0.6436	0.6733	78.58	0.583	9.43
17	0.160	0.166	0.1042	0.1081	0.8081	0.8384	78.24	0.601	8.340	0.7921	0.8218	78.01	0.603	8.99
18	0.210	0.216	0.1368	0.1407	1.0606	1.0909	82.92	0.637	7.589	1.0396	1.0693	77.12	0.633	8.30
19	0.260	0.266	0.1694	0.1733	1.3131	1.3434	86.26	0.663	7.053	1.2871	1.3168	76.45	0.656	7.78
20	0.320	0.326	0.2085	0.2124	1.6162	1.6465	89.93	0.691	6.464	1.5842	1.6139	75.76	0.680	7.24
21	0.390	0.396	0.2541	0.2580	1.9697	2.0000	93.46	0.718	5.897	1.9307	1.9604	74.94	0.708	6.60
22	0.460	0.466	0.2997	0.3036	2.3232	2.3535	97.22	0.747	5.294	2.2772	2.3069	74.29	0.731	6.10
23	0.540	0.546	0.3518	0.3557	2.7273	2.7576	100.43	0.771	4.778	2.6733	2.7030	73.58	0.755	5.54
24	0.630	0.636	0.4104	0.4143	3.1818	3.2121	104.60	0.803	4.109	3.1188	3.1485	72.80	0.782	4.94
25	0.720	0.726	0.4691	0.4730	3.6364	3.6667	107.88	0.829	3.583	3.5644	3.5941	72.12	0.805	4.41
26	0.820	0.826	0.5342	0.5381	4.1414	4.1717	111.85	0.859	2.945	4.0594	4.0891	71.35	0.832	3.81
27	0.940	0.946	0.6124	0.6163	4.7475	4.7778	115.46	0.887	2.366	4.6335	4.6832	70.53	0.860	3.17
28	1.080	1.086	0.7036	0.7075	5.4545	5.4848	120.30	0.924	1.589	5.3465	5.3762	69.61	0.891	2.46
29	1.240	1.246	0.8078	0.8117	6.2626	6.2929	124.07	0.953	0.984	6.1386	6.1683	68.66	0.924	1.72
30	1.440	1.446	0.9381	0.9420	7.2727	7.3030	127.72	0.981	0.398	7.1287	7.1584	67.85	0.952	1.09
31	1.690	1.696	1.1010	1.1049	8.5354	8.5657	129.96	0.998	0.039	8.3663	8.3960	67.03	0.980	0.45
32	1.940	1.946	1.2638	1.2678	9.7980	9.8283	130.22	1.000	-0.003	9.6040	9.6337	66.74	0.990	0.23
33	2.190	2.196	1.4267	1.4306	11.0606	11.0909	130.17	1.000	0.005	10.8416	10.8713	66.61	0.995	0.12
34	2.440	2.446	1.5896	1.5935	12.3232	12.3535	130.21	1.000	-0.002	12.0792	12.1089	66.55	0.997	0.08
35	2.690	2.696	1.7524	1.7564	13.5859	13.6162	130.23	1.000	-0.005	13.3168	13.3465	66.45	1.000	0.00

MEAN VELOCITY AND TEMPERATURE PROFILE - UINF=130 FT/SEC F=0.000

RUN	= 071374-6	UINF	= 130.60	DELM	= 1.740	REX	= 0.581E 07
PLATE	= 22	TWALL	= 95.47	DELM1	= 0.328	REM	= 15142.00
X(IN)	= 86.	TINF	= 66.34	DELM2	= 0.234	REH	= 15412.40
X-XO(IN)	= 86.0	F	= 0.000	H	= 1.464	REK	= 99.30
Z(IN)	= 0.000	CF/2	= 0.00224	DELH	= 1.964	UTAU	= 6.18
POINTS	= 34	ST	= 0.00215	DELH2	= 0.228	TTAU	= 1.258

I	Y	YS	Y/DELM	YS/DELM	Y/DELM2	YS/DELM2	U	U/UINF	UDE	Y/DELH2	YS/DELH2	T	TBAR	TDE
1	0.007	0.013	0.0040	0.0075	0.0299	0.0556	38.84	0.297	14.848	0.0307	0.0570	85.30	0.349	15.07
2	0.008	0.014	0.0046	0.0080	0.0342	0.0598	39.40	0.302	14.757	0.0351	0.0614	85.23	0.352	15.02
3	0.009	0.015	0.0052	0.0086	0.0385	0.0641	40.61	0.311	14.561	0.0395	0.0658	85.02	0.359	14.85
4	0.011	0.017	0.0063	0.0098	0.0470	0.0726	42.44	0.325	14.265	0.0482	0.0746	84.66	0.371	14.56
5	0.014	0.020	0.0080	0.0115	0.0598	0.0855	44.84	0.343	13.877	0.0614	0.0877	84.22	0.386	14.21
6	0.019	0.025	0.0109	0.0144	0.0812	0.1068	48.02	0.368	13.362	0.0833	0.1096	83.58	0.408	13.70
7	0.026	0.032	0.0149	0.0184	0.1111	0.1368	51.81	0.397	12.749	0.1140	0.1404	82.99	0.428	13.24
8	0.035	0.041	0.0201	0.0236	0.1496	0.1752	55.97	0.429	12.076	0.1535	0.1798	82.30	0.452	12.69
9	0.047	0.053	0.0270	0.0305	0.2009	0.2265	59.59	0.456	11.490	0.2061	0.2325	81.60	0.476	12.13
10	0.062	0.068	0.0356	0.0391	0.2650	0.2906	63.27	0.484	10.895	0.2719	0.2982	80.79	0.504	11.49
11	0.080	0.086	0.0460	0.0494	0.3419	0.3675	67.09	0.514	10.277	0.3509	0.3772	80.15	0.526	10.93
12	0.100	0.106	0.0575	0.0609	0.4274	0.4530	70.25	0.538	9.765	0.4386	0.4649	79.58	0.545	10.52
13	0.130	0.136	0.0747	0.0782	0.5556	0.5812	74.37	0.569	9.099	0.5702	0.5965	78.77	0.573	9.88
14	0.170	0.176	0.0977	0.1011	0.7265	0.7521	78.25	0.599	8.471	0.7456	0.7719	77.98	0.600	9.25
15	0.220	0.226	0.1264	0.1299	0.9402	0.9658	82.12	0.629	7.845	0.9649	0.9912	77.35	0.622	8.75
16	0.280	0.286	0.1609	0.1644	1.1966	1.2222	86.06	0.659	7.207	1.2281	1.2544	76.48	0.652	8.06
17	0.350	0.356	0.2011	0.2046	1.4957	1.5214	90.01	0.689	6.568	1.5351	1.5614	75.77	0.676	7.50
18	0.430	0.436	0.2471	0.2506	1.8376	1.8632	93.77	0.718	5.960	1.8860	1.9123	74.94	0.705	6.84
19	0.520	0.526	0.2989	0.3023	2.2222	2.2479	97.41	0.746	5.371	2.2807	2.3070	74.22	0.729	6.26
20	0.620	0.626	0.3563	0.3598	2.6496	2.6752	101.80	0.779	4.660	2.7193	2.7456	73.41	0.757	5.62
21	0.740	0.746	0.4253	0.4287	3.1624	3.1880	105.88	0.811	4.000	3.2456	3.2719	72.63	0.784	5.00
22	0.880	0.886	0.5057	0.5092	3.7607	3.7863	110.26	0.844	3.291	3.8596	3.8860	71.65	0.818	4.22
23	1.040	1.046	0.5977	0.6011	4.4444	4.4701	115.51	0.884	2.442	4.5614	4.5877	70.72	0.850	3.48
24	1.220	1.226	0.7011	0.7046	5.2137	5.2393	119.94	0.918	1.725	5.3509	5.3772	69.68	0.885	2.66
25	1.420	1.426	0.8161	0.8195	6.0684	6.0940	124.91	0.956	0.921	6.2281	6.2544	68.50	0.926	1.72
26	1.640	1.646	0.9425	0.9460	7.0085	7.0342	128.14	0.981	0.398	7.1930	7.2193	67.44	0.962	0.87
27	1.880	1.886	1.0805	1.0839	8.0342	8.0598	130.46	0.999	0.023	8.2456	8.2719	66.76	0.986	0.33
28	2.130	2.136	1.2241	1.2276	9.1026	9.1282	130.60	1.000	0.000	9.3421	9.3684	66.55	0.993	0.17
29	2.380	2.386	1.3678	1.3713	10.1709	10.1966	130.76	1.001	-0.026	10.4386	10.4649	66.52	0.994	0.14
30	2.630	2.636	1.5115	1.5149	11.2393	11.2650	130.73	1.001	-0.021	11.5351	11.5614	66.49	0.995	0.12
31	2.880	2.886	1.6552	1.6586	12.3077	12.3333	130.67	1.001	-0.011	12.6316	12.6579	66.43	0.997	0.07
32	3.130	3.136	1.7989	1.8023	13.3761	13.4017	130.60	1.000	0.000	13.7281	13.7544	66.38	0.999	0.03
33	3.230	3.236	1.8563	1.8598	13.8034	13.8291	130.56	1.000	0.006	14.1667	14.1930	66.34	1.000	0.00
34	3.330	3.336	1.9138	1.9172	14.2308	14.2564	130.56	1.000	0.006	14.6053	14.6316	66.34	1.000	0.00

D.4 Reynolds Stress Tensor Components (Isothermal)

This section contains the isothermal data of the Reynolds stress tensor components for the uniformly blown and unblown cases. The following is a summary of the test cases and abbreviations used in the data listings (see also D.3 for the explanation of other abbreviations).

U_∞ (ft/sec)	F
52	0.000
89	0.000
130	0.000
89	0.002
89	0.004

UTAU	Friction velocity, $U_\infty \sqrt{C_f/2} = U_\tau$	(ft/sec)
DELM	Momentum boundary layer thickness	(inch)
U'2/UINF2	$\overline{u'^2}/U_\infty^2$	-
V'2/UINF2	$\overline{v'^2}/U_\infty^2$	-
W'2/UINF2	$\overline{w'^2}/U_\infty^2$	-
Q2/UINF2	q^2/U_∞^2	-
-U'V'/UINF2	$-\overline{u'v'}/U_\infty^2$	-
RUV	correlation coefficient, $-\overline{u'v'}/\sqrt{\overline{u'^2}}\sqrt{\overline{v'^2}}$	-
RQ	correlation coefficient, $-\overline{u'v'}/q^2$	-

REYNOLDS STRESS TENSOR COMPONENTS
ISOTHERMAL - UINF= 52 FT/SEC F=0.000 PLATE 10

RUN = 070174-2
UINF = 52.30
CF/2 = 0.00247
UTAU = 2.61
DELM = 0.684

Y	Y/DELM	U	U'2/UINF2	V'2/UINF2	W'2/UINF2	Q2/UINF2	-U'V'/UINF2	RUV	RQ
0.007	0.0102	17.29	0.00964						
0.009	0.0132	18.51	0.01030						
0.014	0.0205	21.10	0.01003						
0.020	0.0292	22.91	0.00971						
0.030	0.0439	25.18	0.00939						
0.043	0.0629	27.27	0.00920						
0.062	0.0906	29.34	0.00892						
0.094	0.1374	31.96	0.00869						
0.130	0.1901	34.30	0.00825	0.00305	0.00[illegible]35	0.01665	0.00238	0.474	0.142
0.155	0.2266	35.66	0.00793	0.00320	0.00[illegible]26	0.01639	0.00236	0.468	0.144
0.185	0.2705	37.12	0.00751	0.00317	0.00514	0.01582	0.00229	0.469	0.144
0.215	0.3143	38.52	0.00711	0.00300	0.00469	0.01507	0.00218	0.472	0.145
0.250	0.3655	39.92	0.00664	0.00290	0.00485	0.01439	0.00208	0.474	0.144
0.290	0.4240	41.51	0.00609	0.00257	0.004[illegible]6	0.01302	0.00189	0.477	0.145
0.330	0.4825	43.04	0.00555	0.00241	0.00400	0.01196	0.00167	0.456	0.140
0.380	0.5556	44.73	0.00490	0.00218	0.00366	0.01074	0.00150	0.459	0.140
0.500	0.7310	48.46	0.00298	0.00175	0.00215	0.00683	0.00091	0.398	0.133
0.600	0.8772	50.70	0.00141	0.00091	0.00102	0.00334	0.00041	0.362	0.123
0.700	1.0234	51.88	0.00038	0.00040	0.00[illegible]2	0.00120	0.00011	0.282	0.092
0.850	1.2427	52.23	0.00006						

REYNOLDS STRESS TENSOR COMPONENTS
ISOTHERMAL - UINF= 52 FT/SEC F=0.000 PLATE 19

RUN = 070174-1
UINF = 52.41
CF/2 = 0.00213
UTAU = 2.42
DELM = 1.325

Y	Y/DELM	U	U'2/UINF2	V'2/UINF2	W'2/UINF2	Q2/UINF2	-U'V'/UINF2	RUV	RQ
0.007	0.0053	15.13	0.01012						
0.009	0.0068	15.78	0.00977						
0.014	0.0106	18.31	0.00968						
0.021	0.0158	20.69	0.00925						
0.032	0.0242	23.43	0.00875						
0.048	0.0362	25.60	0.00866						
0.074	0.0558	27.88	0.00854						
0.108	0.0815	29.98	0.00840						
0.130	0.0981	31.21	0.00833	0.00289	0.00480	0.01602	0.00210	0.428	0.131
0.160	0.1208	32.33	0.00824	0.00287	0.00455	0.01566	0.00212	0.436	0.135
0.200	0.1509	33.98	0.00800	0.00297	0.00446	0.01540	0.00214	0.439	0.139
0.250	0.1887	35.32	0.00764	0.00293	0.00441	0.01498	0.00209	0.442	0.140
0.310	0.2340	37.15	0.00725	0.00288	0.00431	0.01444	0.00202	0.442	0.141
0.380	0.2868	38.45	0.00676	0.00282	0.00413	0.01371	0.00192	0.440	0.140
0.460	0.3472	40.42	0.00622	0.00270	0.00390	0.01282	0.00180	0.439	0.140
0.650	0.4906	44.13	0.00503	0.00210	0.00342	0.01055	0.00144	0.443	0.136
0.890	0.6717	47.85	0.00327	0.00140	0.00189	0.00656	0.00094	0.439	0.143
1.210	0.9132	51.29	0.00115	0.00075	0.00060	0.00250	0.00033	0.358	0.132
1.600	1.2075	52.41	0.00003	0.00006	0.00003	0.00012	0.00001	0.059	0.018

REYNOLDS STRESS TENSOR COMPONENTS
ISOTHERMAL - UINF= 89 FT/SEC F=0.000 PLATE 10

RUN = 071174-2
UINF = 88.45
CF/2 = 0.00252
UTAU = 4.44
DELM = 0.836

Y	Y/DELM	U	U'2/UINF2	V'2/UINF2	W'2/UINF2	Q2/UINF2	-U'V'/UINF2	RUV	RQ
0.007	0.0084	29.17	0.00824						
0.009	0.0108	31.20	0.00840						
0.015	0.0179	34.68	0.00843						
0.024	0.0287	38.14	0.00856						
0.038	0.0455	42.07	0.00926						
0.056	0.0670	45.78	0.00950						
0.082	0.0981	49.17	0 00958						
0.130	0.1555	54.43	0.00940	0.00347	0.00524	0.01821	0.00250	0.438	0.137
0.160	0.1914	56.96	0.00910	0.00341	0.00500	0.01750	0.00245	0.440	0.140
0.200	0.2392	60.50	0.00850	0.00336	0.00504	0.01690	0.00240	0.449	0.142
0.240	0.2871	63.09	0.00803	0.00343	0.00502	0.01648	0.00234	0.446	0.142
0.280	0.3349	65.89	0.00752	0.00343	0.00515	0.01610	0.00227	0.447	0.141
0.330	0.3947	68.59	0.00698	0.00338	0.00487	0.01521	0.00216	0.445	0.142
0.380	0.4545	71.45	0.00629	0.00307	0.00492	0.01429	0.00200	0.455	0.140
0.440	0.5263	74.75	0.00558	0.00272	0.00406	0.01236	0.00173	0.444	0.140
0.500	0.5981	77.85	0.00466	0.00258	0.00369	0.01093	0.00153	0.441	0.140
0.575	0.6878	80.98	0.00375	0.00191	0.00276	0.00842	0.00117	0.437	0.139
0.650	0.7775	83.97	0.00268	0.00120	0.00177	0.00565	0.00078	0.435	0.138
0.800	0.9569	87.50	0.00057	0.00036	0.00052	0.00145	0.00019	0.420	0.131

REYNOLDS STRESS TENSOR COMPONENTS
ISOTHERMAL - UINF= 89 FT/SEC F=0.000 PLATE 19

RUN = 071174-1
UINF = 88.49
CF/2 = 0.00226
UTAU = 4.21
DELM = 1.424

Y	Y/DELM	U	U'2/UINF2	V'2/UINF2	W'2/UINF2	Q2/UINF2	-U'V'/UINF2	RUV	RQ
0.007	0.0049	26.27	0.00751						
0.009	0.0063	27.65	0.00758						
0.014	0.0098	30.94	0.00818						
0.020	0.0140	33.95	0.00840						
0.029	0.0204	37.10	0.00870						
0.043	0.0302	40.68	0.00925						
0.065	0.0456	44.52	0.00978						
0.095	0.0667	48.37	0.00979						
0.130	0.0913	51.48	0.00968	0.00275	0.00455	0.01698	0.00225	0.436	0.133
0.155	0.1088	53.43	0.00950	0.00285	0.00447	0.01682	0.00226	0.434	0.134
0.185	0.1299	55.57	0.00930	0.00277	0.00440	0.01647	0.00224	0.441	0.136
0.220	0.1545	57.24	0.00900	0.00278	0.00407	0.01601	0.00221	0.442	0.138
0.260	0.1826	59.07	0.00861	0.00265	0.00421	0.01547	0.00215	0.450	0.138
0.310	0.2177	61.32	0.00810	0.00280	0.00421	0.01511	0.00213	0.447	0.141
0.370	0.2598	63.84	0.00770	0.00285	0.00413	0.01468	0.00207	0.442	0.141
0.445	0.3125	66.35	0.00721	0.00285	0.00402	0.01408	0.00200	0.441	0.142
0.520	0.3652	68.87	0.00665	0.00262	0.00376	0.01303	0.00185	0.443	0.142
0.700	0.4916	73.88	0.00528	0.00232	0.00344	0.01105	0.00158	0.451	0.143
0.925	0.6496	79.51	0.00388	0.00189	0.00255	0.00832	0.00119	0.439	0.143
1.200	0.8427	84.98	0.00165	0.00123	0.00148	0.00436	0.00062	0.435	0.142

REYNOLDS STRESS TENSOR COMPONENTS
ISOTHERMAL - UINF= 89 FT/SEC F=0.002 PLATE 19

RUN = 073174-3
UINF = 87.93
CF/2 = 0.00158
UTAU = 3.50
DELM = 2.022

Y	Y/DELM	U	U'2/UINF2	V'2/UINF2	W'2/UINF2	Q2/UINF2	-U'V'/UINF2	RUV	RQ
0.007	0.0035	19.07	0.00713						
0.010	0.0049	19.29	0.00750						
0.015	0.0074	24.16	0.00799						
0.022	0.0109	26.60	0.00845						
0.033	0.0163	30.02	0.00884						
0.048	0.0237	33.45	0.00928						
0.070	0.0346	36.49	0.00988						
0.105	0.0519	40.39	0.01076						
0.130	0.0643	42.99	0.01085	0.00284	0.00446	0.01815	0.00245	0.441	0.135
0.160	0.0791	45.42	0.01080	0.00287	0.00451	0.01818	0.00249	0.447	0.137
0.200	0.0989	47.16	0.01073	0.00317	0.00463	0.01853	0.00252	0.432	0.136
0.250	0.1236	49.49	0.01065	0.00321	0.00463	0.01849	0.00257	0.439	0.139
0.310	0.1533	52.41	0.01043	0.00328	0.00482	0.01829	0.00256	0.440	0.140
0.380	0.1879	54.93	0.00984	0.00330	0.00500	0.01814	0.00254	0.436	0.140
0.550	0.2720	60.06	0.00917	0.00355	0.00495	0.01767	0.00258	0.452	0.146
0.770	0.3808	65.47	0.00803	0.00352	0.00498	0.01653	0.00248	0.457	0.147
0.910	0.4500	68.86	0.00728	0.00325	0.00476	0.01529	0.00214	0.444	0.140
1.090	0.5391	73.02	0.00634	0.00290	0.00424	0.01347	0.00190	0.443	0.141
1.290	0.6380	76.89	0.00525	0.00254	0.00324	0.01102	0.00161	0.441	0.146
1.490	0.7369	80.63	0.00412	0.00180	0.00234	0.00826	0.00119	0.437	0.144

REYNOLDS STRESS TENSOR COMPONENTS
ISOTHERMAL - UINF= 89 FT/SEC F=0.004 PLATE 19

RUN = 080674-4
UINF = 89.75
CF/2 = 0.00100
UTAU = 2.83
DELM = 2.536

Y	Y/DELM	U	U'2/UINF2	V'2/UINF2	W'2/UINF2	Q2/UINF2	-U'V'/UINF2	RUV	RQ
0.007	0.0028	13.58	0.00594						
0.012	0.0047	16.68	0.00667						
0.019	0.0075	19.85	0.00765						
0.038	0.0150	25.05	0.00879						
0.075	0.0296	30.85	0.01003						
0.130	0.0513	36.36	0.01149	0.00262	0.00396	0.01808	0.00253	0.461	0.140
0.220	0.0868	42.46	0.01179	0.00318	0.00448	0.01946	0.00280	0.457	0.142
0.280	0.1104	45.37	0.01178	0.00345	0.00473	0.01997	0.00295	0.463	0.148
0.350	0.1380	47.44	0.01167	0.00402	0.00499	0.02068	0.00301	0.439	0.145
0.430	0.1696	49.96	0.01145	0.00429	0.00532	0.02106	0.00310	0.442	0.147
0.520	0.2050	53.17	0.01120	0.00396	0.00534	0.02049	0.00302	0.453	0.147
0.730	0.2879	58.68	0.01066	0.00412	0.00598	0.02075	0.00302	0.456	0.146
1.000	0.3943	64.54	0.00971	0.00424	0.00546	0.01941	0.00300	0.466	0.154
1.300	0.5126	70.75	0.00835	0.00382	0.00461	0.01679	0.00284	0.466	0.156
1.700	0.6703	78.50	0.00626	0.00259	0.00331	0.01216	0.00185	0.459	0.152
2.100	0.8261	84.92	0.00348	0.00151	0.00168	0.00677	0.00099	0.434	0.149

REYNOLDS STRESS TENSOR COMPONENTS
ISOTHERMAL - UINF=130 FT/SEC F=0.000 PLATE 10

RUN = 071274-2
UINF = 129.60
CF/2 = 0.00252
UTAU = 6.51
DELM = 0.867

Y	Y/DELM	U	U'2/UINF2	V'2/UINF2	W'2/UINF2	Q2/UINF2	-U'V'/UINF2	RUV	RQ
0.007	0.0081	40.40	0.00725						
0.009	0.0104	42.35	0.00741						
0.016	0.0185	47.99	0.00821						
0.025	0.0288	53.39	0.00904						
0.038	0.0438	58.67	0.00973						
0.056	0.0646	64.82	0.01026						
0.084	0.0969	70.95	0.01041						
0.130	0.1499	78.00	0.01005	0.00325	0.00514	0.01844	0.00252	0.441	0.137
0.160	0.1845	81.55	0.00977	0.00322	0.00491	0.01792	0.00248	0.441	0.139
0.195	0.2249	85.32	0.00932	0.00325	0.00484	0.01741	0.00242	0.440	0.139
0.235	0.2710	89.45	0.00914	0.00322	0.00471	0.01707	0.00239	0.441	0.140
0.275	0.3172	93.28	0.00853	0.00321	0.00476	0.01650	0.00236	0.451	0.143
0.325	0.3749	97.65	0.00806	0.00314	0.00438	0.01556	0.00229	0.455	0.147
0.400	0.4614	103.83	0.00695	0.00297	0.00409	0.01401	0.00206	0.453	0.147
0.475	0.5479	109.45	0.00606	0.00264	0.00371	0.01241	0.00180	0.450	0.145
0.550	0.6344	114.46	0.00481	0.00230	0.00318	0.01028	0.00146	0.439	0.142
0.625	0.7209	119.26	0.00351	0.00191	0.00262	0.00805	0.00118	0.454	0.146
0.725	0.8362	124.29	0.00215	0.00135	0.00156	0.00506	0.00066	0.386	0.130

REYNOLDS STRESS TENSOR COMPONENTS
ISOTHERMAL - UINF=130 FT/SEC F=0.000 PLATE 19

RUN = 071274-3
UINF = 129.20
CF/2 = 0.00229
UTAU = 6.18
DELM = 1.549

Y	Y/DELM	U	U'2/UINF2	V'2/UINF2	W'2/UINF2	Q2/UINF2	-U'V'/UINF2	RUV	RQ
0.007	0.0045	38.39	0.00748						
0.009	0.0058	40.35	0.00755						
0.015	0.0097	45.21	0.00808						
0.022	0.0142	49.91	0.00859						
0.032	0.0207	54.05	0.00913						
0.045	0.0291	58.43	0.00957						
0.065	0.0420	63.75	0.01000						
0.100	0.0646	69.74	0.01009						
0.130	0.0839	74.50	0.01004	0.00267	0.00459	0.01730	0.00229	0.442	0.132
0.160	0.1033	77.12	0.01002	0.00264	0.00459	0.01725	0.00227	0.441	0.132
0.210	0.1356	81.07	0.00957	0.00277	0.00441	0.01674	0.00226	0.440	0.135
0.260	0.1679	84.86	0.00907	0.00281	0.00424	0.01612	0.00224	0.444	0.139
0.320	0.2066	88.49	0.00864	0.00285	0.00432	0.01581	0.00215	0.433	0.136
0.390	0.2518	91.91	0.00811	0.00280	0.00409	0.01500	0.00213	0.447	0.142
0.460	0.2970	95.63	0.00767	0.00275	0.00391	0.01433	0.00202	0.440	0.141
0.540	0.3486	98.95	0.00710	0.00269	0.00384	0.01363	0.00195	0.446	0.143
0.630	0.4067	102.65	0.00651	0.00270	0.00365	0.01286	0.00189	0.451	0.147
0.820	0.5294	109.94	0.00519	0.00232	0.00325	0.01076	0.00156	0.450	0.145
1.080	0.6972	118.36	0.00352	0.00169	0.00195	0.00716	0.00106	0.434	0.148
1.440	0.9296	126.52	0.00110	0.00053	0.00089	0.00252	0.00034	0.430	0.130

D.5 Velocity and Temperature Fluctuation Profiles Data

This section contains the velocity and temperature fluctuation data for the uniformly blown and unblown cases. The following is a summary of the test cases and abbreviations used in the data listings (see also D.3 for the explanation of other abbreviations).

U_∞ (ft/sec)	F
52	0.000
89	0.000
130	0.000
89	0.002
89	0.004

TW - T	$T_w - T_{\infty,o}$	(°F)
DELM	Momentum boundary layer thickness	(inch)
U'	RMS value of longitudinal velocity fluctuation $\sqrt{\overline{u'^2}}$	(ft/sec)
UTAU	Friction velocity, $U_\infty\sqrt{C_f/2} = U_\tau$	(ft/sec)
U'2/UINF2	$\overline{u'^2}/U_\infty^2$	-
T'	RMS value of temperature fluctuation, $\overline{t'^2}$	(°F)
TTAU	$(T_w - T_{\infty,o})\ St/\sqrt{C_f/2} = T_\tau$	(°F)
RUT	correlation coefficient, $\overline{u't'}/\sqrt{\overline{u'^2}}\sqrt{\overline{t'^2}}$	-

VELOCITY AND TEMPERATURE FLUCTUATION PROFILES
UINF= 52 FT/SEC F=0.000 PLATE 10

RUN = 070274-3	TW-T = 26.93	CF/2 = 0.00247	UTAU = 2.61
UINF = 52.29	DELM = 0.700	ST = 0.00251	TTAU = 1.360

Y	Y/DELM	U'	U'/UTAU	U'2/UINF2	T'	T'/TTAU	T'/(TW-T)	RUT
0.007	0.0100	5.13	1.967	0.00964	2.003	1.473	0.074	-0.72
0.009	0.0129	5.31	2.033	0.01030	2.060	1.515	0.076	-0.69
0.014	0.0200	5.24	2.006	0.01003	2.068	1.521	0.077	-0.75
0.020	0.0286	5.15	1.974	0.00971	2.043	1.502	0.076	-0.76
0.030	0.0429	5.07	1.941	0.00939	1.985	1.460	0.074	-0.77
0.043	0.0614	5.02	1.922	0.00920	1.905	1.401	0.071	-0.71
0.062	0.0886	4.94	1.892	0.00892	1.820	1.338	0.068	-0.71
0.094	0.1343	4.87	1.868	0.00869	1.713	1.260	0.064	-0.70
0.130	0.1857	4.75	1.820	0.00825	1.633	1.201	0.061	-0.61
0.185	0.2643	4.53	1.736	0.00751	1.541	1.133	0.057	-0.65
0.330	0.4714	3.90	1.493	0.00555	1.381	1.015	0.051	-0.65
0.600	0.8571	1.96	0.752	0.00141	0.998	0.734	0.037	-0.60

VELOCITY AND TEMPERATURE FLUCTUATION PROFILES
UINF= 52 FT/SEC F=0.000 PLATE 19

RUN = 070274-4	TW-T = 27.73	CF/2 = 0.00213	UTAU = 2.42
UINF = 52.41	DELM = 1.325	ST = 0.00215	TTAU = 1.292

Y	Y/DELM	U'	U'/UTAU	U'2/UINF2	T'	T'/TTAU	T'/(TW-T)	RUT
0.007	0.0053	5.27	2.180	0.01012	2.079	1.609	0.075	-0.71
0.009	0.0068	5.18	2.142	0.00977	2.113	1.635	0.076	-0.72
0.014	0.0106	5.16	2.133	0.00968	2.178	1.686	0.079	-0.66
0.021	0.0158	5.04	2.085	0.00925	2.186	1.692	0.079	-0.72
0.032	0.0242	4.90	2.028	0.00875	2.147	1.662	0.077	-0.68
0.048	0.0362	4.88	2.017	0.00866	2.094	1.621	0.076	-0.64
0.074	0.0558	4.84	2.003	0.00854	2.028	1.570	0.073	-0.62
0.108	0.0815	4.80	1.987	0.00840	1.950	1.509	0.070	-0.60
0.160	0.1208	4.76	1.968	0.00824	1.878	1.454	0.068	-0.59
0.250	0.1887	4.58	1.895	0.00764	1.793	1.388	0.065	-0.38
0.550	0.4151	3.92	1.621	0.00559	1.567	1.213	0.057	-0.60
1.040	0.7849	2.40	0.993	0.00210	1.251	0.968	0.045	-0.60

VELOCITY AND TEMPERATURE FLUCTUATION PROFILES
UINF= 89 FT/SEC F=0.000 PLATE 10

RUN = 071674-6
UINF = 88.45

TW-T = 26.54
DELM = 0.836

CF/2 = 0.00252
ST = 0.00244

UTAU = 4.45
TTAU = 1.290

Y	Y/DELM	U'	U'/UTAU	U'2/UINF2	T'	T'/TTAU	T'/(TW-T)	RUT
0.007	0.0084	8.03	1.804	0.00824	1.626	1.260	0.061	-0.75
0.009	0.0108	8.11	1.822	0.00840	1.642	1.273	0.062	-0.76
0.015	0.0179	8.12	1.825	0.00843	1.646	1.276	0.062	-0.73
0.024	0.0287	8.18	1.839	0.00856	1.674	1.298	0.063	-0.77
0.038	0.0455	8.51	1.913	0.00926	1.668	1.293	0.063	-0.72
0.056	0.0670	8.62	1.937	0.00950	1.640	1.271	0.062	-0.72
0.082	0.0981	8.66	1.945	0.00958	1.603	1.243	0.060	-0.76
0.130	0.1555	8.58	1.927	0.00940	1.534	1.189	0.058	-0.73
0.200	0.2392	8.15	1.833	0.00850	1.457	1.129	0.055	-0.79
0.280	0.3349	7.67	1.724	0.0[illegible]32	1.364	1.057	0.051	-0.77
0.500	0.5981	6.04	1.357	0.00466	1.170	0.907	0.044	-0.71
0.800	0.9569	2.11	0.475	0.00057	0.738	0.572	0.028	-0.71

VELOCITY AND TEMPERATURE FLUCTUATION PROFILES
UINF= 89 FT/SEC F=0.000 PLATE 19

RUN = 071674-4
UINF = 88.49

TW-T = 26.80
DELM = 1.424

CF/2 = 0.00226
ST = 0.00221

UTAU = 4.22
TTAU = 1.246

Y	Y/DELM	U'	U'/UTAU	U'2/UINF2	T'	T'/TTAU	T'/(TW-T)	RUT
0.007	0.0049	7.67	1.817	0.00751	1.693	1.359	0.063	-0.77
0.009	0.0063	7.70	1.826	0.00758	1.708	1.371	0.064	-0.82
0.014	0.0098	8.00	1.897	0.00818	1.759	1.412	0.066	-0.73
0.020	0.0140	8.11	1.922	0.00840	1.791	1.437	0.067	-0.80
0.029	0.0204	8.25	1.956	0.00870	1.831	1.470	0.068	-0.77
0.043	0.0302	8.51	2.017	0.00925	1.840	1.477	0.069	-0.73
0.065	0.0456	8.75	2.074	0.00978	1.835	1.473	0.068	-0.74
0.095	0.0667	8.76	2.075	0.00979	1.838	1.475	0.069	-0.75
0.130	0.0913	8.71	2.063	0.00968	1.810	1.453	0.068	-0.74
0.185	0.1299	8.53	2.022	0.00930	1.768	1.419	0.066	-0.77
0.370	0.2598	7.76	1.840	0.00770	1.608	1.291	0.060	-0.78
0.700	0.4916	6.43	1.524	0.00528	1.392	1.117	0.052	-0.74
0.925	0.6496	5.51	1.306	0.00388	1.100	0.883	0.041	-0.68
1.200	0.8427	3.59	0.852	0.00165	0.979	0.786	0.037	-0.71

VELOCITY AND TEMPERATURE FLUCTUATION PROFILES
UINF= 89 FT/SEC F=0.002 PLATE 19

RUN = 080474-1 TW-T = 29.77 CF/2 = 0.00158 UTAU = 3.49
UINF = 87.85 DELM = 2.074 ST = 0.00143 TTAU = 1.071

Y	Y/DELM	U'	U'/UTAU	U'2/UINF2	T'	T'/TTAU	T'/(TW-T)	RUT
0.007	0.0034	7.42	2.125	0.00713	2.086	1.948	0.070	-0.49
0.010	0.0048	7.61	2.180	0.00750	2.138	1.996	0.072	-0.60
0.015	0.0072	7.85	2.250	0.00799	2.206	2.060	0.074	-0.63
0.022	0.0106	8.08	2.314	0.00845	2.251	2.102	0.076	-0.60
0.033	0.0159	8.26	2.367	0.00884	2.299	2.147	0.077	-0.61
0.048	0.0231	8.46	2.425	0.00928	2.325	2.171	0.078	-0.65
0.070	0.0338	8.73	2.502	0.00988	2.338	2.183	0.079	-0.63
0.105	0.0506	9.11	2.611	0.01076	2.340	2.185	0.079	-0.61
0.160	0.0771	9.13	2.616	0.01080	2.327	2.173	0.078	-0.59
0.250	0.1205	9.07	2.598	0.01065	2.377	2.219	0.080	-0.59
0.770	0.3713	7.87	2.256	0.00803	1.899	1.773	0.064	-0.56
1.290	0.6220	6.37	1.824	0.00525	1.672	1.561	0.056	-0.59
1.690	0.8149	4.44	1.274	0.00256	1.404	1.311	0.047	-0.57

VELOCITY AND TEMPERATURE FLUCTUATION PROFILES
UINF= 89 FT/SEC F=0.004 PLATE 19

RUN = 081074-1 TW-T = 28.88 CF/2 = 0.00100 UTAU = 2.81
UINF = 88.74 DELM = 2.586 ST = 0.00082 TTAU = 0.749

Y	Y/DELM	U'	U'/UTAU	U'2/UINF2	T'	T'/TTAU	T'/(TW-T)	RUT
0.007	0.0027	6.84	2.434	0.00594	2.128	2.841	0.074	-0.62
0.012	0.0046	7.25	2.579	0.00667	2.267	3.027	0.078	-0.58
0.019	0.0073	7.76	2.762	0.00765	2.361	3.152	0.082	-0.63
0.038	0.0147	8.32	2.961	0.00879	2.457	3.280	0.085	-0.61
0.075	0.0290	8.89	3.163	0.01003	2.542	3.394	0.088	-0.60
0.170	0.0657	9.62	3.423	0.01175	2.537	3.387	0.088	-0.61
0.280	0.1083	9.64	3.429	0.01179	2.521	3.366	0.087	-0.59
0.430	0.1663	9.50	3.379	0.01145	2.445	3.264	0.085	-0.62
0.620	0.2398	9.33	3.320	0.01105	2.344	3.130	0.081	-0.58
0.850	0.3287	8.99	3.199	0.01026	2.235	2.984	0.077	-0.60
1.400	0.5414	8.47	3.016	0.00912	2.041	2.725	0.071	-0.62
2.000	0.7734	7.85	2.793	0.00782	1.781	2.378	0.062	-0.57

VELOCITY AND TEMPERATURE FLUCTUATION PROFILES
UINF=130 FT/SEC F=0.000 PLATE 10

RUN = 071474-1 TW-T = 26.86 CF/2 = 0.00252 UTAU = 6.53
UINF = 130.30 DELM = 0.857 ST = 0.00240 TTAU = 1.284

Y	Y/DELM	U'	U'/UTAU	U'2/UINF2	T'	T'/TTAU	T'/(TW-T)	RUT
0.007	0.0082	11.09	1.695	0.00725	1.494	1.164	0.056	-0.72
0.009	0.0105	11.22	1.718	0.00741	1.530	1.192	0.057	-0.67
0.016	0.0187	11.81	1.808	0.00821	1.579	1.230	0.059	-0.73
0.025	0.0292	12.39	1.897	0.00904	1.621	1.262	0.060	-0.75
0.038	0.0443	12.85	1.968	0.00973	1.640	1.277	0.061	-0.78
0.056	0.0653	13.20	2.021	0.01026	1.640	1.277	0.061	-0.79
0.084	0.0980	13.29	2.036	0.01041	1.620	1.262	0.060	-0.80
0.130	0.1517	13.06	2.000	0.01005	1.554	1.210	0.058	-0.80
0.195	0.2275	12.58	1.926	0.00932	1.469	1.144	0.055	-0.77
0.275	0.3209	12.03	1.843	0.00853	1.385	1.079	0.052	-0.72
0.400	0.4667	10.86	1.664	0.00695	1.275	0.993	0.047	-0.72
0.725	0.8460	6.04	0.925	0.00215	0.994	0.774	0.037	-0.71

VELOCITY AND TEMPERATURE FLUCTUATION PROFILES
UINF=130 FT/SEC F=0.000 PLATE 19

RUN = 071474-5 TW-T = 27.72 CF/2 = 0.00229 UTAU = 6.23
UINF = 130.20 DELM = 1.535 ST = 0.00222 TTAU = 1.286

Y	Y/DELM	U'	U'/UTAU	U'2/UINF2	T'	T'/TTAU	T'/(TW-T)	RUT
0.007	0.0046	11.26	1.807	0.00748	1.631	1.268	0.059	-0.61
0.009	0.0059	11.31	1.816	0.00755	1.659	1.290	0.060	-0.62
0.015	0.0098	11.70	1.879	0.00808	1.731	1.346	0.062	-0.69
0.022	0.0143	12.07	1.937	0.00859	1.782	1.386	0.064	-0.71
0.032	0.0208	12.44	1.997	0.00913	1.819	1.414	0.066	-0.72
0.045	0.0293	12.74	2.044	0.00957	1.857	1.444	0.067	-0.75
0.065	0.0423	13.02	2.090	0.01000	1.876	1.459	0.068	-0.78
0.100	0.0651	13.08	2.099	0.01009	1.884	1.465	0.068	-0.78
0.160	0.1042	13.03	2.092	0.01002	1.839	1.430	0.066	-0.76
0.260	0.1694	12.40	1.990	0.00907	1.737	1.351	0.063	-0.79
0.390	0.2541	11.73	1.882	0.00811	1.612	1.253	0.058	-0.71
0.720	0.4691	9.85	1.581	0.00572	1.410	1.096	0.051	-0.76
1.080	0.7036	7.72	1.240	0.00352	1.162	0.904	0.042	-0.75

D.6 Turbulent Prandtl Number Data

This section contains the turbulent Prandtl number data for the uniformly blown and unblown cases. The following is a summary of the test cases and abbreviations used in the data listings (see also D.3 for the explanation of other abbreviations).

U_∞ (ft/sec)	F
52	0.000
89	0.000
130	0.000
89	0.002
89	0.004

TW - T	$T_w - T_{\infty,o}$	(^oF)
UTAU	Friction velocity, $U_\infty\sqrt{C_f/2} = U_\tau$	(ft/sec)
TTAU	$(T_w - T_{\infty,o})\ St/\sqrt{C_f/2} = T_\tau$	(^oF)
-U'V'	Longitudinal - normal velocities correlation, $-\overline{u'v'}$	(ft^2/sec^2)
-U'V'/UINF2	$-\overline{u'v'}/U_\infty^2$	-
UV+	$-\overline{u'v'}/U_\tau^2$	-
V'T'	Normal velocity-temperature correlation, $\overline{v't'}$	(^oF ft/sec)
RVT	Correlation coefficient, $\overline{v't'}/\sqrt{\overline{v'^2}}\sqrt{\overline{t'^2}}$	-
VT+	$\overline{v't'}/U_\tau T_\tau$	-
PRT	Turbulent Prandtl number	-

TURBULENT PRANDTL NUMBER
UINF= 52 FT/SEC F=0.000 PLATE 10

RUN = 070274-2	TW-T = 26.62	CF/2 = 0.00249	UTAU = 2.63
UINF = 52.72	DELM = 0.700	ST = 0.00251	TTAU = 1.339

Y	Y/DELM	-U'V'	-U'V'/UINF2	UV+	V'T'	RVT	VT+	PRT
0.130	0.1857	6.615	0.00238	0.956	3.247	0.70	0.922	0.935
0.155	0.2214	6.559	0.00236	0.948	3.250	0.70	0.923	0.926
0.185	0.2643	6.365	0.00229	0.920	3.222	0.72	0.915	0.987
0.215	0.3071	6.059	0.00218	0.876	3.095	0.73	0.879	0.898
0.250	0.3571	5.781	0.00208	0.836	2.877	0.73	0.817	0.922
0.290	0.4143	5.253	0.00189	0.759	2.712	0.72	0.770	0.889
0.330	0.4714	4.642	0.00167	0.671	2.557	0.73	0.726	0.836
0.380	0.5429	4.169	0.00150	0.603	2.384	0.75	0.677	0.803
0.500	0.7143	2.529	0.00091	0.366	1.757	0.71	0.499	0.764
0.600	0.8571	1.140	0.00041	0.165	0.838	0.54	0.238	0.833
0.700	1.0000	0.306	0.00011	0.044	0.317	0.46	0.090	0.756

TURBULENT PRANDTL NUMBER
UINF= 52 FT/SEC F=0.000 PLATE 19

RUN = 070274-1	TW-T = 27.73	CF/2 = 0.00213	UTAU = 2.42
UINF = 52.41	DELM = 1.325	ST = 0.00215	TTAU = 1.292

Y	Y/DELM	-U'V'	-U'V'/UINF2	UV+	V'T'	RVT	VT+	PRT
0.130	0.0981	5.768	0.00210	0.987	2.990	0.55	0.957	0.925
0.160	0.1208	5.823	0.00212	0.956	2.880	0.55	0.922	0.970
0.200	0.1509	5.878	0.00214	1.005	2.912	0.55	0.932	0.968
0.250	0.1887	5.741	0.00209	0.982	2.868	0.57	0.918	0.960
0.310	0.2340	5.549	0.00202	0.949	2.884	0.58	0.923	0.923
0.380	0.2868	5.274	0.00192	0.902	2.746	0.58	0.879	0.921
0.460	0.3472	4.944	0.00180	0.846	2.677	0.60	0.857	0.886
0.650	0.4906	3.955	0.00144	0.677	2.156	0.59	0.690	0.880
0.890	0.6717	2.582	0.00094	0.442	1.596	0.61	0.511	0.868
1.210	0.9132	0.906	0.00033	0.155	0.765	0.55	0.245	0.858

TURBULENT PRANDTL NUMBER
UINF= 89 FT/SEC F=0.000 PLATE 10

RUN = 071174-6 TW-T = 26.54 CF/2 = 0.00252 UTAU = 4.45
UINF = 88.45 DELM = 0.836 ST = 0.00244 TTAU = 1.290

Y	Y/DELM	-U'V'	-U'V'/UINF2	UV+	V'T'	RVT	VT+	PRT
0.130	0.1555	19.558	0.00250	0.988	5.287	0.66	0.921	1.024
0.160	0.1914	19.167	0.00245	0.968	5.253	0.67	0.915	0.993
0.200	0.2392	18.776	0.00240	0.948	5.178	0.69	0.902	0.985
0.240	0.2871	18.307	0.00234	0.924	4.920	0.67	0.857	1.009
0.280	0.3349	17.759	0.00227	0.897	4.943	0.68	0.861	0.968
0.330	0.3947	16.899	0.00216	0.853	4.420	0.65	0.770	1.018
0.380	0.4545	15.647	0.00200	0.790	4.133	0.67	0.720	1.028
0.440	0.5263	13.534	0.00173	0.683	3.892	0.68	0.678	0.958
0.500	0.5981	11.970	0.00153	0.604	3.347	0.63	0.583	0.982
0.575	0.6878	9.153	0.00117	0.462	2.819	0.67	0.491	0.954
0.650	0.7775	6.102	0.00078	0.308	2.245	0.71	0.391	0.891
0.800	0.9569	1.486	0.00019	0.075	0.867	0.70	0.151	0.760

TURBULENT PRANDTL NUMBER
UINF= 89 FT/SEC F=0.000 PLATE 19

RUN = 071174-7 TW-T = 26.80 CF/2 = 0.00226 UTAU = 4.22
UINF = 88.49 DELM = 1.424 ST = 0.00221 TTAU = 1.246

Y	Y/DELM	-U'V'	-U'V'/UINF2	UV+	V'T'	RVT	VT+	PRT
0.130	0.0913	17.697	0.00226	0.994	5.221	0.62	0.993	0.939
0.155	0.1088	17.619	0.00225	0.989	5.190	0.61	0.987	0.941
0.185	0.1299	17.540	0.00224	0.985	5.132	0.61	0.976	0.947
0.220	0.1545	17.305	0.00221	0.972	5.090	0.63	0.968	0.943
0.260	0.1826	16.836	0.00215	0.945	5.027	0.64	0.956	0.926
0.310	0.2177	16.679	0.00213	0.937	4.990	0.64	0.949	0.925
0.370	0.2598	16.209	0.00207	0.910	4.964	0.65	0.944	0.905
0.445	0.3125	15.661	0.00200	0.879	4.748	0.64	0.903	0.915
0.520	0.3652	14.486	0.00185	0.813	4.527	0.66	0.861	0.887
0.700	0.4916	12.372	0.00158	0.695	3.923	0.66	0.746	0.873
0.925	0.6496	9.318	0.00119	0.523	3.008	0.69	0.572	0.365
1.200	0.8427	4.855	0.00062	0.273	1.935	0.64	0.368	0.811

TURBULENT PRANDTL NUMBER
UINF= 89 FT/SEC F=0.002 PLATE 19

RUN = 080474-2   TW-T = 29.77   CF/2 = 0.00158   UTAU = 3.49
UINF = 87.85   DELM = 2.074   ST = 0.00143   TTAU = 1.071

Y	Y/DELM	-U'V'	-U'V'/UINF2	UV+	V'T'	RVT	VT+	PRT
0.130	0.0627	18.908	0.00245	1.552	5.951	0.55	1.592	0.967
0.160	0.0771	19.217	0.00249	1.578	6.216	0.57	1.663	0.941
0.200	0.0964	19.448	0.00252	1.597	6.250	0.56	1.672	0.947
0.250	0.1205	19.834	0.00257	1.628	6.339	0.55	1.696	0.952
0.310	0.1495	19.757	0.00256	1.622	6.276	0.57	1.679	0.958
0.380	0.1832	19.603	0.00254	1.609	6.261	0.55	1.675	0.982
0.550	0.2652	19.911	0.00258	1.635	6.085	0.58	1.628	0.996
0.770	0.3713	19.140	0.00248	1.571	5.816	0.59	1.556	1.001
0.910	0.4388	16.516	0.00214	1.356	5.289	0.58	1.415	0.950
1.090	0.5256	14.663	0.00190	1.204	4.986	0.61	1.334	0.906
1.290	0.6220	12.425	0.00161	1.020	4.261	0.56	1.140	0.907
1.490	0.7184	9.184	0.00119	0.754	3.312	0.56	0.886	0.878

TURBULENT PRANDTL NUMBER
UINF= 89 FT/SEC F=0.004 PLATE 19

RUN = 081074-2   TW-T = 28.88   CF/2 = 0.00100   UTAU = 2.81
UINF = 88.74   DELM = 2.586   ST = 0.00082   TTAU = 0.749

Y	Y/DELM	-U'V'	-U'V'/UINF2	UV+	V'T'	RVT	VT+	PRT
0.130	0.0503	19.923	0.00253	2.523	6.731	0.59	3.198	0.971
0.170	0.0657	21.498	0.00273	2.723	7.583	0.61	3.603	0.930
0.220	0.0851	22.286	0.00283	2.822	7.859	0.61	3.734	0.930
0.350	0.1353	23.624	0.00300	2.992	8.149	0.59	3.872	0.951
0.520	0.2011	24.254	0.00308	3.072	8.375	0.60	3.979	0.950
0.730	0.2823	24.097	0.00306	3.052	7.794	0.59	3.703	1.014
1.000	0.3867	2[illegible]73	0.00293	2.922	7.194	0.57	3.418	1.052
1.300	0.5027	[illegible].474	0.00260	2.593	7.032	0.62	3.341	0.955
1.600	0.6187	16.222	0.00206	2.054	6.137	0.64	2.916	0.867
1.900	0.7347	12.048	0.00153	1.526	4.538	0.60	2.156	0.871

TURBULENT PRANDTL NUMBER
UINF=130 FT/SEC F=0.000 PLATE 10

RUN = 071474-4	TW-T = 26.58	CF/2 = 0.00252	UTAU = 6.53
UINF = 130.20	DELM = 0.857	ST = 0.00240	TTAU = 1.271

Y	Y/DELM	-U'V'	-U'V'/UINF2	UV+	V'T'	RVT	VT+	PRT
0.130	0.1517	42.719	0.00252	1.002	7.885	0.69	0.950	0.981
0.160	0.1867	42.041	0.00248	0.986	7.802	0.70	0.940	0.976
0.195	0.2275	41.024	0.00242	0.962	7.719	0.71	0.930	0.962
0.235	0.2742	40.515	0.00239	0.950	7.719	0.73	0.930	0.950
0.275	0.3209	40.007	0.00236	0.938	7.553	0.74	0.910	0.960
0.325	0.3792	38.820	0.00229	0.910	7.470	0.77	0.900	0.941
0.400	0.4667	34.921	0.00206	0.819	6.889	0.76	0.830	0.918
0.475	0.5543	30.514	0.00180	0.716	6.391	0.77	0.770	0.881
0.550	0.6418	24.750	0.00146	0.580	4.980	0.77	0.600	0.900
0.625	0.7293	20.003	0.00118	0.469	4.731	0.77	0.570	0.848
0.725	0.8460	11.188	0.00066	0.262	3.154	0.69	0.380	0.781

TURBULENT PRANDTL NUMBER
UINF=130 FT/SEC F=0.000 PLATE 19

RUN = 071474-3	TW-T = 27.72	CF/2 = 0.00229	UTAU = 6.23
UINF = 130.20	DELM = 1.535	ST = 0.00222	TTAU = 1.286

Y	Y/DELM	-U'V'	-U'V'/UINF2	UV+	V'T'	RVT	VT+	PRT
0.130	0.0847	38.820	0.00229	1.000	7.691	0.62	0.960	0.944
0.160	0.1042	37.973	0.00224	0.978	7.611	0.62	0.950	0.933
0.210	0.1368	38.312	0.00226	0.987	7.531	0.61	0.940	0.951
0.260	0.1694	37.973	0.00224	0.978	7.611	0.63	0.950	0.933
0.320	0.2085	36.447	0.00215	0.939	7.371	0.63	0.920	0.925
0.390	0.2541	36.108	0.00213	0.930	7.211	0.64	0.900	0.937
0.460	0.2997	34.243	0.00202	0.882	7.050	0.65	0.880	0.909
0.540	0.3518	33.056	0.00195	0.852	6.810	0.65	0.850	0.907
0.630	0.4104	32.039	0.00189	0.825	6.650	0.66	0.830	0.901
0.820	0.5342	26.445	0.00156	0.681	5.929	0.70	0.740	0.854
1.080	0.7036	17.969	0.00106	0.463	4.647	0.73	0.580	0.813
1.440	0.9381	5.764	0.00034	0.148	1.602	0.64	0.200	0.814